NMR Studies of Cellulose Dissolution in Ionic Liquids

Asanah Radhi

Submitted in accordance with the requirements for the degree of
Doctor of Philosophy

The University of Leeds

School of Physics & Astronomy

October 2014

The candidate confirms that the work submitted is her own, except where work which has formed part of jointly authored publications has been included. The contribution of the candidate and the other authors to this work has been explicitly indicated below. The candidate confirms that appropriate credit has been given within the thesis where reference has been made to the work of others.

The work in Chapter 4 of the thesis has appeared in publication as follows:

Journal of Physical Chemistry B, January 7, 2015, Asanah Radhi, Kim Anh Le, Michael E. Ries, and Tatiana Budtova.

I was responsible for collecting the data and analyses the result. The contribution of the other authors was analyses the result and writing up the publication.

The work in Chapter 6 of the thesis has appeared in publication as follows:

Journal of Biomacromolecules, February 10, 2014, Michael E. Ries, Asanah Radhi, Alice S. Keating, Owen Parker, and Tatiana Budtova.

I was responsible for collecting the data and analyses the result. The contribution of the other authors was analyses the result and writing up the publication.

Acknowledgements

First and foremost, I would like to express my special appreciation and thanks to my supervisor Dr. Michael E. Ries, you have been a tremendous mentor for me. Your advices on this research have been invaluable. Without your guidance and constant feedback this PhD would not have been achievable.

I greatly appreciate the support received through the collaborative work undertaken with the Centre de Mise en Forme des Materiaux, Sophia Antipolis, France - thank you to Prof. Tatinana Budtova and team for your help in collecting the viscosity data.

I would like to say a big thank you to Robin A. Damion for his spare time in problem solving with the NMR spectroscopy and also Simon Wellings for his help with the glove box and sample preparations.

I would like to thank my sponsor Ministry of Higher Education (Malaysia) for the financial support during the years I was here pursuing my PhD. More than that I would like to give thanks to the people of Malaysia in general. Effectively the people of my country are my real sponsors. It is through their daily hard work that the government of my country is able to send people like me to study abroad.

A special thanks to my family. Words can not express how grateful I am to my mother-in law, father-in-law, my mother, and father for all of the sacrifices that you've made on my behalf. Your prayer for me was what sustained me thus far.

At last but not least I would like to thank the person who is my biggest supporter, my husband Hazim Omar. The beginning in a new country was not easy for us and maybe more challenging for him but not for a moment was he hesitant. He has always supported me throughout our years here. I am in debt to him and I hope I will be able to return all the dedication he devoted to me.

Abstract

This study examines the properties of ionic liquid and co-solvent mixtures, investigating fundamental aspect of cellulose dissolution in ionic liquids and developes a new technique to study the kinetics of cellulose coagulation.

The first system that we studied is the mixture of 1-Ethyl-3-Methylimidazolium Acetate (EMIMAc) and Dimethyl Sulfoxide (DMSO). The motivation behind this study is that the use of DMSO as a co-solvent for cellulose dissolution in ionic liquid makes the cellulose processing more efficient and cost effective. Detailed studies of solutions are carried out to probe the macro- and micro-scopic changes of the ionic liquid properties as well as DMSO in the mixtures. The results suggest that ionic liquid and DMSO mixtures behave almost like an ideal solution.

Solutions of 1-Butyl-3-Methylimidazolium Chloride (BMIMCl)-cellulose are investigated across a range of cellulose concentrations and temperatures using NMR- spectroscopy and relaxometry, diffusion and viscosity measurements. Using Bloemberg-Purcell-Pound (BPP) theory, NMR relaxation times T_1 and T_2 have been expressed in terms of an isotropic correlation time, τ_c for molecular motion. The derivation of the relation between correlation time and translational diffusion shows that the rotational motion can be best correlated to translational motion in term of hydrodynamic radius and activation energy.

Mixtures of ionic liquids and carbohydrates (glucose, cellobiose and cellobiose) are investigated using viscosity and NMR spectroscopy, relaxometry and diffusion measurements. The results give the interaction stoichiometry of ionic liquid:hydroxyl group, 1:1. Analysis of the dynamic properties of the mixtures suggests that in solutions the bulk viscosity, η is best replaced by a microviscosity, $\eta_\mu = f_\mu \eta$, where f_μ is the microviscosity correction factor.

A new method to study the kinetics of cellulose coagulation in water from cellulose/IL/co-solvent using NMR has been successfully developed. Diffusion coefficients of EMIMAc and DMSO are found not to be significantly affected by cellulose and DMSO concentrations within the range studied, which suggests that if

we want to change the coagulation rate and therefore the morphology, we would need to change the anti-solvent.

Table of Contents

List of Tables

List of Figures

Abbreviations

$[C_4mpy]Cl$	1-Butyl-3-Methylpyridium Chloride
AGU	Anhydroglucopyranose units
AMIMCl	1-Allyl-3-Methylimidazolium Chloride
AMIMFo	1-Allyl-3-Methylimidazolium Formate
BMIMAc	1-Butyl-3-Methylimidazolium Acetate
$BMIMBF_4$	1-Butyl-3-Methylimidazolium Tetrafluoroborate
BMIMCl	1-Butyl-3-Methylimidazolium Chloride
BMIMFo	1-Butyl-3-Methylimidazolium Formate
$BMIMNtf_2$	1-Butyl-3-Methylimidazolium Bistriflimide
$BMIMPF_6$	1-Butyl-3-Methylimidazolium Hexafluorophosphate
BMIMTfO	1-Butyl-3-Methylimidazolium Trifluoromethanesulfonate
BPP	Bloemberg-Purcell-Pound
CAC	Critical aggregation concentration
CS_2	Carbon disulfide
DFT	Density Functional Theory
DMF	*N*,*N* dimethylformamide
DMSO	Dimethyl Sulfoxide
DP	Degree of polymerization
DSC	Differential scanning calorimetry
EMIMAc	1-Ethyl-3-Methyl-Imidazolium Acetate
EMIMCl	1-Ethyl-3-Methyl-Imidazolium Chloride
FTIR	Fourier transform infrared
H_2SO_4	Sulfuric acid
HBA	Hydrogen bond acceptor
IL	Ionic Liquid
IR	Infrared
MCC	Microcrystalline cellulose
NaOH	Sodium hydroxide
NMNO	*N*-methylmorpholine-*N*-oxide
NMR	Nuclear Magnetic Resonance

OES	Organic electrolyte solutions
OH	Hydroxyl groups
PFGSTE	Pulsed field gradient stimulated spin-echo
ppm	Parts per million
RF	Radio frequency
SB	Solvent basicity
$scCO_2$	Supercritical fluids CO_2
SED	Stokes-Einstein-Debye
TGA	Thermogravimetric analysis
$TMGHEtCO_2$	*N*,*N*,*N*,*N*-tetramethylguanidium propionate

Nomenclature

μ	Magnetic moment
a	Associated fraction
B_o	External magnetic field
B_{sec}	Secondary magnetic field
D	Self-diffusion coefficient
D_o	Self-diffusion coefficient pre-exponential factor
E	Potential energy
$E_a[D]$	Diffusion activation energy
$E_a[\eta]$	Viscosity activation energy
$E_a[\tau_c]$	Correlation time activation energy
F	Force
f_μ	Microviscosity correction factor
$\hbar$	Plank's constant
I	Spin quantum number
$\mathcal{J}(\omega_o)$	Spectral density function
I_m	Moment of inertia
k_B	Boltzmann constant
m	Magnetic quantum number
M	Molar mass
N	Interaction stoichiometry
N_A	Avogadro number
$N\rho$	Number of spin per unit volume
P	Spin angular momentum
R_H	Hydrodynamic radius
r_j	Inter-distance proton
T	Temperature
T_1	Spin-lattice relaxation
T_2	Spin-spin relaxation
V	Molar volume

v_o	Frequency
α	Hydrogen bond acidity
β	Hydrogen bond basicity
γ	Gyromagnetic ratio
$\Delta\delta$	Chemical shift change
η	Viscosity
η_μ	Microviscosity
σ	Shear stress
τ_c	Correlation time
τ_{FR}	Free rotor reorientation time
τ_o	Correlation time pre-exponential factor
τ_{rot}	Rotational correlation time
ω_o	Angular frequency

Chapter 1
Introduction

1.1 Background

In the continuously growing consumptions and over-exploitation of non-renewable resources, the utilization of natural polymers has become attractive. Biodegradable polymers and biocompatible composites generated from renewable resources are regarded as potential materials that could replace synthetic polymers and lessen the dependence on fossil fuel resources. Increasing global awareness of environmental responsibility and the concept of sustainability has generated the exploration of new products and processes that are more environmentally friendly. In this context, the use of the renewable resource cellulose exactly meets the requirement of this eco-friendly plan. Cellulose, which consists of β-(1-4)-linked glucose repeating units, is a natural polymer and the largest renewable biological resource in our environment.

Cellulose is the major component in the rigid cell wall in plants that gives plants most of their structural strength. Other organisms such as green algae and oomycetes can also produce it. Some species of micro-organism such as *Acetobacter xylinum* sp. also produces abundant amounts of cellulose. On average, about 33% of plant matter is cellulose (cellulose content in cotton is 90% while about 50% in wood). Cellulose can be modified in many different ways to produce new compounds that are useful in a range of applications. It has been broadly used in industry, e.g. in the paperboard, paper, rayon, textile and food industries [1, 2]. However due to the strong glycosidic bonds and the huge degree of both intra- and intermolecular hydrogen bonding, it is a challenge to find suitable solvents for its dissolution.

The main challenge to the more wide ranging use of cellulose until now was a lack of suitable solvents for the chemical dissolution process. The well-developed intermolecular hydrogen bonding hinders it from being easily dissolved in water or other organic solvent. Its unsolvable properties in water and common organic solvents have affected its development and utilization [3].

1.2 Motivation

Most of the typical solvents currently employed in cellulose processing often have environmentally unfriendly characteristics. The viscose process, for example, is the most important and also the oldest process that is still currently used to produce cellulose. However, this process has economic and ecological drawbacks as the derivatization and dissolution process of cellulose involves the production of environmentally unfriendly by-products such as sulphur compounds (i.e. carbon disulfide, CS_2) which need to be completely removed or chemically disposed of before being discharged into the environment.

As shaping of cellulose can only be accomplished by dissolution and coagulation/regeneration, therefore the search for suitable cellulose solvents is of great importance. It is a challenge for researchers and academia to design the most powerful solvent with excellent environmental and eco-friendly properties. One of the main alternatives for cellulose fibre production is the lyocell process which was first developed in the late 1960s. The use of *N*-methylmorpholine-*N*-oxide (NMMO) as a new organic solvent for cellulose opens up new perspective for the cellulose dissolution process. The NMMO process is a direct dissolution process and essentially involves physical phenomena, where no chemical reaction takes place and there are no chemical by-products produced [4, 5]. Even though the NMMO process offers many advantages, however as of today, it fails to totally replace the viscose process. The severe fibrillation found in manufactured fibres and its relatively low surface energy makes it difficult for dyes to bind to it resulting in a finished product that is more expensive. In addition, the thermally unstable properties of NMMO require major investment in safety technology [6, 7].

Introduction of ionic liquid as a new type of cellulose direct solvent with greater dissolving power a decade ago had filled in these gaps. It was found that without a pre-treatment, certain ILs have an ability to dissolve up to 20 wt% of cellulose [8]. However, the cost of ILs is rather expensive up until now. ILs are currently produced only on the laboratory scale. The cost of ILs may be reduced if ILs are produced on an industrial scale instead. In order to further the use of ILs commercially as solvents, a comprehensive understanding of ILs properties and their

interaction with solute or other solvents is important. As a potential replacement solvent for reactions and separations, they are still under intense investigation. At present, numerous studies on ILs have been carried out across various fields of chemical research, including biomass-processing. Understanding the mechanism of cellulose solvation and how ILs properties can affect their capability to dissolve cellulose at microscopic level is therefore very important. In addition, a study of new cellulose solvent that could potentially reduce the cost of using ILs through more rapid dissolution time and temperature for cellulose dissolution is essential for industrial purposes.

1.3 Overview of the Thesis

1.3.1 Objectives

The research conducted for this thesis focused on studying the mechanism of cellulose dissolution in ILs as well as developing a novel cellulose solvent and a new technique to study the kinetics of cellulose regeneration. In this work, the focus is only on the most popular imidazolium-based ILs that are widely used in cellulose processing. The ILs investigated were 1-Ethyl-3-Methyl-Imidazolium Acetate (EMIMAc) and 1-Butyl-3-Methyl-Imidazolium Chloride (BMIMCl).

Generally, most of the ILs used in cellulose/biomass processing are more viscous with the viscosity of two or three orders of magnitude than those of typical molecular solvents. For practical use, the relatively high viscosity of ILs give significant disadvantage as it will lead to difficulty in mass transfer and consume a lot of energy during the mixing process. This problem is amplified with the increasing cellulose concentration in IL. Adding organic co-solvent is an effective way to reduce the viscosity of the mixture which subsequently improves processing efficiency including heat and mass transfer rates. The use of co-solvent in cellulose processing not only improves the processing efficiency but also reduces the processing cost as less IL and energy are consumed. On the basis of this consideration, the first goal of this research was focused on the development of new cellulose solvent with low viscosity by combined ionic liquid with co-solvent. In order to promote the application of mixture IL and co-solvent, the physicochemical

properties of these mixtures are needed. Understanding physicochemical properties of IL/co-solvent mixtures that affect their performance in the interaction with solute are essential to determine and identify their potential for a wide variety of applications. Physiochemical properties are not only informative in the understanding of IL-solvent interactions from a theoretical standpoint but also significant in the design and control of the practical process.

Nuclear Magnetic Resonance (NMR) has been proven to be a valuable technique to provide information concerning the dynamics and molecular interactions that occur in the liquid state. Understanding the dynamic properties of ILs and their molecular organization in cellulose/IL solutions is an essential pre-requisite for successful cellulose processing. Therefore, this work is focused on studying the mechanism of cellulose dissolution in ILs by using the NMR technique. Different types of ILs and carbohydrates are used to provide a better understanding of molecular interactions relative to each other and their dynamic behaviour in solution.

The condition of the coagulation is the most crucial procedure to the formation of the regenerated cellulose structure. It is of considerable importance to investigate the diffusion rate of the solvent molecules as it determines the microstructure of the cellulose membrane/fibre [9]. There are only a few studies investigating the kinetics of cellulose regeneration from ILs [10, 11]. It has never been carried out for ternary mixtures, cellulose/IL/co-solvent solution. Therefore, the final work of this research is focused on the use of a new technique to study the kinetics of cellulose regeneration from the cellulose/IL/co-solvent system. The NMR technique can provide the self-diffusion coefficient of both components (IL and co-solvent) simultaneously by measuring their molecular concentration throughout the regeneration process. The present study can provide reliable features of transport properties of both IL and co-solvent and important information about the kinetics of cellulose regeneration from cellulose/IL/co-solvent solutions.

1.3.2 Organization of the Thesis

This chapter introduces the background, the motivation behind using ILs for cellulose dissolution and the aims and objectives of this thesis in the context of the literature reviewed.

Chapter 2 of this thesis provides an overview of the literature pertinent to the research presented in this thesis. The literature covers the cellulose dissolution in ILs as well as the interaction of ILs with both co-solvent and anti-solvent in the context of research carried out. It also covers the motivation for using co-solvent combined with IL for the dissolution of cellulose. This chapter also provides a detailed review of the ILs, co-solvent and carbohydrate used in this research.

Chapter 3 briefly discusses the fundamental theory, models and instrumentation issues related to this work. It summarizes the necessary NMR experiment used for this work and gives an overview of typical measurement that were employed.

Chapter 4 shows the results of performed experiments on ionic liquid/co-solvent solutions. The idea is to use ILs combined with co-solvent as new cellulose solvent for cellulose processing. Here, the density, viscosity, chemical shift, self-diffusion coefficient and NMR relaxation of EMIMAc-DMSO mixtures was measured. The changes of macro- and micro-scopic properties of ionic liquid, EMIMAc in the presence of various co-solvent concentrations at different temperatures have been analysed using ideal mixing law.

Chapter 5 describes the dissolution mechanism of cellulose in BMIMCl. The structure and the dynamic properties of this solution have been investigated mainly using both high field and low field NMR. This chapter contains both basic data analysis and a ^{1}H NMR relaxation analysis of the BMIMCl. In this work, ^{1}H NMR relaxation data of the ILs was examined and analysed to draw a useful qualitative picture of the reorientational microdynamics of the ILs. The Bloembergen-Purcell-Pound (BPP) method is then used to further analyse the ^{1}H NMR relaxation data. These results are then correlated with the viscosity data. Other models are also used to analyse the structure and dynamics of the BMIMCl at different temperatures and cellulose concentrations.

Chapter 6 describes the dissolution of three different types of carbohydrates; glucose, cellobiose and cellulose in EMIMAc. The study of cellulose monomer, dissolved in IL provides a fundamental overview of how IL interacts with cellulose during the dissolution process. In this work, glucose and cellobiose are chosen as the model of cellulose to investigate the interaction between EMIMAc and cellulose at molecular level. Similar to Chapter 5, this chapter contains both basic data analysis and a ^{1}H NMR relaxation analysis of the EMIMAc. As a complement, results from diffusion and viscosity studies are also presented.

Chapter 7 demonstrates how the NMR technique is used to study cellulose coagulation. The kinetics of cellulose coagulation is tracked using NMR giving molecular concentration and dynamics information of EMIMAc and DMSO that were released from cellulose/EMIMAc-DMSO solutions. The information obtained is analysed using a diffusion controlled model that was derived from Fick's second law of diffusion.

Chapter 8 summarizes the findings and provides a brief outlook for possible follow-up experiments.

Chapter 2
Literature Review

2.1 Conventional methods for cellulose dissolution

2.1.1 Viscose process

The viscose process is the most important and the oldest process that is still currently used to produce cellulose. The viscose process was first discovered by British chemist Charles Cross, Edward Bevan and Clayton Beadle in 1891. It was then successfully commercialized in 1905 and since then viscose rayon is leading the worldwide fibre market. The manufacturing of rayon and cellophane using the viscose process involves four primary operations; 1) steeping 2) aging 3) xanthation and 4) spinning. In a steeping operation cellulosic raw materials and aqueous caustic solution, sodium hydroxide (NaOH) were added to the slurry tank. Inside the slurry tank, cellulose is finally converted into alkali cellulose. Prior to aging, the solution has undergone several processes, such as pressing and shredding, which leave the solution in a form of "white crumb". In the aging step, the white crumb is then exposed under controlled conditions to oxygen to oxidize and depolymerise it. This step requires careful monitoring so that the length of the fibres is short enough to manage the viscosity to the spinning solution but long enough to produce good fibres. Then the aged white crumb (alkali cellulose) is transported to the xanthator. In the xanthator, the aged white crumb is reacted with gaseous or liquid carbon disulfide (CS_2) to produce cellulose xanthate. In this process, the amount of carbon disulfide for xanthation of the alkali cellulose depends upon the product being manufactured. After that, cellulose xanthate is again dissolved in aqueous caustic solution. However, cellulose xanthate cannot be dissolved completely as there are blocks of unxanthated hydroxyl groups inside the crystalline regions of cellulose. Before spinning or casting, the viscose is filtered and ripened. In a spinning stage, the solution is mixed with sulfuric acid (H_2SO_4) and other additives. As soon as the solution reacted with the sulfuric acid, the xanthate groups are converted to unstable xantheic acid groups that release carbon disulphide to form filaments or rayon

fibres. During this process, carbon disulphide is released and can be recycled [12, 13]. The schematic diagram of viscose process is shown in Figure 2.1.

The viscose process can produce variable types of fibre properties. Although the viscose process is broadly employed in the fibres industry, it still has economic and ecological drawbacks. Its derivatization and dissolution process for cellulose involves the production of environmentally unfriendly by-products such as sulphur compounds (i.e.; carbon disulfide, CS_2) which need to be completely removed or chemically disposed of before being discharged into the environment. Because of the demanding stringent environmental regulations, the search for alternative processes to generate cellulose fibre has been extensively investigated and only the lyocell process has become an important industrial alternative.

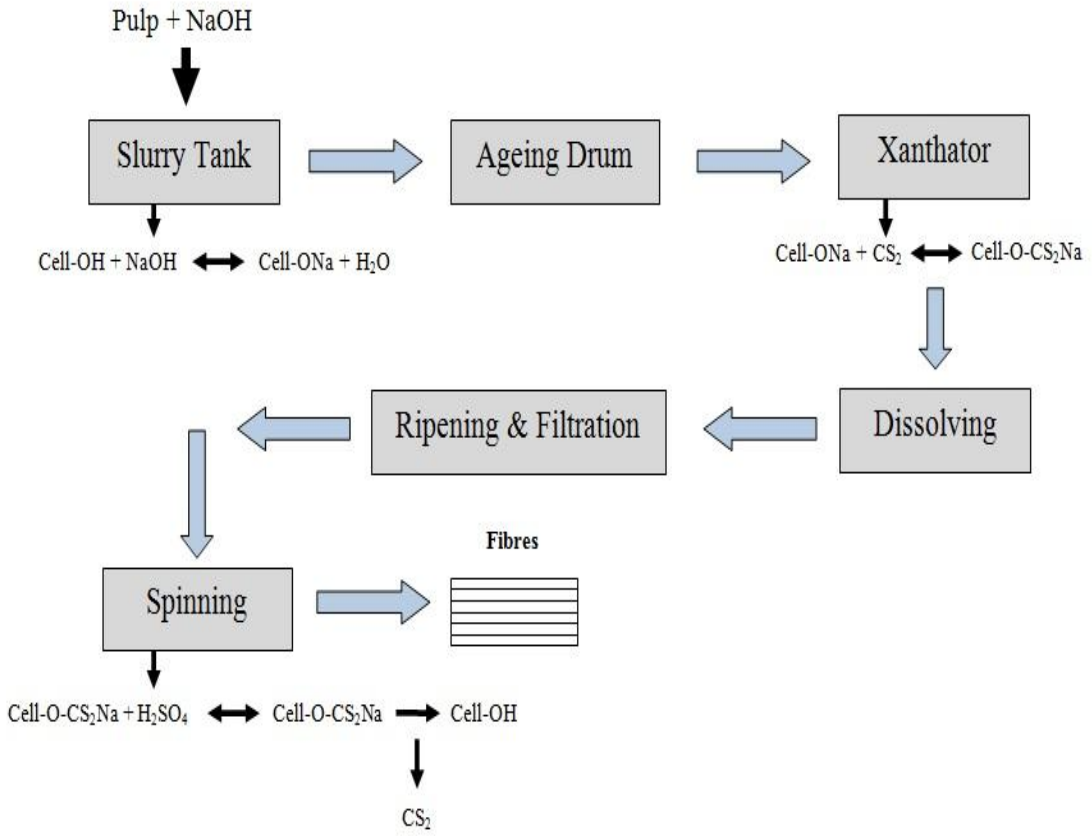

Figure 2.1: The viscose process.

2.1.2 Lyocell process

One of the main alternatives for cellulose fibre production is the lyocell process that was first developed in the late 1960's. The use of *N*-methyl morpholine-*N*-oxide (NMMO) (*see* Figure 2.2) as a new organic solvent for cellulose opens up new perspectives for the cellulose dissolution process. Lyocell or NMMO process is a direct dissolution process and essentially involves physical phenomena which has no chemical reaction taking place and no chemical by-product produced [4, 5]. The lyocell process is characterized by direct dissolution of wood pulp in *N*-methyl morpholine-*N*-oxide monohydrate (NMMO.H_2O) without prior derivatization of the cellulose. In relation to the viscoss process, the lyocell process involves a comparatively low number of process steps. Cellulose fibres are directly obtained from cellulose solution in NMMO without undergoing derivatization such as alkalization and xanthation in the case of rayon fibre [14].

The NMMO process is based on an NMMO-water-cellulose system (3 phase diagram). The range for the water content in NMMO that allows dissolving of cellulose is varied from 4 to 17%. Cellulose solution up to 30% can be produced depending of the characteristic of the pulp and the amount of water content in the system [15]. NMMO belongs to the family of cyclic, aliphatic, tertiary amide oxides. The most important features of NMMO are the highly polar of the N-O group with the highest electron density located at the oxygen atom. Although the NMMO process has been employed in industry for several decades, the physicochemical process of the cellulose dissolution and the structure of the dissolved cellulose are still far from being comprehensively understood. The mechanism for dissolution of cellulose has been intensively investigated with various scientific efforts including thermo-analytical analysis, rheology, and quantum mechanical computations [16, 17]. Using NMR, Gagnaire et al. has shown that cellulose derivatization in NMMO-water-cellulose solution did not occurr [18]. Today, consensus has been reached that the dissolution of cellulose in NMMO originates from the ability of the strong dipolar N-O group in NMMO to disrupt the hydrogen bond network of cellulose and form a solvent complex (hydroxylated compounds), with a new hydrogen bond between cellulose and solvent being formed.

The production of cellulose fibres, films and membranes via the NMMO process that is free from hazardous by-product cannot be denied as a good alternative for cellulose processing. Nevertheless, this process suffers from a number of weaknesses and drawbacks. The fibres produced suffer from high fibrillation. In addition, the NMMO process gives rise to several side reactions which in an NMMO/cellulose mixture, both solvent and cellulose undergo degradation reaction. At the elevated process temperature used, cellulose undergoes severe degradation and this causes NMMO/cellulose mixture to become unstable.

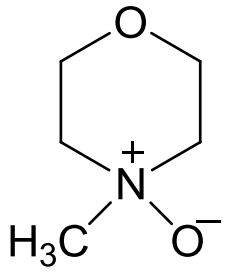

Figure 2.2: Structure of *N*-methylmorpholine-*N*-oxide.

2.2 Ionic Liquids

Ionic liquids (ILs) are organic salts with relatively low melting points (<100^{o}C). Like other salts, they are composed of anions and cations. ILs have many interesting properties such as extremely low vapour pressure, high ionic conductivity, good thermal stability and excellent solubility for polar and non-polar compounds [19-22]. ILs can participate in ionic, hydrophobic and hydrogen bond interactions. Owing to their good solvent capabilities for a broad variety of compounds, they can potentially replace conventional solvents in many applications. Apart from that, their unique properties have been applied in diverse fields, such as synthesis, catalysis, biocatalysis, separation technology and nanotechnology [19, 23]. IL can be tailored with a huge variety of possible ion combinations. Therefore, in order to meet its desired application, the selection of an appropriate cation and anion contained in an ionic liquid is crucial, as it will determine the physical and chemical properties of the IL itself. Typically, ILs consist of a bulky, asymmetric organic cation such as imidazolium, aliphatic ammonium and pyrrolidinium ions. Alkylphosphonium and alkylsulfonium cations are also in use. Many anions are widely employed with these

cations. Most ILs reported in the literature consists of organic and inorganic anion. For examples, 1-Butyl-3-Methylimidazolium Chloride BMIMCl consists of organic cation and inorganic anion, and 1-Ethyl-3-Methylimidazolium Acetate (EMIMAc) consists of organic cation and organic anion.

2.2.1 Imidazolium based ionic liquids

There is a large volume of literature which has been published on imidazolium-based ILs. However, among all ILs, the most common and extensively investigated are the 1-alkyl-3-methylimidazolium-based ILs with its short abbreviation $[C_n\text{mim}]^+$, *n* represents the length of the alkyl chain. This is reflected by a growing numbers of publications dealing with the physicochemical properties of these ILs in the pure state and of its mixture with co-solvents [24-26]. Such cations of the general formula $[C_n\text{mim}]^+$ possess a charge-rich imidazolium core and hydrophobic alkyl chain. The region where the imidazolium core formed a hydrogen-bonded network with anions can be regarded as the polar region where as the region where the alkyl chain linked by short-range van der Waals forces is referred to as a non-polar region [26].

This imidazolium core consisted of a delocalized 3-centre-4-electron configuration across the N^1-C^2-N^3 moiety, a double bond between C^4 and C^5 at the opposite side of the ring and a weak delocalization in the central region (*see* Figure 2.3). This configuration resulted in the larger positive charge on the C^2-H, C^4-H and C^5-H groups, which become the main attractive sites with the anion [27-29].

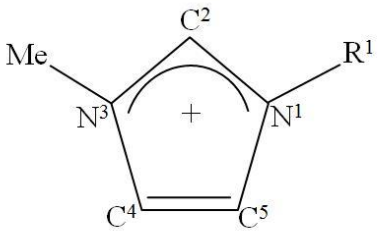

Figure 2.3: Denotation and electronic structure of 1-alkyl-3-methylimidazolium ions. (adapted from H. Weingartner) [30].

A. Bagno et al. demonstrated that resonance of H2 (proton attached to the C^2) is strongly influenced by the local arrangement of the anion. MD simulation on pair distribution function and co-ordination number demonstrated that hydrogen H2 followed by H4 and H5 are the ones which appear to interact most closely with the anion, (H2 > H4 = H5) [31]. It concludes that protons of the *n*-butyl chain are quite insensitive to the presence of the anion, while H2, H4 and H5 are the major site of interaction with the anion [32]. However, different types of anion form different hydrogen bonds with cations. For example, for anions with single atom such as chloride, bromide and iodide, there is only one C-H----X (X = Cl, Br, I) hydrogen bond formed between anion and cation. However, in the case of anion with multiple atoms like acetate, Ac^- and tetrafluoroborate, BF_4^-, there is more than one hydrogen bond formed between anion and cation [33-35]. Three imidazolium ring protons are involved to form this strong hydrogen bond. Interactions between these three imidazolium rings form a three dimensional ion network with aromatic π-stacking interaction between the imidazoilum cores [36, 37].

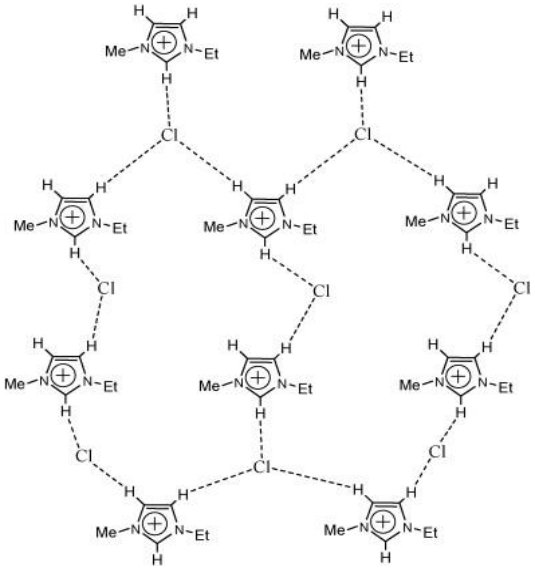

Figure 2.4: Three dimensional network of hydrogen-bonding between ring protons (adapted from [38]).

Hydrogen bonding in ionic liquid also determines the properties of ILs such as melting points, viscosities, density and vaporization enthalpies. Studies on imidazolium IL-water have suggested that the density trend for this system is mainly determined by hydrogen bonding between ILs and water [39, 40]. Apart from that,

Seddon et al. have shown that the viscosity of the 1-Butyl-3-Methylimidazolium Chloride (BMIMCl) increases with the increase of chloride concentration which indicates that hydrogen bonding via cohesive force between chloride ions and the protons of the imidazolium ring increases [41].

An increase in the length of alkyl chain in the imidazolium cation increases the hydrophobicity of the IL [26, 42]. The charge distribution in the imidazolium cation is greatly affected by the length and number of alkyl radicals. This alters the strength of the cation-anion bond which determines the dissolving power of ionic liquid [42]. ILs have relatively higher viscosity than conventional organic solvents. The viscosity is one of the important properties as it influences chemical reaction rate. The rate of chemical reaction decreases as the viscosity increases. L.A.S. Ries et al. indicate that the viscosity of an IL solution can be correlated with the supramolecular structure of the liquid network [43, 44]. Intermolecular interaction changes dramatically with the addition of water even for small amounts [45]. The viscosity of ionic liquid is very sensitive to impurities. Addition of water in a high viscosity ionic liquid can reduce the viscosity of the system, which permits the chemical reactions to occur at a faster rate. S. Seki et al. demonstrated that the viscosity did not depend on molecular weight of cations and anions but on the molecular shape of the ions [46].

2.2.2 Ionic liquids for cellulose dissolution

In order to completely replace conventional cellulose solvent, ideally ILs should meet several other criteria. If possible their melting point should be below 20 ^{o}C with high a decomposition point (>100^{o}C). Apart from that, in order to implement newest (efficient) processing technology their cost effective process must be better than the conventional process (e.g: uncomplicated and higher recovery of ILs and easy cellulose regeneration). In the biomass processing industry for example, the effective pre-treatment of cellulosic biomass is essential to its bioconversion into a usable biofuel. An effective pretreatment enhances the accessibility and reactivity of the polysaccharide to maximize the release of fermentable sugars.

In 2002, Swatloski et al. reported the use of an ionic liquid as a solvent for cellulose regeneration. Other experiments also proved that many ILs such as 1-Allyl-3-Methylimidazolium Chloride (AMIMCl), 1-Ethyl-3-Methylimidazolium Acetate (EMIMAc), 1-Butyl-3-Methylimidazolium Acetate (BMIMAc), and 1-Allyl-3-Methylimidazolium Acetate (AMIMAc) can effectively dissolve the biomass from wood, wool, silk and so forth [47-49]. Their biodegradability and low toxicity make them potential substitutes for environment-friendly green solvents in sustainable processes. However, how can these ILs dissolve biomass/cellulose easily? Several factors might influence their capability to efficiently dissolve cellulose such as the lengths of the alkyl side-chain and the substitute anion.

Several studies investigating the dissolution of cellulose in ILs suggest that the solubility power of ILs to dissolve cellulose depends on its physiochemical properties; the polarity parameter [50-52]. Doherty and co-workers have carried out direct studies of the relationship between the solvent polarity parameter for a set of ILs and their ability to reduce cellulose crystallinity. They found that the crystallinity index of regenerated cellulose decreases with an increase in hydrogen bond basicity, β of the ILs [50].

Table 2.1: Selected results for cellulose dissolution in ILs

Ionic liquids	Types of cellulose	Condition	Solubility	References
		Temperature (^{o}C)		
BMIMCl	Avicel	100	20%	[53]
BMIMCl	Pulp (1000)	-	10%	[8]
BMIMAc	MCC	70	15.5%	[54]
BMIMAc	MCC	40	11.5%	[54]
BMIMAc	Avicel	100	12%	[55]
EMIMAc	Avicel (225)	110	28%	[56]
EMIMAc	Avicel	100	8%	[55]
EMIMCl	Avicel	100	10%	[53]

2.2.2.1 1-Butyl-3-Methylimidazolium Chloride (BMIMCl)

1-Butyl-3-Methylimidazolium Chloride, (BMIMCl) with the molecular formula ($C_8H_{15}ClN_2$) is a prominent example of a chloride-based ionic liquid. To date, a

number of researchers have studied the thermodynamic properties of this IL [57, 58]. For example, the Raman scattering and X-ray diffraction studies revealed that BMIMCl has two polymorphs designated as crystal (1) and (2). BMIMCl exists in a solid form at room temperature with its melting point at about 70 ^{o}C. This fairly high melting point resulted in the high viscosity of this solution [58]. O. Yamamuro et al. reported that BMIMCl has an orientationally-disordered structure and has been regarded as a fragile liquid in the same way glass-forming molecular liquids behave [59].

As reported by Swatloski et al. BMIMCl can dissolve up to 25% of cellulose without any pre treatment [8]. Of many ILs, BMIMCl is found to be a good solvent for cellulose dissolution with no side reactions occurring in the dissolving process of cellulose in BMIMCl. High chloride content and activity in BMIMCl was suggested to be the main reason for dissolving cellulose in ILs. Besides that, chloride anions which are strong hydrogen bond acceptors make BMIMCl effective as a cellulose solvent [8]. Structures of BMIMCl are shown in Figure 2.5 and a summary of its physical properties is shown in Table 2.2.

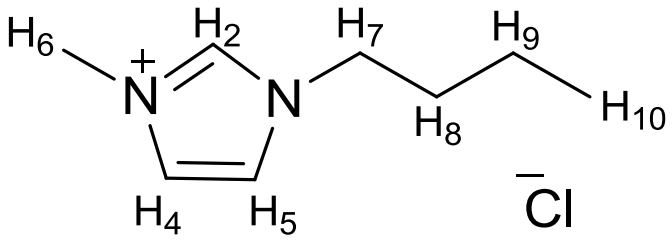

Figure 2.5: Schematic structure of 1-Butyl-3-Methylimidazolium Chloride BMIMCl.

2.2.2.2 1-Ethyl-3-Methylimidazolium Acetate (EMIMAc)

1-Ethyl-3-Methylimidazolium Acetate (EMIMAc) with the molecular formula ($C_8H_{14}N_2O_2$) is one of the ILs that has been widely studied in the research of cellulosic biomass processing. The cation consists of a five-membered ring with two nitrogen and three carbon atoms while the anion consists of an acetate ion. The structure of EMIMAc is shown in Figure 2.6. EMIMAc has properties that make it favourable as a solvent such as relatively low viscosity (132.91 mPas) [60] at room

temperature and low melting point. These make its handling easier. Furthermore, EMIMAc exists in liquid form at room temperature and it has been described as the most suitable reaction medium because the acetate anion catalyzes ring opening of the oxiranes and the reaction with polysaccharide. EMIMAc have shown great promise in the dissolution of biomass and lignocellulosic materials. Experimental data on its physicochemical properties such as density, viscosity, surface tension have been reported in many studies [61, 62]. The presence of a good hydrogen bond acceptor such an acetate ion makes EMIMAc able to strongly co-ordinate with a hydrogen bond donator such as –OH groups. The capability of EMIMAc to strongly co-ordinate with –OH groups make it more promising as a cellulosic biomass solvent [49]. Bowron et al. has investigated the liquid state structure of EMIMAc by molecular dynamic simulations and neutron diffraction. Bowron et al. have reported that the main anion-cation features are in-plane interactions of anion with three acidic hydrogens of the imidazolium ring [35]. The physical properties of EMIMAc are summarized in a Table 2.2:

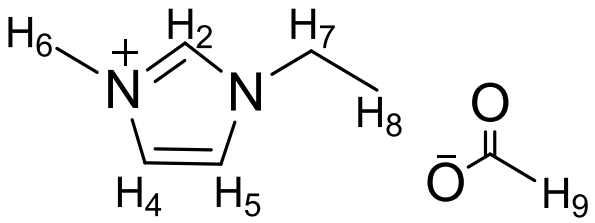

Figure 2.6: Schematic structure of 1-Ethyl-3-Methylimidazolium Acetate.

Table 2.2: Physical properties of ionic liquid BMIMCl and EMIMAc.

Physical properties	BMIMCl	Ref.	EMIMAc	Ref.
Molecular mass (g/mol)	174.7	-	170.22	-
Density (g/cm^3) at 25 ^{o}C	-	-	1.09778	[60]
Melting point (^{o}C)	~70, 41	[26, 42]	<-20	
Viscosity at 25 ^{o}C (mPas)	-	-	132.91	[60]

2.2.3 Role of cation

A considerable amount of literature has been published describing the role of cation in cellulose dissolution. It has been suggested that even though the cation only play

a secondary role in cellulose solubility, and its influence is less important than its counterpart anion, its role cannot be neglected. The existence of weak interaction between cation of ionic liquid and cellulose have been proved by several studies. It was suggested that the imidazolium cation interact with glucose rings through van der Waals interactions [63-65]. Therefore, cation-cellulose interactions also appear to be an important compensator for lost cellulose intersheet interactions.

Chiappe et al. found that as the combination of cation and anion is changed, the polarity of the ILs is significantly affected [66]. This explains why the solubility power of ILs changes when the anion is combined with different types of cation. On the other hand, the author also points out that the alkyl chain length has only a moderate effect on the polarity of the ILs [66].

A number of studies have found that the amount of cellulose that can be dissolved in ILs depends on the charge carrying moiety of the cation and the length of its alkyl chain [67]. Introduction of OH groups on the alkyl chain or imidazolium ring are found to increase polarity and the dielectric constant of the ILs [66, 68]. Zhao et al. investigated the effect of cationic structure on cellulose dissolution in ILs. In their study a series of imidazolium based choride ILs with different alkyl chain length and 1-Butyl-3-Methylpyridium Chloride [C_4mpy]Cl were simulated to study the effect of varying the heterocyclic structure and alkyl chain length. Their study showed that an ionic liquid with shorter alkyl chain achieved higher cellulose solubility than the longer one. On the other hand, [C_4mpy]Cl which has the same alkyl chain length with BMIMCl dissolved more cellulose than BMIMCl [67]. The authors also investigated the effect of the electron-withdrawing group within the alkyl chain of the cation on the dissolution of cellulose by using $AMIM^+$ as a model. It has been suggested that the presence of an electron withdrawing group in the alkyl chain of the cation enhanced the interaction between cation and cellulose.

2.2.4 Role of anion

It has been conclusively shown that it is the IL anion that mainly governs the dissolution of cellulose. In the same line of research, later on, it was identified that the increase in the hydrogen bond accepting ability of the anions composing the ILs caused an increase on their dissolving capability for cellulose. Recent studies

pointed out that high dissolution of cellulose in ILs requires an IL with hydrogen bond basicity [28, 52, 69, 70]. For example, Xu et al. investigated the influence of anionic structure of the ILs on the solubility of cellulose and found that anions with different hydrogen bond basicity, β had a significant effect on the amount of cellulose that can be dissolved [70]. This is not surprising as cellulose polymer behaves preferentially like a hydrogen-bond donor in solution. Therefore, selection of anion is important to determine the maximum cellulose that can be dissolved in ILs. Although IL with a high value of β was found to be a good cellulose solvent, there are however certain limits of the β value in which IL can be classified as a good cellulose solvent. In addition, a necessary balance between acidity, α and basicity, β is also an important aspect that needs to be considered. Studies have shown that IL with a β value range from 0.80 to 1.20 with the net basicity (β - α) neither lower than 0.35 nor exceeding 0.90 is regarded as a good cellulose solvent [71]. Selected ILs that are or are not able to dissolve cellulose is summarize in Table 2.3.

Table 2.3: Hydrogen bond basicity, β for selected ILs.

Ionic liquids	β parameter	References
Cellulose solvent		
AMIMCl	0.83	[51]
AMIMFo	0.99	[51]
BMIMAc	1.09	[72]
BMIMCl	0.87	[72]
BMIMFo	1.008	[54]
EMIMAc	1.09	[73]
Non cellulose solvent		
BMIMPF$_6$	0.207	[74]
BMIMTfO	0.464	[28]
BMIMBF$_4$	0.376	[28]
BMIMNtf$_2$	0.243	[75]

2.3 Carbohydrates

Carbohydrate or saccharide is the most abundant class of biomolecules and consists only of carbon, hydrogen and oxygen. The empirical formula of carbohydrate is $C_m(H_2O)_n$ where the ratio of hydrogen to oxygen atom is usually 2:1. The simplest carbohydrate is called a monosaccharide, or sugar. Principally the chemical grouping of carbohydrates is based on the number of monosaccharides that combine with each other to form a more complex carbohydrate. Therefore these groups are divided into four groups ranging from the most simple to the most complex form; monosaccharide, disaccharide, oligosaccharide and polysaccharide. Disaccharides are a combination of two monosaccharides, while oligosaccharide consists of two to ten monosaccharides. Polysaccharide consists of a large number of monosaccharide and form more complex structures. In this study only glucose, cellobiose and cellulose which represent monosaccharide, disaccharide and polysaccharide group respectively are used.

2.3.1 Cellulose

Cellulose is the most common organic polymer and considered as an almost inexhaustible resource in nature. Cellulose has an important place in the history of polymers because it was used to make some of the first synthetic polymers. Cellulose is divided into four different polymorphs, which are cellulose I, II, III, and IV. Each of these forms can be identified by their characteristic x-ray diffraction pattern. The characteristics of cellulose I, II, III and IV are described below. Cellulose that is commonly found in nature is called cellulose I. Cellulose I has two different polymorphs; monoclinic phase (Iα) and triclinic phase (Iβ), that can occur in variable proportions depending on the source of the cellulose. Cellulose Iα is commonly found in cellulose that has been produced by primitive organisms (bacteria and algae) whereas Cellulose Iβ comes mainly from cellulose of higher plants (woody tissues, cotton, etc.).

Elemental composition of cellulose was first determined by Payen in 1838. Cellulose contains 44 to 45% carbon, 6 to 6.5% hydrogen, the rest consisting of oxygen and its generic chemical formula is $(C_6H_{10}O_5)_n$. Cellulose is a very strong substance with the straight-chain molecules hydrogen bonding with one another.

Cellulose is derived from *D*-anhydroglucopyranose units (AGU). These units are linked together by $\beta(1\rightarrow4)$ glycosidic bonds between C-1 and C-4 of adjacent glucose. Each AGU unit consists of three hydroxyl (OH) groups at C-2, C-3 and C-6 positions. Each glucose unit is rotated through 180^{o} with respect to its neighbour (*see* Figure 2.7). Thus the structure repeat is a cellobiose unit. The terminal groups at either end of the cellulose molecule are different from each other. The C-1 OH at one chain end has a reducing hemiacetal group while C-4 OH at the other end has an alcoholic hydroxyl (OH-) group and thus is called the non-reducing end [76-78].

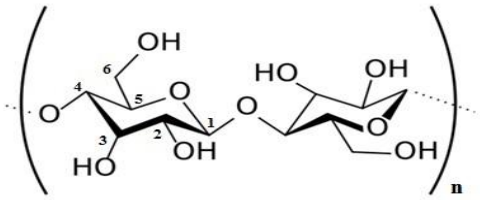

Figure 2.7: Molecular structure of cellulose representing the cellobiose unit as a repeating unit showing reducing (right) and non-reducing (left) end groups. Repeated anhydroglucopyranose units (AGU) are rotated 180^{o} with respect to each other.

The size of cellulose chains depends on the number of repeating units of glucose which is called the degree of polymerization (DP). The value of DP is greatly dependent on the method of isolation. In the case of laboratory-synthesized cellulose, the DP ~ 20 and is more ~10 000 for bacterial cellulose [79].

The presence of three equatorially positioned OH groups in the AGU, one primary and two secondary, determine the chemical character and reactivity of cellulose. Besides, the β-glycosidic linkages of cellulose are susceptible to the hydrolysis process. Cellulose is insoluble in conventional solvents and water due to its hydrogen bonding and partially crystalline structure. Thus, these hydrogen bonds must be broken in order to dissolve cellulose. OH groups in cellulose molecules form hydrogen bonds by intramolecular and intermolecular interactions. Intramolecular hydrogen bonds formed between C2-OH and C6-OH groups and C3-OH with endocyclic oxygen while intermolecular hydrogen bonds interact via their C3-OH and C6-OH groups (*see* Figure 2.8) [80, 81].

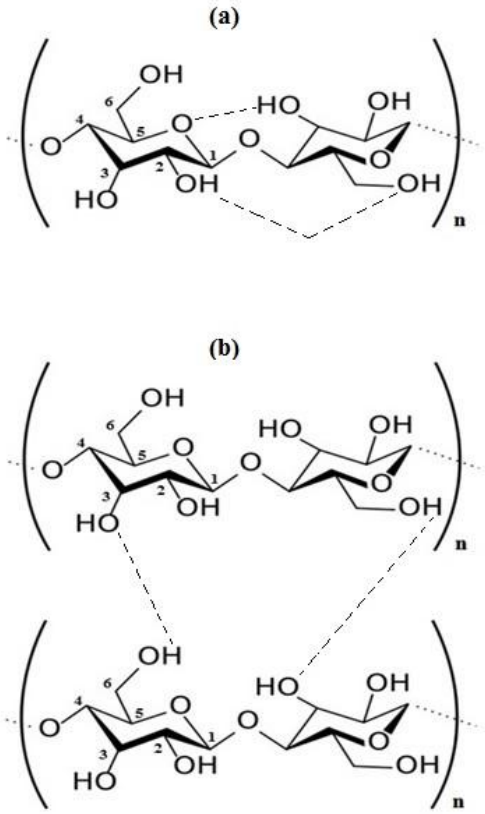

Figure 2.8: Cellulose structures showing a) the intramolecular hydrogen bonding between C2-OH and C6-OH, and C3-OH with endocyclic oxygen and b) the intermolecular hydrogen bonding between C3-OH and C6-OH.

By noting the placement of O6-C6 with respect to the O5-C5 and C4-C5 bonds, the conformation of the hydroxymethyl group in cellulose can be characterized. The conformation is called *gt* if the O6-C6 is *gauche* to O5-C5 and *trans* to C4-C5. Another possibility of hydroxymethyl group conformation is *gg* and *tg*. In cellulose I, the orientation of hydroxymethyl group is in *tg* in which their O6 atom point toward the O2 hydroxyl groups of neighbouring glucose units and subsequently create a second intermolecular hydrogen bond.

Cellulose I can be converted to cellulose II via physical treatment such as regeneration or mercerization. Cellulose II is thermodynamically the most stable form. Mercerization involves a treatment of cellulose I with alkali whereas regeneration involves the dissolution of cellulose I in solvent, then followed by regeneration process. Cellulose II has a monoclinic structure which is based on a two-chain unit cell, arranged in antiparallel. These two chains have different

backbone and glucose conformation. During the conversion process (regeneration or mercerization), the hydroxymethyl group rotates from *tg* to the *gt* conformation. This rotation causes the second intermolecular hydrogen bond to be lost and new inter-sheet hydrogen bonds are established. Cellulose III_I and III_{II} can be obtained through aqueous ammonia treatment of cellulose I or II. The chains in cellulose III are parallel as in cellulose I. However, the conformation of hydroxymethyl groups is oriented in the *gt* conformation and the inter-sheet hydrogen bonds are similar to those in cellulose II.

2.3.2 Cellobiose

Cellobiose is a form of disaccharide which consists of two *D*-Glucopyranoses or sugars linked by $\beta(1\rightarrow4)$ bond. The molecular formula of cellobiose is $C_{12}H_{22}O_{11}$. Cellobiose can be obtained by partial hydrolysis of cellulose. Since cellobiose is a combination of two monosaccharides, it has eight free hydroxyl groups (OH). The bonding between two glucopyranose rings in cellobiose is from the anomeric carbon in ring 1 to the C-4 hydroxyl group on ring 2 where one of the glucopyranose rings is rotated by 180º (*see* Figure 2.9). This linkage gives rise to strong to inter- and intra-molecular hydrogen bonding.

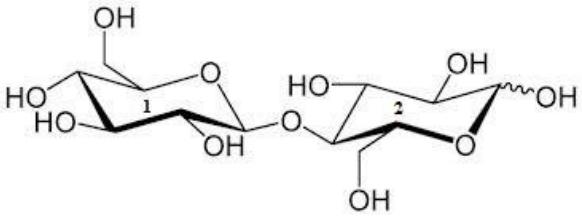

Figure 2.9: Two glucopyranose rings in cellobiose is linked by $\beta(1\rightarrow4)$ bond from the anomeric carbon in ring 1 to the C-4 hydroxyl group on ring 2.

2.3.3 Glucose

Glucose is called a simple monosaccharide since it is made up of only one unit. The molecular formula of glucose is $C_6H_{12}O_6$. Glucose can be thought of as a derivative of hexane, (a 6-carbon chain) with an OH- group attached to every carbon except the endmost one. Therefore, glucose has five free hydroxyl groups. Due to the flexibility of the chain, it can wrap around until the two ends react together to form a ring

structure. The numerous OH groups in glucose makes it highly soluble in water as it can easily form a hydrogen bond with water molecules.

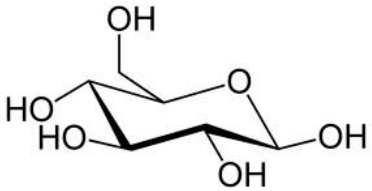

Figure 2.10: The ring form of glucose.

2.4 Influence of water on ILs

ILs and mixtures with water have aroused much interest among scientists in the last few decades. Being composed solely of ions, most of the ILs are miscible in water. However the hydrophilic property of ILs dramatically alters the properties of ILs such as density, viscosity, polarity, conductivity and solubility [43, 82]. In aqueous solution, water molecules interact with the cation and anion of the ILs which result in a change in the nature of IL and its relevant physical properties. In most cases, this limits the application of ILs especially when anhydrous conditions are required. For example, the presence of water in ILs significantly changes their solubility power to dissolve cellulose. Studies have shown that the amount of cellulose that can be dissolved in ILs drops when a small amount of water is present [50]. In addition the presence of water in a mixture may also affect the rates and selectivity of reaction [83]. On the other hand, the hydrophilic property of ILs also offers an advantage in the cellulose regeneration process.

Numerous theoretical and experimental investigations have been carried out to study the interaction of ILs with water molecules [84-86]. For instance, a study by Ding and co-workers using the Density Functional Theory (DFT) and infrared (IR) spectroscopy gave an insight at the molecular level into the interactions between water and EMIMAc. A similar technique has also been employed by Wang and co-workers to investigate the interaction of imidazolium-based ionic liquid with different types of anion with water. It has been suggested that the interaction between water molecules and IL is mainly via hydrogen bond and the anionic part of IL plays a major role in this interaction. The interaction of water molecules with

cations, anions as well as ion pairs is also investigated. It has been proposed that the strengths of interaction in these categories follow the trend anion-water > cation-water > ion pair-water [86]. Hall et al. applied ideal mixing law to study the interactions between water molecules and EMIMAc at macroscopic and microscopic levels. They found that the highest deviation of viscosity, NMR relaxometry, self-diffusion coefficient occurred at water concentration that corresponds to three water molecules per EMIMAc molecule [40].

Studies have shown that the presence of water in ILs reduces their hydrogen bond acceptor (HBA) capacity which was indicated by a decrease of (hydrogen bond basicity, β value. Therefore, it is not surprising that the solubility power of ionic liquid decreases when water is present in the system. This is because net basicity (β-α) value is decreased with the addition of water. Nevertheless, the presence of water alters the net basicity of the ILs in different magnitude [71]. For example, the addition of water up to 16 wt% in EMIMAc did not dramatically decrease the net basicity of EMIMAc to the extent which it is no longer able to dissolve cellulose. However, in the case of *N*,*N*,*N*,*N*-tetramethylguanidium propionate, (TMGHEtCO_2), addition of water, even at 1 wt%, dramatically caused the net basicity of this IL to drop and completely hold down its solubility power to dissolve cellulose [71].

An interesting characteristic of imidazolium-based ILs is that its cation possesses an inherent amphiphilicity and exhibits surfactant character. Therefore in order to understand how ILs participate as components in a mixed solvent system, it is vital to examine the aggregation behaviour of ILs. Some studies of aqueous ionic liquid claim that ILs with long alkyl chain with *n* more than 4 or 6 depending on the type of ILs, formed micelle-like aggregation in high concentration of IL aqueous solution [87]. Aggregation behaviour of ILs in aqueous solution have been investigated using various methods including NMR spectroscopy, small angle neutron scattering, electrospray ionization mass spectroscopy and also by means of surface tension, conductivity and turbidity [87-90]. Bowers at al. investigated the aggregation formation of 1-Butyl-3-Methylimidazolium Tetrafluoroborate ($BMIMBF_4$) in aqueous solution and proposed that above a critical aggregation concentration (CAC) this IL can be modelled as a dispersion of polydisperse spherical aggregates [88]. The study of the microscopic structure of the aggregates

by means of T_1 relaxation suggested that in the aggregated state the imidazolium rings are exposed to water and that the molecular motion of the aggregates is more restricted [87, 91].

2.5 Influence of organic solvents on ILs

It should be pointed out that the viscosity of the cellulose/solvent solution is the main concern of industry in cellulose processing. The viscosity of the cellulose/solvent solutions is not only important during the cellulose dissolution process, but also important in handling of the solutions. At the final stage, mainly during the spinning process of the fibres, the viscosity of the solution also plays a vital role as it determines the spinnability of the spinning fluid which subsequently affects the fibre quality produced. In the case of ILs, the addition of the cellulosic polymer also causes the solution to become more viscous. Nevertheless, the adverse effect of the high viscosity of the solutions can be reduced by adding an organic solvent such as dimethyl sulfoxide (DMSO), *N*,*N* dimethylformamide (DMF), or acetonitrile as a co-solvent, to the solutions. For example, Sui et al. prepared a homogenous cellulose solution by adding DMF as co-solvent as a dilutent to cellulose/AMIMCl solution [92]. In other studies a class of solvent systems for cellulose called organic electrolyte solutions (OESs) which contained a polar aprotic solvent (DMSO, DMF, *N*,*N*-dimethylacetamide, 1,3-Dimethyl-2-Imidazolidinone) and a small fraction of ILs has been successfully developed by Rinaldi. It was found that the polarity of solvent systems increases considerably when IL and co-solvent is mixed. An increased polarity of the solvent system results in improvement of ILs ability to dissolve cellulose more quickly [93]. Tian et al. conducted a similar series of experiments in which they mixed AMIMCl with DMSO to evaluate the pre-treatment effectiveness of dissolution and regeneration of cellulose in an OES for enzymatic hydrolysis [94]. Using only 0.7 mole fraction of AMIMCl, this OES dissolved cellulose rapidly and was able to yield an amount of glucose which was only slightly lower than the value obtained using neat AMIMCl.

Detailed examination of the effects of molar ratio on the aprotic polar solvent to IL and the nature of the co-solvents on cellulose solubility have been studied by Xu et al [70]. The authors proposed that the higher dissolution of cellulose in this

system (IL/co-solvent) mainly results from the preferential solvation of cation by the aprotic polar solvents. It has been speculated that addition of aprotic polar solvents in ILs will result in the solvation of cation, which leaves the anions more free. For that reason, anions in an IL/aprotic polar solvent system can more easily reach the hydroxyl protons of cellulose than those in the neat ionic liquid. More accessibility of anion to disrupt hydrogen bond networks in cellulose offers a great advantage as it can enhance the maximum amount of cellulose dissolved in the ionic liquid.

Though the use of co-solvent is good to reduce the viscosity of the cellulose/IL solution, careful selection of co-solvent is important. As cellulose polymer behaves like a hydrogen bond donor in solution, therefore the co-solvent should have high hydrogen bond basicity, β and preferentially no hydrogen acidity, α in order to avoid any competition with cellulose for hydrogen bond basicity of ILs [93]. Based on the previous findings, it was proposed that the OES pre-treatment offers economic benefits as it can reduce the high cost of ILs as well as less time and energy required for stirring and transporting of the mixture owing to the low viscosity of the OES.

2.5.1 Dimethyl Sulfoxide (DMSO)

DMSO is widely used as a co-solvent because of its effectiveness and its favourable toxicological properties. DMSO $(CH_3)SO$ has been in use as a commercial solvent for decades. As shown in Figure 2.11, DMSO consists of a highly polar S=O group and two hydrophobic methyl groups. DMSO forms a tetrahedral structure with sulphur, oxygen and carbon atoms at the corner which divided DMSO molecules into two regions; polar and non-polar regions. Polar region is the region where sulphur and oxygen atoms bond together. The bonding causes the oxygen atom to become more electronegative and makes DMSO have a high dielectric constant, ε = 46.7 at 293.15 K [95]. DMSO is a considerably high polar solvent with its dipole moment is 3.96 D. Meanwhile, the non-polar region is the two methyl groups that are attached to the sulphur atom. The presence of two methyl groups can contribute to the effect of the hydrophobic association of DMSO molecules.

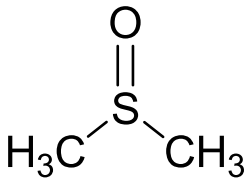

Figure 2.11: Schematic structure of dimethyl sulfoxide (DMSO).

Some physicochemical properties of DMSO suggest that DMSO is highly associated in its neat liquid. High self-association of DMSO molecules observed in neat DMSO were explained as arising from the high polarity of DMSO as well as its geometry. DMSO molecules were associated into polymer chains by dipole attraction. The self-association of DMSO may take place via a few possible bridgings. However, the strongest bridging was via $S \cdots O$ bridging while the other bridging's such as $O \cdots H$ and $S \cdots H$ are improbable because of the very low $C \cdots H$ acidity.

Due to electro negativity of the oxygen atom, DMSO tended to solvate cations rather than anions. DMSO solvates cations through dipole-dipole attraction and it attaches to the cation through the oxygen. This explains why self-association of DMSO disassociated in the presence of proton-donor solvents such as water and methanol. DMSO is fairly basic with its solvent basicity, (SB) is 0.647 [96]. High SB of DMSO resulted from the enhanced electron density at the oxygen atom. This explained why DMSO is considered as a good hydrogen bond acceptor.

Owing to the remarkable importance in chemistry, biotechnology and medicine, examining the role of DMSO as a co-solvent is of high importance. DMSO has been reported as a good organic co-solvent for ILs with polysaccharides [94]. A few experimental and computer simulation studies on the bulk structure, physical properties and dynamics of DMSO have been carried out in previous studies [97-101]. The physical properties of DMSO are summarized in Table 2.4:

Table 2.4: Summary of physical properties of liquid DMSO

Property	Value	References
Density (g/cm^3) at 25 ^oC	1.0958	[100]
Freezing point (^oC)	18.55	[102]
Boiling point (^oC)	189.0	[103]
Shear viscosity (mPa.s) at 25 ^oC	2.010	[100]
Diffusion coefficient (m^2s^{-1}) at 25 ^oC	$1.1x10^{-9}$	[104]
Dielectric constant at 20^oC	46.7	[95]
Dipole moment, (D)	3.96 ± 0.04	[105]
Kamlet-Taft		
Hydrogen bond acidity (α)	0	[101]
Hydrogen bond basicity (β)	0.76	[101]

2.6 Cellulose coagulation

Cellulose can be easily regenerated from the ionic liquid solution by precipitation into water or organic solvent such as ethanol or acetone. A range of structural forms of regenerated cellulose such as powder, tube, fibre and film can be produced. This all depends on their regeneration process. The regeneration process is crucial as it has impact on the microstructure of the regenerated cellulose. Generally, regeneration of cellulose can be accomplished by using the phase inversion technique; immersion precipitation. In this technique, cellulose-ionic liquid solution (polymer solution) is immersed into a precipitation bath that contains non-solvent mentioned above. After immersion, the ionic liquid molecules from the polymer solution diffuse into a precipitation bath while the non-solvent molecules diffuse into polymer solution. The changes in composition as well as the liquid-liquid demixing process are promoted because of mass transfer between bath and solution. The schematic diagram of the immersion precipitation process is presented in Figure 2.12.

It is already established and well known that hydrogen bonding between anion and hydroxyl groups of cellulose is formed during cellulose dissolution. However, during the regeneration process, as soon as the polymer solution is in contact with water, cellulose-anion interaction strength slowly diminishes. Diffusion of water into polymer solution leads to the destruction of the cellulose-anion

hydrogen bond and subsequently formation of cellulose-cellulose and anion-water hydrogen bonds.

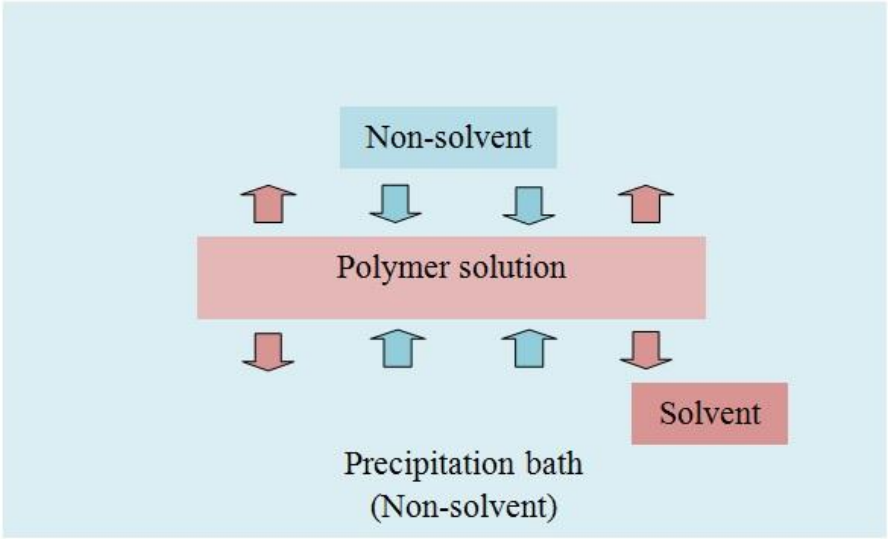

Figure 2.12: Phase inversion technique by immersion recovery.

Numerous studies have been carried out to examine the effect of physical factors such as temperature, concentration and types of coagulation bath on the regeneration process. It has been found that the number of cellulose molecules in contact (aggregated) rises as the temperature is increased which suggests that cellulose regeneration is more rapid at higher temperatures [106]. On the other hand, it has been suggested that the selection of non-solvent as the precipitation bath does not appear to affect the resulting regenerated cellulose. Morphologies of the membranes (regenerated cellulose) obtained may vary depending on the thermodynamic parameters involved as well as on the kinetics of precipitation of the polymer solution.

2.7 Regenerated cellulose

In terms of regenerated cellulose produced, there must be no cellulose decomposition and its properties should be at least as good as with the NMMO and viscose processes. Several studies investigating the structural differences between

the untreated cellulose and regenerated cellulose have been carried out using X-ray diffraction, Fourier transform infrared (FTIR) spectroscopy, thermogravimetric analysis (TGA) and differential scanning calorimetry (DSC). From these studies, it has been demonstrated that cellulose regenerated from ILs were found to be essentially amorphous and more prone to cellulose saccharification [92, 107, 108]. Gupta et al. performed MD simulations to investigate the cellulose regeneration process and found that the torsional angle distributions of hydroxymethyl groups in regenerated cellulose chains are substantially different from those in cellulose crystal and follow the order of *gg* > *gt* > *tg*, which indicated that the regenerated cellulose has an amorphous structure [106].

2.8 Recyclability of ionic liquids

Due to the high cost of ILs, the recyclability of ILs is necessary to make them economic for commercial and industrial use. Recyclability/recovery of ILs is not only an important issue in respect of economics, but also important in the perspective of ecology. To date, however, there have been only a few papers discussing IL recovery [109, 110]. Studies have shown that, there are several possible ways to recover ILs. For example, using the application of supercritical fluids CO_2 ($scCO_2$), Scurto et al. have demonstrated that the separation of IL from IL-saturated aqueous solution was possible [110]. Apart from that, other techniques such as direct vacuum distillation and membrane separation technology were also developed to recover ILs [111]. However, each of these techniques has its disadvantages such as energy consuming and loss of IL during the recovery process. It can be conclusively said that the major drawback of these approaches is that they are not amenable to industrial implementation. Therefore, the major challenge for the researcher is to find better ways to recycle ILs before they are further used in a large-scale industrial application.

Chapter 3
Experimental and Theoretical Background

3.1 NMR Spectroscopy

Nuclear magnetic resonance (NMR) is a versatile spectroscopic technique for elucidating information on chemical compounds such as molecular structure, motion and conformation. It involves reorientation of the nuclear spins with respect to the static external magnetic field which give rise to the so-called NMR phenomena. This process can be explained either by quantum theory or classical mechanical theory, but works best if both are considered.

The introduction of NMR presented in this section has been collated from texts by Levitt [112], Callaghan [113], Hore [114], Keeler [115], and Balci [116].

3.1.1 Quantum Description of NMR

Quantum mechanically subatomic particles (protons, neutrons and electrons) have an intrinsic property called spin. Spin is a form of angular momentum, a vector that is represented by the symbol ***P***. Spin angular momentum, ***P*** is an intrinsic property of the particle itself and it is not produced by a rotation of the particles.

The total spin angular momentum can be quantized as:

$$P = \hbar[I(I+1)]^{1/2} \tag{3.1}$$

where I is the spin quantum number and $\hbar$ is the reduced Planck's constant. Each elementary particle has a particular value for the spin quantum number I. The rules for determining the net spin of a nucleus are as follows; 1) The nucleus has no spin if the number of neutrons and the number of protons are both even. 2) The nucleus has a half-integer spin (i.e. 1/2, 3/2, 5/2) if the number of neutrons plus the number of protons is odd. 3) The nucleus has an integer spin (i.e. 1, 2, 3) if the number of neutrons and the number of protons are both odd.

In this thesis, only the ^{1}H nuclei is considered. In the hydrogen atom (^{1}H), with one unpaired electron, one unpaired proton, and no neutron, the total nuclear spin is 1/2. Nuclei that have spin angular momentum also have magnetic moments, μ given by:

$$\mu = \gamma P \tag{3.2}$$

In the absence of a strong external magnetic field, the nuclear spins of protons are randomly oriented and energy levels are degenerate. However, in the presence of an external magnetic field, the degeneration is broken. The energy levels split into energy levels depending on their magnetic quantum number and are quantized accordingly. The splitting between the nuclear spin levels is called nuclear Zeeman splitting. Since the energy of a dipole in a magnetic field is quantized, therefore it can only have a certain value. This value depends on their magnetic quantum number, *m*. For a proton with spin ½ it has two magnetic quantum numbers, *m* = +1/2 and *m* = -1/2.When a magnetic dipole of any nucleus is placed in a static magnetic field B_o, the potential energy *E* of a dipole is:

$$E = \mu B_o \tag{3.3}$$

where μ is the magnetic moment of the nucleus that has already been calculated in the previous section. Combining Equation 3.2 and Equation 3.3 together, gives the new potential energy expression:

$$E = \gamma \hbar m B_o \tag{3.4}$$

In Equation 3.4, γ, $\hbar$ and B_o are constant, thus the potential energy *E*, depends only on magnetic quantum number, *m*. Figure 3.1 shows the nuclear Zeeman levels of a ^{1}H nucleus as a function of external magnetic field.

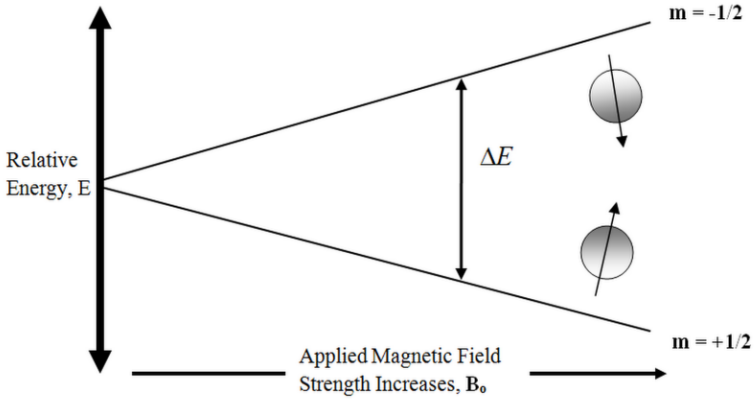

Figure 3.1: Nuclear Zeeman sub-levels of the ^{1}H as a function of external magnetic field. The ^{1}H nucleus with spin ½ splits into two sub-levels according to Equation 3.4 (adapted from [116]**.**

When a sample is placed in a magnetic field, some of the components of magnetic moments will align parallel (lower energy level) with the external magnetic field and some against (higher energy level). Net absorption of energy that is responsible for producing the NMR signal is dependent on the difference in populations of the two levels. The distribution of magnetic moments between energy levels is given by Boltzmann distribution:

$$\frac{N_{upper}}{N_{lower}} = e^{-\Delta E/k_B T} \qquad 3.5$$

where N_{upper} and N_{lower} represent the population of magnetic moments in upper and lower energy states respectively, k_B is the Boltzmann constant and T is the temperature. It should be noted that in NMR spectroscopy the differences of the two energy levels are very small (i.e, 1 in 10^4 - 10^6). The distribution of the magnetic moments gives rises to a bulk magnetization, M_o, of the sample and can be calculated from:

$$M_o \cong \frac{1}{4}\gamma^2\hbar^2 N_o B_o / k_B T \qquad 3.6$$

where N_o is the total number of spins. The strength of the NMR signal depends on the population difference between the spin states.

3.1.2 Classical Description of NMR

The motion of the ensemble of spins is described in terms of the precession of the magnetization vector around a magnetic field B_o with a frequency, υ_o, the Larmor frequency,

$$\upsilon_o = \frac{\gamma}{2\pi} B_o \qquad 3.7$$

where γ is the gyromagnetic ratio (sometimes called the magnetogyric ratio). γ is a physical property of each nucleus. For a given abundance, nuclei with higher values of γ produce larger NMR signal.

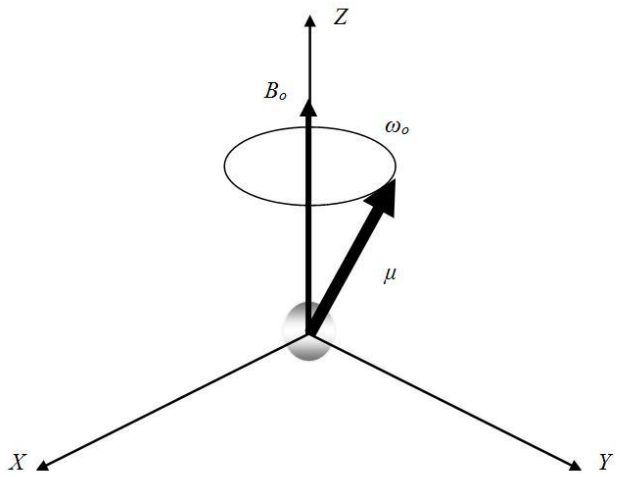

Figure 3.2: The nuclear magnetic moment of a nucleus precessing around B_o with the Larmor frequency ω_o.

When a radio frequency (RF) pulse at the frequency υ_1 is applied along the y-axis and absorbed by the nucleus with spin, the spin will be excited and the angle θ_p will change. The angle through which it is tipped is:

$$\theta_p = \gamma \tau_p B_1 \qquad 3.8$$

In Equation 3.8 the angle θ_p is called the pulse angle, and τ_p is the duration of the radio-frequency pulse. Typically RF pulses are applied to tip the magnetization

either completely into the transverse plane (θ = 90^o) or onto the negative Z-direction (θ = 180^o). At the instance when the pulse is switched off, radio frequency energy will be re-emitted and the spin will over time, return to its equilibrium state. The spins now revert to their equilibrium state (Boltzmann equilibrium) by a relaxation process, with M_z growing back to its original value M_o. As the relaxation processes return the spin system to the equilibrium state, the NMR signal is detected in the *X*-*Y* (transverse) plane, and the signal decays typically exponentially.

The potential energy *E*, of the precessing spins is dependent on the precessing angle, θ_p between the B_o and the spin and is given by:

$$E = -\mu_z B_o = -\mu B_o cos\ \theta \qquad 3.9$$

where μ_z is the z-direction magnetic moment of the spin.

3.1.3 High Field & Low Field NMR

As mentioned in Section 3.1.1, the difference in the thermodynamic equilibrium populations of the spin states, which depends on the strength of the magnetic field, is responsible for producing the NMR signal. Hence, instruments operating with higher magnetic fields give better resolution and sensitivity than those operating with lower magnetic fields. For example, the chemical shift acquired from high field NMR can be used to distinguish molecular species in a substance. With this advantage, high field NMR is used to determine the molecular motion of each molecular species in a substance, such as local segmental rotation and vibration [117]. Being sensitive to very rapid motion, high resolution spectra of solutions obtained from high field NMR might be due to the internal molecular motions (i.e., vibrations and rotations of some internal molecular groups) of the molecules rather than their overall reorientation [112, 118].

For low field NMR, due to the low intensity and low frequency of the magnetic field, the different molecular species cannot be distinguished. Therefore, the low field NMR is widely used to determine the average value of the motion of the whole molecule [118]. The relaxation times obtained from low field NMR result from molecular rotations and molecular translations of the whole molecule. In this study, low field NMR is used to study the relaxation time of EMIMAc and

BMIMCl. The study of the relaxation times using low field NMR is in line with the purpose of this study, which is the connection of microscopic to macroscopic properties.

3.1.4 Chemical Shift

In NMR spectroscopy, all protons do not have a single resonance frequency as described in Equation 3.7. Each proton resonates at a different frequency depending on its chemical environment. The fact that not all protons have a single resonance frequency has led to the study of structural analysis using chemical shift data. The presence of electrons surrounding protons have a significant effect on the resonance frequency experienced by each proton. Electrons under the influence of an external magnetic field generate their own magnetic field (secondary magnetic field, B_{sec}), either increasing or decreasing the influence of the external magnetic field. The magnitude of the secondary magnetic field, B_{sec} is dependent on the strength of the external magnetic field B_o and expressed by:

$$B_{sec} = \sigma B_o \tag{3.10}$$

where σ is the shielding constant. Since the protons are influenced by both external magnetic field and magnetic field induced by the electrons, the effective magnetic field sensed by the protons can be written as follows.

$$B_{eff} = B_o - B_{sec} \tag{3.11}$$

As a result, the resonance frequencies of protons of a given molecule will be different when their chemical environments are different.

Since NMR spectrometers operate at many different magnetic field strengths, the chemical shift will vary from one instrument to another. Thus, in order to quantify the chemical shift, δ independent of the strength of the magnetic field, the measured frequency is expressed in relation to the frequency of a reference substance.

$$\delta/ppm = \frac{v_{sample} - v_{reference}}{v_{spectrometer}} \, x \, 10^6 \tag{3.12}$$

The abbreviation *'ppm'* stands for 'parts per million'. Proton chemical shifts are very important in analytical NMR spectroscopy as they provide a means to distinguish protons in different chemical environments. In the case of proton NMR, the chemical shifts are typically of ~10 ppm.

3.1.5 NMR Relaxation

NMR relaxation is described as the restoration process of the magnetization M_o to its equilibrium state after the Boltzmann distribution of oriented magnetic moment has been disrupted by radio frequency pulses. The two main relaxation processes are longitudinal (T_1) relaxation and transversal (T_2) relaxation. Longitudinal relaxation describes the restoration process of magnetization M_o in the direction of the external magnetic field, B_o. Longitudinal relaxation (T_1) process depends on the exchange of energy between the spin system and the surrounding thermal reservoir, known as the lattice while returning to their lower state of energy. Due to this process, the longitudinal relaxation is also known as spin lattice relaxation. The phenomenological description of this process is given by Equation 3.13 [113].

$$\frac{dM_Z}{dt} = -\frac{(M_Z - M_o)}{T_1} \qquad 3.13$$

Several dynamic processes such as molecular rotation, diffusion or vibration have contributed to the accomplishment of this energy exchange. The processes that lead to the spin lattice relaxation will be discussed further in the next section.

On the other hand, transverse relaxation T_2 describes the phenomenon where the spins lose their phase coherence. This process does not require energy transitions but depends on the local variation of the magnetic field strength that leads to the dispersion of phase coherence of the precessing spins. The greater the magnetic field strength variation, the faster the dispersion of phase coherence of the spins. The phenomenological description for transverse relaxation is given by [113]:

$$\frac{dM_{X,Y}}{dt} = -\frac{M_{X,Y}}{T_2} \qquad 3.14$$

3.1.5.1 Relaxation Mechanism

The mechanism of NMR relaxation is mainly caused by fluctuations of magnetic fields. In an NMR relaxation measurement, right after the RF pulse is switched off, the protons get out of phase due to the fluctuations in the local magnetic field. There are many sources of fluctuation of magnetic field, but in the case of spin ½ nuclei only two tend to be dominant: the dipolar mechanism and the chemical shift anisotropy. For that reason only these mechanism will be discussed in this thesis.

3.1.5.1.1 The Dipolar Mechanism

In liquids, all the molecules are well packed and thus the molecular distances between spin groups are very short. The short distance between spin groups leads to short range dipolar interaction that can contribute significantly to the spin relaxation. This process is called dipole-dipole interaction. Dipole-dipole interaction refers to the interaction between two magnetic dipoles (protons) with one of the dipoles generating the fluctuation field and another one experiencing it. Assuming that there is a molecule containing two protons, as illustrated in Figure 3.3.

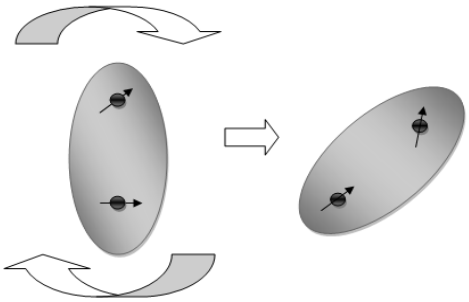

Figure 3.3: Dipole-dipole interaction of two protons.

When these molecules tumble in solution these two dipole-dipole couplings do not change in synchrony. Thus the fluctuation of local magnetic field experienced by each proton is different as the molecules rotate or tumble in a solution. This fluctuation causes the relaxation to occur. However, different fluctuations have different ability to bring about relaxation. Only when the fluctuation has a frequency that matches with transition frequency will the relaxation occur efficiently. Transition frequency is the frequency that protons should have in order to transfer their energy to the lattice efficiently. In this case, T_1 will be short as the transfer of

energy to the lattice is efficient. However, if the molecule tumbles too fast or too slow, the protons experience difficulty in transferring energy to the lattice, then, T_1 will be very long. The motion of the molecule depends on the size of the molecule itself and it is characterized by a correlation time, τ_c. Therefore, the relaxation is efficient when the correlation time, τ_c is about $1/2\pi\upsilon_o$ where υ_o is the frequency of the spectrometer. However, molecular tumbling is not the only motion that causes relaxation as there is rotational motion around local axes that is also involved.

The main parameter that causes the fluctuation of magnetic field due to neighbouring spin is the distance, *r*, between the two spins. The interaction falls of rather quickly to the inverse r^3. The second parameter is the gyromagnetic of the spin itself. According to Equation 3.2, the magnetic moment is proportional to the gyromagnetic ratio. Thus the larger the gyromagnetic ratio, the larger the magnetic moment and the larger the fluctuation of the magnetic field. This explains why protons give rise to the larger magnetic field fluctuation than ^{13}C nuclei. The third parameter is the orientation of the vector joining the two spins relative to the external magnetic field.

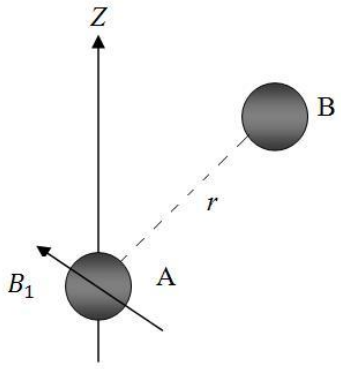

Figure 3.4: Spin A experiences fluctuation of the magnetic field, B_1 due to the magnetic moment of its neighbour, spin B. The magnitude and direction of fluctuation magnetic field depends on the distance *r* between the two spins and the orientation of the vector joining the two spins with respect to the external magnetic field.

3.1.5.1.2 Chemical shift anisotropy

In chemical shift anisotropy, similar to the chemical shift isotropy the fluctuations of magnetic field are caused by molecular electron currents induced by the external magnetic field. As discussed in the previous section, for chemical shift isotropy the nucleus experiences the sum of the external magnetic field and the induced field subsequently shifting the Larmor frequency. This is because in liquid samples, the molecules are tumbling so rapidly that the nuclei see an average fluctuation in the magnetic field. Nevertheless at any instant, for molecules that orientated at certain orientation with respect to the external magnetic field, the fluctuation of the magnetic field experienced by them is different. Hence the size of their chemical shifts is different. This is called chemical shift anisotropy. This fluctuation of magnetic field varies in direction and size as the molecules tumble in liquid. This variation becomes a source of relaxation.

3.1.5.2 Spin Lattice Relaxation

In this section, two experiments for measuring spin lattice relaxation are described; Inversion recovery method and saturation recovery method.

3.1.5.2.1 Measurement of T_1 by Inversion Recovery

A common method to measure T_1 is inversion recovery. In this method, the spins are inverted with 180^o pulse from $+Z$ direction to the $-Z$ direction, followed by a variable waiting period, τ. The magnetization recovers toward the $+Z$ direction during the period of τ. By applying 90^o pulse after τ, the magnetization and signal intensity is recorded. The pulse sequence for the inversion recovery method is shown in Figure 3.5.

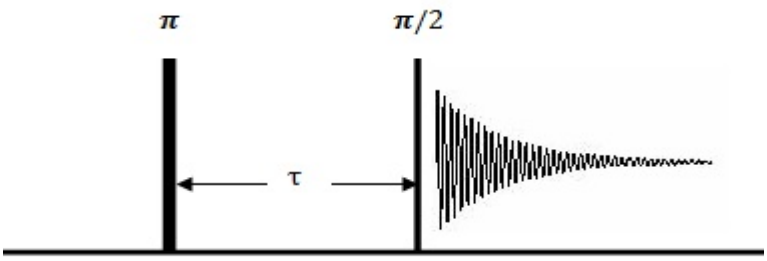

Figure 3.5: The pulse sequence to measure spin-spin lattice relaxation.

The signal intensity yields from the Inversion Recovery sequence can be described by:

$$M_\tau = M_o\left[1 - 2\exp\left(-\frac{\tau}{T_1}\right)\right] \qquad 3.15$$

3.1.5.2.2 Measurement of T_1 by Saturation Recovery

The saturation recovery technique measures T_1 more quickly than inversion recovery. In the saturation recovery method, the magnetization is flipped from the *Z*-direction to the *X*-*Y* plane and allowed to completely dephase during a period τ. Saturation recovery sequences consist of multiple (n) 90^o pulses that are required to ensure no net magnetization exists in any direction and the magnetization is saturated. After a period of τ, the magnetization then recovers, growing along the Z-direction. This magnetization recovery is monitored by flipping it again into the transverse plane by another 90^o pulse. The NMR signal is acquired immediately after this.

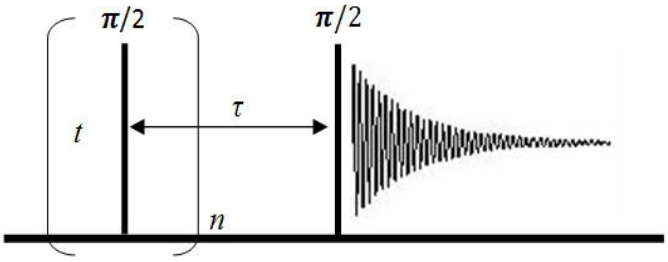

Figure 3.6: Saturation recovery pulse sequence.

The saturation recovery equation is given by:

$$M_\tau = M_o\left[1 - \exp\left(-\frac{\tau}{T_1}\right)\right] \qquad 3.16$$

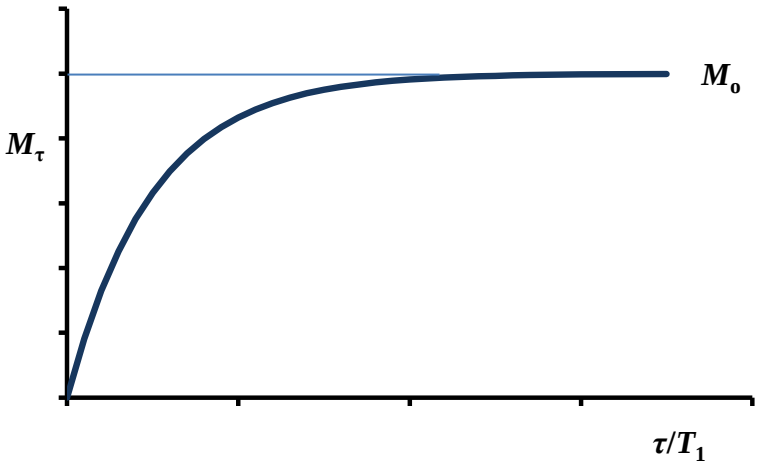

Figure 3.7: Longitudinal magnetization, M_τ as a function of τ/T_1. At $\tau = 0$, M_τ is zero and at $\tau = \infty$, M_τ reach equilibrium where $M_\tau = M_o$.

3.1.5.3 Spin Spin Relaxation T_2

T_2 relaxation corresponds to the decoherence of the transverse nuclear spin magnetization and is called spin-spin or transverse relaxation. T_2 relaxation involves dephasing of precessing nuclear magnetization, rather than exchange of energy between the nuclei and the environment (lattice). Similar to T_1, spin-spin relaxation is longer at high frequency (short τ_c) motions. However, it becomes short when frequency motions or other frequency processes are slow. Thus, T_2 decreases with increasing τ_c. T_2 relaxation is commonly measured using the Hann Spin-Echo sequence. The Hahn echo is constituted first by a 90^o pulse that flips the magnetization in the X-Y plane. After a period of τ, a 180^o pulse is applied and the magnetization is inverted. Following this pulse, another τ delay is applied and the magnetization will start to refocus during this period.

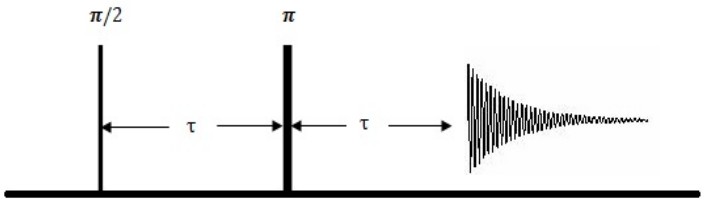

Figure 3.8: The Hahn Spin-Echo sequence.

3.1.5.4 Bloemberg-Purcell-Pound (BPP) Theory

The basis of relaxation such as dipolar, quadrupolar and magnetic coupling and spin rotation, are formed by several physical mechanisms. As mentioned before, for a system containing protons, the most important relaxation mechanism is the dipole-dipole interaction. This interaction depends on a few factors that have been explained in the previous section such as the strength of the dipolar coupling (dependent on γ), orientation or distance between interacting nuclei and the type of motion.

The Bloemberg-Purcell-Pound (BPP) theory has described the relaxation times of simple systems such as bulk water in terms of correlation time, τ_c. In general, the BPP theory has put together three assumptions; 1) Pairwise dipolar interactions; 2) The assignment of single reorientational correlation time, τ_c to the molecular motion responsible for relaxation; 3) Isotropic motions described by a Hamiltonian which have zero average over the motion, as in ideal liquids [119].

The authors explained how the spin lattice relaxation of a single nuclear spin in a liquid was induced by the fluctuations of local magnetic field from neighbouring spins. If the relaxation spin and the spin which induces relaxation are attached to the same molecule the fluctuating field is produced by molecular reorientational motion. The contribution of this mechanism to the overall T_1 is denoted by $(T_1)_{rot}$. Conversely, if the relaxation spin and the spin which induces spin relaxation are attached to a different molecule, the contribution of this mechanism to the overall T_1 is denoted by $(T_1)_{trans}$. Thus for the overall relaxation, one can write

$$\left(\frac{1}{T_1}\right) = \left(\frac{1}{T_1}\right)_{rot} + \left(\frac{1}{T_1}\right)_{trans} \qquad 3.17$$

For the spin lattice relaxation due to a pair of nuclear moments of spin ½ on the same molecule, its general equation is given by:

$$\frac{1}{T_1} = K\{\mathcal{J}(\omega_o) + 4\mathcal{J}(2\omega_o)\} \qquad 3.18$$

$\mathcal{J}(\omega_o)$ is a spectral density function which gives the probability of finding the frequency (energy) ω_o within the thermal motion of the molecule and it can be written as:

$$\mathcal{J}(\omega_o) = \frac{\tau_c}{1 + \omega_o^2 \tau_c^2} \qquad 3.19$$

For spin ½ nuclei, the relaxation constant, *K* is defined as:

$$K = \frac{3}{10}\left(\frac{\mu_o}{4\pi}\right)^2 \gamma^4 \hbar^4 \sum_l \frac{1}{r_l^6} \qquad 3.20$$

Combining Equation 3.19 and Equation 3.20, the spin lattice relaxation rate constant for molecular reorientaional motion therefore becomes:

$$\frac{1}{T_1} = \frac{3}{10}\left(\frac{\mu_o}{4\pi}\right)^2 \gamma^4 \hbar^4 \sum_i \frac{1}{r_i^6}\left[\frac{\tau_c}{1 + \omega_o^2 \tau_c^2} + \frac{4\tau_c}{1 + 4\omega_o^2 \tau_c^2}\right] \qquad 3.21$$

In Equation 3.20, r_i is the inter-proton distance within the molecule while γ, $\hbar$ and ω_o are constants. The total rotational contribution to T_1 is approximately equal to the sum over all spins on the same molecule of the contributions of the individual spin pairs. In the extreme narrowing condition, where $\omega_o \tau_c \ll 1$, Equation 3.21 now becomes:

$$\left(\frac{1}{T_1}\right)_{rot} = 5K\tau_c \qquad 3.22$$

In this condition the relaxation is said to be controlled by molecular rotation. Therefore, the term correlation time, τ_c in Equation 3.22 can be best replaced with rotational correlation time, τ_{rot}. In this case, it is helpful to directly state the rotational correlation time in terms of measurable variable. This can be developed by assuming that the molecule is a sphere and undergoing rotation by Brownian motion. In classical theory, rotational correlation time, τ_{rot} is related to the bulk viscosity by the Stokes-Einstein-Debye, SED relation as [120]:

$$\tau_{rot} = \frac{4\pi R_H^3 \eta}{3k_B T} \qquad 3.23$$

In Equation 3.23, T is the absolute temperature, k_B is the Boltzmann constant and R_H is the hydrodynamic radius often called the Stoke's radius.

In the limit of motional narrowing, when all magnetic nuclei in the liquid have spin ½ and are identical, the BPP equation for $(T_1)_{trans}$ can be written as [113] :

$$\left(\frac{1}{T_1}\right)_{trans} = \left(\frac{\mu_o}{4\pi}\right)^2 \frac{\pi\gamma^4\hbar^2 N_\rho}{4R_H D} \qquad 3.24$$

where N_ρ is the number of spin per unit volume, R_{H} is a radius of molecule and D is the diffusion coefficient of the liquid. If combining the Stokes-Einstein relationship in Equation 3.44, the Equation 3.24 above becomes [121]:

$$\left(\frac{1}{T_1}\right)_{trans} = \left(\frac{\mu_o}{4\pi}\right)^2 \frac{3\pi^2\gamma^4\hbar^2\rho\eta}{2k_B T} \qquad 3.25$$

Molecular motion is not only causing spin relaxation but also T_2 relaxation. Therefore, the BPP theory can also possibly be applied to describe T_2 relaxation. In the case of intramolecular dipole-dipole relaxation, the transverse relaxation rate ($1/T_2$) takes the following value:

$$\frac{1}{T_2} = \frac{K}{2}[3\mathcal{J}(0) + 5\mathcal{J}(\omega_o) + 2\mathcal{J}(2\omega_o)] \qquad 3.26$$

Combining Equation 3.19 and 3.26, T_2 relaxation can be expressed in terms of correlation time, τ_{c} according to the equation below:

$$\frac{1}{T_2} = \frac{3}{10}\left(\frac{\mu_o}{4\pi}\right)^2 \gamma^4\hbar^4 \sum_i \frac{1}{r_i^6}\left[3\tau_c + \frac{5\tau_c}{1+\omega_o^2\tau_c^2} + \frac{2\tau_c}{1+4\omega_o^2\tau_c^2}\right] \qquad 3.27$$

The correlation time, τ_{c} obtained from spin relaxation explains the time it takes by a nucleus to interact with a nucleus of a neighbouring molecule before it diffuses or rotates away by thermal motion of the corresponding molecules. In liquids the correlation time, τ_{c} is about nanoseconds to picoseconds while much longer in solid. The relaxation time constants T_1 and T_2 are compared in Figure 3.9.

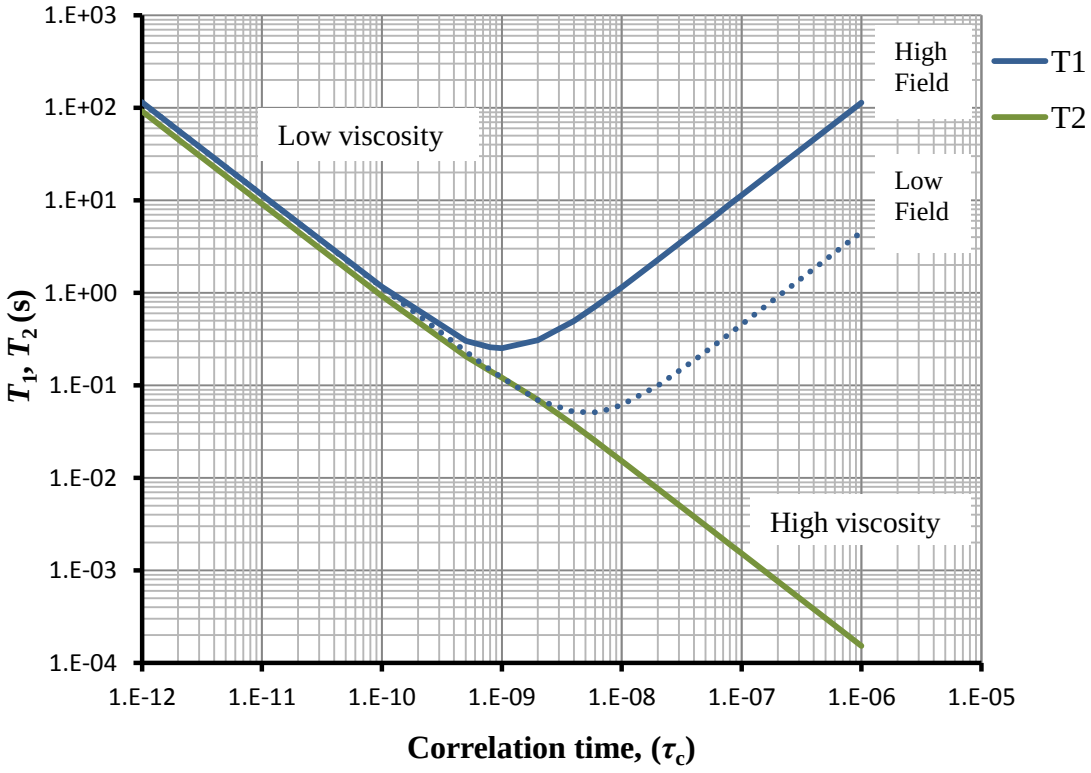

Figure 3.9: Dependence of T_1 and T_2 on rotational correlation time, τ_c with relaxation constant, K, 1.74 x 10^9 s^{-2}. The regions of the graph corresponding to fast and slow tumbling of the molecules.

The values of T_1 and T_2 are equal at very short rotational correlation times. This region is called the extreme narrowing limit. T_1 passes a minimum and then increases as the correlation time is increased. On the other hand, the transverse relaxation time constant T_2 continues to decrease. In practice, it means that the NMR peaks get progressively broader as the molecular size or viscosity increases. Thus, the relaxation time and hence the spectral resolution also depend on the size of the molecule under study, and the viscosity, η, of the solution, which decreases exponentially with increasing temperature.

If there is only a single correlation time, τ_c responsible for relaxation, therefore only a single activation energy will be present. For a thermally activated reorientation, the correlation time, τ_c for ^{1}H NMR also follows an Arrhenius law,

$$\tau_c = \tau_o exp\left(\frac{E_a[\tau_c]}{k_B T}\right) \quad 3.28$$

where the parameters $E_a[\tau_c]$ and τ_o are the activation energy and the pre-exponential factor respectively. τ_o can be equated with classical free rotor reorientation time, τ_{FR} which is given by [120]:

$$\tau_{FR} = \left(\frac{2\pi}{9}\right)\sqrt{\frac{I_m}{k_B T}} \quad 3.29$$

where I_m is the moment of inertia of the molecule [120].

3.1.6 Diffusion

Diffusion is a random translational (or Brownian) motion of particles that is driven by thermodynamic driving force (a chemical potential barrier). It is one of the most important modes of molecular transport. It can be characterized quantitatively by the so-called *self-diffusion coefficient*, *D*. Diffusion is the basic process by which molecules in a substance are dispersed in space. In 1855, Adolf Fick derived two laws to describe diffusion which can be solved for the diffusion coefficient. Fick's first law relates the diffusive flux of the particles (**J**) at position **r** which is directly proportional to the concentration gradient ∇C:

$$\mathbf{J}(\mathbf{r}, t) = -D\nabla c(\mathbf{r}, t) \quad 3.30$$

where *D* is the self-diffusion coefficient ("Diffusion" as described throughout) when the chemical potential gradient is zero (m^2s^{-1}) and *C*(**r**, t) is the solute concentration. When applying the law of conservation of masses:

$$\partial c\,(\mathbf{r}, t)/\partial t = -\nabla.\mathbf{J}(\mathbf{r}, t) \quad 3.31$$

combining Equations 3.30 and 3.31 Fick's second law of diffusion is derived:

$$\partial c\,(\mathbf{r}, t)/\partial t = D\nabla^2.c(\mathbf{r}, t) \quad 3.32$$

D is assumed to be independent of the solute concentration, which is presumed to be low. For analysing NMR diffusion measurement and its derivation, it is important to

introduce the concept of a diffusion propagator, $P(\mathbf{r}_o|\mathbf{r},t)$. $P(\mathbf{r}_o|\mathbf{r},t)$ is the conditional probability of finding a solute molecule initially at position $\mathbf{r}_o$ at a position $\mathbf{r}$ after a time t. Since the propagator $P(\mathbf{r}_o|\mathbf{r},t)$ obeys Equation 3.32, therefore the Equation 3.32 can be written as:

$$\partial P\,(\mathbf{r}_o|\mathbf{r},t)/\partial t = D\nabla^2.P(\mathbf{r}_o|\mathbf{r},t) \qquad 3.33$$

For the case of diffusion in an isotropic and homogenous medium (i.e, boundary condition $P(\mathbf{r_o}|\mathbf{r},t) \rightarrow 0$ as $\mathbf{r} \rightarrow \infty$) the solution of Equation 3.33 yields the dependence of $P(\mathbf{r}_o|\mathbf{r},t)$ on the displacement;

$$P(\mathbf{r}_o|\mathbf{r},t) = 4\pi Dt^{-3/2}\exp[-(\mathbf{r}-\mathbf{r}_o)^2/4Dt] \qquad 3.34$$

Equation 3.34 indicates that the volume occupied by a molecule is a Gaussian distribution that broadens with the increase in the diffusion time t. It should be noted that the distribution function in Equation 3.34 depends on the displacement of the molecules but not on their initial position. Therefore, the mean displacement $\langle(\mathbf{r}-\mathbf{r_o})\rangle$ of a molecule under these conditions in three dimensional by random walk is zero. However, the self diffusion root mean square displacement $\langle(X^2)\rangle^{1/2}$ in such systems is given by Einstein's equation where:

$$\langle(X^2)\rangle^{1/2} = (nDt)^{1/2} \qquad 3.35$$

In this equation n = 2,4 and 6 for one, two and three dimensional respectively. It states that for free isotropic diffusion the mean square displacement increases linearly with the diffusion time t. The self-diffusion is therefore a measure of the rate of mean square displacement of a molecule and consequently has a unit of m^2s^{-1} [122].

3.1.6.1 NMR Methods for Measuring Diffusion

NMR can be used to replace the conventional method of measuring the self-diffusion coefficient. Diffusion rates can be measured by NMR by applying gradient pulses. The basis of this technique is the fact that a magnetic field gradient can be used to label the position of NMR active nuclei through their Larmor frequency. In this technique, the constant magnetic field B_o is superimposed with an

inhomogeneous fields over the short time intervals, δ. Typically the gradients of the magnetic field produced by this gradient can be described by Equation 3.36:

$$\widehat{\boldsymbol{G}} = \frac{\partial B_z}{\partial x}\hat{\boldsymbol{\imath}} + \frac{\partial B_z}{\partial y}\hat{\boldsymbol{\jmath}} + \frac{\partial B_z}{\partial z}\widehat{\boldsymbol{k}} \qquad 3.36$$

where $\hat{\boldsymbol{\imath}}$, $\hat{\boldsymbol{\jmath}}$ and $\widehat{\boldsymbol{k}}$ are the unit vectors in the *x*, *y* and *z* directions respectively. Thus, the total magnetic field produced at position $\hat{\boldsymbol{r}}$ along $\boldsymbol{B_o}$ becomes:

$$B(\hat{\boldsymbol{r}}) = B_o + \widehat{\boldsymbol{G}}.\hat{\boldsymbol{r}} \qquad 3.37$$

With the presence of $\widehat{\boldsymbol{G}}$, thus the Larmor equation is modified in which angular frequency, ω becomes a function of $\hat{\boldsymbol{r}}$,

$$\omega(\hat{\boldsymbol{r}}) = -\gamma B(\hat{\boldsymbol{r}}) \qquad 3.38$$

For a spin located at $\hat{\boldsymbol{r}}$ after the application of magnetic gradient pulse of duration δ, the phase angle, Φ is given by:

$$\Phi(\hat{\boldsymbol{r}}) = -\gamma B(\hat{\boldsymbol{r}})\delta \qquad 3.39$$

This equation shows that the magnetic field gradient can be used to encode the position of spin along the *Z*-direction.

With the NMR method, molecular motion is measured based on the attenuation of the NMR signal resulting from the de-phasing of nuclear spin. In principle, de-phasing of nuclear spin is caused by the combination of translational motion and the imposition of spatially well-defined gradient pulses. The diffusion coefficient is then calculated from the measured attenuated intensity.

The most common approach to measure the diffusion coefficient of molecules in heterogeneous systems such as the ionic liquid system where $T_1 \gg T_2$ is to use the pulsed field gradient stimulated spin-echo (PFGSTE) with the bipolar gradients technique. In this sequence, the net spin is stored in the longitudinal direction by applying a second 90^o pulse. As a result, the presence of any gradient in the longitudinal direction will not affect the net spin.

When performing experiments with this sequence for a heterogeneous system, the experimental time or diffusion time is usually fixed to a constant value and only the applied gradient field is varied. In that manner, the number of existing molecules will be unchanged as they are not affected by relaxation effects. The PFGSTE sequence with bipolar gradient is shown in Figure 3.10 [123].

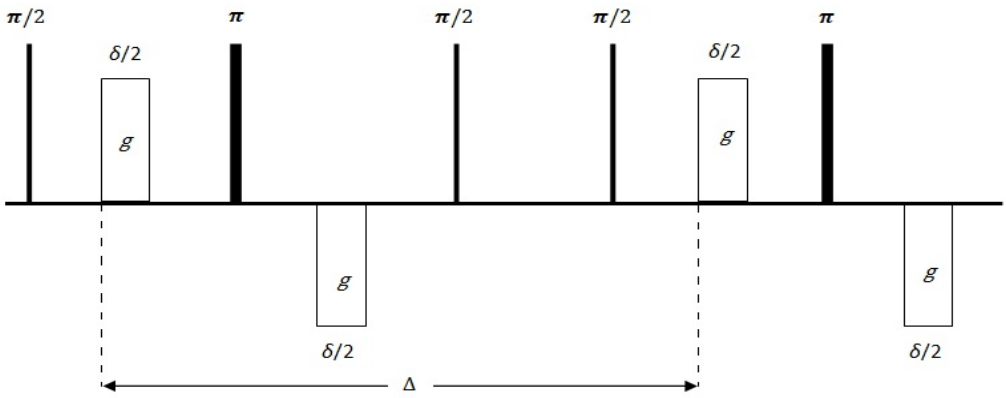

Figure 3.10: The PFGSTE sequence with bipolar gradients.

The signal intensity of this sequence can be described by Equation 3.40:

$$\ln(S_i/S_{i0}) = -D\gamma^2 g^2 \delta^2 (\Delta - \delta/3 - \tau/2) \qquad 3.40$$

where S_i is the observed signal and echo intensity of species i, S_{i0} is defined as the initial signal intensity, γ is the proton gyromagnetic ratio, δ is the pulse duration of a combined pair of bipolar pulses, τ is the period between bipolar gradients, Δ is the period separating the beginning of each pulse pair (i.e. diffusion time) and g is the gradient strength.

3.2 Viscosity

3.2.1 Definition of Viscosity

Viscosity is a fundamental transport property that characterizes the resistance of fluids (gas or liquids) to flow. It is described as the internal friction of moving fluids. The viscosity of a fluid can be depicted by assuming a confined fluid between

two large plates of area *A*, where the top one is moveable and the bottom one is stationary. When a shearing force, *F* is exerted on the upper plate, it causes the fluid between the plates to move in the *x*-direction with a constant velocity, v_o, in which the intermediate layers will flow at different velocities relative to each other. Therefore, a velocity gradient, $\frac{dv_x}{dz}$ also known as shear rate, $\dot{\gamma}$ will start to develop. In this case, the maximum velocity, v_o will be experienced by the layer of fluids that is located near to the top boundary, whereas the velocity of the in-between layers decreases in the z-direction towards the bottom plate.

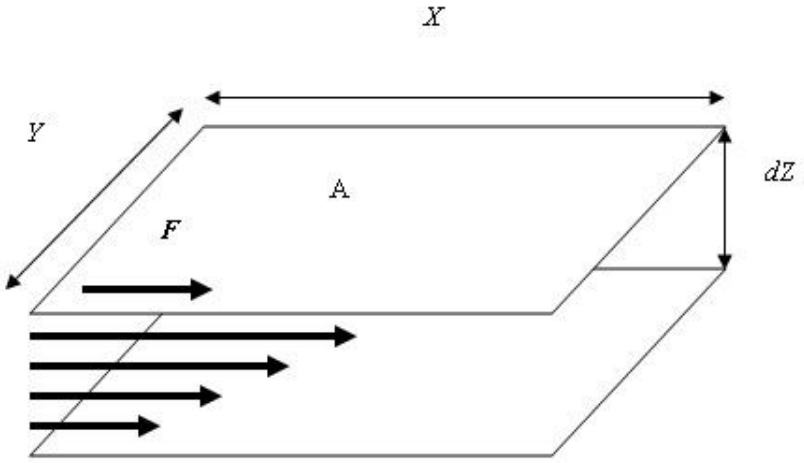

Figure 3.11: Simple sketch defining the coefficient of viscosity based on simple laminar flow.

Shear stress, τ, the tangential force, *F* (in the plane of the laminar) divided by the area, *A* across which the force acts (the area vector is at right angles to the plane of the laminar) is in the direction of the negative velocity gradient and is proportional to the velocity gradient and is expressed by the Newton's law as:

$$\tau_{x,z} = \frac{F_{x,z}}{A} = -\eta \frac{dv_x}{dz} = -\eta\dot{\gamma} \qquad 3.41$$

$\tau_{x,z}$ can be viewed as the viscous rate of flow of x-momentum in the z-direction. Momentum is transferred from a region of high velocity to a region of low velocity. In this case the velocity gradient is the driving force for momentum transfer. From the equation above, η is the proportionality factor called dynamic viscosity. As a $F_{x,z}/A$ has the units of pressure, i.e. Pascal (Pa) while dv_x/dz has the units of s^{-1}, therefore, the viscosity coefficient has the unit of Pas.

3.2.2 Relation between Viscosity and Diffusion

The dynamics in fluids are governed by two closely related properties: viscosity and atomic diffusion. In liquid state research, a quantitative understanding of this relationship is vital and has been one of the long-standing goals. The former describes the molecular transport of momentum by the collective motion of the molecules whereas the latter describes diffusive transport of a single molecule. By studying the molecular diffusion in a solution of viscosity, η an insight into a range of physical molecular properties including molecular size, shape, aggregation, encapsulation and hydrogen bonding can potentially be obtained. This can be related by remembering the classical Einstien relation which says:

$$D = \frac{k_B T}{\xi} \qquad 3.42$$

In Equation 3.42 ξ is the molecular friction constant that is defined as a force needed to pull a single molecule through the solvent with viscosity, η. For a sphere in a continuous medium of viscosity η, ξ can be derived as:

$$\xi = c\pi\eta R_H \qquad 3.43$$

where R_{H} is assumed to be much larger than the solvent molecular radius and may be treated as an adjustable parameter in the case of molecular particles. Combining Equation 3.42 and 3.43, results in the following expression of the Stokes-Einstein (SE) equation.

$$D = \frac{k_B T}{c\pi R_H \eta} \qquad 3.44$$

In Equation 3.44, the constant c depends on the choice of boundary condition. Constant c is said to be 4 in the case of the slip boundary and 6 in the case of the stick boundary. However, it should be noted that different theories described the molecular friction constant with different values depending on the geometries of the molecular species.

A number of studies have been carried out to explore the validity of the SE relationship. Among the aspects considered are: the viscosity, mass, density, size of

solutes and nature of the interactions. Molecular dynamics simulations of pure water by R. Walser *et al.* showed that the product of diffusion and viscosity is dependent on the mass of the simulated water molecules, which deviates from the SE expression that states that the product should be independent of mass. Hence, they concluded that this relation is not always valid for small molecules [124]. Cappelezzo *et al.* have investigated the validity of the SE relationship for pure simple fluids with a broad range of temperatures and densities [125]. According to the authors, at low reduced densities, the value of constant c is smaller than 4 while at intermediate densities, c has a value around 5-6 for a hard sphere fluid, however the slip boundary conditions (c = 4) is fully satisfied in a large range of high densities.

The application of SE relationship is not only limited to single component system but also applicable in miscible blend systems [126]. Previous studies have shown that in aqueous solutions, the relationship between diffusion and viscosity can be best described by the SE relationship. Ribeiro *et al*. studied the aqueous solutions of glucose, sucrose, lactose and fructose over a wide range of temperatures. They found that the variations of hydrodynamic radius with temperature are relatively small (< 3%) [126]. A study by Berner and Kivelson, found that the reciprocal relation between D and η holds reasonably well over nearly five orders of magnitude of η [127]. However, other studies have shown that this relationship breaks down as the system approaches the glass transition [128, 129].

Apart from single component systems and miscible blend systems, the SE relationship is also employed in immiscible systems. For instance, in diluted colloidal systems, due to the large size and mass differences between colloidal particles and solvent molecules, the colloid dynamics can be modelled in term of diffusion in a homogenous solvent [130]. Using the SE relationship, the dynamics of a colloidal system can be estimated if its continuous phase viscosity, particle size and solvent density are changed. However, in concentrated dispersions where there are solvent-mediated many-particles hydrodynamic interactions, this relation is no longer valid. In concentrated dispersions, the influence of hydrodynamic interactions and direct interactions between the colloids reduces the diffusion of the colloidal

particles. The applicability of SE to diffusion of spheres in concentrated colloidal systems is still under active investigation [131-133].

In the previous test of the Stokes-Einstein relation, the hydrodynamic radius, R_H, was related to the molar volume of the liquids by the approximation

$$R_H = \frac{1}{2}\left(\frac{V}{N_A}\right)^{1/3} \qquad 3.45$$

where N_A is the Avogadro number and V the molar volume of the liquid. It has been shown that this empirical relation agrees with most of the experimental data [134].

3.3 Thermodynamics of Mixing

A mixture is formed when two or more components (solids, liquids or gases) are mixed together. The mixing of these components will leads to a change in thermodynamic quantities such as enthalpy, entropy and Gibbs free energy of the system [135].

However the magnitude of change for each thermodynamic quantity depends on the type of reaction. For example, the change in enthalpy is positive in endothermic reactions while negative in heat-releasing exothermic processes [135]. Despite the fact that a decrease in the enthalpy makes a process more favourable (spontaneous) the change in enthalpy alone cannot be used to predict whether an overall change is spontaneous or non-spontaneous. There is another thermodynamic quantity that must be considered and that is entropy. The change in entropy is the changes in disorder that occurs when particles of the solute mix with those of the solvent. However, similarly to the enthalpy, change in entropy alone cannot be used to predict whether the mixing is spontaneous or not. For that reason, another thermodynamic quantity called Gibbs free energy of mixing is then used. Gibbs free energy of mixing combines both enthalpy and entropy terms along with the temperature to predict the direction of a chemical reaction. The Gibbs free energy of mixing is written as:

$$\Delta G = \Delta H - T\Delta S \qquad 3.46$$

where ΔG is the free energy of mixing, ΔH the change in enthalpy, ΔS the change in entropy and T the absolute temperature. The process will be spontaneous if the sign of the Gibbs free energy of mixing is negative and non-spontaneous if the sign is positive.

There are conditions for ΔH and ΔS, which make a process spontaneous, or non-spontaneous [135]. At a constant temperature and pressure, if the change is exothermic and is accompanied by increase in entropy, the process will be spontaneous. On the other hand, the process will be non-spontaneous if the change is endothermic and is accompanied by a lowering of the entropy. The process can also be non-spontaneous if ΔH and ΔS are either both positive or both negative. In a former condition, the absolute value of ΔH must be larger than the value of $T\Delta S$, while in the later condition the absolute value of the $T\Delta S$ must be larger than the value of ΔH [135].

When a hydrophobic substance such as oil is added to water, a phase separation occurs. The immiscibility of the system implies that mixing is non-spontaneous, hence the value of the Gibbs free energy change, ΔG must be positive. It has been reported that ΔH of binary liquid mixtures of nonpolar solutes and aqueous solvents is approximately zero [136, 137]. Therefore, the reason for the immiscibility of oil in water must be entropy and not enthalpy. Based on Equation 3.46, if ΔG is positive and ΔH is zero for dissolving oil in water, then ΔS must be negative [136]. The decrease of entropy upon dissolving oil in water can be explained in term of conformational entropy [136]. In liquid water, the water molecules attain a tetrahedral arrangement by forming two covalent bonds between hydrogen atoms and an oxygen atom, while the hydrogen atoms are bonded to neighbouring oxygen atoms by hydrogen bonding [138]. Introducing solute (hydrophobic) molecules that cannot form hydrogen bonds with water molecules will reduce the number of possible hydrogen bonding configurations surrounding the water molecules [139]. The loss of possible hydrogen bond configurations reduces the conformational entropy of the system. The entropy loss accompanied by the zero enthalpy of the system results in a positive value for the free energy of mixing.

3.4 Ideal Mixing Law

In the processing of materials, fluid flow plays a very important role as most of the processes are based on the use of the fluid and its mixture. The behaviour of a fluid in flow is associated with its main intrinsic property; viscosity. Thus, understanding and predicting how the intrinsic property of pure components changes when they are mixed is vital. Constraints on the availability of time, facilities and expertise often force the experimentalist to use an estimated value despite the fact that it would be ideal to measure the viscosities of the solutions and mixtures at the condition of interest. However, the modelling of mixture viscosities from their pure components is still challenging and requires a deeper understanding of the interaction between components. Various models have been proposed and were reported in the literature. Nevertheless, none of them appeared to be universal.

A general theory of viscosities, diffusion, thermal and ionic conductivity based on the reaction rate theory have been developed by Eyring and co-workers decades ago and are the most powerful and widely used models [140]. With these models, the viscosity of mixtures and even non-ideal mixtures can be predicted with high accuracy. According to this theory, viscous flow can be regarded as an activated process. It assumes that liquid is in dynamic equilibrium where there is continual rearrangement of the structure by the shearing stress where one molecule at a time escapes from the cage to fill an adjoining hole. Since this process is an activated process, thus activation energy, $E_a[\eta]$ is required for molecules to jump from their cage to the adjoining hole [140].

The work by Powell et al. also included the case of liquid mixtures of molecules with different sizes interdiffusing. According to the author, the flow of fluid is not dependent on its properties but rather the availability of a hole to be occupied by a molecule. In order for a molecule to flow or jump over its neighbour, a hole of a certain size must be available into which the given unit of flow can move. Therefore, solvent is said to be responsible for providing this empty hole. We may say that the fluidity is proportional to the number of holes present in a liquid. The indication of the relationship between holes and viscosity has been found in the mechanism of liquid expansion and behaviour of viscosity at the melting point. From this

approach, they derive a mixing law for a mixture viscosity arising from combining two liquids.

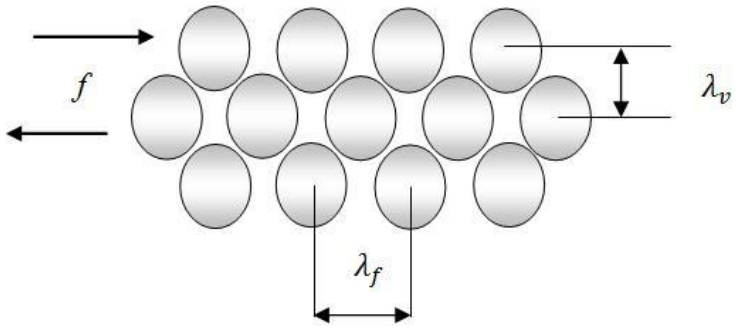

Figure 3.12: Eyring model illustrating fluid flow.

In a mixture of two liquids, originally the viscosity activation energy, $E_a[\eta]$ for this mixture is expressed by:

$$E_a[\eta] = x_1 E_a[\eta_1] + x_2 E_a[\eta_2] + 2RT\ln\frac{V_A}{V_G} \qquad 3.47$$

However, the last term has been described as an excess free energy of mixing. Thus for the liquid mixture system with zero excess free energy of mixing, the activation energy in above relation will vary linearly with mole fraction. This is also shown by Vignes and Cullinan that for non-associated liquid systems, the activation energy for diffusion varies linearly with mole fraction between the infinitely dilute extremes [141, 142].

Since the fluid flow is an activated process, thus the fluid flow also varies in a similar linear manner. For molecules of approximately equal size, a mixing rule based on mole fractions was derived.

$$\ln\eta = x_1 \ln\eta_1 + x_2 \ln\eta_2 \qquad 3.48$$

where η is the mixture viscosity, η_i is the viscosity of species *i* and x_x is the mole fraction of species *i*.

For the diffusion of a Brownian particle of radius $R_{H,}$ in a solvent medium of viscosity η, the Stokes-Einstein expression given in Equation 3.44 relates the

transport properties. Since the processes of viscous flow and diffusion are similar and the viscosity and diffusion coefficient are interrelated, thus a similar relation can also be used to express the binary diffusion coefficient.

$$\ln\left(\frac{1}{D_i}\right) = x_1 \ln\frac{1}{D_{i,1}} + x_2 \ln\frac{1}{D_{i,2}} \qquad 3.49$$

where D_i is the self diffusion coefficient for species i in the mixture, and $D_{i,j}$ is the self diffusion coefficient of i in liquid j.

A similar concept of the ideal mixing rule is now applied for NMR relaxometry measurement T_1 and T_2. As shown in Figure 3.9, in the extreme narrowing condition, the curves of T_1 and T_2 are overlapped. As mentioned before, in this region both relaxations, T_1 and T_2 are predominantly caused by molecular rotation.

$$\frac{1}{T_1} = \frac{1}{T_2} = 5K\tau_{rot}$$

If we rewrite Equation 3.23 where:

$$\tau_{rot} = \frac{4\pi R_H^3 \eta}{3kT}$$

it means that the relaxation times depend on the size of the molecule under study and viscosity of the solution. Combining Equations 3.22 and 3.23, the relationship between relaxometry data and viscosity can be explained by:

$$\frac{1}{T_1} = \left(\frac{20\pi}{3} K R_H^3\right)\frac{\eta}{kT} \qquad 3.50$$

If the logarithm of the viscosity follows an ideal mixing law then so will the logarithm of the inverse NMR relaxation times. Therefore, the binary relaxation time can be written as:

$$\ln\left(\frac{1}{T_1}\right) = x_1 \ln\frac{1}{T_{1,1}} + x_1 \ln\frac{1}{T_{1,2}} \qquad 3.51$$

where $T_{1,i}$ is the relaxation time of the neat components. Similar to the case of viscosity and diffusion, any positive or negative deviations from ideal mixing law

will have the same sense as those of deviations from viscosity and diffusion ideal mixing rules.

Chapter 4
Macroscopic and Microscopic Study of 1-Ethyl-3-Methyl-Imidazolium Acetate - Dimethyl Sulfoxide (DMSO) Mixtures

4.1 Introduction

The properties of ILs such as viscosity, polarity and conductivity change if they are employed together with other co-solvents such as water, ethanol, methanol, acetonitrile and dimethyl sulfoxide (DMSO). ILs and their mixtures have aroused much interest among researchers in recent years [40, 60, 143-149]. The mixture of IL/co-solvent displays interesting intermediate behaviour not seen in neat ILs and departs from ideal behaviour. Both the theoretical and experimental approaches have been considered extensively for studying the mixture of ILs with co-solvent in order to understand the nature and extent of various intermolecular interactions existing between different species present in the mixtures as well as structural changes induced by co-solvent [148] [143, 150].

Among the co-solvents mentioned above, the aprotic solvent DMSO has become a more desirable co-solvent due to its excellent solubility in both inorganic and organic compounds. DMSO is well known as a solvent that plays an important role in the area of industrial medicine, biology and chemistry. DMSO has been used extensively in industry for biomass processing. In cellulose processing particularly, DMSO has been found to reduce the viscosity of the cellulose-IL solutions which gives an advantage to the cellulose processing. However, information on the properties of IL-DMSO mixtures is still limited. Despite a knowledge of physical properties such as vapour pressure, surface tension, viscosity and enthalpy of mixing, complementary information such as spectroscopic (IR and NMR) data for the two mixing components is also necessary to appropriately characterize IL-DMSO mixtures [151].

The behaviour of IL-DMSO mixtures has been studied recently using molecular dynamic simulation. This study has allowed the transport properties of the mixtures to be elucidated [150]. From this transport diffusivities study, it was found that dissociation into ions in ILs is less likely to occur in IL-DMSO mixtures. Other

than that, infrared spectroscopy and theoretical investigation have been carried out to elucidate the formation of hydrogen bonding between DMSO and pyridinium-based IL, 1-Butylpyridinium Tetrafluoroborate ($BupyBF_4$). From this study it was found that DMSO forms a hydrogen bond with $BuPy^+$ cation through $S = O$ group. Therefore, obtaining information on the interactions between the co-solvent (DMSO) molecule and ILs is important to improve the properties and performance of ILs, especially in the industry and biomass processing.

Taking into account the published data concerning the structure of IL EMIMAc [35], and DMSO [97, 152, 153] and previous studies on mixtures of EMIMAc with water [40], it seemed appropriate to extend these studies to the IL-DMSO binary mixtures. In this work, we combined both physical properties such as density, viscosity, diffusivity and relaxation time and spectroscopic studies to gain a better understanding of EMIMAc-DMSO mixtures behaviour. The changes of these parameters must be the result of the molecular interactions in their bulk; consequently they could be of assistance in interpreting their macroscopic and microscopic properties. This study will provide results in to help interpret this binary mixture at both macroscopic and microscopic levels.

4.2 Experimental Methods

4.2.1 Materials and Sample Preparation

The EMIMAc (97%) and DMSO (99.9%) were purchased from Sigma Aldrich and were used without further purification. In this work pure EMIMAc and DMSO and a series of EMIMAc-DMSO (0.5, 3, 10, 20, 40, 50, 60, 70, 80, 85 and 90 wt%) binary mixtures were prepared by weight fraction. All the sample preparations were made in an MBraun Labmaster 130 atmospheric chamber under nitrogen. Both EMIMAc and DMSO were mixed and stirred in a small container. After 2 hours, the mixtures were transferred into 5 mm NMR tubes. Since both EMIMAc and DMSO are hygroscopic, all containers and NMR tubes used in sample preparation were dried in the oven at 50 ^oC prior to use to make sure they were free from atmospheric moisture. Once the correct amount of solution had been transferred into the sample tubes, all tubes were subsequently sealed within the chamber.

4.2.1.1 Density

The density of pure EMIMAc and DMSO and a series of seven EMIMAc-DMSO (20%, 40%, 50%, 60%, 70%, 80% and 85%) binary mixtures were measured using a capillary pycnometer. The pycnometer was first calibrated with distilled water prior to the measurement. All the measurements were carried out at room temperature (25 ^{o}C).

4.2.1.2 Viscosity

The viscosity data presented in this section was collected in collaboration with Prof. Tatiana Budtova from the Centre de Mise en Forme des Materiaux, Sophia Antipolis, France.

The Bohlin Gemini Advanced Rheometer equipped with a 4^{o}-40 mm cone plate was used to measure the viscosity of pure EMIMAc and DMSO and a series of five EMIMAc-DMSO (20, 40, 50, 60, 80 wt%) binary mixtures. Shear rate dependent viscosity was measured at temperatures ranging from 20-100 ^{o}C in 10 ^{o}C increments. A thin film of low viscosity silicon oil was placed around the borders of the measuring cell in order to prevent moisture uptake and evaporation at higher temperatures.

4.2.1.3 NMR Relaxometry

^{1}H NMR relaxation time for all samples was measured using a low-field spectrometer operating at 20 MHz. The ^{1}H-T_1 and ^{1}H-T_2 values of EMIMAc-DMSO solution were obtained as a function of temperature in the range 10 ^{o}C to 80 ^{o}C. The measurement of T_1 and T_2 was performed using inversion recovery and Carr-Purcell-Meiboom-Gill pulse sequences respectively. The radio frequency pulse strength of this instrument is 3.7 μs for a 90^{o} pulse width.

4.2.1.4 NMR Diffusion

Diffusion experiments were carried out on a Bruker AV 400 spectrometer operating at 400MHz using a Diff60 probe (Bruker Biospin) for ^{1}H NMR with variable temperature control (accurate to ± 0.1 ^{o}C). At each temperature the RF coil was tuned, the static magnetic field shimmed and pulse lengths measured. Following this, an FID was acquired, and the spectrum was examined. Calibration was performed by measuring the self-diffusion coefficient of pure water at each

temperature prior to the experimental measurements. The reference value of the temperature dependence of the diffusion coefficient of water is referred to the results published by Holz et al. [98]. Experiments for all samples were performed at temperatures ranging from 20 to 60 ^{o}C in 10 ^{o}C increments. Diffusion coefficients for ions in EMIMAc-DMSO mixtures were obtained using the ^{1}H-detected PFG-STE bipolar sequence that has been explained in Chapter 3.

4.3 Results

4.3.1 Density and Excess Molar Volume

The density measurement for EMIMAc-DMSO binary mixtures was carried out for the total concentration at room temperature, 25 ^{o}C. Figure 4.1 shows the density of EMIMAc-DMSO mixtures as a function of DMSO mole fraction. Both pure EMIMAc and DMSO are in good agreement with the reliable published data (*see* Table 4.1). A list of density for both pure liquids obtained from experiment and reference value are summarized in Table 4.1.

Table 4.1: Density of EMIMAc and DMSO obtained from experiment and compared with reference values at 25 ^{o}C.

Ionic Liquid	**Density (g/cm^{3}) at 25 ^{o}C**		
	Experiment	**Literature review**	**References**
EMIMAc	1.1071 ± 0.0028	1.09778	[60]
		1.102	[154]
		1.0993	[155]
DMSO	1.0981 ± 0.0030	1.095295	[156]
		1.099	[153]
		1.0972	[157]

The changes of density from pure EMIMAc to pure DMSO is less than 1%. It was found that the deviation of density from mixing rule which is indicated by a solid line is within an experimental error. This linear behaviour follows additive law:

$$\rho_{calc} = \sum_{i}^{2} x_i \rho_i \qquad 4.1$$

where ρ_{calc} is calculated mixture density, x_i is a molar fraction of each component and ρ_i is the density of the neat components. Ideal behaviour of density for this system indicated that there was neither contraction nor expansion occurring in the mixing of the solutions.

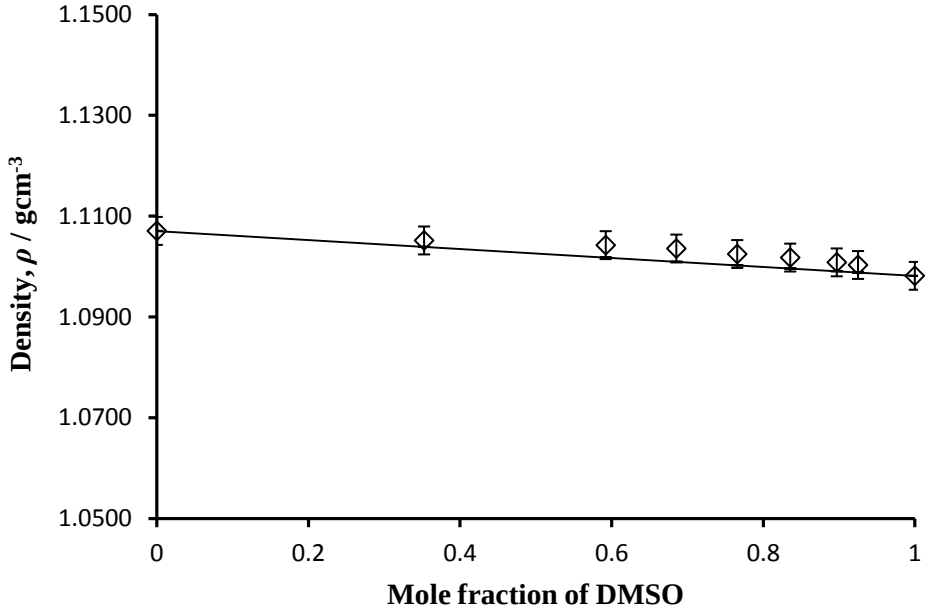

Figure 4.1: Density of EMIMAc-DMSO mixtures as a function of mole fraction of DMSO measured at 25 ^{o}C. The straight line is the ideal mixing law given by Equation 4.1.

Knowing the densities and compositions of the mixtures, it is possible to calculate excess molar volume V_m^E for each solution using, [158]:

$$V_m^E = \left(\frac{x_1 M_1 + x_2 M_2}{\rho}\right) - (x_1 V_1 + x_2 V_2) \qquad 4.2$$

where x_1 and x_2 are mole fractions, M_1 and M_2 are molar masses and V_1 and V_2 are molar volumes of EMIMAc and DMSO respectively. The sign of excess volume of

a system can be either positive or negative depending on the magnitude of density changes which correspond to the expansion or contraction of the solutions.

In general there are several factors that can explain the variation of the observed values of excess molar volumes of the system under investigation. It can be divided into physical, chemical and geometrical contributions. Positive V_m^E value could be due to loss of dipolar association of components. Meanwhile negative V_m^E could be caused by the presence of specific intermolecular interaction between unlike molecules such as hydrogen bond and dipole-dipole interaction. In this study the dependence of excess molar volume on DMSO molar fraction is shown in Figure 4.2.

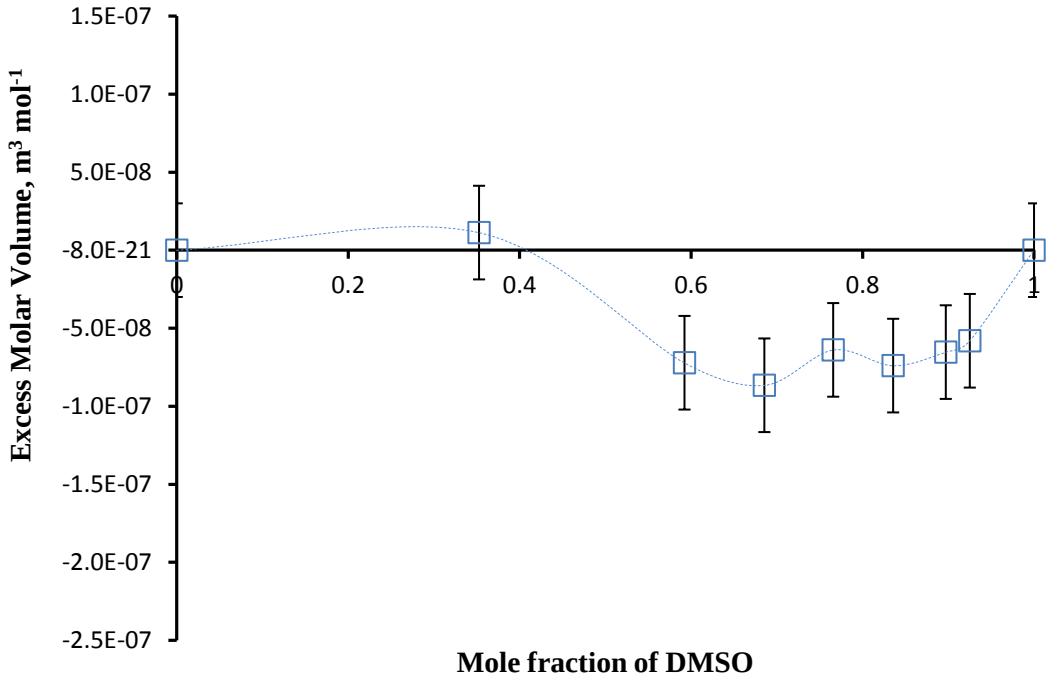

Figure 4.2: Excess molar volume as a function of molar fraction of DMSO measured at 25 ^{o}C.

It was found that the value of excess molar volume obtained in this work is extremely small (2 – 8 x 10^{-8} m^3mol^{-1}), typical values for other IL binary blends are usually ~ 10^{-6} – 10^{-7} m^3mol^{-1} [159, 160]. The extremely small value of excess molar volume showed that this system was very close to ideal mixing behaviour. This indicates that no specific interaction between DMSO and EMIMAc ions.

In the case of EMIMAc-DMSO mixtures the small excess molar volume again revealed that no attractive interaction occurred when EMIMAc and DMSO were mixed. The formation of any hydrogen bonds between DMSO and EMIMAc, if they occur, must be compensated by the breaking of bonds between the $EMIM^+$ and Ac^- ions. Thus no net volume expansion or contraction takes place. In addition as mentioned before, the variation of excess molar volume is also contributed to by the geometrical contribution; the presence of different sized and shaped component molecules in the system. In this case, the size of $EMIM^+$, Ac^- and DMSO are similar with their molecular radii calculated as 2.74 Å, 2.24 Å and 2.45 Å respectively. (These radii are calculated using Equation 3.45 explained in Chapter 3). A small excess molar volume ($2 – 8 \times 10^{-8}$ m^3mol^{-1}) exhibited by this mixture agrees with the findings of a previous study for [BMIM][PF_6]/DMSO mixtures with its excess molar volume *ca.* ($1 – 2 \times 10^{-7}$ m^3mol^{-1}) and found no minimum for excess molar volume. The authors suggested that similarity of polarity between the two solvents led them to behave like an ideal solution [156].

The correlation between the magnitude of excess molar volume and dielectric constant has also been observed for a number of binary solvent systems, V_m^E being larger as the dielectric constant of co-solvent is larger. This is clearly seen when comparing the excess molar volume of this system with the EMIMAc-water system [40]. Since the dielectric constant of water was larger than DMSO, the value of V_m^E was found to be larger in EMIMAc-water mixtures compared to EMIMAc-DMSO mixtures.

4.3.2 NMR Chemical Shift

The changes of proton chemical shift for each spectral band in EMIMAc and DMSO have been examined to investigate the microscopic structure of EMIMAc and DMSO mixtures. In Scheme 1, the proton numbering (H2-H9) for EMIMAc that represents a spectral band in the spectrum is described. To simplify the analysis of chemical shift changes ($\Delta\delta$), H6 is then defined to have a fixed chemical shift. The choice of H6 as a reference point follows previous studies in which this spectral band was found not to be dependent on temperature and concentration of solute [49, 87].

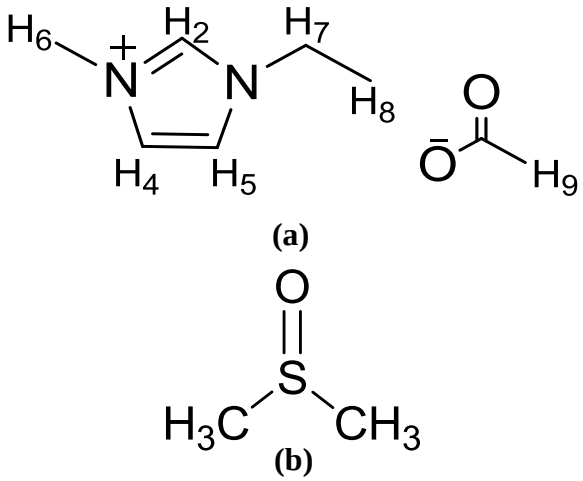

Scheme 1: Schematic representation of the a) EMIMAc and b) DMSO used in this study.

In Figure 4.3, $\Delta\delta$ of individual hydrogen atoms in EMIMAc-DMSO mixtures as a function of DMSO concentration at 20 ^{o}C is displayed. The positive and negative value of $\Delta\delta$ in the figure indicates the downfield and upfield movement of protons respectively. The $\Delta\delta$ relative to 0.5 wt% of DMSO is considerably small for all protons (< 0.5 ppm) where the magnitude of the $\Delta\delta$ being three times smaller than that observed in the EMIMAc-watersystem. For example, $\Delta\delta$ for H2 is about -0.3 ppm in an EMIMAc-DMSO system but showed changes in the EMIMAc-water system with the maximum $\Delta\delta$ was about -1.5 ppm [40]. The relatively small $\Delta\delta$ observed in the EMIMAc-DMSO system implies that weak interactions occurred between EMIMAc and DMSO molecules.

The magnitude and nature of the shifts reflects changes of their environment. Compared with other protons in $EMIM^{+}$, imidazolium protons H2, H4 and H5 show larger variation in its $\Delta\delta$ owing to the fact that they are the most acidic protons and most affected by any environmental changes. Many studies have reported that these three protons are the preferred interaction sites of the imidazolium cation relative to the solute as compared to its alkyl protons [161, 162]. Thus, addition of DMSO does not really affect the chemical environment of protons in the alkyl chain much. This explains the smaller variation of $\Delta\delta$ experienced by these protons. However, it is suggested that the relatively larger variation of $\Delta\delta$ in the tail proton, H8 can be explained by the solvation of the cluster in pure EMIMAc upon addition of the

solvent. The solvation of a cluster of pure IL upon addition of a co-solvent results in the exposure of the tail to a new chemical environment.

It is worth noting that while the $\Delta\delta$ of other spectral bands showed a common trend in chemical shift changes either completely downfield or upfield movement over the whole DMSO concentration studied, the $\Delta\delta$ of the most informative proton H2 deviates from this common trend. H2 moved downfield to a 60% mass fraction of DMSO before it dramatically moved upfield with a further increase of DMSO. This anomalous trend of $\Delta\delta$ of H2 has been observed previously by Remsing et al. in their study of BMIMCl-DMSO mixtures [163].

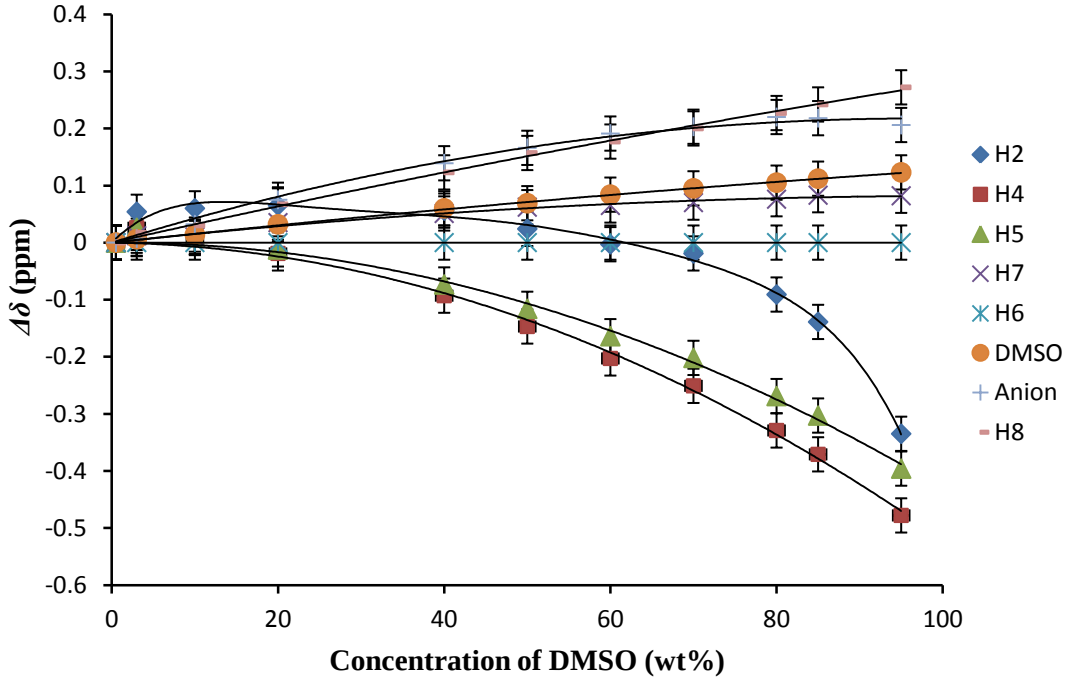

Figure 4.3: The variation in chemical shift changes ($\Delta\delta$) of protons in EMIMAc-DMSO mixtures with increasing DMSO concentration at 20 ^{o}C. The solid lines are guides to the eye.

There are two possibilities for a downfield movement of H2; it is either the DMSO molecules interact with H2 and forms stronger hydrogen bond as anion does, or the cation and anion form stronger hydrogen bonds upon the addition of DMSO. However, taking into consideration that DMSO is not a good hydrogen bond acceptor relative to the anion, Ac^-, then the former assumption is probably wrong.

Thus in this case we believe that the latter is the main reason for the downfield movement of H2. This is in agreement with recent simulation results that showed the peak of radial distribution function of anion-cation became higher with the addition of DMSO which then suggested that the interaction between cations and anions is strengthened in the presence of DMSO [163]. The upfield movement of ring protons can be attributed to the breaking of the hydrogen bond in EMIMAc molecules that leaves these three protons more shielded. Since DMSO is not a good hydrogen bond acceptor as Ac^-, the upfield movement of ring protons also suggests that EMIMAc has been dissolved in DMSO in a form of ion pair rather than isolated ions. All alkyl protons show the downfield movement indicated that there are interactions occurring between them and DMSO. Compared to the H2, protons of anions show a smaller magnitude of $\Delta\delta$ that suggest the direct interaction between $C-H\,(DMSO)\cdots Ac^-$ is far weaker than interaction between $S=O\cdots C-H2$. This weaker interaction arises from the very low $C\cdots H$ acidity possessed by methyl groups of DMSO that cause Ac^- to be less likely to interact with them. Weak interaction between polar aprotic solvent with anion in ionic liquid had been observed in Dimethylimidazolium Chloride (DMIM) and dimethyl ether (DME) mixtures studied by Hanke and co-workers. They found that interaction of DME with the imidazolium cation is more important than anion [85]. Complementary information from radial distribution functions and three-dimensional probability functions of their study showed that there was no such DME around the anion and the nearest site is on a cation.

Since the assigned spectral band for DMSO in the spectrum belongs to methyl groups, it is worth noting that the magnitude of $\Delta\delta$ is also small. Due to its low $C\cdots H$ acidity, it is less likely that methyl groups can form a hydrogen bond with the anion. Thus it is suggested that the changes in the chemical shift probably contributed from the indirect effect from $S=O\cdots C-H2$ interactions. As suggested by Zhang et al., upon the formation of hydrogen bond between $S=O$ and imidazoilum cation, DMSO methyl groups donate their negative charge to $S=O$. Therefore this phenomenon could possibly gives rise to the changes of $\Delta\delta$ of DMSO methyl groups [143]. From their study, they also did not observe any evidence that showed any direct interaction between the DMSO methyl group and the anion taking place in the system.

4.3.3 Viscosity

The viscosity η for EMIMAc-DMSO mixture as a function of DMSO concentration for temperatures ranging from 20 ^{o}C to 100 ^{o}C was studied. Figure 4.4 shows the variation of the viscosity of the EMIMAc-DMSO mixture throughout the mole fraction range at 20 ^{o}C, 40 ^{o}C and 50 ^{o}C. According to the ideal mixing rule discussed in Section 3.4, the viscosity of the binary mixture can be writen as:

$$\ln \eta = x_1 \ln \eta_1 + x_2 \ln \eta_2 \qquad 4.3$$

where η, is the viscosity of the mixture; x_i is the mole fraction of component *i* of the mixture and η_i is the viscosity of the pure component *i* of the mixture; subscript *i* = 1 is for EMIMAc and *i* = 2 is for DMSO. It is known that the addition of a low viscosity co-solvent to an ionic liquid results in a significant decrease of its viscosity. In this system, the natural logarithm of viscosities of all mixtures decreases approximately linear with a mole fraction of DMSO. The decreasing of viscosity with the addition of DMSO arises from the intermolecular attractions between the EMIMAc molecules being screened by the DMSO [164]. Generally, pure ILs are characterized by the presence of clusters/nanosegregation [35]. Here the presence of DMSO has disrupted these clusters [165, 166] subsequently making the resultant blend easier to shear. In this study, the viscosity deviations are positive over the whole composition range (*see* Figure 4.4). However, the deviations from the ideal mixing behaviour are very weak and almost behave like an ideal solution. This result corroborates the earlier result from density and excess molar volume, which suggested that there was no strong specific interaction occurring in this system. The viscosity drop in a liquid mixture is not only associated with the amount of free volume in the system, but it is also related to the strength of the molecular interactions between the components in the system. In this study, the former has been quantified by the volumetric properties; excess molar volume of the mixture as discussed above.

The correlation between viscosity deviation and excess molar volume have been observed for a number of binary mixture systems [167]. Viscosity deviation is positive when the excess molar volume is negative and vice-versa. In EMIMAc-DMSO mixtures, a small positive deviation of viscosity from ideal mixing behaviour

is consistent with the extremely small negative value of excess molar volume. It is known that the polarity of both EMIMAc and DMSO are very close [66]. As a result, DMSO will less likely contribute to the dissociation of IL into their ionic components. Therefore, there will be an increase in hydrophobic interactions between the alkyl chain of EMIMAc and the methyl groups of DMSO.

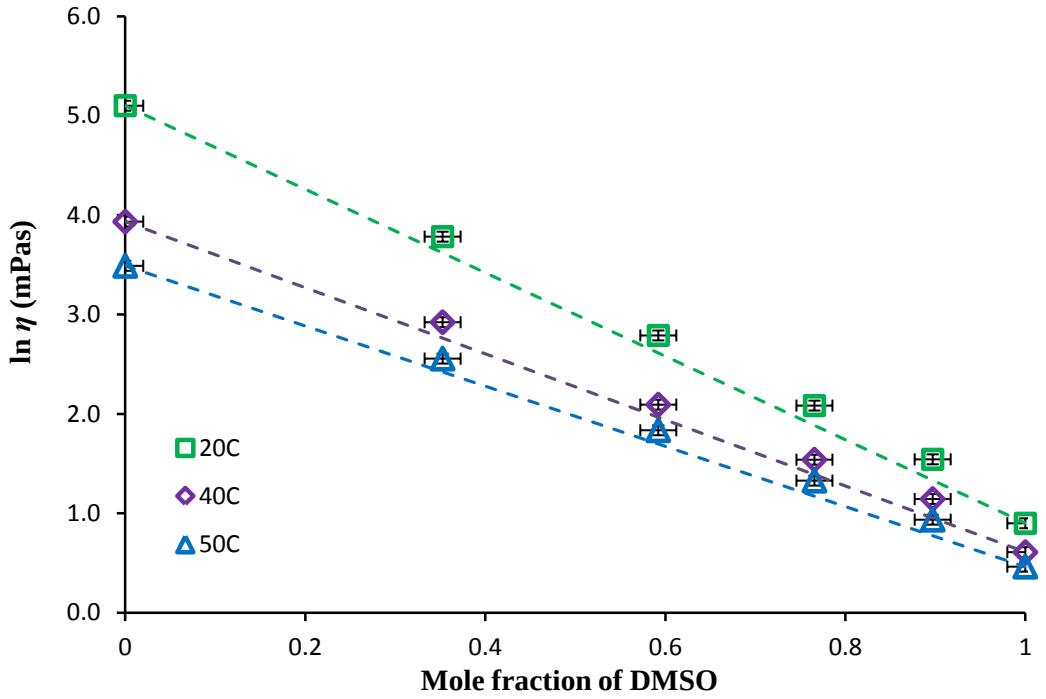

Figure 4.4: Viscosity of EMIMAc-DMSO mixtures as a function of mole fraction of DMSO at three temperatures as an example. The viscosity of the mixture decreases with the addition of DMSO. The straight line indicated the ideal mixing rule given by Equation 4.3.

4.3.4 NMR relaxometry

Investigation of the relaxation dynamics of EMIMAc-DMSO systems has been done using low field ^{1}H NMR. In this study, both T_1 and T_2 are equal, within the experimental uncertainty. In this case, they are therefore said to be in a high temperature limit where the relaxation rates are proportional to a correlation time, τ_c. From now on, we shall therefore only consider one relaxation time, T_1. No minimum point in T_1 was observed in the range of concentration and temperatures studied indicating that the systems are not undergoing transition from the high temperature limit to the diffusion limit. Based on the relationship discussed in Chapter 3,

$$\tau_c \propto \frac{1}{T_1} \propto \frac{1}{D} \propto \frac{\eta}{T} \qquad 4.4$$

if the logarithm of the viscosity follows an ideal mixing law then so will the logarithm of the inverse NMR relaxation times. ln $1/T_1$ against mole fraction are therefore plotted in Figure 4.5.

$1/T_1$ decreases with the addition of DMSO. Introduction of DMSO into the system has lengthened the NMR relaxation time, with this resulting from the faster rotational motion of the molecules giving rise to a smaller τ_c. This is also related to the viscosity in that the viscosities of the mixtures decrease with increase of DMSO. As shown in Figure 4.5, the measured relaxation rates are slightly larger than those predicted by a simple mixing rule, which means that the correlation times responsible for NMR relaxation are slightly longer than expected. The mobility of molecules in an EMIMAc-DMSO mixture are more hindered and therefore find it more difficult to reorient due to intermolecular interaction between DMSO and EMIMAc ions. This is particularly true if the hydrophobic interaction between DMSO and EMIMAc exists. Hydrophobic interaction between DMSO and EMIMAc will result in larger clusters which cause the reorientation of molecules to become longer. However, similar to the case of viscosity, the deviation from ideal mixing behaviour is very weak and considerably small. As shown in Figure 4.5, the deviation becomes less pronounced as the temperature increases. This is due to the weakening of the interactions between different kinds of ions with temperature increase.

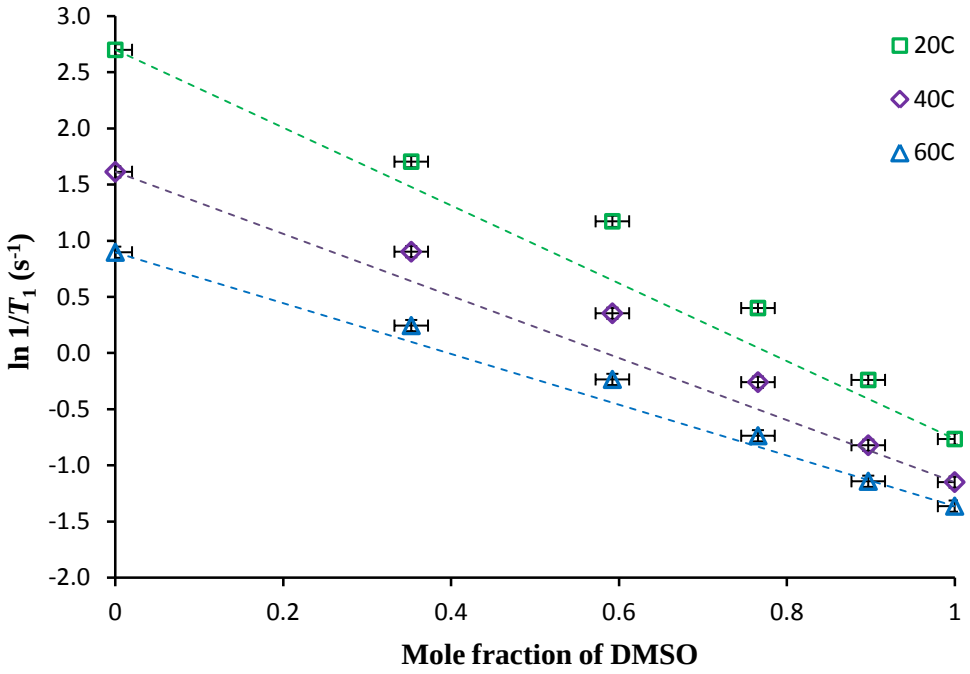

Figure 4.5: T_1 relaxation rates of EMIMAc-DMSO mixtures as a function of mole fraction of DMSO at three temperature 20 ^{o}C, 40 ^{o}C and 60 ^{o}C. The relaxation times decrease with the addition of DMSO.

4.3.5 Diffusion

The resulting self-diffusion coefficients as a function of mole fraction for EMIMAc and DMSO are presented in Figure 4.6. Natural logarithm of inverse diffusion coefficient is plotted following the relationship mentioned in the previous section. Due to the strong interaction between cation and anion in the IL, it was observed that the diffusion coefficient of the anion and cation in the range of temperatures and concentration studied is smaller than DMSO. However, both cation and anion are observed to have very similar self-diffusion coefficient values in all the mixtures.

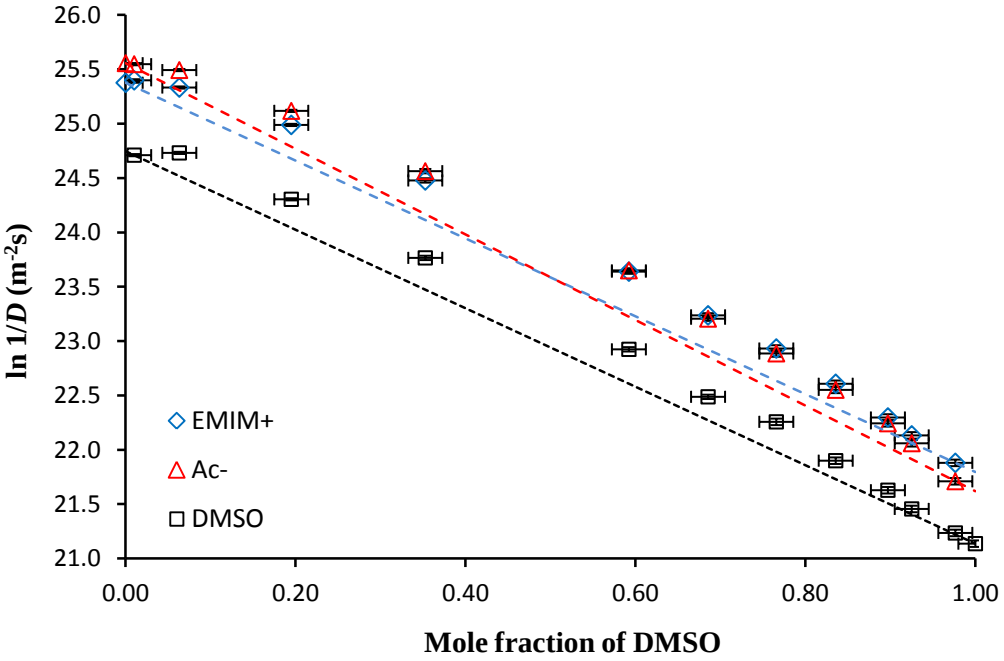

Figure 4.6: The plots of diffusion coefficient of cation, anion and DMSO in EMIMAc-DMSO mixtures as a function of mole fraction of DMSO at 20 ^{o}C. The diffusion coefficients increase with the addition of DMSO. The straight lines are the ideal mixing rule. The error bars are much smaller than the symbol sizes.

As predicted, the diffusion coefficient of both EMIMAc and DMSO molecules increases in the presence of DMSO. The strong coulomb interactions between the $EMIM^{+}$ cation and Ac^{-} anion are weakened upon mixing with the DMSO, which leads to a higher mobility of the ions. All components in the mixture show a deviation from ideal mixing in the same sense, diffusing slower than expected. However, the positive deviations for all cases are very weak. The self-diffusion

coefficient of EMIMAc ions and DMSO are therefore only slightly lower than those expected from ideal mixing rule.

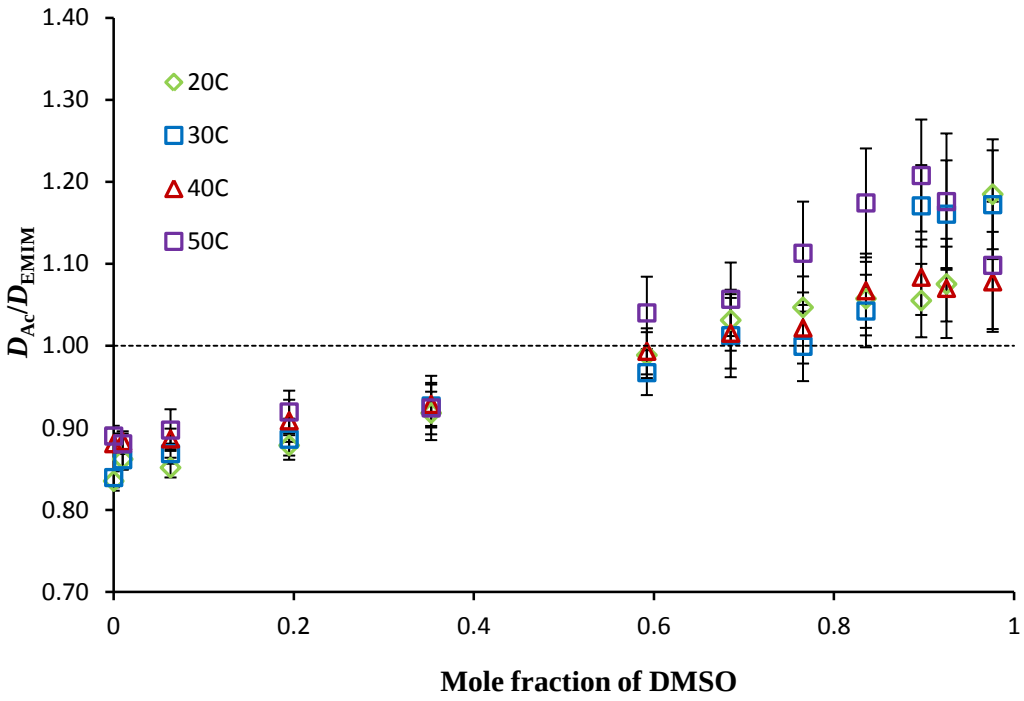

Figure 4.7: DMSO concentration dependence of the ratio of Ac^- to $EMIM^+$ diffusivities at various temperatures.

In pure EMIMAc, it was found that the larger cation diffuses faster than the anion. The faster diffusion of the cation has been explained by a computational study that showed that the preferable direction of cation motion is along the ring plane and perpendicular to the long axis of its alkyl chain, while the anion displacement is isotropic [168]. Some studies also suggested that because of the strong interaction that occurs between counter-ions, the ions may diffuse as a complex rather than a single ion [63]. The addition of DMSO has reduced the magnitude of the differences between diffusivities of the cations and anions. The ratio of Ac^- to $EMIM^+$ diffusivities tends to unity as the DMSO concentration is increased. With a further dilution, at molar fraction more than ~0.6, the anion starts to diffuse faster than the cation. This suggests that at this concentration and above, the presence of DMSO perturbs the ionic liquid-ionic liquid association. This is supported by an infrared spectroscopy study on $BMIMBF_4$/DMSO mixtures that showed at low concentration of DMSO that is 0.4 mole fraction, no drastic change in

imidazolium C-H band frequency observed. The author suggested that at low concentration of DMSO, there is a clustering of IL in the polar region and this cluster was perturbed with the further addition of DMSO [169].

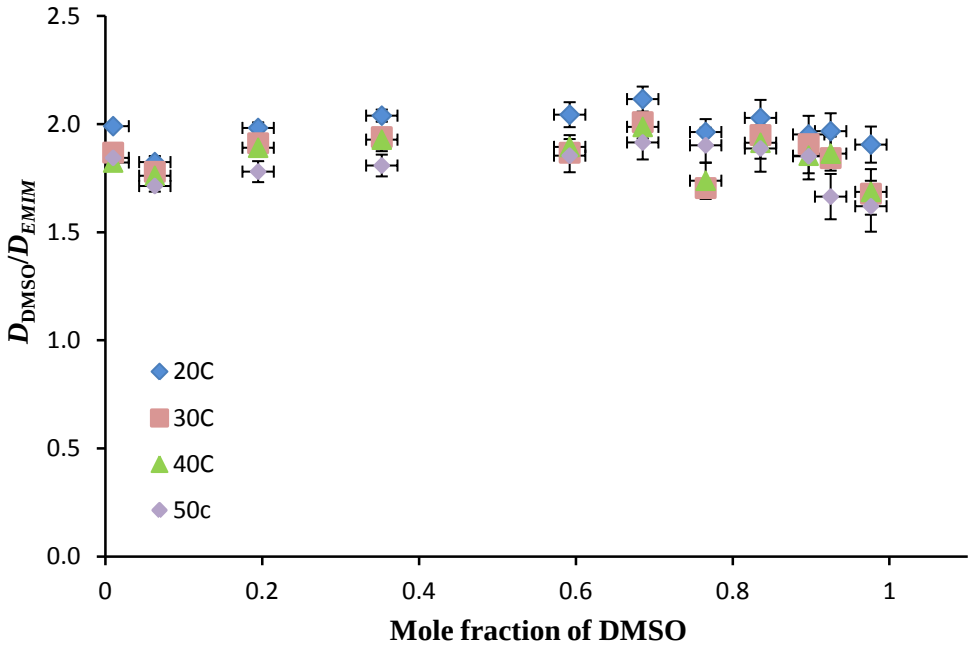

Figure 4.8: DMSO concentration dependence of the ratio of D_{DMSO} to D_{EMIM} diffusivities at various temperatures.

The ratio of the D_{DMSO} to that of the D_{EMIM} is plotted in Figure 4.8. It is found that the diffusivity of DMSO is almost two times larger than the diffusivity of the cation over the entire composition of DMSO. Even at a very small amount of DMSO (~0.010 mole fraction), the ratio of diffusion coefficient of DMSO to cation is similar to that of the dilute region (0.980 mole fraction). This is true for all temperatures studied and suggests that highly self-associated DMSO exists even at very small amounts of DMSO. This is supported by a mutual diffusivity study of IL-DMSO mixtures by Liu and co-workers which demonstrated that the mutual diffusion of anions and cations in ILs does not vary with mixture composition [150]. The negligible effect of DMSO on mutual diffusion of cations and anions has led them to the conclusion that the direct interaction between anions and cations is not disrupted by the presence of DMSO. Some physicochemical properties of DMSO suggest that this neat liquid solvent forms temporary polymer chains by interaction between its sulphur and oxygen atoms. Thus the negligible effect of DMSO on the

ratio of D_{DMSO} to that D_{EMIM} for the entire composition may be a result of the strongly associative nature of DMSO itself. This also suggests that the local organization of cation and anion in DMSO is not perturbed by the presence of DMSO.

In Figure 4.9, relative self-diffusion coefficients, $D(c)/D(o)$ against mole fraction of DMSO is plotted to see the variation of self-diffusion with composition. In Figure 4.9, $D(c)$ is a diffusion coefficient of $EMIM^+$, Ac^- and DMSO at a particular DMSO concentration and $D(o)$ is a diffusion coefficient of $EMIM^+$, Ac^- and DMSO at 0.01 mole fraction of DMSO. It shows that the variation of $EMIM^+$, Ac^- and DMSO is different over the range of concentration studied. Below ~0.60 molar fraction of DMSO, all the self-diffusion coefficients, $EMIM^+$, Ac^- and DMSO have been affected in the same order of magnitude. However Ac- starts to diffuse faster with further increase of DMSO. This can be related to the nature of interaction between DMSO and ionic liquid. As mentioned before, DMSO preferentially interacts with cation rather than anion due to its poor hydrogen bond donor. Favourable interaction of DMSO with cations may leave anions to more free, consequently able to diffuse faster than its counterpart at higher DMSO concentration [170]. Preferential of DMSO to solvate cation might also explains similar changes of the $D(c)/D(o)$ for $EMIM^+$ and DMSO over the range of concentration studied.

Earlier study focusing on liquid mixture of 1-Butyl-3-Methylimidazolium bis(trifluoromethanesulfonyl)imide, ($BMIMNtf_2$) and molecular solvent suggested that dipolar molecular solvents with large non-polar moiety were not fully dissolved near the polar network of IL. Hence, they are not able to interact directly with the ions in IL. Instead, they are partially dissolved into the non-polar regions of the IL [146]. Preferential DMSO molecules interact with non-polar regions of IL resulting in the formation of clusters between cation and DMSO molecules which cause the D_c/D_o for both cation and DMSO to be affected in a similar manner over the entire composition studied.

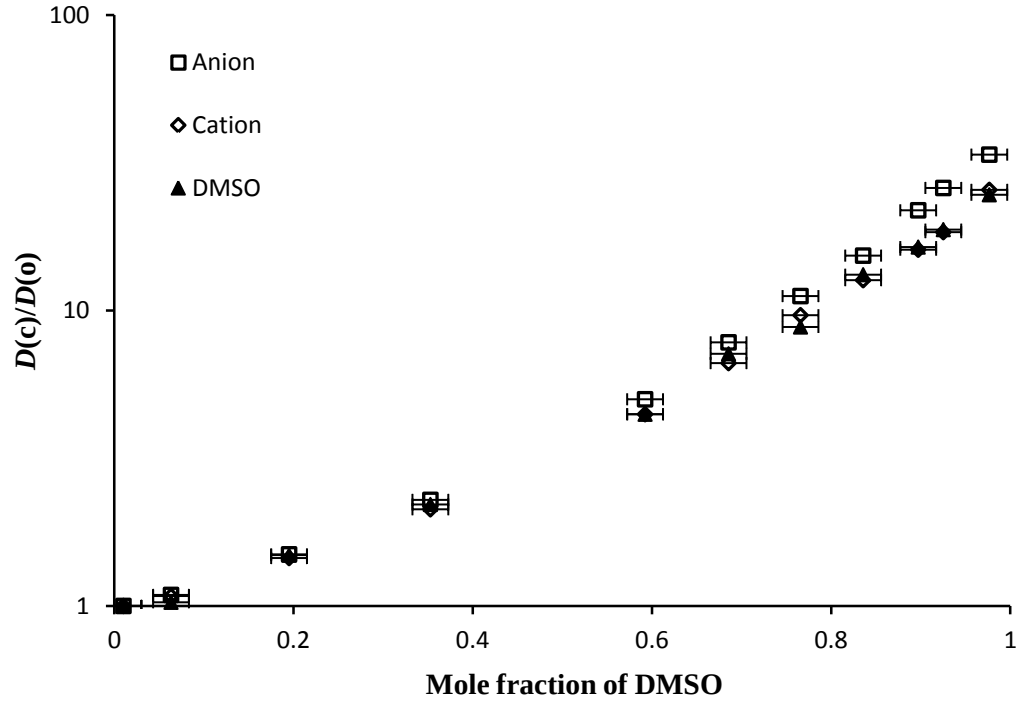

Figure 4.9: Relative self-diffusion coefficients, D(c)/D(o) against mole fraction of DMSO. The error bars are much smaller than the symbol sizes.

4.4 Discussion

4.4.1 Stokes-Einstein

Correlations between temperature dependence of self-diffusion coefficients and viscosities can be analyzed using the Stokes-Einstein relationship that has been discussed in Section 3.2.2. For a spherical molecule with a hydrodynamic radius R_H moving in a medium of viscosity η, the diffusion rate is given by:

$$D = \frac{kT}{c\pi R_H \eta} \qquad 4.5$$

The resistance of motion experienced by molecules in this viscous liquid is described by the friction coefficient, $\zeta = c\pi R_H \eta$. In classical Stokes-Einstein relation, the constant c is said to be 6. Therefore, for this analysis the value of 6 is taken as a constant value. In Figure 4.10, the plot of D against T/η for all species in EMIMAc-DMSO solutions is presented. For all our solutions it was found that, the plots of D against T/η showed linear relationships. The linear correlation in the experimental data demonstrates that the Stokes-Einstein equation provides a suitable description of the relationship between D and T/η for the EMIMAc-DMSO system.

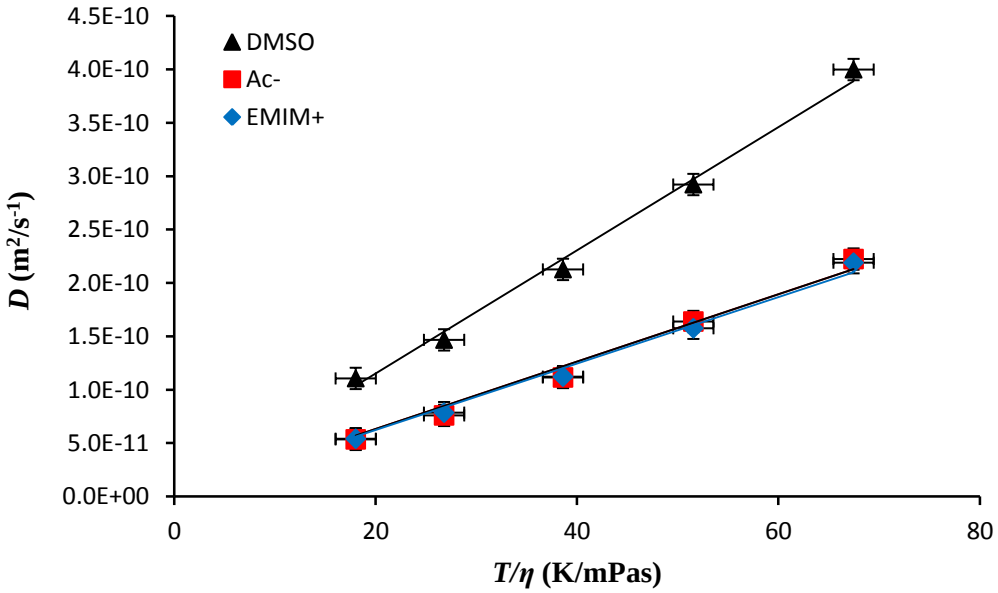

Figure 4.10: Relationship between D and T/η for the DMSO molecules, cations and anions for 0.35 mol fraction DMSO in the EMIMAc-DMSO mixture. The solid lines are fits to the Stokes-Einstein equation.

4.4.2 Microviscosity correction factor

An adjustment of the Stokes-Einstein relationship can be made by introducing a microviscosity correction factor f_μ (*see* Equation 4.6). In classical Stokes-Einstein relationship, f_μ is unity. However, this value can deviate from unity under certain circumstances. There are four circumstances for this deviation: i) molecules undergoing an anisotropic diffusion with this reducing f_μ; ii) the size of the diffusing molecule is small relative to the mixture in which it diffuses, again reducing f_μ iii) the diffusing molecules interact with environment in which it diffuses via e.g. hydrogen bonding, making f_μ larger and finally; iv) an increase of effective hydrodynamic radius of the diffusing molecules due to the formation of aggregates with this increasing f_μ [40].

$$D = \frac{kT}{6\pi f_{\mu} R_H \eta} \qquad 4.6$$

In order to determine the microviscosity correction factor, f_μ, the hydrodynamic radius, R_H is calculated separately using an empirical relationship (the calculation is detailed in Chapter 3, Equation 3.45). From this formula the hydrodynamic radius, R_H for $EMIM^+$, Ac^- and DMSO were found to be 2.74 Å, 2.24 Å and 2.45 Å respectively. For the $EMIM^+$, Ac^- and the DMSO, f_μ was determined at 0.7 ± 0.1, 0.9 ± 0.2 and 0.49 ± 0.04 respectively.

Since constant *c* in Equation 4.5 is an adjustable parameter that can vary from 4 to 6 depending on the boundary condition, therefore, the selection value of 6 in this case is almost appropriate. If 6 is referring to the stick boundary condition while 4 is referring to the slip boundary condition, therefore the value of f_μ for anion which very close to unity might suggest that the anion is in the stick condition. The stick condition experienced by the anion was probably caused by its interaction with surrounding molecules or formation of aggregates as explained above. Look back on the value of f_μ for the cation (0.7 ± 0.1), it is approximately equivalent to the f_μ = 4/6, which indicates that the cation is exposed to slip boundary conditions with the constant *c* equivalent to 4. Finally, this analysis reveals that, it is the DMSO molecules that experience the lowest microviscosity where $\eta_{\mu} = f_{\mu}\eta$.

4.4.3 NMR Relaxometry – Viscosity

It is well known that T_1 and T_2 provided information about molecular motion. T_1 is determined by both translational and rotational motion while T_2 principally by rotational motion. As mentioned earlier, our T_1 and T_2 values are the same in the range of concentration and temperature studied. As previously discussed, within this limit, the relaxation rate is said to be predominantly caused by rotational motion rather than translational motion. If it is assumed that the Stokes-Einstein-Debye (SED) model is adequate to give the rotational contribution to T_1, therefore the relationship between relaxometry data and viscosity can be investigated in detail, (*recall* Section 3.4),

$$\frac{1}{T_1} = \left(\frac{20\pi}{3} K R_H^3\right)\frac{\eta}{k_B T} \qquad 4.7$$

This equation provides a convenient means for comparing relaxation time data with the form of the BPP equation and the macroscopic transport coefficient. In order to verify the direct proportionality of $1/T_1$ and η predicted in Equation 4.7 a graph of $1/T_1$ against η/T is plotted (*see* Figure 4.11). As shown in Figure 4.11, $1/T_1$ shows a linear dependence with η/T and this dependence was true for all compositions studied. It is interesting to note that this result and the Stokes-Einstein plots in Figure 4.10 together reveal that microscopically the local microviscosity for both rotational and translational motion is proportional to the macroscopic viscosity.

The linear dependence of $1/T_1$ with viscosity provides more information pertaining to the relaxation constant, K in the BPP equation. Since k_B is a constant and R_H is predicted from the empirical relation, it is therefore possible to calculate the value of relaxation constant, K. It was found that the value of K obtained from the slope is $1.09 \times 10^9\ s^{-2}$. As explained in Section 3.1.5.4, K can be written as:

$$K = \frac{3}{10}\left(\frac{\mu_o}{4\pi}\right)\gamma^4 \hbar^2 \sum_j \frac{1}{r_j^6} \qquad 4.8$$

Note that the last term in Equation 4.8 is the sum of the inter-proton distances within the molecule. Since it is the summation of the inverse of the sixth power of inter-distance proton, therefore it can be approximated that only the nearest proton

neighbours contribute to the relaxation. Considering this approximation, this term is best replaced by:

$$\sum_j \frac{1}{r_j^6} = \frac{1}{r_j^6} \qquad 4.9$$

with r_j is now described as an effective inter-distance proton. The constant value of K calculated from the slope of the graph yields an effective inter-proton distance, r_j equivalent to 2.33 Å. The average inter-proton distance calculated from this equation is close to the actual inter-distance protons in aliphatic and aromatic protons which are 1.77 Å and 2.48 Å respectively [171].

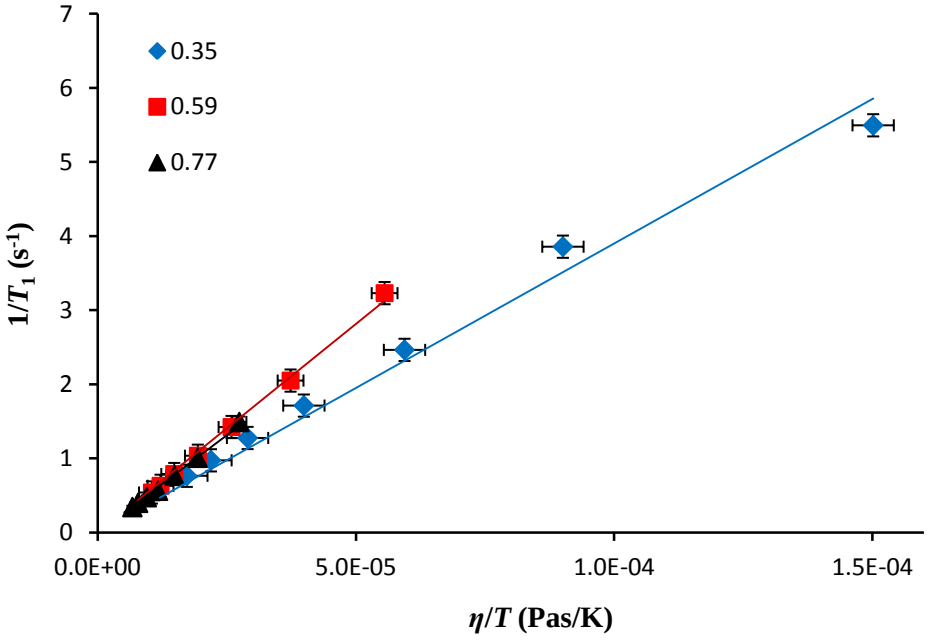

Figure 4.11: $1/T_1$ against viscosity over temperature for selected composition is shown as an example. The solid line fits the Equation 4.7.

4.4.4 Ideal Mixing Law

The percentage of deviation (% diff) from the simple ideal mixing laws for the various parameters measured is defined by:

$$\%\ diff = \frac{\left(X_{exp} - X_{mix\ rule}\right)}{X_{mix\ rule}} \text{X } 100 \qquad 4.10$$

(where $X = \eta$ or $1/T_1$ or $1/T_2$ or $1/D$). The percentage of deviation for all techniques employed are plotted as a function of DMSO mole fraction in Figure 4.12. It can be seen that the maximum deviation from ideal mixing rules for both macroscopic and microscopic properties occurs at 0.6 ± 0.1 mole fraction of DMSO.

This suggests that EMIMAc and DMSO molecules form the strongest associations at this concentration which causes the molecular dynamic to deviate most pronouncedly from simple ideal mixing compared to other concentrations. This also proposes that EMIMAc interacts with DMSO with the ratio of 1 EMIMAc:2 DMSO. However the deviation of EMIMAc-DMSO mixtures from ideal mixing behaviour are still considerably small in contrast to aqueus ILs reported from other study [40]. If comparing with the EMIMAc-water system from our previous study, the percentage of deviation for this system is far lower. In this system the percentage of deviation is ranging from 50-70 % whereas in EMIMAc-water system the percentage deviation is ranging from 200-500%. This figure is an order magnitude larger than that in the EMIMAc-DMSO system which reflects that stronger interactions occuring in aqueous ILs.

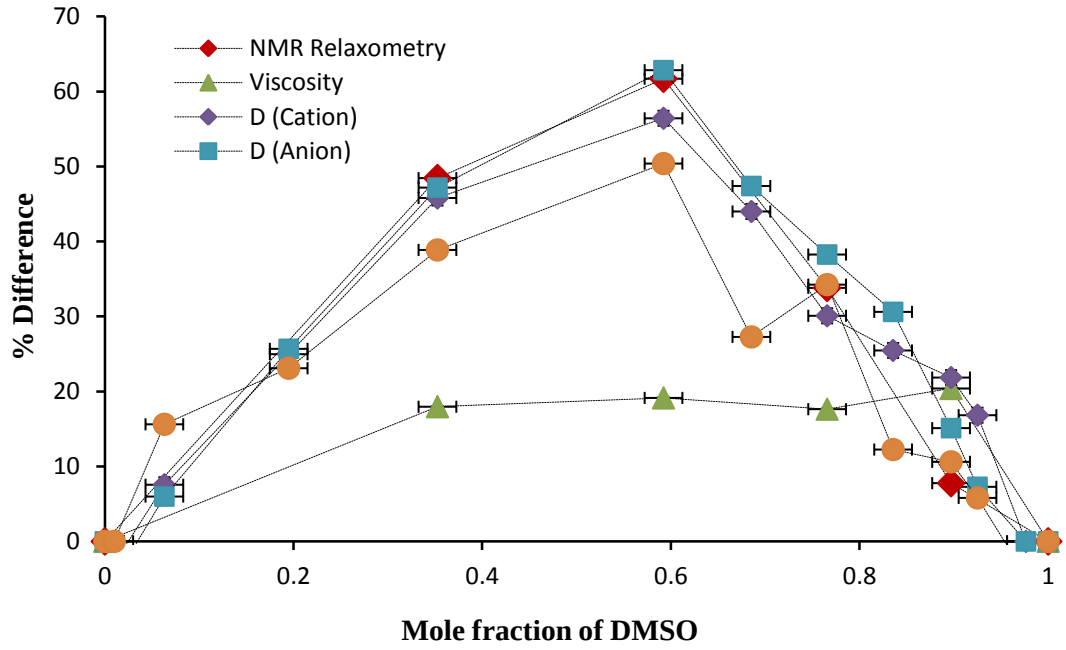

Figure 4.12: Percentage difference between measured parameters and the corresponding simple ideal mixing prediction for viscosity, anion inverse diffusion, DMSO inverse diffusion and inverse spin-lattice relaxation. The solid lines are guides for the eye.

These mixtures exhibit a different trend from EMIMAc-water mixtures which showed very strong non-ideality of its physicochemical properties with composition. Because DMSO is a hydrogen bond acceptor while EMIMAc can be both hydrogen-bond donors and acceptors, the network of hydrogen bonding in EMIMAc-DMSO mixtures is not strongly composition dependent. Weak interaction between EMIMAc and DMSO is believed to be responsible for the weakly non-ideal mixing behaviour reflected in small maxima in the variation of the above properties with the mole fraction of DMSO.

4.5 Conclusions

In this work, we have presented an experimental study of both macroscopic and microscopic properties of mixtures composed of EMIMAc and DMSO over the entire concentration range. The objective was to explore the changes of these properties due to the addition of a co-solvent to the ionic liquid. Our experiments on the transport property of the mixture at macroscopic level i.e. viscosity at all temperatures, is in quantitative agreement with the transport properties at microscopic level, that is a diffusion coefficient and NMR relaxations. All measurements deviated from ideal mixing law and show a maximum at DMSO molar fraction $x = 0.6 \pm 0.1$. The composition range of EMIMAc-DMSO mixtures within which macro- and micro-scopic properties attain their highest value should be interpreted as a region characterized by maximal intermolecular interaction between EMIMAc and DMSO.

From the experimental results for density, viscosity, diffusion coefficient and NMR relaxation, deviation from ideal mixing rules were calculated. It was found that all of these deviations from ideal mixing rule have the same sense. However, we have found that in most cases the macroscopic and microscopic properties of the mixture only deviate slightly from ideal mixing behaviour. Weak interactions between EMIMAc and DMSO molecules are believed to be responsible for the weakly non-ideal mixing behaviour.

The density of the mixture followed an additive law (*see* Equation 4.1) within experimental error. The excess molar volumes which were calculated from the density measurements also exhibit similar behaviour. The values were found to be extremely small ~ ($2 – 8 \times 10^{-8}$ m^3mol^{-1}).

The change in ^1H chemical shift positions, $\Delta\delta$, revealed that the resonance of H2, H4 and H5 belonging to the imidazolium ring protons had weaker dependencies on DMSO composition than in the EMIMAc-water system. This indicates that the presence of DMSO did not significantly alter the environment of the EMIMAc molecules.

The viscosities of all our samples were measured. The viscosities showed a small positive deviation from simple ideal mixing with the percentage difference

being only 15-20 %. This figure is far smaller than what was observed in the EMIMAc-water system with percentage difference of viscosity from the ideal mixing rule being 450-500%. Indeed the measured viscosity of the solution behaved almost like an ideal solution.

The self-diffusion coefficient for each component ($EMIM^+$, Ac^- and DMSO) in the mixtures was measured using high field NMR (400 MHz). It was found that larger $EMIM^+$ diffuses faster than its counterpart Ac^- in the pure EMIMAc. However, with further increase of DMSO, Ac^- gradually diffuses faster and eventually had a similar diffusion coefficient to $EMIM^+$ at molar fraction $x = 0.59$ before it then starts to diffuse faster than $EMIM^+$. Over the range of concentration studied, DMSO molecules had a diffusion coefficient two times that of $EMIM^+$.

Introduction of the microviscosity correction factor, f_μ in the Stokes-Einstein relation showed that anion molecules are diffusing in stick boundary conditions which could be caused by their interaction with the environment or formation of the aggregates. The result also shows the microviscosity of cations is less than unity which indicates that cations diffused faster, i.e. slip boundary conditions.

For all measurements, the maximum of percentage difference of the deviation from ideal mixing law in the EMIMAc-DMSO system was smaller (20-65%) than in the EMIMAc-water system that fell between 200-500%. This suggested that interaction between IL and polar aprotic solvent such as DMSO is much weaker than its interaction with polar solvent through hydrogen bonding.

Chapter 5

1-Butyl-3-Methylimidazolium Chloride/cellulose Solutions

5.1 Introduction

Over the last decade, 1-Butyl-3-Methylimidazolium Chloride (BMIMCl) has been the subject of many studies concerning its ability to dissolve cellulose. BMIMCl exists in two polymorphic forms, monoclinic and orthorhombic with melting points 41 ^{o}C and ~70 ^{o}C respectively [26, 172]. BMIMCl is a very powerful solvent for cellulose. Its superior efficiency to dissolve up to 25% of cellulose concentration [8] has drawn it to the attention of researchers to further investigate its physical properties as well as its interaction with cellulose and other types of polysaccharides. High chloride content and activity in BMIMCl was suggested to be the main reason for dissolving cellulose in this IL. Chloride anions which are strong hydrogen bond acceptors make BMIMCl effective as a cellulose solvent. Dissolution of cellulose in IL is predominantly explained by the formation of hydrogen bonds between the anion and the equatorial hydroxyl groups and side chain of glucan units. The formation of hydrogen bonds between them subsequently weakens the hydrogen bonding between glucan strands. This is supported by NMR relaxation times of Cl^- anion from carbohydrates dissolved in BMIMCl that showed the stoichiometry of the affected cellulose anion to that of hydroxyl groups possessed by these carbohydrates is 1:1 [173]. The formation of hydrogen bonds between the hydroxyl groups and anion have also been observed in MD simulation studies of solvated oligosaccharides and single glucan chain in ILs [63, 65, 163]. However, there are other views of the interactions between ILs and cellulose which suggest that the cation also plays a non-negligible role in the dissolution process of cellulose in ILs. Some experimental studies showed that the cationic structure and alkyl chain length of the ILs has affected the ability of ILs to dissolve cellulose [67, 174, 175]. Even though cation plays a secondary role in the cellulose dissolution process, their effect cannot be neglected.

Herein, Nuclear Magnetic resonance (NMR) has been used to study the mechanism of cellulose dissolution in BMIMCl. Since the processing of cellulose

from an ionic liquid depends on the properties of the solvent itself, thus the understanding of the dynamic properties of IL as well as its molecular organization in cellulose-IL systems is an essential prerequisite for successful cellulose processing. In this work a comprehensive investigation of the structure and dynamics of BMIMCl that dissolve microcrystalline cellulose at different concentrations and temperatures is presented.

5.2 Experimental

5.2.1 Material and sample preparation

Avicel PH-101 microcrystalline cellulose, (cellulose) with the degree of polymerization 180 was purchased from Sigma Aldrich. Prior to the sample preparation, cellulose was dried under vacuum at 80 ^{o}C for a period of 12 hours. BMIMCl (purity ≥ 97 %) was used without further purification. The BMIMCl was purchased from Sigma-Aldrich. In this work, a series of cellulose (1.0, 2.0, 5.0, 8.0 and 10.0 wt%) in BMIMCl were prepared by heating a mixture to 80 ^{o}C with constant stirring in a container for about 12 hours. Upon complete dissolution, the samples were transferred into 5 mm NMR tubes that were subsequently sealed to prevent atmospheric moisture contamination. A sample of the neat BMIMCl was prepared analogously. A 2.0 - 2.5 cm high sample was put into the tube to ensure there would be enough NMR signal whilst not being too much to cause thermal gradients. To avoid impurities and their impact on the physical properties of BMIMCl, the preparation of the samples carried out in a glove box.

The concentration of cellulose dissolved in BMIMCl was calculated using the equation below:

$$C_{cellulose} = \frac{m_{cellulose}}{m_{cellulose} + m_{BMIMCl}} .100\%$$

where $C_{\text{cellulose}}$ is the concentration of cellulose, $m_{\text{cellulose}}$ and m_{BMIMCl} are the mass of cellulose dissolved in BMIMCl and the mass of BMIMCl respectively.

5.2.2 NMR instrumentation and experiment

5.2.2.1 High Field NMR (General)

Experiments were acquired on a Bruker AV 400 spectrometer operating at 400 MHz using a Diff60 probe (Bruker Biospin) for ^{1}H NMR with variable temperature control (accurate to ± 0.1 ^{o}C). At each temperature the RF coil was tuned, the static magnetic field shimmed and pulse lengths measured. Following this, an FID was acquired and the spectra examined. In particular, the proton spin-lattice, proton spin-spin relaxation times and diffusion, T_1, T_2 and D respectively have been measured. Calibration was performed by measuring T_1 relaxations and the self-diffusion coefficient of pure water at each temperature prior to the experimental measurements. The reference value of temperature dependence of the T_1 relaxation and the diffusion coefficient of water is referred to results published elsewhere [98, 176]. The temperature was set and controlled with an air flow of 1035 l h^{-1} in order to avoid any fluctuation due to sample heating during the magnetic field pulse gradients. Experiments for all samples were performed at temperature ranging from 20 to 70 ^{o}C in 10 ^{o}C increments.

5.2.2.2 Measurement of T_1 Relaxation

Longitudinal (T_1) ^{1}H relaxation data for the $BMIM^{+}$ ions were obtained with standard ^{1}H saturation recovery pulse sequence. In this study, all the measurements were acquired with 8 scans.

5.2.2.3 Measurement of T_2 Relaxation

Transverse (T_2) ^{1}H relaxation data for the $BMIM^{+}$ ions were obtained with standard ^{1}H Carr–Purcell–Meiboom–Gill (CPMG) pulse sequence. A total of 8 scans were also acquired for this measurement.

5.2.2.4 Measurement of Diffusion Coefficient

Since the relatively high viscosities of these systems lead to short ^{1}H T_2 times, PFG-STE bipolar sequence techniques were employed to carry out the measurements. Diffusion coefficients for ions in pure BMIMCl and BMIMCl-cellulose solutions were obtained using the ^{1}H-detected PFG-STE bipolar sequence that has been explained in detail in Chapter 3. The self-diffusion coefficient of $BMIM^{+}$ in

BMIMClc/cellulose solutions was obtained as a function of temperature in the range from 20 ^{o}C to 70 ^{o}C.

5.2.2.5 Low Field NMR

The ^{1}H-T_1 and ^{1}H-T_2 values of BMIMClc/cellulose solutions were obtained as a function of temperature in the range from 30 ^{o}C to 100 ^{o}C. The protocols and parameters used for this acquisition are similar to those mentioned in the previous chapter (*see* Section 4.2.1.3).

5.2.3 Viscosity

The viscosity data presented in this section was collected in collaboration with Prof. Tatiana Budtova from the Centre de Mise en Forme des Materiaux, Sophia Antipolis, France.

Shear rate dependent viscosity was measured at temperatures ranging from 70 - 130 ^{o}C in 10 ^{o}C increments.

5.3 Results

5.3.1 ^{1}H NMR Studies of Cellulose in BMIMCl

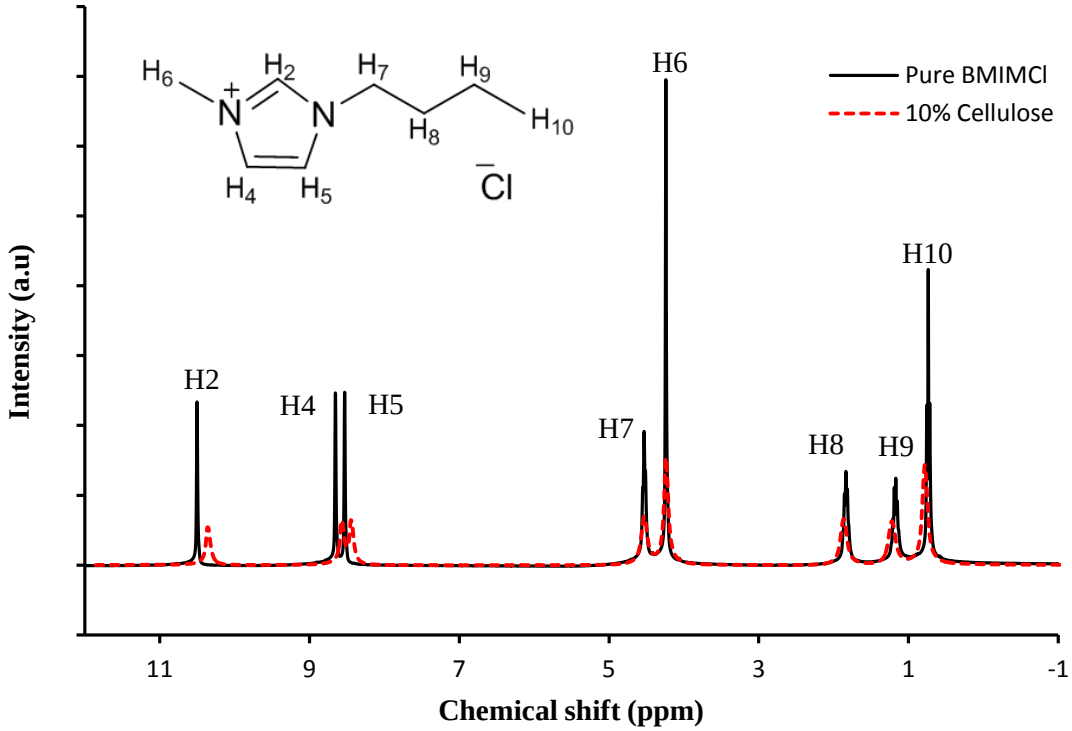

Figure 5.1: ^{1}H NMR spectra of pure BMIMCl and 10% cellulose solution at 70 ^{o}C. (Insert: Chemical structure of BMIMCl labelled with H2-H10).

^{1}H NMR spectra obtained for 10 wt% cellulose in BMIMCl-cellulose solution at 70 ^{o}C is shown in Figure 5.1. The assignment of chemical shift for each spectral band, labelled H2-H10, is made with reference to the chemical structure of BMIMCl shown in Figure 5.1 (*see* insert).

Owing to its asymmetric structure, BMIMCl molecules have non-equivalent sets of protons. Thus all protons that attached to the carbon site produced their own individual signal. As seen in Figure 5.1, it is clearly shown that there are eight peaks all together in the NMR spectra. The first three peaks from the left belong to the protons attached to the imidazolium ring followed by methylene (-CH_2) and methyl (-CH_3) groups adjacent to the imidazolium ring respectively and the last three peaks belong to -CH_2 and -CH_3 groups of the alkyl chain.

It has been observed that none of the signals from cellulose molecule appeared in the spectra. It is well known that the acquisition and assignment of cellulose signals in ^{1}H NMR spectra is a difficult task. One of the major problems is their signal lying within a crowded region. This is because most of the protons in cellulose lie in rather similar chemical environment. Density Functional Theory (DFT) and Molecular Dynamic (MD) simulation by Bagno et al. showed that most of their signals are within less than 0.5 ppm, with some signal almost isochronous. This difficulty becomes worse in the presence of solvent such as ionic liquid. The solvation of cellulose in this solvent leads to the changes in solute geometry and electronic structure of cellulose that subsequently affect the NMR parameter (i.e. shielding constant). Direct interaction between cellulose and ionic liquid also affects the cellulose signal. Ionic liquid forms intermolecular hydrogen bonding with hydroxyl groups that were previously conceived by intramolecular hydrogen bonding [177-179].

From the spectra acquired, it has been confirmed that no new compound is formed during the solvation of cellulose in BMIMCl. This is shown from the well resolved peaks of the spectra and no unidentified peaks are observed. Apart from that, due to the high hydrophilicity of chloride based ILs, careful examination on the spectra is essential to verify the purity of the BMIMCl. From the observation of the spectra, there are no peaks or signal between peak H5 and H7, which indicates that our samples were free from water contamination. Since only ^{1}H NMR is employed in this study, therefore it only allows us to probe the spectra and molecular dynamics of $BMIM^{+}$. Thus our investigations are concerned only with the $BMIM^{+}$ ion.

5.3.2 Chemical Shift Changes Analysis

Proton spectra for a series of concentrations were recorded to study the chemical shift changes. To simplify the analysis of chemical shift changes, H6 is then defined as having a fixed chemical shift. The choice of H6 as a reference point follows previous studies in which this spectral band was found not to be dependent on the concentration of the solute [49, 87]. NMR spectroscopic studies of cellobiose solvation in EMIMAc found that the methyl group in imidazolium cation exhibited almost no change in chemical shift upon addition of cellulose concentration [49]. Chemical shift of protons in neat BMIMCl is used as a starting reference value. Any

changes of chemical shift with cellulose concentration correspond to the change from this reference value. In Figure 5.2, the chemical shift change of individual protons in BMIMCl as a function of concentration at 40 ^{o}C is displayed. In this study, it can be seen that the chemical shift of imidazolium proton H2 followed by H4, and H5 had the most significant changes and they move upfield ($\Delta\delta < 0$) upon addition of cellulose concentration. In contrast alkyl proton H7, H8, H9 and H10 moved downfield ($\Delta\delta > 0$), with a smaller magnitude, as the concentrations of cellulose increased.

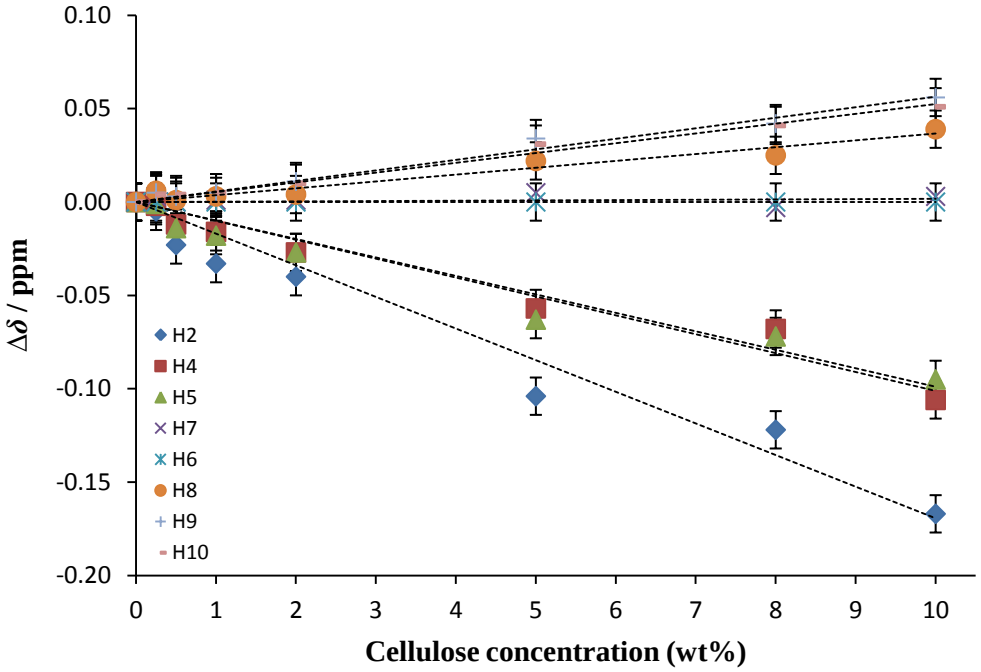

Figure 5.2: The changes of proton chemical shift difference in BMIMCl with increasing cellulose concentration (wt%) at 40 ^{o}C. ($\Delta\delta = \delta - \delta_{neat}$). The dotted lines are presented as an aid to the eye.

Generally, the formation of a hydrogen bond gives a downfield shift to the proton resonance. This is due to the fact that during the formation of a hydrogen bond, the electron density around the proton has been reduced and subsequently caused the proton to resonate at a lower field. In this case, one might expect H2, H4 and H5 to move downfield since dissolution of cellulose in BMIMCl involves formation of hydrogen bond between the hydroxyl group of cellulose and BMIMCl, especially with imidazolium ring protons. However, the greatest upfield shift of these protons can be explained as follows. In BMIMCl itself, cations and anions formed hydrogen

bonds in which the strongest hydrogen bonding always involved the most acidic H2 of imidazolium cation followed by H4 and H5. The hydroxyl group of cellulose preferred to interact with H2 rather than with H4 and H5 owing to the fact that the H2 is positively charged due to the electron deficit in the imidazolium ring [35, 180, 181]. Since the hydrogen atoms in hydroxyl groups are stronger hydrogen bond donors than those in imidazolium protons, the chloride anions formed stronger hydrogen bonds with hydrogen atoms in cellulose hydroxyls. Formation of new hydrogen bonds between chloride anions and hydrogen atoms in hydroxyls therefore breaks up the interaction between anions and ring protons of cations. Consequently, hydroxyls interact with aromatic protons and form weaker hydrogen bonds. This weaker hydrogen bonding causes an upfield shift of the imidazolium protons.

5.3.3 ^{1}H NMR Relaxation

A change in ^{1}H NMR relaxation provides information pertaining to the dynamics of the cation, their interaction with cellulose, phase changes and molecular conformations. In this section the changes in the relaxation times of proton nuclei of the $BMIM^{+}$ as a function of concentration and temperature will be discussed.

5.3.3.1 T_1 relaxation

5.3.3.1.1 Influence of cellulose concentration on T_1 relaxation

In this study, the changes in relaxation times of proton nuclei of the $BMIM^{+}$ as a function of concentration and temperature probed by low field (20 MHz) and high field (400 MHz) NMR have been observed. However, probing the $BMIM^{+}$ relaxation time as a function of concentration using a high field (400MHz) spectrometer did not provide much more information on the changes of relaxation time among all protons. In this case, the high transition frequency of the spectrometer might not be efficient at bringing about relaxation for the BMIMCl-cellulose system. Figure 5.3 shows the changes in T_1 relaxation over the whole concentration range for the H2, methyl group of imidazolium proton, H6 and alkyl proton, H9 and H10. A similar trend is also observed for the other protons. H2 and H6 which attached to the imidazolium ring display almost negligible change in T_1 over the whole cellulose concentration studied. Alkyl protons on the other hand,

displayed a little change in T_1 due to the mobility nature of the alkyl chain itself which is less restricted in the IL solutions.

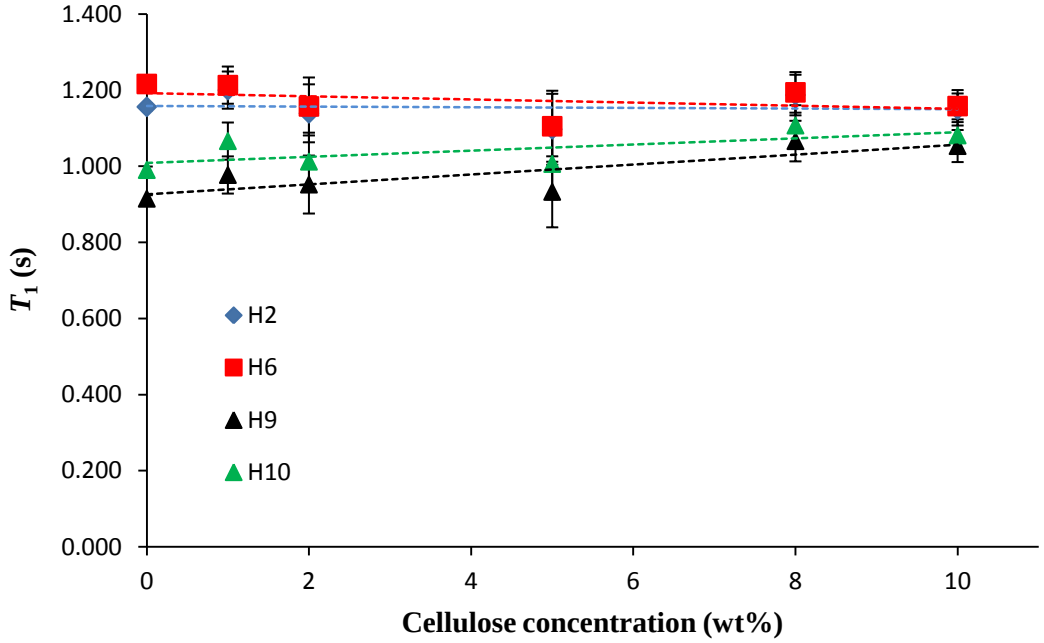

Figure 5.3: ^{1}H-T_1 values of BMIM$^+$ protons as a function of the cellulose concentration at 40 ^{o}C using 400 MHz NMR spectrometer.

Conversely, measurement of BMIM$^+$ relaxation by low-field NMR showed a significant change in T_1 relaxation time over the whole concentration studied. The dependence of T_1 on cellulose concentration is shown in Figure 5.4. It is found that T_1 relaxation decreases with the further increase of cellulose concentration. Due to the lower resonance frequency, i.e. 20 MHz, the obtained ^{1}H relaxation time is averaged over all protons for the BMIM$^+$ ions. Although it only provides information on relaxation time for the whole cations, its changes in relaxation time have demonstrated that concentrations of solute also affect the relaxation rate. This is opposed to the findings of Remsing et al. which suggested that relaxation rates of carbon constituting the cation changed very little with cellobiose concentration, subsequently leading to the conclusion that the interaction between cation and cellobiose is negligible [173]. In contrast, from a recent simulation, it is shown that a small, but non-negligible interaction between carbohydrate molecules and the ILs cation exists [174]. Thus the decreasing of relaxation rates of proton with cellulose

concentration in our study might indicates that it resulted from this interaction, though viscosity might also contribute to the changes of relaxation.

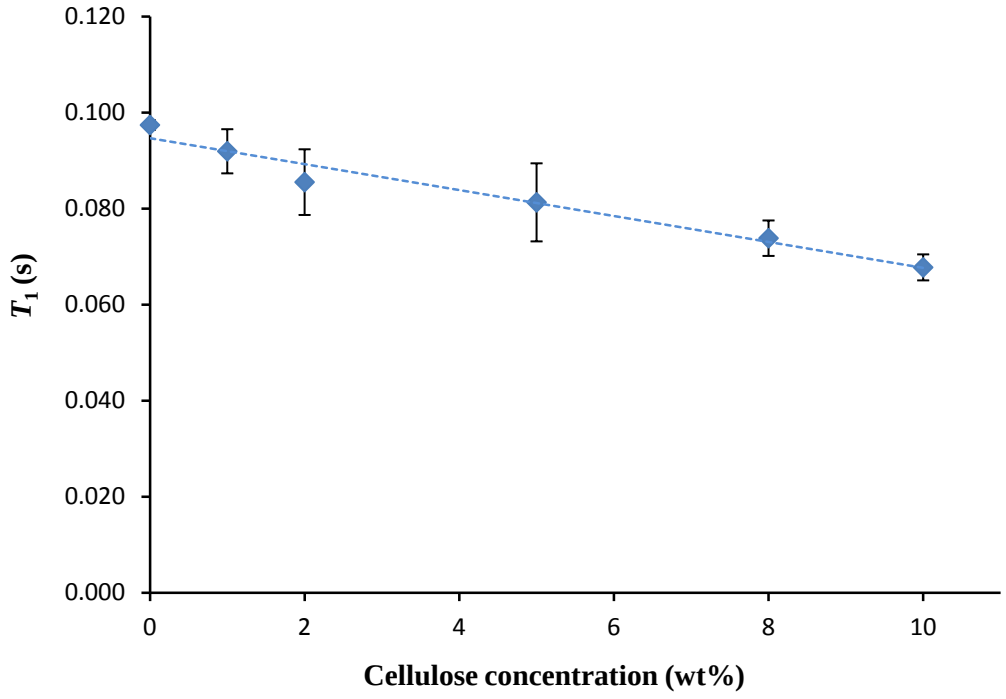

Figure 5.4: ^{1}H-T_1 values of BMIM^{+} cation as a function of the cellulose concentration at 70 ^{o}C using 20 MHz NMR.

5.3.3.1.2 Influence of temperature on T_1 relaxation

In order to study the influence of temperature on the dynamics of the cation in the presence of cellulose, the temperature dependency of the relaxation rates of ^{1}H nuclei of all samples was studied. Using 400 MHz NMR measurement, the relaxation rate for each proton constituting the BMIM^{+} is observed. The relaxation profiles suggest that upon heating, the T_1 values of the alkyl protons decrease, whereas those of the ring protons or methyl protons directly attached to the the ring did not change. As can be seen, the relaxation rates for H2 and H6 do not vary with temperature (*see* Figure 5.5). This is owing to the restiction in mobility of the imidazolium ring and the adjacent proton atoms in the system. This is in good agreement with the dynamic behaviour of other imidazolium salts [182-184]. Conversely, due to higher mobility of the butyl chain, relaxation rates of all *n*-butyl chain protons change with further increase in temperature. In Figure 5.5, relaxation

rates of the chain protons is represented by both H9 and H10 protons. For both protons, the T_1 value decreased with raising of the temperature indicating that these protons are within the diffusion limit regime. The other *n*-butyl protons also exhibit similar trends. However, any minimum of T_1 was not observed for all protons in the range of temperature studied. This means that the protons did not undergo transition from the diffusion limit ($\omega_o\tau_c >> 1$) to the extreme narrowing ($\omega_o\tau_c << 1$).

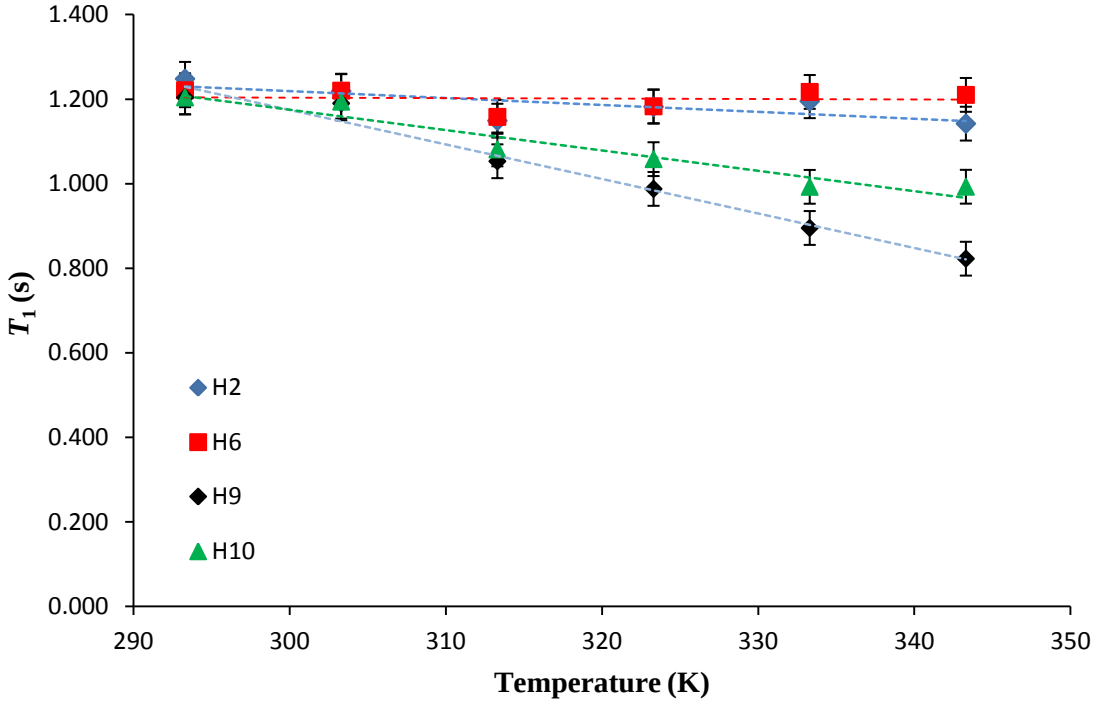

Figure 5.5: ^{1}H-T_1 values of selected BMIM$^+$ protons as a function of temperature for 10% cellulose concentration using 400 MHz NMR spectrometer.

However longitudinal relaxation rates of the whole BMIM$^+$ cations probed by 20 MHz NMR spectrometer showed a different trend. Figure 5.6 shows the temperature dependence of relaxation times, T_1 of BMIM$^+$ at various cellulose concentrations. The pronounced increase of T_1 relaxation in high temperature limits with rising temperature correlates with the observed changes in viscosity. However the most informative point within this data is the location of T_1 minimum as a function of temperature. The ability of the proton nucleus to reach a minimum within the range of temperature studied indicated that they undergo a transition from relatively restricted to unrestricted motion. From our study it is clearly shown that the T_1 relaxation has a minimum at 323 ± 5 K ~ (5 ± 5 ^{o}C). The regime on the left side of

minimum is called the diffusion limited side. Here molecules reorient slowly on the NMR time scale as a result of viscosity.

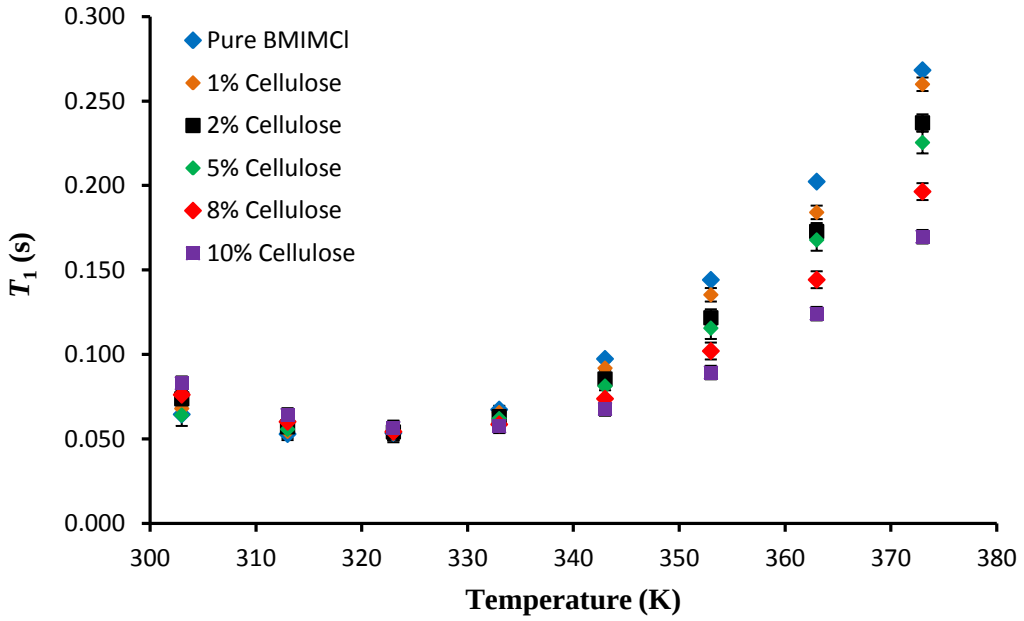

Figure 5.6: ^{1}H-T_1 values of $BMIM^{+}$ as a function of temperature for all BMIMCl-cellulose solutions studied using low field NMR (20MHz).

The reorientational motion of molecules can be characterized by correlation time τ_c, where τ_c is a measure of the average time that a molecule spends in a given orientation. Thus, in the diffusion limited regime correlation time, τ_c is said to be much larger than inverse of the transition frequency ω_o ($\tau_c >> 1/\omega_o$). The area on the right side of the minimum is called the extreme narrowing region. In this region, molecules tumble very fast where their correlation time is much smaller than the transition frequency ($\tau_c << 1/\omega_o$). In this study, the observed T_1 minimum correspond rather well with the melting point of this ionic liquid at 314 K (41 ^{o}C) reported by a previous study [26].

The experimental value of T_1 can be expressed in terms of an isotropic correlation time, τ_c, for molecular motion by using the Bloembergen-Purcell-Pound (BPP) theory. From the ^{1}H NMR T_1 data shown in Figure 5.6, we can derive the correlation time, τ_c for the reorientation of cations in BMIMCl-cellulose solutions. This topic will be discussed further in the next section.

5.3.3.2 T_2 Relaxation

5.3.3.2.1 Influence of cellulose concentration on T_2 relaxation

The dependency of T_2 relaxation times with cellulose concentration is shown in Figure 5.7 and Figure 5.8. T_2 was probed by high field and low field NMR and showed a decrease in cellulose concentration. In Figure 5.7, T_2 relaxation probed by high field NMR exhibit similar trend with T_1 relaxation. It was found that the relaxation of protons that attached to the imidazolium ring is much shorter and does not significantly vary with cellulose concentration. Conversely, the alkyl chain protons exhibited longer T_2 relaxation and significantly decreased with cellulose concentration. This is due to the nature of the alkyl chain itself that is more free than the imidazolium ring part. In addition, the ability of imidazolium ring protons to interact with cellulose might also contribute to the short T_2 relaxation of these protons.

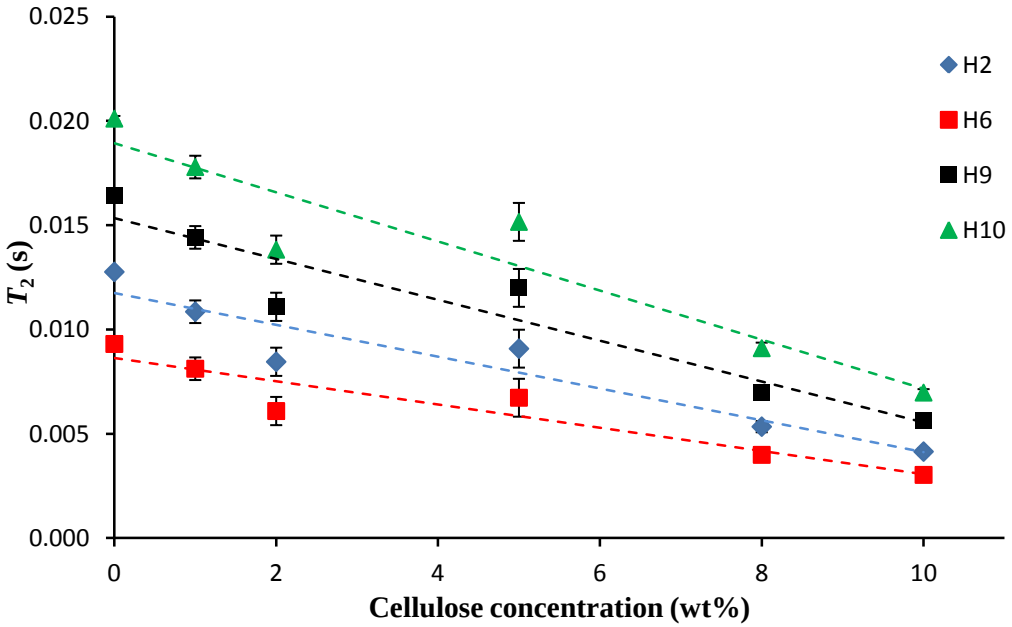

Figure 5.7: The ^{1}H-T_2 values of different protons constituting BMIM$^+$ cation as a function of the cellulose concentration at 70 ^{o}C probed by high field NMR (400 MHz). Dashed lines are linear fits to data.

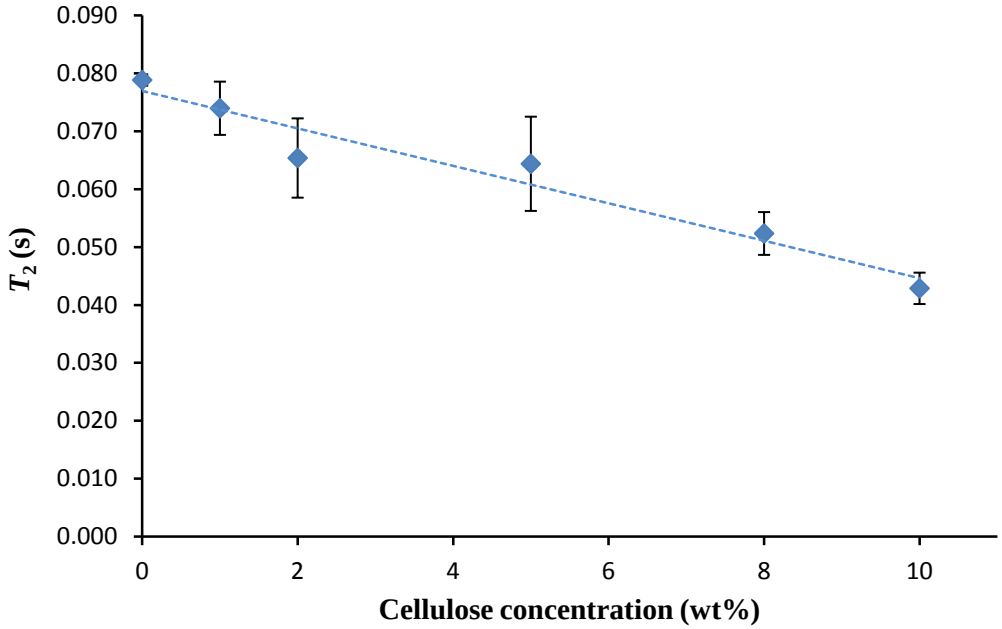

Figure 5.8**:** ^{1}H-T_2 values of $BMIM^{+}$ cation as a function of the cellulose concentration at 70 ^{o}C probed by low field NMR (20 MHz).

5.3.3.2.2 Influence of temperature on T_2 relaxation

The dependency of T_2 relaxation times on temperature is shown in Figure 5.9 and Figure 5.10. As expected, in both cases, the relaxation profiles showed that upon heating, the T_2 values of the protons increased. As the temperature increased, protons became more mobile. This phenomenon caused the T_2 to become longer.

Figure 5.9 shows the T_2 value for selected protons constituting the $BMIM^{+}$ in 10% cellulose solution. Again, a similar trend is observed in which the alkyl chain protons are found to be more affected with the temperature increase compared to the imidazolium protons.

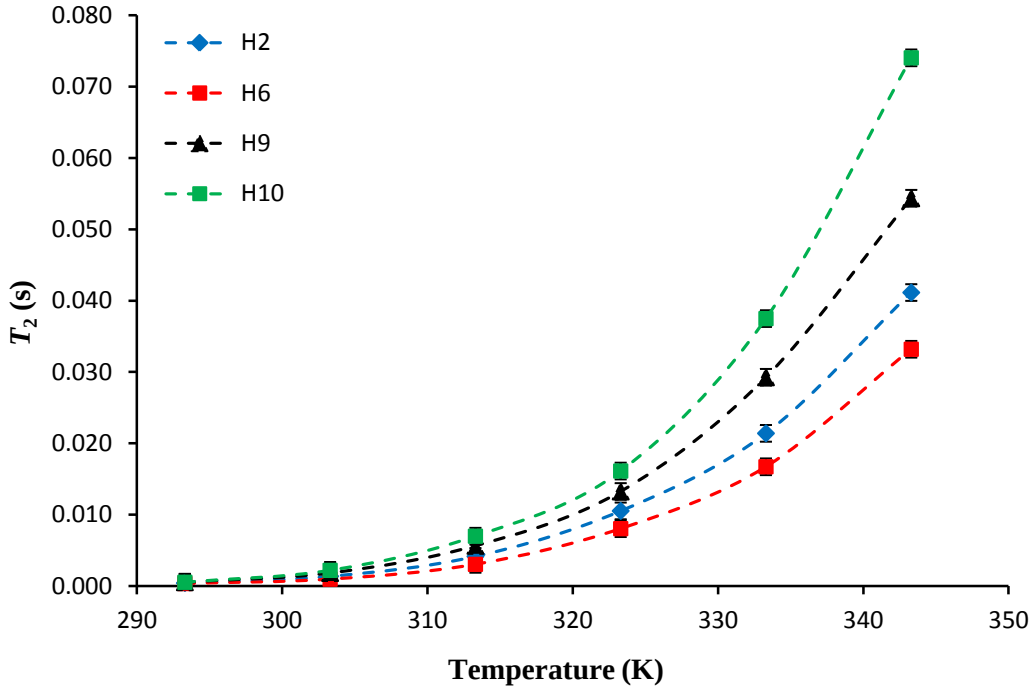

Figure 5.9: ^{1}H-T_2 values of selected BMIM$^+$ protons as a function of temperature for 10% cellulose concentration in BMIMCl-cellulose solution using a 400 MHz NMR spectrometer.

As mentioned before, due to the lower resonance frequency, i.e. 20 MHz, the obtained T_2 relaxation times (*see* Figure 5.10) are averaged over all protons for the BMIM$^+$ ions. This can be verified by comparing the value of T_2 acquired from low field NMR with the average value of the T_2 acquired from high field NMR.

For example, in the case of 10% cellulose solution, at 70 ^{o}C, the average value of T_2 probes by high field NMR is 0.046 ± 0.015 s. This value coincides with the T_2 value acquired from low field NMR which is 0.043 s. It seems that, this value very well represents the average value of T_2 relaxation for all protons constituting the BMIM$^+$. This result is reasonable since the value of T_2 relaxation is not dependent on the frequency of the NMR spectrometer.

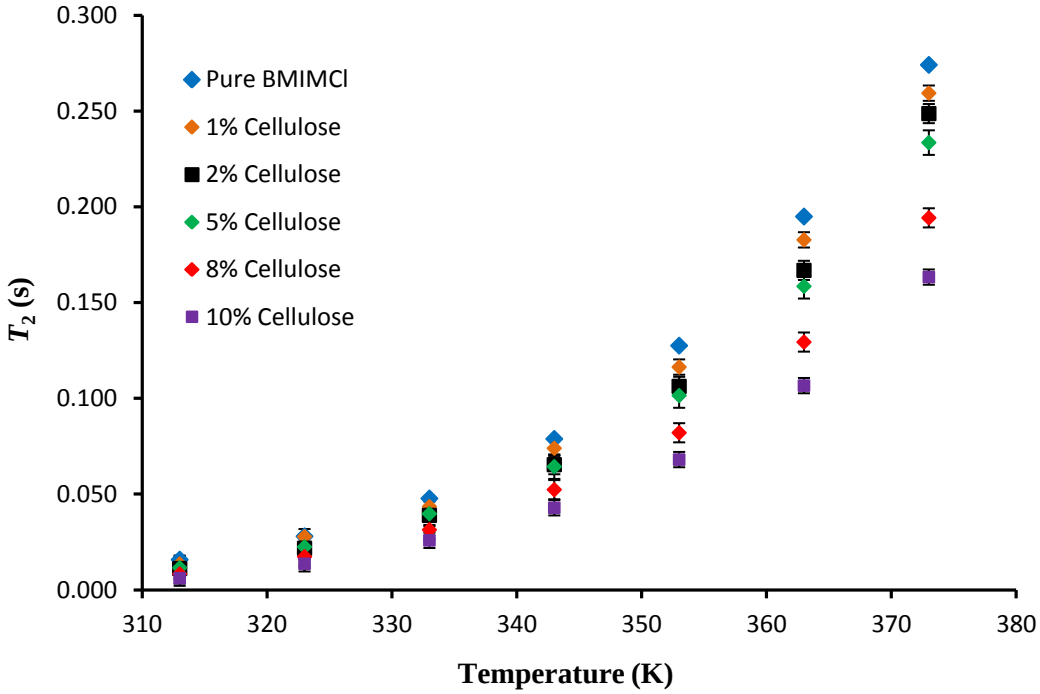

Figure 5.10: Spin-spin relaxation T_2 for neat BMIMCl as well as BMIMCl-cellulose solutions vs. temperature probe by 20 MHz NMR.

5.3.4 Diffusion coefficient measurement

The dependence of diffusivities of $BMIM^+$ on cellulose concentration is shown in Figure 5.11. As can be seen, there is a significant reduction in the diffusivities of $BMIM^+$ ion as the concentration of cellulose is increased. This is generally observed when solvent molecules diffuse in a polymer system. For a polymer solution one of the reasons for the diffusion coefficient to decrease with polymer concentration is the power-law increase of the solution viscosity [172].

To understand the transport properties and polymer-solvent interaction in this system, it is important to describe the relationship between cellulose concentration and the ion diffusivities. One of the most common approaches is Stokes-Einstein. However, due to the physical nature of the BMIMCl and BMIMCl-cellulose solutions is that they are solid at room temperature (melting temperature of BMIMCl is around 70 ^oC), therefore it was not possible to measure the viscosity of this solution below 70 ^oC. Hence, the temperature ranges for diffusion measurement (20-70 ^oC) do not match with the temperature range from the viscosity

measurements (70-130 ^{o}C) therefore the relationship between diffusivities and viscosity using the Stokes-Einstein (SE) equation cannot be analysed.

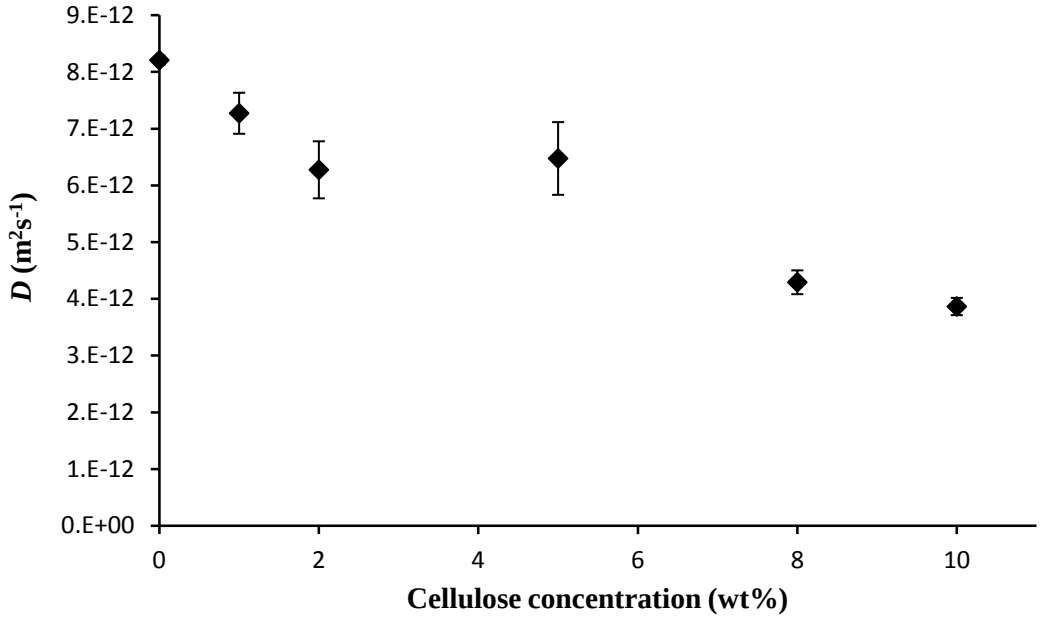

Figure 5.11: Cellulose concentration dependence of $BMIM^{+}$ self-diffusion coefficient at 70 ^{o}C.

In diffusion, there are two processes involved:; 1) a molecule must overcome the interstitial potential; and 2) a vacancy at the nearest lattice is created. A molecule must overcome the interstitial potential, which is given by $E_a[\tau_c]$ regardless of whether the nearest lattice is occupied or not. To create a vacancy at an adjacent lattice, an energy ΔE, is required. For a molecule to diffuse, it needs to overcome these two potential barriers. Therefore, the activation energy for diffusion, Ea[D] can be expressed as [185]:

$$\Delta E_a[D] = E_a[\tau_c] + \Delta E \qquad 5.1$$

To study the temperature dependence of the self-diffusion coefficient, the Arrhenius approach is used. The Arrhenius equation is written as below.

$$D = D_o \exp(-E_a[D]/k_B T) \qquad 5.2$$

In Equation 5.2, k_B is a Boltzmann constant, D_o is a diffusion pre-exponential factor and $E_a[D]$ is interpreted as the average amount of energy that is required to perform translational of the cation to another position. Based on this equation the resulting

self-diffusion coefficient of $BMIM^+$ was fitted using a least-squares analysis in order to determine the value of D_o and diffusion activation energy, $E_a[D]$. For this purpose, the value of D_o across all the samples was treated as a global fitting parameter while the diffusion activation energy, $E_a[D]$ is treated as a variable parameter depending on the concentration of the solutions. It was found that the self-diffusion data across all concentrations are best fit with an Arrhenius equation with the value of diffusion pre-exponential factor, D_o given by 1.05×10^{-1} m^2s^{-1}. The plot of ln D versus reciprocal absolute temperature for all solutions is shown in Figure 5.12. The solid lines represent the theoretical value of the self-diffusion coefficient acquired from least-squares analysis. The value of diffusion activation energy, $E_a[D]$ for each concentration is summarize in Table 5.1.

Table 5.1: Arrhenius parameters fit to the temperature dependences on the $BMIM^+$ self-diffusion coefficient.

Percentage of cellulose concentration (wt%)	**Activation energy, $E_a[D]$ (kJ/mol)**
0	66.2 ± 1
1	66.5 ± 1
2	66.9 ± 1
5	66.8 ± 2
8	67.8 ± 2
10	68.3 ± 2

As seen from Table 5.1, the values of activation energies calculated from self-diffusion coefficients are not significantly altered as the cellulose concentration increases. Thus the Arrhenius description did not suggest an increase in the energy required for diffusive steps as cellulose concentration increases in BMIMCl.

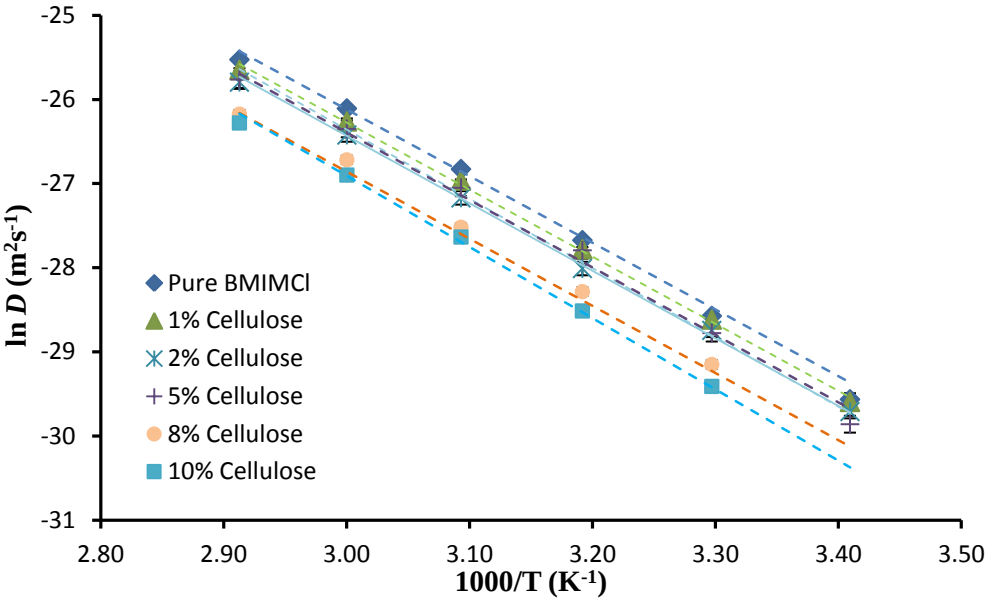

Figure 5.12: $BMIM^+$ self-diffusion coefficient against reciprocal temperature for pure BMIMCl and each BMIMCl-cellulose solution. The solid lines passing through the data points were obtained by performing least-squares analysis and are fits to Equation 5.2. Some error bars are smaller than plotted symbol size.

5.4 Discussion

5.4.1 BPP Analysis

As shown in Figure 5.13, our T_1 and T_2 relaxation values exhibit simple dipolar relaxation behaviour as described by the BPP theory. As can be seen, T_1 shows the transition from extreme narrowing to diffusion limit in the range of temperature studied while T_2 simply decreased with falling temperature as expected. Thus by using BPP theory the experimental value of T_1 and T_2 can be expressed in terms of an isotropic correlation time τ_c for molecular motion.

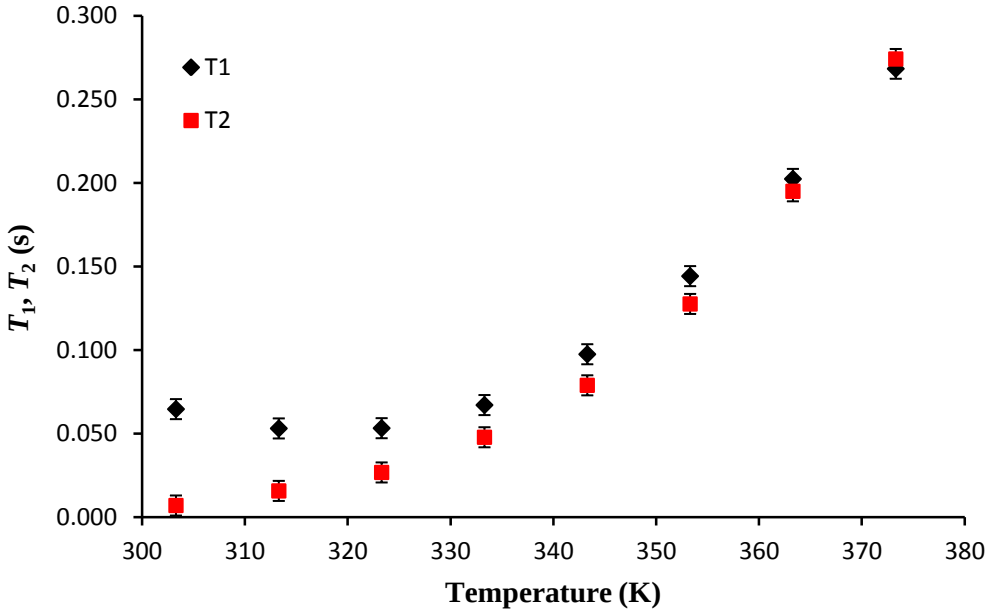

Figure 5.13: The observed T_1 and T_2 values exhibit simple dipolar relaxation as described in BPP theory.

As discussed in Section 3.1.5.4, T_1 and T_2 can be described as [119]:

$$\frac{1}{T_1} = K\left[\frac{\tau_c}{1 + \omega_0{}^2\,\tau_c^2} + \frac{4\tau_c}{1 + 4\omega_o^2\tau_c^2}\right] \qquad 5.3$$

$$\frac{1}{T_2} = \frac{K}{2}\left[3\tau_c + \frac{5\tau_c}{1 + \omega_o^2\,\tau_c^2} + \frac{2\tau_c}{1 + 4\omega_o^2\tau_c^2}\right] \qquad 5.4$$

Due to the terms in parentheses in Equation 5.3, the spin lattice relaxation time, T_1 is minimum when $\omega_o\tau_c = (2\pi\ \upsilon_o)\ \tau_c = 0.616$. In this study, the ^{1}H observed frequency, υ_o is 20 MHz. Therefore, the τ_c at this minimum is simply calculated to be 4.90 x 10^{-9} s. From Figure 5.13, it has been shown that all solutions show a minimum at a similar temperature around 323 ± 5 K ~ (50 ± 5 ^{o}C).

Again, recall Section 3.1.5.4, the relaxation constant, *K* is written as:

$$K = \frac{3}{10}\left(\frac{\mu_o}{4\pi}\right)^2 \gamma^4\hbar^2 \sum_j \frac{1}{r_j^6} \qquad 5.5$$

If the value of T_1 is 0.0542 ± 0.002 s at this minimum point and τ_c is calculated to be 4.90 x 10^{-9} s, it is therefore possible to determine the value of *K*. For this system, it was found that the value of *K* was 1.66 x 10^9 s^{-2}. This value yields the effective inter-proton distance, r_j equivalent to 2.16 Å. The effective inter-proton distance calculated from this equation is also close to the value of inter-distance proton (2.33 Å) obtained from the slope of $1/T_1$ against η/T of EMIMAc-DMSO solution (*see* Section 4.4.4). Again this value lies in between the actual inter-distance protons in aliphatic and aromatic protons which are 1.77 Å and 2.48 Å respectively [171].

Knowing the *K* value, both the observed values of T_1 and T_2 were then fitted simultaneously using a least-squares analysis to determine the τ_c across all temperatures and concentrations studied. Since both NMR relaxation times exhibit simple dipolar relaxation, therefore only single correlation time and activation energy is responsible for the molecular motion in each system. With the narrow range of the temperatures studied, the system is presumed to follow Arrhenius behaviour (*recall* Section 3.1.5.4).

$$\tau_c = \tau_o \exp\left(\frac{E_a[\tau_c]}{k_B T}\right) \qquad 5.6$$

The parameters $E_a[\tau_c]$ and τ_o are the correlation time activation energy and correlation time pre-exponential factor respectively. For this purpose the value of τ_o across all the sample will be treated as one global fitting parameter while the correlation time activation energy, $E_a[\tau_c]$ for each concentration is treated as a variable parameter.

From a least square analysis, it was found that the correlation time, τ_c for all concentrations were best fit with an Arrhenius equation with the value of pre-exponential factor, τ_o is 2.92 x 10^{-16} s. The values of T_1 and T_2 calculated using the BPP equation were also obtained. The comparison of experimental and fitting value of T_1 and T_2 are shown in Figure 5.14.

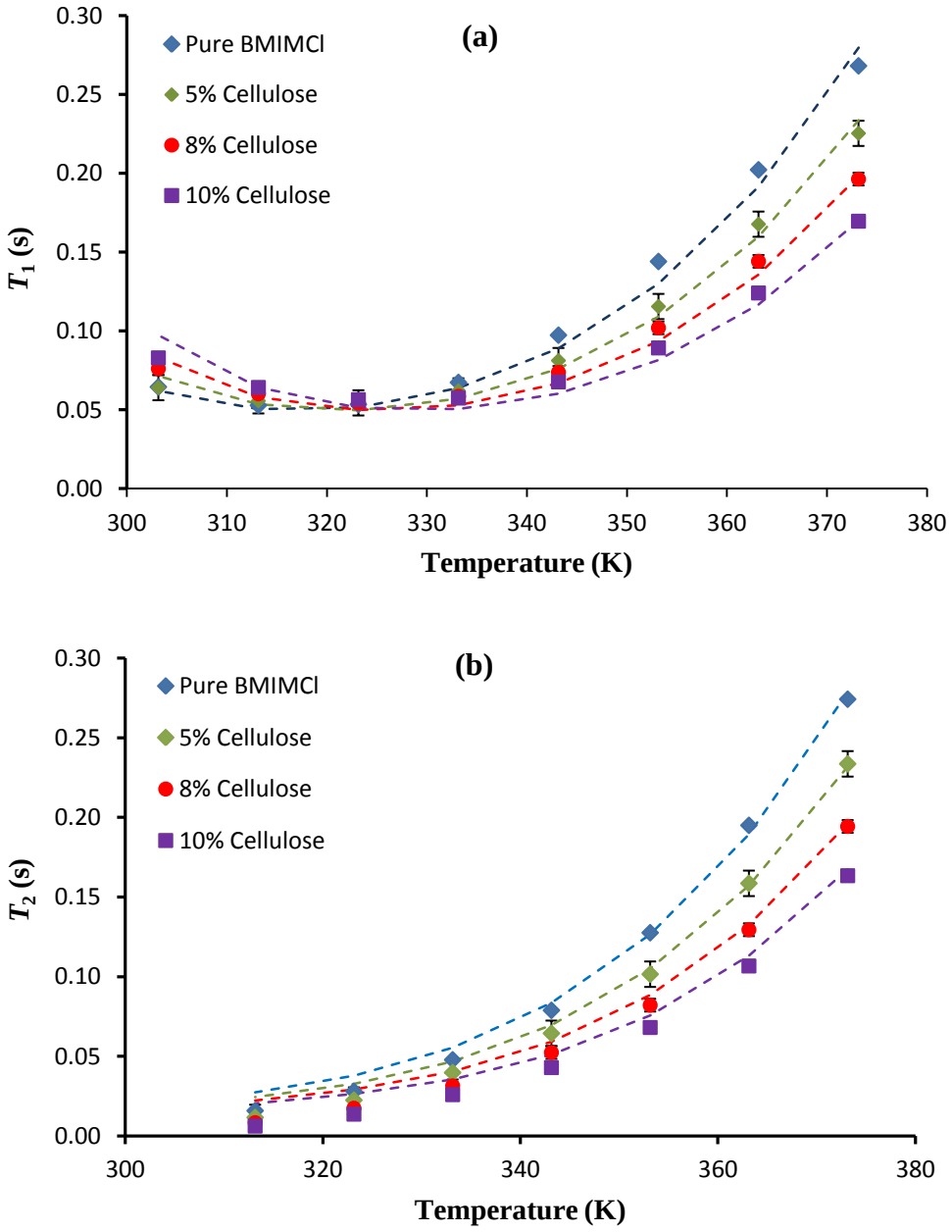

Figure 5.14: The observed a) T_1 and b) T_2 values of the imidazolium cation. The dotted lines passing through the data points were obtained by performing a least-squares fit. Only the T_1 and T_2 of pure BMIMCl and 5%, 8% and 10% of cellulose concentration are shown as examples. Some error bars are smaller than plotted symbol size.

The value of activation energies, $E_a[\tau_c]$ for each system are summarized in Table 5.2:

Table 5.2: The value of activation energies, $E_a[\tau_c]$ for pure BMIMCl and BMIMCl-cellulose solutions.

Percentage of cellulose concentration (wt%)	**Activation energy, $E_a[\tau_c]$ (kJ/mol)**
0	43.9
1	44.1
2	44.3
5	44.4
8	45.0
10	45.0

From Table 5.2, it can be readily seen that the activation energies are almost constant with the increase in cellulose concentration. This is parallel to the value of activation energies determined from diffusion coefficients where the values do not vary over the whole concentration studied.

It worth noting that at the same cellulose concentration, the activation energies of correlation time, $E_a[\tau_c]$ is always smaller than the activation energies of diffusion, $E_a[D]$. This show that the approximation in Equation 5.1 correctly relating the $E_a[\tau_c]$ and $E_a[D]$. Details about the relationship between τ_c and D will be explained in a subsequent section.

The activation energies of correlation time are also compared with activation energies of viscosity from previous studies [172]. From rheological study, it was found that the activation energy increases monotonously with cellulose concentration. It should be noted that these two activation energies largely differ: $E_a(\tau_c)$ = 44.5 ± 0.6 kJ/mol across all cellulose concentrations, whereas $E_a[\eta]$ ranges from 42 kJ/mol for pure BMIMCl to 62 kJ/mol for BMIMCl-cellulose solution with 10% cellulose concentration [172]. This suggests that rotational motion of $BMIM^+$ in pure BMIMCl and BMIMCl-cellulose solutions has little to do with the shear viscosity of the solutions.

In other words, it suggests that the changes in T_1 and T_2 relaxation are not predominantly caused by the viscosity of the solution. This is opposite to the findings of Remsing et al., that have pointed out the decreasing of ^{13}C relaxation rates of the imidazolium carbons with carbohydrates concentration is due to the increase of solution viscosity, which leads to the conclusion that cation did not play a role in cellulose dissolution [173]. For that reason it is possible to suggest that the changes of T_1 and T_2 relaxation in our results were not predominantly caused by the changes of viscosity in polymer solutions.

5.4.2 NMR Relaxometry-Viscosity

Using a model proposed by Bloembergen, Purcell and Pound the microscopic motion that is associated with rotational and translational motions can be related to the macroscopic properties of the liquids [119]. For a spherical particle undergoing isotropic rotation, its rotational correlation time, τ_{rot}, is expressed in terms of the viscosity based on the Stokes-Einstein-Debye (SED) formula (*recall* Section 3.1.5.4) which is given by:

$$\tau_{rot} = \frac{4\pi {R_H}^3 \eta}{3k_B T} = \frac{V\eta}{k_B T} \qquad 5.7$$

Nevertheless, comparison of experimental data with correlation time calculated from Equation 5.7 is generally unsuccessful as the calculated correlation times (SED) are generally too large by a factor of 10 [186-188].

For correlation times determined by NMR relaxation times, the relationship between τ_c and temperature dependence of viscosity is given by Equation 5.8 [120]:

$$\tau_c = \tau_o + (\eta\tau_{red}/T) \qquad 5.8$$

$\tau_{red} = V/k_B$ is a reduced correlation time which depends only upon the size and molecular shape of the molecule. In Figure 5.15, a plot correlation time, τ_c, for $BMIM^+$ at cellulose concentration versus viscosity function η/T is shown. τ_c shows a linear relationship with viscosity in pure BMIMCl and BMIMCl-cellulose solutions

with the R^2 lies between 0.97 – 0.99. All the straight lines in Figure 5.15 have the same intercept at, $\tau_o = 3.0 \pm 0.3 \times 10^{-10}$ s.

τ_{red} which was represented by the slope of the of the graph, can be analysed to provide a value of hydrodynamic radius, R_H. For pure BMIMCl and 10% cellulose, analysis of the slope gave a value of R_H for $BMIM^+$ 1.88 Å and 0.32 Å respectively. However, the value of R_H obtained from this type of analysis is somewhat small compared to the expected value which ranges from 3.07 to 3.60 Å calculated from molar volume and gas phase calculation [22, 189]. This discrepancy suggests that the bulk viscosity, η, is not the effective viscosity at the surface of a molecule. Nevertheless this unrealistic value can be corrected to a more reasonable value using frictional correction factors [120]. Though the slope of the graph does not give the actual value of the radius of rotating molecules, R_H, it is still worth noting that in all systems, the microscopic dynamic properties are always proportional to the macroscopic properties of the solution. This suggested that, in solutions the bulk viscosity, η is best replaced by a microviscosity, $\eta_\mu = f_\mu \eta$, where f_μ is a constant that is the microviscosity correction factor, dependent on the boundary conditions of the system.

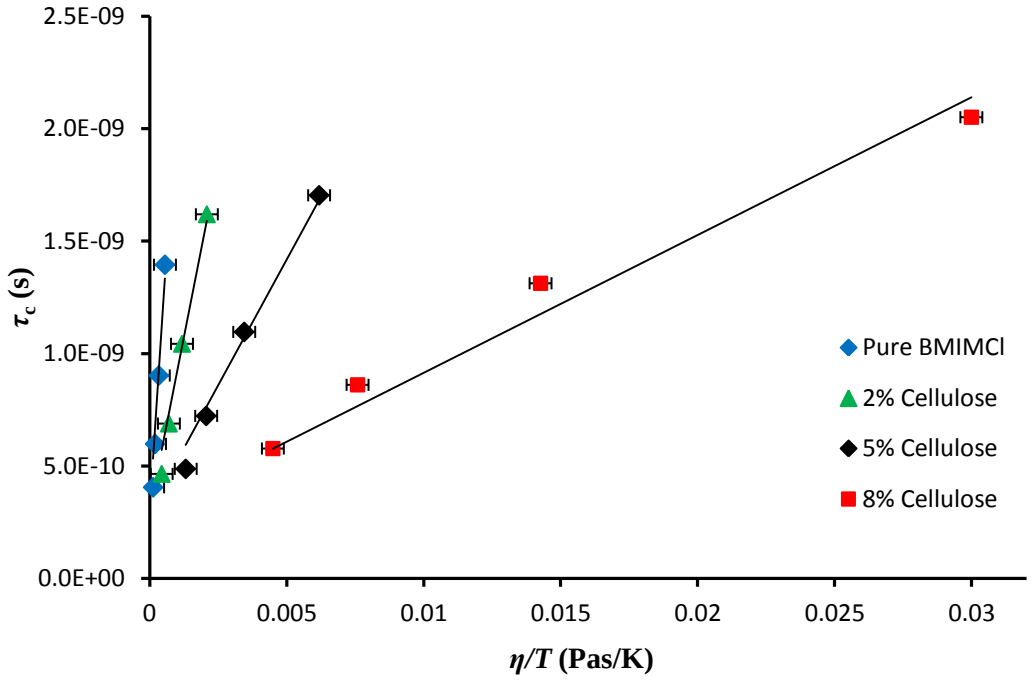

Figure 5.15: Correlation time, τ_c against viscosity over temperature. Pure BMIMCl and three selected BMIMCl-cellulose solutions are shown as an example. The solid lines are fit to Equation 5.8 and have the same intercept at $3.0 \pm 0.3 \times 10^{-10}$ s.

The Hu-Zwanzig (HZ) model introduces a rotational microviscosity correction factor f_{HZ} which is dependent on the shape of the molecule [190]. Many of the ionic liquid molecules are not spherical and often regarded as prolate (cigar-shaped; $a = b < c$) or oblate (pancake-shape; $a < b = c$) spheroids that result in anisotropic rotational motion. Hu-Zwanzig (HZ) slipping boundary model takes into account the rotational friction coefficient of both prolate and oblate spheroids over a range of a/c values [190].

In the case of the butyl side chain in the BMIMCl, it seems reasonable to presume that $BMIM^+$ cation has a prolate spheroid shape that undergoes anisotropic rotational motion. Based on a density functional study of molecular structure of 1-Ethyl-3-Methylimidazolium Acetate, (EMIMAc) by Dhumal et al. [191], it is possible to estimate the distance from the methyl group adjacent to imidazolium ring to the end of the butyl side chain (*see* Figure 5.16). The details of the bond distance value are summarized in Table 5.3. From estimation, it is found that the distance is approximately 12 Å. The other axes are estimated to be 3.2 Å. The ratio of min axis

to max axis (0.27) from these values results in a f_{slip} correction factor of 0.12 [190]. Introduction of correction factor, f_{slip} would effectively increase the R_H value (SED) of $BMIM^+$ for pure BMIMCl from 1.88 Å to 3.80 Å. This increment corresponds to the 106 % improvement of R_H (SED) from the theoretical gas-phase R_H value (3.60 Å) [189]. Based on this result the introduction of Hu-Zwanzig microviscosity correction factor, f_{HZ}, using slip boundary conditions has been successfully applied to rotational motion of $BMIM^+$ in pure BMIMCl solution.

For the system which contained solute, introduction of microviscosity correction factor f_{GW} introduced by Gierer and Wirtz is more appropriate as this model takes into account the ratio of rotating molecule radius to environment molecule radius in the system. According to this model, if the environment molecules are too large, the rotation molecules 'rattle' in the interstices between environment molecules and hence the frictional resistance to rotation is very small. In our system, the presence of large cellulose molecules might provide a slipping boundary condition to BMIMCl molecules in which the BMIMCl molecules rattle in the interstices and experience less friction. In this case, the microviscosity factor f_{GW} can have a value of 1/10 up to 1/50 if the size of environment molecules is two to ten times larger than the rotating molecule.

Table 5.3: Bond distance (in Å) in $BMIM^+$ cation.

	Distance (Å).	**References**
N1 - C2	1.338	[191]
C2 - N3	1.339	[191]
N3 - C4	1.383	[191]
C4 - C5	1.364	[191]
N3 - C6	1.470	[191]
N1 - C7	1.483	[191]
C7 - C8	1.526	[191]
C8 - C9	1.526	a
C9 - C10	1.526	a
C2 - H	1.079	[191]
C4 - H	1.079	[191]
C5 - H	1.078	[191]
C6 - H	1.091	[191]
C10 -H	1.093	b
N1 - N3	2.218	c
H2 - (C4 - C5)	2.121	c

[a] Predicted from C7 - C8, [b] Predicted from C8 - H from ref [27], [c] Calculated from the geometry of molecule.

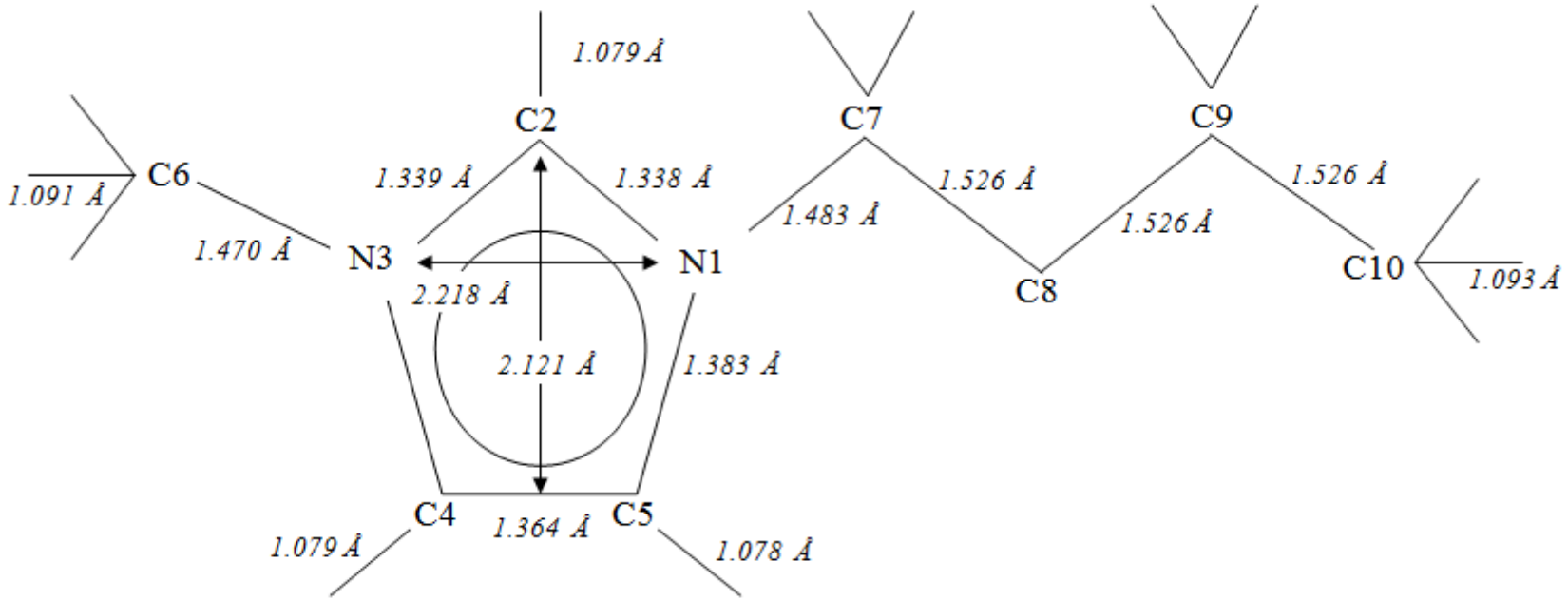

Figure 5.16: Sketch of the structure of the $BMIM^+$ cation along with the bond distance between atoms as summarized from Table 5.3.

In the Arrhenius and SED equations, the value of τ_o can be estimated independently from classical free rotor theory and is given by the corresponding expression (*recall* Section 3.1.5.4),

$$\tau_o = \left(\frac{2\pi}{9}\right)\sqrt{\frac{I_m}{k_B T}} \qquad 5.9$$

In this equation, I_m is the moment of inertia. Taking the value of the moment of inertia for $BMIM^+$ from the literature, 1.3 x 10^{-45} kgm^2 [192], it is then possible to calculate the value of τ_o using free rotor theory. The corresponding values of τ_o determined from the Arrhenius equation, Stokes-Einstein-Debye equation and free rotor theory are listed in Table 5.4.

Table 5.4: The value of τ_o determined from three different methods.

Method	**τ_o (s)**
Least square analysis (Arrhenius equation) (*see* Figure 5.14)	2.92 x10^{-16}
Stokes-Einstein-Debye (*see* Figure 5.15)	3.0 x 10^{-10}
Free rotor theory (*see* Equation 5.9)	3.92 x 10^{-13}

As shown in Table 5.4, the value of τ_o obtained from the intercept of graph τ_c against η/T is three to six orders of magnitude larger than the value of τ_o determined from other methods. The largest value of τ_o obtained from Figure 5.15 might be explained by the existence of Coulomb interactions between $BMIM^+$ and its counterpart Cl^- which cause the molecular motion to be much slower. IL which consists solely of ions should be expected to have strong interaction/bonding between them. Therefore, during the rotational process $BMIM^+$ has to drag the Cl^- together and rotate as a complex rather than a single ion. In addition, other studies also suggested that there is an existence of dynamical heterogeneities in IL which would cause SED not be valid for this system [193].

For the value of τ_o calculated from free rotor theory, it is in agreement with the value of τ_o from the literature study by Boeré et al. According to the authors, in cases where the correlation time, τ_c exceeds 10 ps, the pre-exponential factors, τ_o

estimated from free rotor theory may be less than 1 ps [120]. This is in agreement with our finding where the correlation time τ_c is three order magnitude larger (ns), and the value of τ_o calculated from free rotor theory is less than 1 ps.

If compared the values of τ_o calculated from classical free rotor theory with the value of τ_o determined from the least-square analysis, it is clearly show that the calculated values (free rotor theory) is three orders of magnitude larger the than experimental value. Comparison of experimental data with τ_o calculated from free rotor theory is generally unsuccessful as the theoretical correlation times are generally too large by two or three order magnitude [183].

5.4.3 Self-Diffusion Coefficients and Reorientational Correlation Times

Here, a derivation of the relation between τ_o and D_o is presented. Using the Stokes-Einstein (SE) relation that has been discussed in Section 3.2.2, the translational diffusion of the molecules is expressed in terms of bulk viscosity:

$$D = \frac{k_B T}{6\pi\eta R_H} \qquad 5.10$$

Now, the correlation time of the solvent is also expressed in terms of viscosity by invoking the Stokes-Einstein-Debye (SED) relation.

$$\tau_c = \frac{4\pi R_H^3 \eta}{3k_B T}$$

Combining the SE and SED equations, the viscosity term is eliminated and correlation time, τ_c is only correlated to translational diffusion by hydrodynamic radius and is given by:

$$\tau_c = \frac{2R_H^2}{9D} \qquad 5.11$$

Based on this relationship (Equation 5.11) a graph of τ_c against 1/*D* has been plotted. As can be seen from Figure 5.17, at higher diffusion coefficient, τ_c shows a linear dependence with 1/*D*. The most important feature observed in Figure 5.17 is the correlation time collapsed in one master curve with reciprocal self-diffusion

coefficient. This suggested that from a qualitative point of view, the rotational correlation time, τ_c can be correlated to translational diffusion.

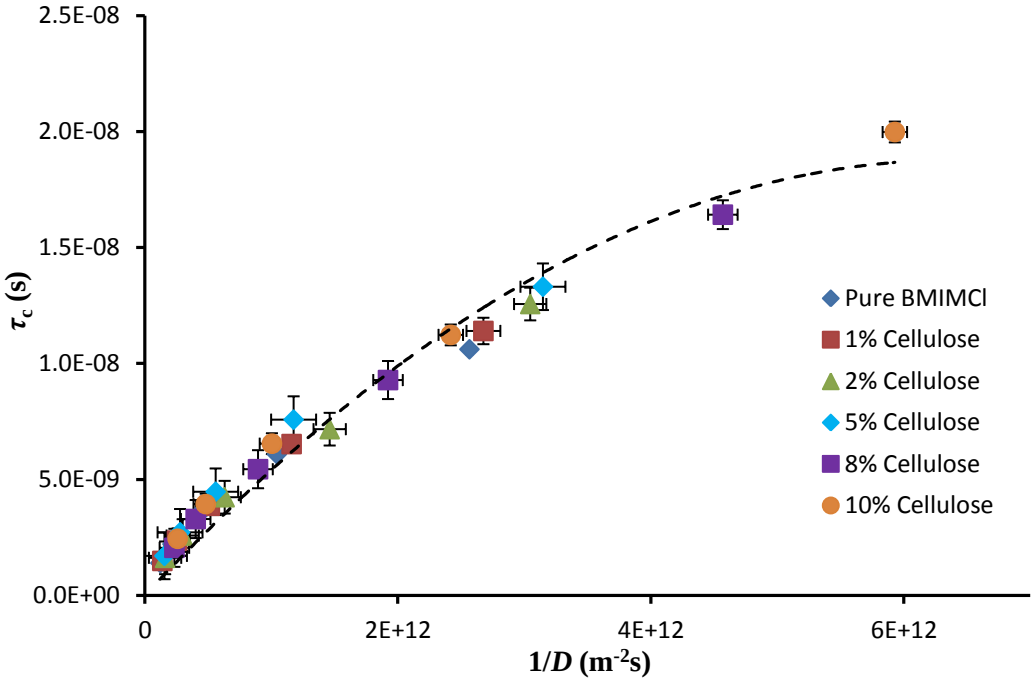

Figure 5.17: Correlation time, τ_c against reciprocal of self-diffusion coefficient of $BMIM^+$ for all systems.

If both τ_c and D terms are expressed based on the Arrhenius equation, Equation 5.11 therefore can be re-written as:

$$\tau_o exp\left(\frac{E_a[\tau_c]}{k_B T}\right) = \frac{2}{9} R_H^2 \frac{1}{D_o} exp\left(\frac{E_a[D]}{k_B T}\right) \qquad 5.12$$

Since the diffusion activation energy, $E_a[D]$ is a summation of activation energy for NMR relaxation and ΔE,

$$\tau_o exp\left(\frac{E_a[\tau_c]}{k_B T}\right) = \frac{2}{9} R_H^2 \frac{1}{D_o} exp\left(\left(\frac{E_a[\tau_c]}{k_B T}\right) + \left(\frac{\Delta E}{k_B T}\right)\right) \qquad 5.13$$

Simplifying Equation 5.13, one obtains the relationship between D_o and τ_o expressed by:

$$D_o = \frac{2}{9} R_H^2 \frac{1}{\tau_o} exp\left(\frac{\Delta E}{k_B T}\right) \qquad 5.14$$

This relationship depends on the hydrodynamic radius of the molecules and the different activation energy between diffusion and rotation.

An attempt has been made to verify this relationship (Equation 5.14). From our study, the values of τ_o and D_o of $BMIM^+$ from a least squares analysis is given by 2.92 x 10^{-16} s and 1.05 x 10^{-1} m^2/s respectively. If we take the average temperature of 333 K and hydrodynamic radius of $BMIM^+$, R_H is determined from the empirical equation (*see* Equation 3.45) giving a value of 3.07 Å, therefore it is possible to determine the value of ΔE. Based on Equation 5.14, and the value of ΔE for $BMIM^+$ is found to be 20.2 kJ/mol. This value, which has been independently determined from the value of τ_o and D_o, matches reasonably well with the ΔE of $BMIM^+$ 22 ± 1 kJ/mol) found from the two separate Arrhenius analyses. This shows that the derivation above is correctly relating the diffusion to the correlation time and vice versa.

5.5 Conclusion

Solutions of BMIMCl-cellulose have been investigated across a range of cellulose concentrations and temperatures using NMR- spectroscopy and relaxometry, diffusion and viscosity measurements.

The change in ^{1}H chemical shift position $\Delta\delta$ is consistent with solutions of EMIMAc-cellulose from our previous study [194]. The change in chemical shift revealed that the resonance of imidazolium ring protons had the strongest dependencies on cellulose concentration with them moving upfield on the addition of cellulose. The least dependence of $\Delta\delta$ for alkyl protons on cellulose concentration indicated that their contribution in cellulose dissolution was negligible. This is consistent with the non-polar region of the alkyl chain proton itself which does not interact with the hydroxyls group of cellulose.

Proton spin-lattice relaxation, T_1 and spin-spin relaxation T_2 times were also measured using low field (20 MHz) NMR. Both T_1 and T_2 of pure BMIMCl and BMIMCl-cellulose solutions were found to be well described by the BPP theory. Using BPP theory, both relaxation times T_1 and T_2 can be expressed in terms of an isotropic correlation time τ_c for molecular motion. The minimum was observed in T_1 relaxation at temperatures around 323 ± K ~ (50 ± 5 ^{o}C). This transition point is consistent with the melting point of BMIMCl (41 ^{o}C). The fitting of T_1 and T_2 data using a least squares analysis with τ_o is treated as a global fitting parameter across all cellulose concentration results in T_1 and T_2 having only a single activation energy for each concentration. However, the activation energies were found to be constant over the whole cellulose concentration studied.

The correlation time τ_c obtained from T_1 and T_2 relaxation was compared with the macroscopic viscosity data and found to follow Equation 5.8. Analysis of the slope from the graph of pure BMIMCl results in an unrealistic hydrodynamic radius, R_H (1.88 Å) of $BMIM^+$ cation. Introduction of correction factor, f_{slip} from the Hu-Zwanzig (HZ) model result gave an improvement to the R_H (SED) from 1.88 Å to 3.80 Å. The corrected hydrodynamic radius, R_H is very close to the theoretical gas-phase R_H value (3.60 Å). In the case of ILs especially, the size of molecules

should be analysed based on their geometry, as the geometry of the molecules provides different effective viscosity at their surface.

Determination of τ_o from the intercept of graph τ_c against η/T shows a discrepancy from the τ_o obtained from Arrhenius analysis and τ_o using the free rotor model (*see* Equation 5.9). The discrepancy between these values can be explained by the existence of Coulomb interaction between $BMIM^+$ cation and Cl^- anion as the determination of τ_o from the intercept of the graph takes into account the contribution from viscosity which results from strong interaction/bonding between $BMIM^+$ and Cl^-.

Diffusion activation energies of $BMIM^+$ were found not to change significantly as the cellulose concentration is increased. This is consistent with the activation energies calculated from NMR relaxation. Thus the Arrhenius description did not suggest an increase in the energy required for diffusive steps and rotational motion as cellulose concentration increases in BMIMCl. Both results showed a discrepancy from what has been observed in viscosity studies which showed an increase of activation energy with cellulose concentration. This indicates that rotational reorientation of $BMIM^+$ cannot be simply interpreted by means of the classical hydrodynamic theory. However, it is worth noting that the diffusion activation energy, $E_a[D]$ is always larger than the correlation time activation energy, $E_a[\tau_c]$.

In this study, the relationship between D_o and τ_o has been derived (*see* Equation 5.14). This relationship which only depends on the hydrodynamic radius of the molecules and the difference of activation energy between diffusion and correlation time, has been verified using the experimental data. It was found that the ΔE for $BMIM^+$ (20.2 kJ/mol) which has been independently determined from D_o and τ_o matched reasonably well with the ΔE of $BMIM^+$ (21.6 ± 0.9 kJ/mol) found from a least-squares analysis. This shows that the derivation above is correctly relating the diffusion to the correlation time and vice versa within 1 order of magnitude.

From NMR relaxometry-viscosity analysis, it is suggested that introduction of microviscosity correction factor, f_μ is needed to account for the shear viscosity dependence of molecular liquids. In solutions, the bulk viscosity, η is then best

replaced by a microviscosity, $\eta_\mu = f_\mu \eta$. Introduction of microviscosity prefactor, f_{HZ}, which was interpreted by Hu and Zwanzig using slip boundary conditions, has been successfully applied to rotational motion of $BMIM^+$ in our cellulose solutions.

Chapter 6
Glucose, Cellobiose and Cellulose Solvation in the Ionic Liquid 1-Ethyl-3-Methylimidazoilum Acetate

6.1 Introduction

Different types of carbohydrate have been used to study the mechanism of solvation in ionic liquids (ILs). This ranges from the most simple monosaccharide, glucose to the long chain polysaccharide, cellulose. Among all those carbohydrates, glucose and cellobiose have been frequently used to study the mechanism of cellulose dissolution in IL owing to the fact that they are the building blocks of cellulose. Many studies have been carried out either by experiment or simulation, to have better understanding of the dissolution process of these carbohydrates in ILs. Among the techniques that have been employed to accomplish this are molecular dynamic (MD) simulations. According to these studies, ILs solvate carbohydrates through the formation of hydrogen bonds between the IL anions and the hydroxyl groups of the sugar solutes. Here, the role of anion in this process is clear. However, opinions about the role of cation are divided; some say that the cation does not interact with the cellulose unit, some say that strong hydrogen bonding between them exists.

In this study, three different types of carbohydrates have been employed to further investigate the mechanism of carbohydrates solvation in ILs at the macrocospic and microscopic levels to probe the nature of solute-solvent interactions. Thus in order to accomplish this, glucose and cellobiose were dissolved at room temperature in ionic liquid 1-Ethyl-3-Methylimidazolium Acetate (EMIMAc). For this purpose, ^{1}H NMR relaxation times (T_1 and T_2), self-diffusion coefficients and viscosity of these binary mixtures in the range of 0-15 wt% have been measured over a range of temperatures. This study was then compared with our previous work on cellulose solvation in EMIMAc [194]. The understanding of the concentration-dependent diffusion and relaxation times of different types of carbohydrates dissolved in ILs is an essential step toward understanding their effect on the dynamics of the ions in ILs.

6.2 Experimental Methods

6.2.1 Materials and Sample Preparation:

Glucose and cellobiose were purchased from Sigma Aldrich and were used without further purification. In this work pure EMIMAc and a series of five EMIMAc-glucose and five EMIMAc-cellobiose (1%, 3%, 5%, 10% and 15% by weight fraction) binary mixtures were prepared. Both EMIMAc and glucose/cellobiose were mixed and stirred in a small container. After 24 hours, the mixtures were then transferred into 5 mm NMR tubes. Other preparation procedures are similar to those mentioned in the previous chapter.

Concentration of carbohydrate dissolved in EMIMAc was calculated using the equation below:

$$C_{carb} = \frac{m_{carb}}{m_{carb} + m_{EMIMAc}} .100\%$$

where C_{carb} is the concentration of carbohydrate, m_{carb} and m_{EMIMAC} are the mass of carbohydrates dissolved in EMIMAc and the mass of EMIMAc respectively.

6.2.1.1 Viscosity

The Bohlin Gemini Advanced Rheometer equipped, with 4^{o}-40 mm cone plate was used to measure the viscosity of the solutions. Shear rate dependent viscosity was measured at a temperature ranging from 10-100 °C in 10 °C increments. A thin film of low viscosity silicon oil was placed around the borders of the measuring cell in order to prevent moisture uptake and evaporation at higher temperatures.

6.2.1.2 NMR Relaxometry

The ^{1}H-T_1 and ^{1}H-T_2 values EMIMAc/carbohydrate solutions were obtained as a function of temperature in the range from 30 ^{o}C to 100 ^{o}C. The protocols and parameters used for this acquisition are similar to those mentioned in the previous chapter (*see* Section 4.2.1.3).

6.2.1.3 NMR Diffusion

Diffusion coefficients for ions in EMIMAc-carbohydrate mixtures were obtained using the ^{1}H-detected PFG-STE bipolar sequence that has been explained in detail in

Chapter 3. The self-diffusion coefficient for $EMIM^+$ and Ac^- in EMIMAc/carbohydrates solutions was obtained as a function of temperature in the range from 20 ^oC to 70 ^oC. The protocols and parameters used for this acquisition are similar to those mentioned in the previous chapter (*see* Section 4.2.1.4).

6.3 Results

6.3.1 Viscosity

The flow of glucose/EMIMAc solutions of various concentrations and at various temperatures are shown in Figure 6.1. Similar dependence was obtained for cellobiose/EMIMAc solutions. A Newtonian plateau was observed at all concentrations and temperatures for both solutions. As is to be expected the viscosity of both EMIMAc/glucose and EMIMAc/cellobiose increased with solute concentration and reduced as the temperature was elevated.

It is worth noting that despite their different chemical composition, both EMIMAc/glucose and EMIMAc/cellobiose viscosities are similar within an experimental error over the concentrations studied. This indicates that at macroscopic level the effect of glucose monomer and cellobiose dimer dispersed in EMIMAc cannot be distinguished. In Figure 6.2 the dependence of glucose concentration on viscosity at 10 – 100 ^oC temperature is shown.

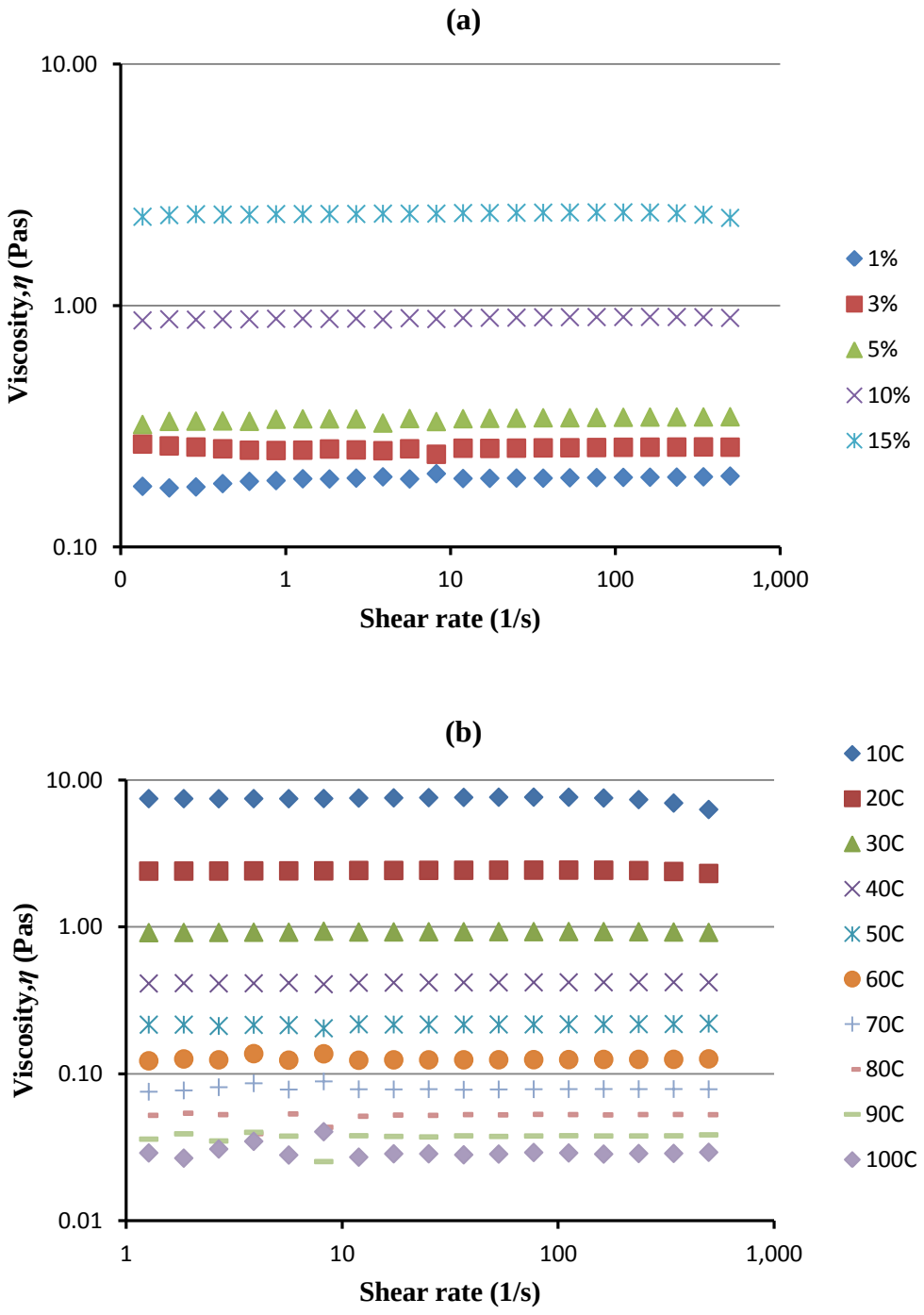

Figure 6.1: Viscosity dependence of shear rate of a) EMIMAc/glucose solutions at 20 ^{o}C and b) 15% glucose in EMIMAc at 10-100 ^{o}C. Newtonian plateau was observed for all concentrations and temperatures studied. EMIMAc/glucose solution is shown as an example. Experimental errors are of the size of the symbols.

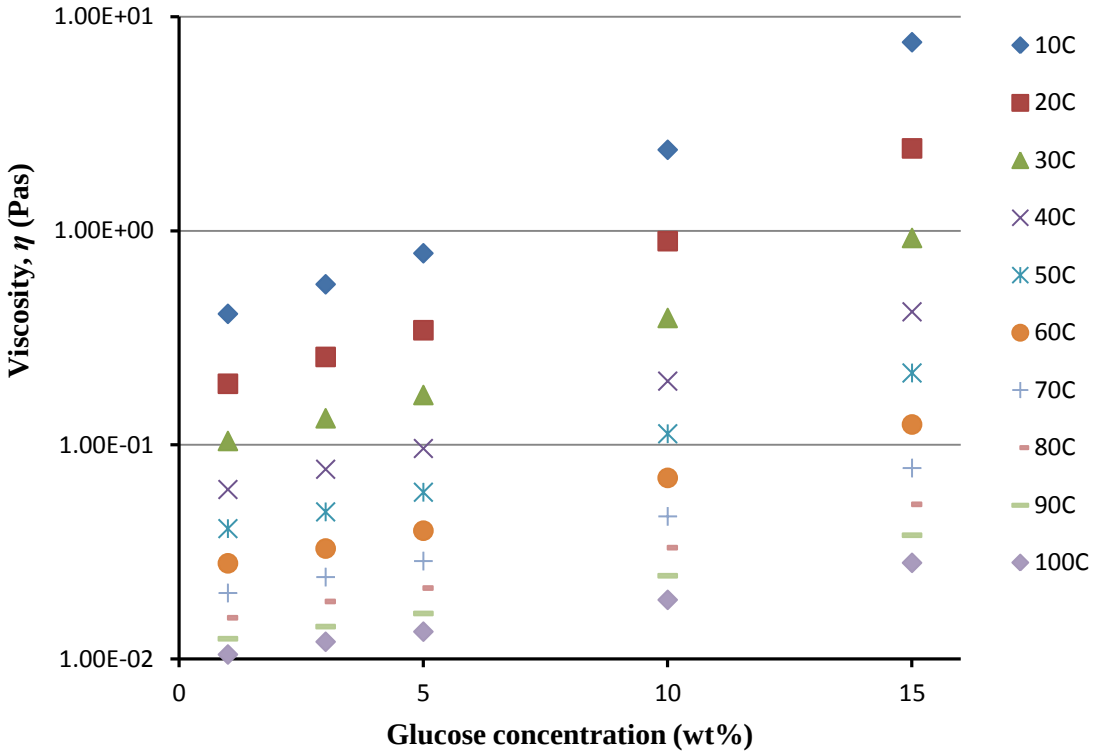

Figure 6.2: Viscosity of EMIMAc/glucose solutions as a function glucose concentration (wt%). The viscosity of the solutions increases with glucose concentration. Experimental errors are of the size of the symbols.

By combining the viscosity data of cellulose/EMIMAc solutions into one graph together with viscosity of these solutions allowed us to make a direct comparison of how these carbohydrates affect the transport properties of solutions. The viscosity data for the EMIMAc/cellulose have been taken from a publication by Sescousse et al. [172]. In Figure 6.3, the zero-shear-rate viscosity of all carbohydrates as a function of concentration at 50 ^{o}C is shown.

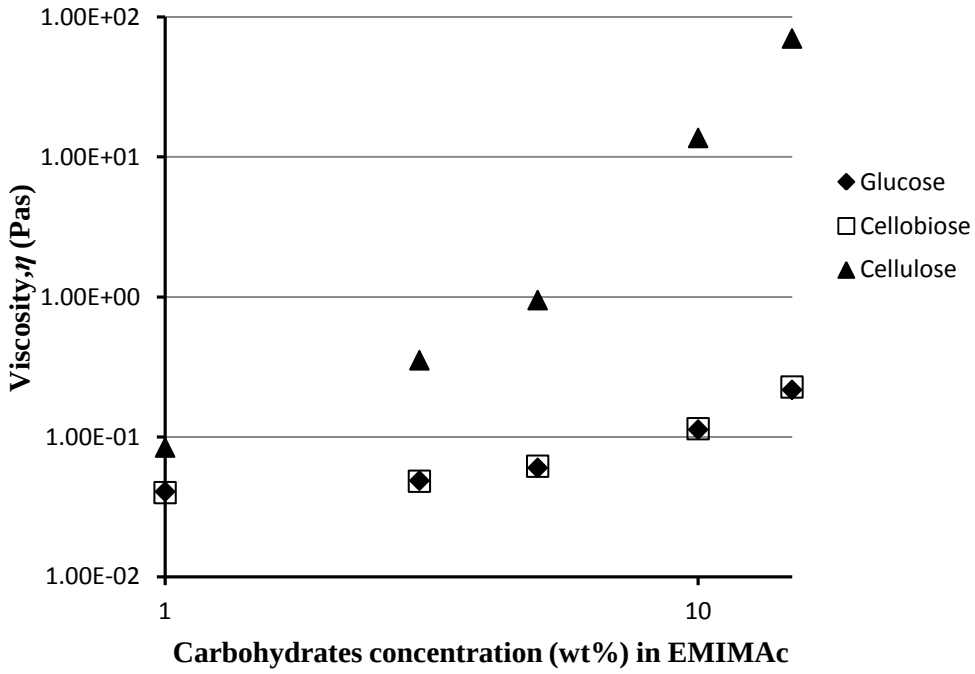

Figure 6.3: Zero-shear-rate viscosity as a function of carbohydrates concentration. Viscosity of EMIMAc/glucose and EMIMAc/cellobiose solutions are similar within experimental error. Experimental errors are of the size of the symbols.

From the graph it is clearly shown that the influence of glucose and cellobiose concentration on viscosity of EMIMAc/glucose and EMIMAc/cellobiose solutions are similar within experimental error. Conversely, the presence of cellulose in EMIMAc formed highly viscous solutions which indicated that cellulose is the most effective molecule for increasing the zero shear rate viscosity. At high concentration of solute, the viscosity of EMIMAc/glucose and EMIMAc/cellobiose solutions can be approximated by linear dependence while EMIMAc/cellulose solution can be approximated by a power law, $\eta \sim C^n$. The power law dependence of cellulose at higher concentrations have been reported previously by various authors for cellulose dissolved in ILs [172].

To study the temperature dependence of viscosity, the Arrhenius approach was used. The Arrhenius equation is written as below:

$$\eta = \eta_o exp\left(\frac{E_a[\eta]}{k_B T}\right) \qquad 6.1$$

where k_B is a Boltzmann constant and $E_a[\eta]$ is interpreted as the activation energy of viscous flow. The plot of ln η versus reciprocal absolute temperature for both solutions is shown in Figure 6.4. The viscosity of the solutions did not obey the Arrhenius equation, instead ln η vs. $1/T$ showed a non-linear dependence. Thus, the activation energies for all concentrations were calculated from the gradient. (*see* Figure 6.4) across three ranges of temperatures: 283-313 K; 313-343 K; and 343-373 K. The activation energies for each range are shown in Figure 6.5.

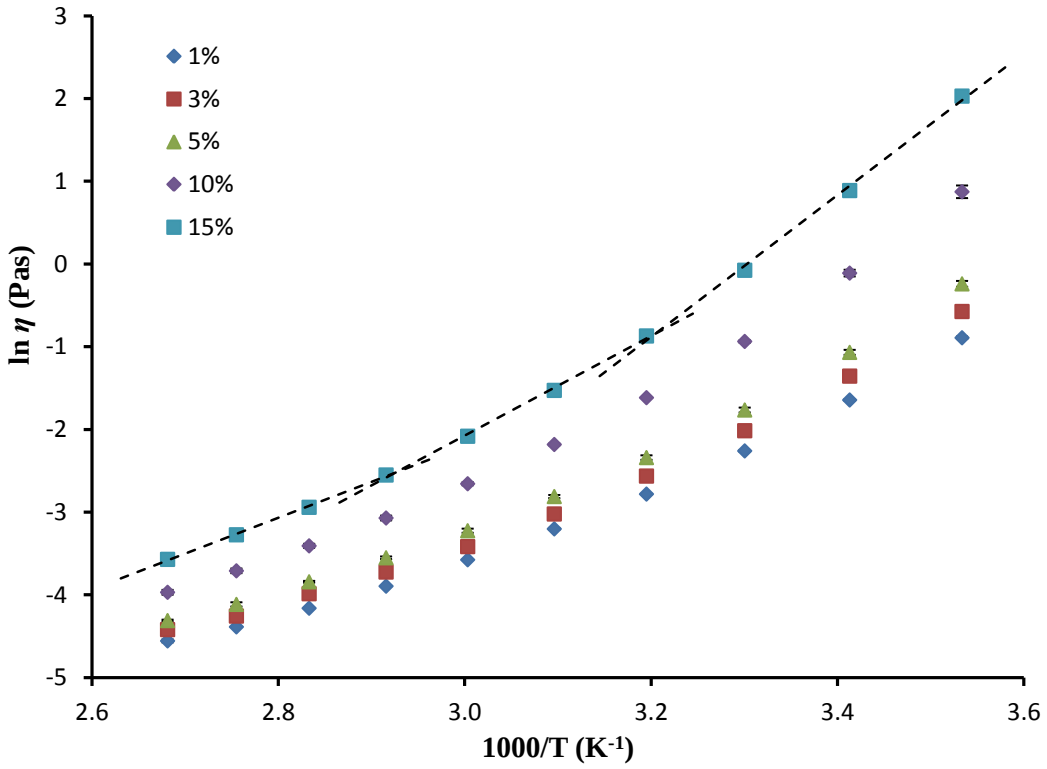

Figure 6.4: ln η against reciprocal temperature for the EMIMAc/glucose solutions. A similar trend was also observed in EMIMAc/cellobiose solutions. Error bars are smaller than the plotted symbol size.

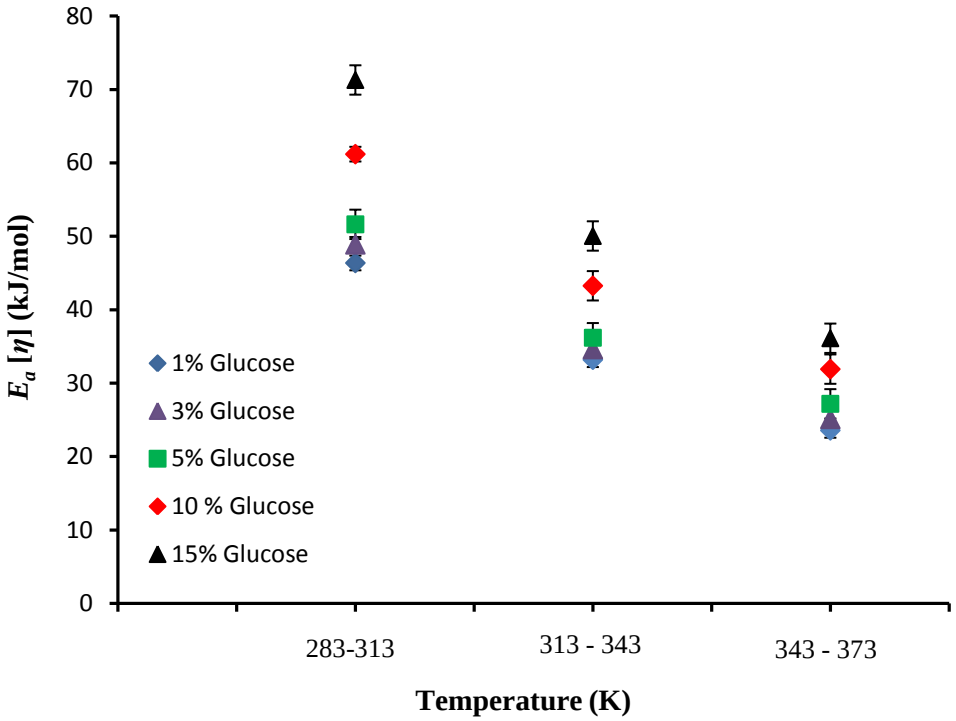

Figure 6.5: The temperature dependence of the activation energy for each EMIMAc/glucose concentration. A similar trend was also observed in EMIMAc/cellobiose solutions.

6.3.2 Diffusion

The EMIMAc diffusivity as a function of carbohydrate concentration for all IL/carbohydrate solutions was studied in the temperature range 10 ^{o}C to 70 ^{o}C. It was found that in dilute solution where the carbohydrate concentration was less than 3 wt%, the diffusion coefficients of EMIMAc ions in glucose, cellobiose and cellulose solutions are similar and not significantly altered by the type of carbohydrate. However, the effect of the type of carbohydrate on the diffusivity of EMIMAc ions becomes more pronounced with the increase of concentration past 5 wt%. This shows that there is a strong dependency of the diffusion coefficient on the type of carbohydrate and its concentration. Figure 6.6 shows the concentration dependence of diffusion coefficient of $EMIM^{+}$ and Ac^{-} in three different solutions at 20 ^{o}C.

It is apparent from the graph that both $EMIM^{+}$ and Ac^{-} were found to diffuse slowest in the glucose solutions. This indicates that glucose has the greatest effect on slowing down the $EMIM^{+}$ and Ac^{-} diffusivity. It should be noted that the magnitude of the diffusivity of ions is influenced by the friction of the translational motion experienced by the ions. The effective friction can be contributed to by several factors such as geometrical shape of the ions, free space around the ions and intermolecular interactions between the ions and their surroundings [195]. However, if the effect of geometrical shape is eliminated, there are only two factors that need to be considered. This will be discussed further in the next section.

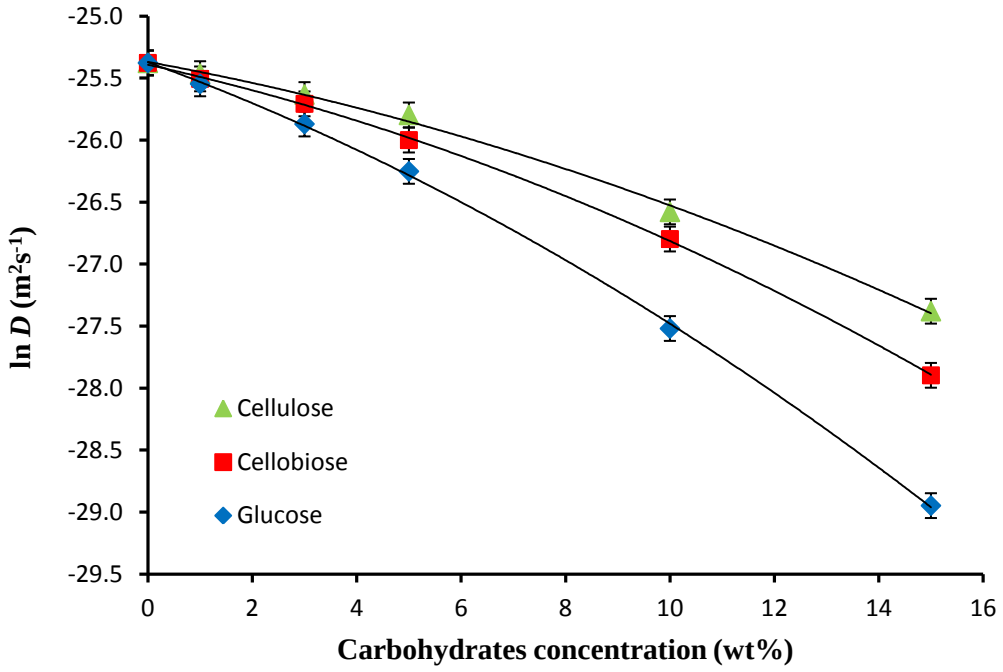

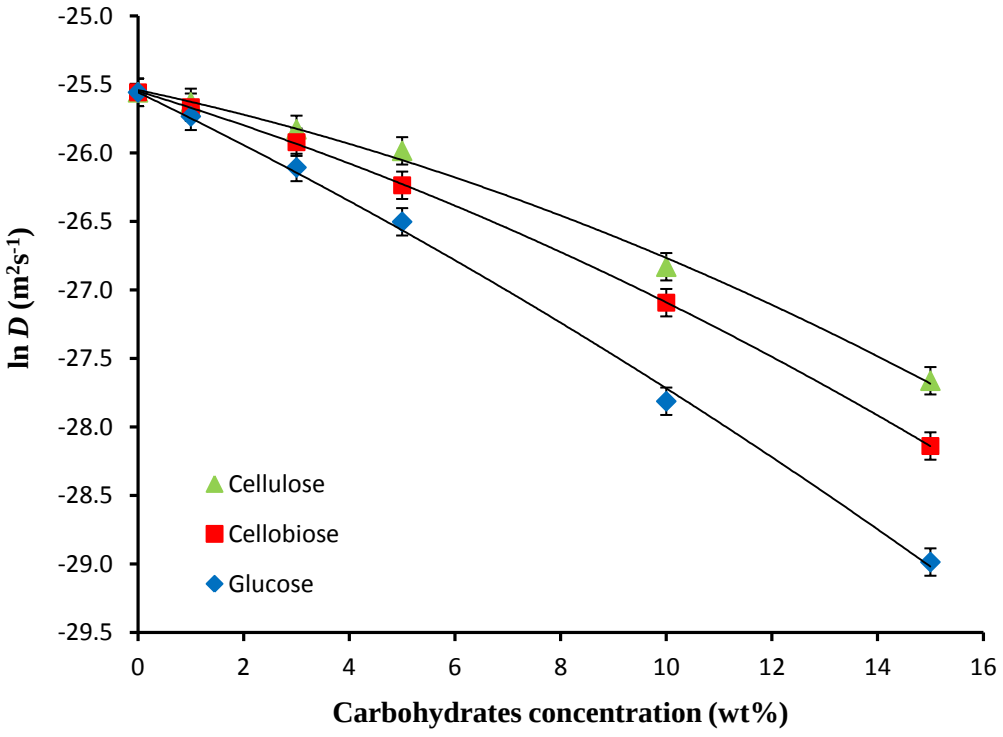

Figure 6.6: Diffusion coefficient of a) $EMIM^+$ and b) Ac^- in EMIMAc/glucose, EMIMAc/cellobiose and EMIMAc/cellulose solutions as a function of solute concentration at 20 ^oC. The effects of carbohydrates on ion diffusivities are more pronounced at higher solute concentration.

Figure 6.7 shows the ratio of the self-diffusion coefficient of Ac^- to $EMIM^+$ as a function of temperature for pure EMIMAc and EMIMAc/glucose solutions. For all concentrations studied, it has been observed that the ratio values deviate from unity. The relatively smaller anion diffused more slowly than the cation. In agreement with previous studies, this peculiarity has been previously observed in NMR studies on several imidazolium based ILs [196-198]. In this study, the deviation becomes more pronounced with the addition of solute in EMIMAc. For pure EMIMAc and dilute solutions, it has been observed that the discrepancy between the self-diffusion coefficient of cation and anion becomes smaller and closer to unity with increasing temperature. Conversely, the ratio of the ion diffusivities displays weaker temperature dependence in concentrated solutions. As can be seen from the graph, the solution with 10% and 15% glucose, the ratio remains approximately at constant value which was $D_{Ac}/D_{EMIM} \approx 0.65$ - 0.70 across the range of temperature investigated. The addition of glucose must alter the ion interaction energies in such a way as to further increase the difference between the counterion diffusivities.

Similar behaviour is also observed in cellobiose and cellulose solutions. However, the magnitude of the discrepancy depends on the type of carbohydrate in the solution. This discrepancy is examined further in Figure 6.8 by showing the concentration and carbohydrate type dependences of the ratio of anion to cation diffusion coefficients. It is shown that at similar concentration, the magnitude of the discrepancy was largest in glucose solution, followed by cellobiose and cellulose solutions. The trend in which the anion to cation ratio was being altered in these solutions is similar to the way the diffusivity of anion and cation is altered. The presence of different carbohydrates is not only affecting the diffusivity of ions, but also the ratio of diffusivity between them. Despite having the smallest molecular weight and size, glucose is found to be the most effective at slowing down the diffusivity of $EMIM^+$ and Ac^-. Conversely, cellulose, which has the largest molecular weight, is the least effective at slowing down the diffusivities of these ions.

These results are different from the viscosity results which found that the viscosity of the solution is highest in the presence of long chain polymer, cellulose.

This finding suggests that, the marcoscopic properties are not always parallel to the microscopic ones. This directly contradicts the Stokes-Einstein relationship which states that the diffusion is inversely proportional to the viscosity. In other words, the effects of the molecules on the macroscopic flow properties (evaluated as viscosity) do not necessarily correlate with the effect on diffusion (i.e. movement at the microscopic scale). This has led to the suggestion that the property known as microviscosity (i.e. a measure of viscosity at the microscopic scale) should be used instead of the macroviscosity to correlate diffusion to a local viscosity.

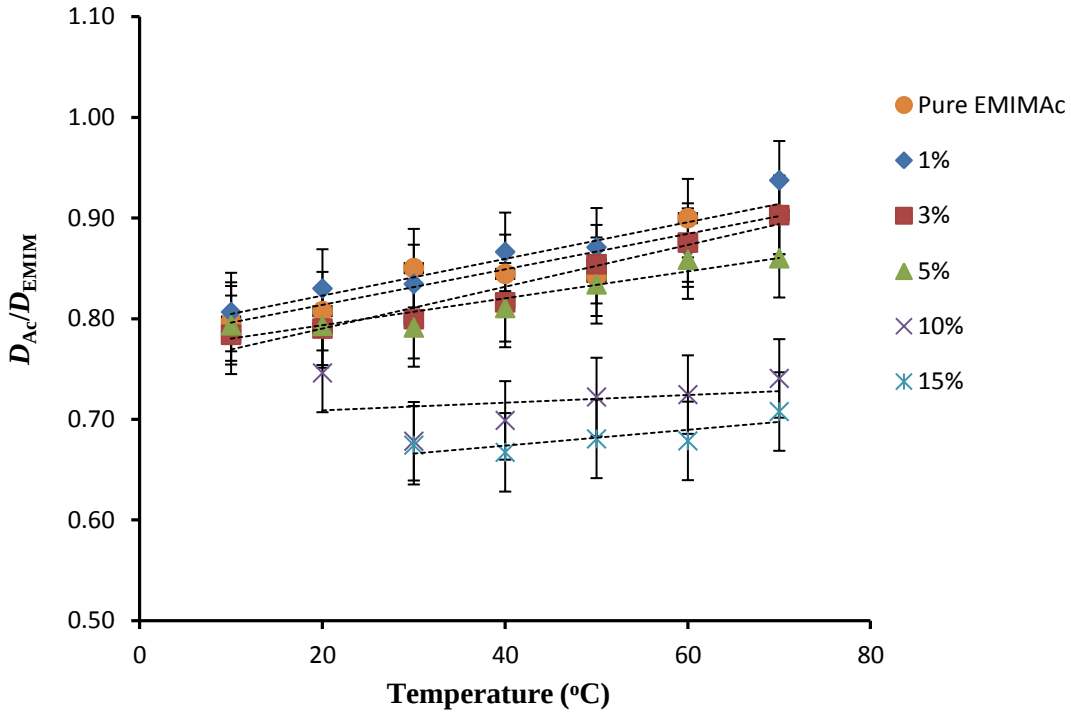

Figure 6.7: Temperature dependence of the ratio of Ac^- to $EMIM^+$ diffusivities at various glucose concentrations. Dashed lines correspond to linear fits.

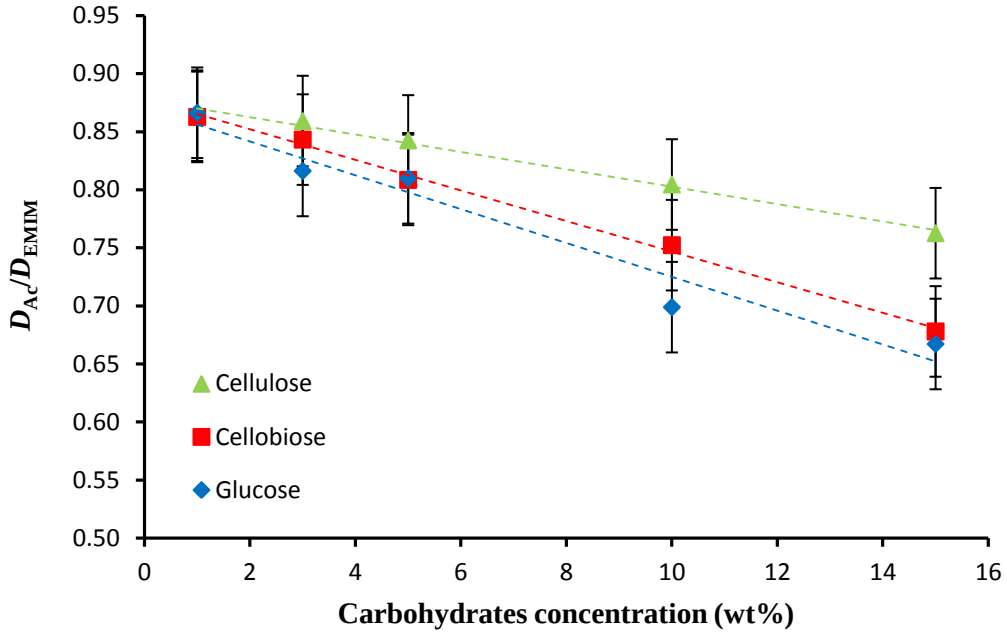

Figure 6.8: D_{Ac}/D_{EMIM} against solute concentration at 40 ^{o}C shows that the ratio varies with the type of carbohydrate. The dashed lines correspond to linear fits and presented as an aid to the eye.

Considering the data in Figure 6.6 and Figure 6.8, a hypothesis is put forward to explain why glucose has the greatest effect on slowing down the $EMIM^+$ and Ac^- diffusivity whilst cellulose with the largest molecular weight is the least effective. As can be seen from Figure 2.10, Figure 2.9 and Figure 2.7 (*recall* Section 2.3), glucose has five hydroxyl (OH) groups per glucose ring while cellobiose and cellulose has four and three OH groups per glucose ring respectively. Hence, it could conceivably be hypothesised that it is the number of OH groups in these system that causes the variation of self-diffusion coefficient in these system. The OH groups that are associated with these carbohydrates can act as both hydrogen bond acceptor and donor to EMIMAc. As a result, the diffusivity of EMIMAc ions becomes slower in EMIMAc/glucose as more ions bound to glucose molecules than cellobiose and cellulose molecules. Herein, an attempt has been made to show that the diffusivity of ions depends on the presence of a hydroxyl group in the solute.

In IL/carbohydrate mixtures, it is assumed that the solutions consist of components of free ions and associated ions (i.e. ions that associated with solute). However, in the case of fast exchange on the NMR time scale, the measured diffusion coefficient (D) is a weighted average of the free and associated diffusion coefficients (D_{free} and D_{assoc} respectively) and can therefore be used to calculate the associated fraction a, as shown in Equation 6.2.

$$D = aD_{assoc} + (1 - a)D_{free} \qquad 6.2$$

In this study, the parameter a refers to the fraction of EMIMAc associated to the solute molecules and is given by the molar ratio of OH groups to EMIMAc molecules. The parameter a can be expressed as:

$$a = N\frac{M_{IL}\phi}{M_{GU}(100 - \phi)} \qquad 6.3$$

In Equation 6.3, M_{IL} is the molar mass of the EMIMAc, 170 g/mol, M_{GU} is the molar mass of a glucose unit (180 g/mol, 171 g/mol, 162 g/mol respectively for glucose, cellobiose and cellulose), ϕ is the solute weight fraction, (wt%) and N is the number of OH groups per glucose unit (5, 4, 3 respectively for glucose, cellobiose and cellulose). A similar approach has been employed by Remsing and co-workers

where they examined the NMR line widths in terms of a bound and free fraction for the 1-Butyl-3-Methylimidazolium Chloride carbohydrate solutions. Here they found an almost 1:1 ratio of chloride ions to carbohydrate hydroxyl groups [199].

The dependence of self-diffusion coefficient on *a* is further examined to see if *a* is the appropriate parameter to quantify the effect of the carbohydrate on the diffusion properties. In Figure 6.9, a graph of ln *D* against *a* is plotted. The most striking result to emerge from these graphs is that the self-diffusion coefficient of each ion merges onto one line and decreases with *a*. This shows that the self-diffusion coefficient of $EMIM^+$ and Ac^- is not dependent on whether the solute they are interacting with is glucose, cellobiose or cellulose. Instead, their diffusion coefficient is predominantly determined by the number of OH groups associated with the solute that they have to satisfy. It is also important to notice that, the graph of ln *D* against *a* is well described by linear fit with the R^2 being greater than 0.98 and the curvature seen in Figure 6.6 when plotting against weight fraction has now been removed. This suggested that the decreasing of the self-diffusion coefficient from its pure ionic liquid state is determined by the number of OH groups per mass of solute in these systems.

The trend which the diffusion coefficient data collapsed together onto one line when plotting against *a* strongly supports the earlier hypothesis which said that the fraction of EMIMAc associates to solute molecules is proportional to the number of hydroxyl group associated with the solute. This support the previous studies that demonstrated the dissolution process of polysaccharides in ILs was primarily due to the formation of hydrogen bonding between ion and hydroxyl groups [65, 200].

Note that the value of *N* used in Figure 6.9 is five, four and three for glucose, cellobiose and cellulose respectively. However, it is possible to vary these numbers to obtain the best overlap. Keeping the cellulose $N = 3$ for glucose value fixed, a least squares analysis yielded the ratio of glucose: cellobiose: cellulose for anion, 5.2: 3.7: 3 and for the cation 6.0: 3.8: 3.0, with uncertainty on all these values of ± 0.4. This result is in parallel with a previous simulation study which found the stoichiometric value of hydrogen bond/per glucose ring of cellulose was in the range 2.5-2.8. In their study, it was suggested that the stoichiometric ratio of hydrogen bond/per hydroxyl group is about 0.9:1 [63].

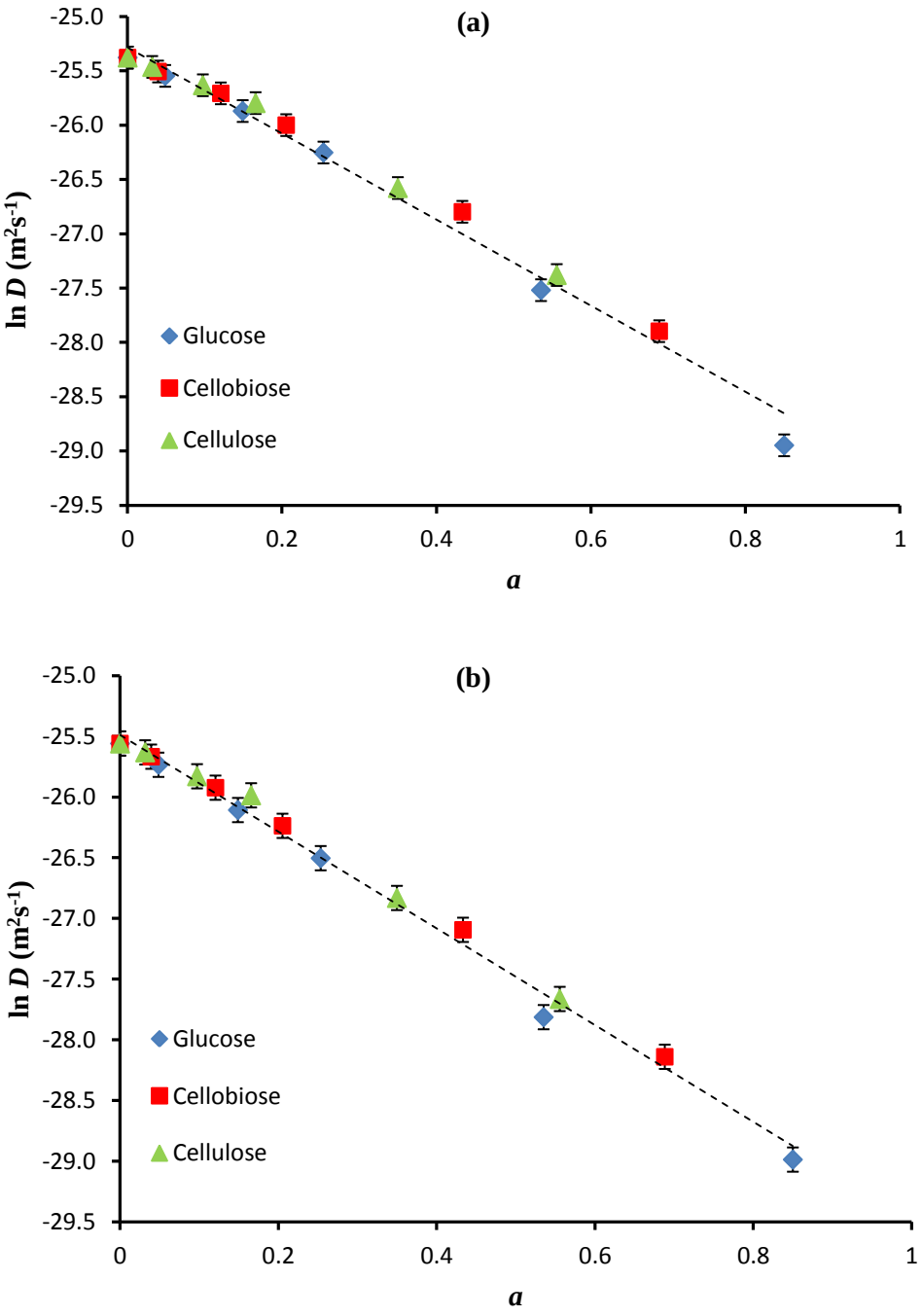

Figure 6.9: Graphs of ln *D* as a function of *a* for a) $EMIM^+$ and b) Ac^- at 20 ^oC. Diffusion coefficients of ions show a linear dependence with *a*, with $R^2 > 0.98$. Dashed lines are linear fits to data.

This study found that the presence of carbohydrates slows down the diffusivity of cations as strongly as that of anions. As proposed by a recent simulation study, anions interact strongly with the hydroxyl groups where its

counterpart cation preferably interacts with the side chain and linker oxygen (i.e. oxygen atom that formed a glycosidic linkage with carbon atom) of the glucose [175]. If referring to the structure of these carbohydrates, it is shown that the free linker oxygen attaches with the glucose, cellobiose and cellulose is essentially proportional to the number of hydroxyl groups associated with them as the linker oxygen originated from the hydroxyl group of the single glucose chain. Hence, it could conceivably be hypothesized that the proportionality of cation diffusivity with *a* (i.e., free hydroxyl groups) does not necessarily means that cation interact with hydroxyl groups but it could result from its interaction with linker oxygen attaching to each glucose ring.

Several studies have suggested that the plane shape and anisotropy of the imidazolium cation led to higher mobility of the cation than its counterpart anion. This offers an advantage to the cation as it can diffuse more freely than the anion and reach the interaction sites more easily. This will indirectly increase the cation-carbohydrate interactions and subsequently increase the solubility power of EMIMAc to dissolve carbohydrates, especially cellulose that has multiple glucan sheets.

To examine the ratio D_{Ac}/D_{EMIM} on the fraction of EMIMAc associated with carbohydrate molecules, a graph of D_{Ac}/D_{EMIM} as a function of *a* is plotted (*see* Figure 6.10). It is shown that D_{Ac}/D_{EMIM} merges onto one line and is linearly dependent on the fraction of EMIMAc associated with solute. This suggested that the diffusivity of ions in solution is predominantly determined by the number of hydroxyl groups associated with the carbohydrates. Again, this indicates that the free hydroxyl group is a site for ions to interact in order to dissolve carbohydrates. Interactions between the ions and hydroxyl groups are clearly evident through the merge of the D_{Ac}/D_{EMIM} data onto one line when plotted against *a*.

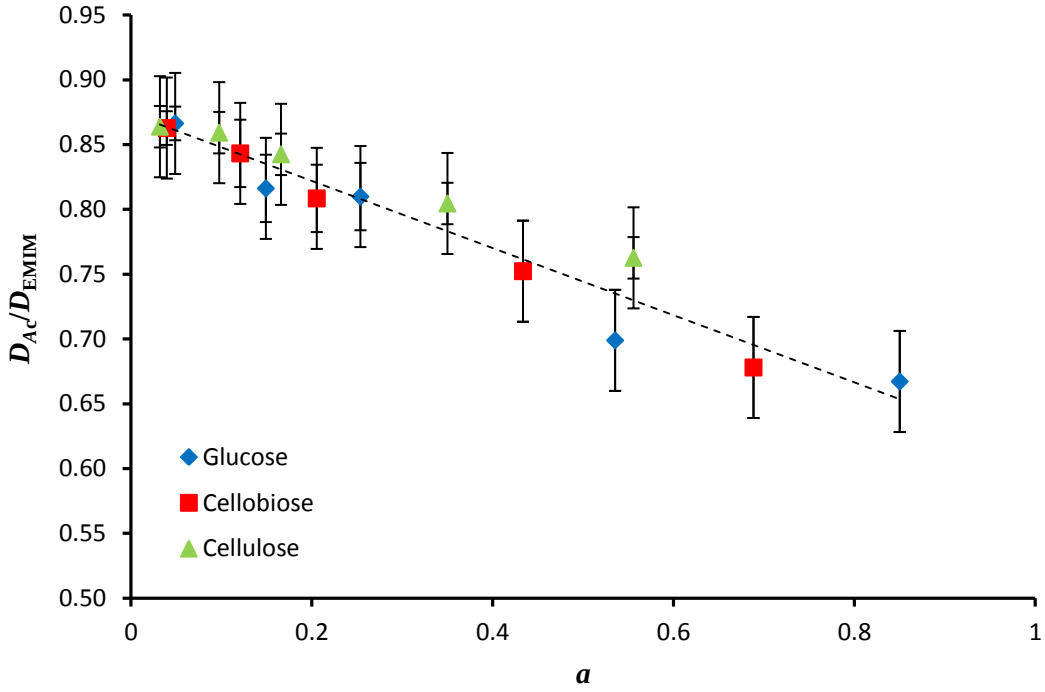

Figure 6.10: D_{Ac}/D_{EMIM} against a shows that the ratio is linear dependent on the relative number of OH groups.

6.3.3 NMR Chemical Shift

In Figure 6.11 the dependence of the change in chemical shift of EMIMAc spectral bands on glucose concentration at 50 ^{o}C is presented. The behaviour of concentration dependence of the chemical shifts observed for all systems had the same trend, even though the changes are very different in magnitude. This indicates that the change of microscopic structure of EMIMAc varied depending on the type of carbohydrates in the solution. The largest change in chemical shift was observed in glucose/EMIMAc solutions, followed by cellobiose/EMIMAc solutions, with the least change in cellulose/EMIMAc solutions.

The largest changes in glucose/EMMAc solutions indicated that the strongest interactions have formed in this system. When carbohydrates were added to EMIMAc, the interaction between the EMIMAc was formed to promote the dissolution of solute. On the basis of sugar dissolution in organic solvent, it is well known that the dissolution is primarily promoted by the interaction of the hydroxyl group with the polar group of the solvent. Therefore, in this case it is reasonable to correlate the different changes in magnitude of chemical shift observed in all

solutions with the different number of hydroxyl groups associated with each carbohydrate. Glucose, which has more hydroxyl groups per ring, will offer more binding sites to the EMIMAc and hence cause the microscopic environment of the EMIMAc to change more significantly compared to the others.

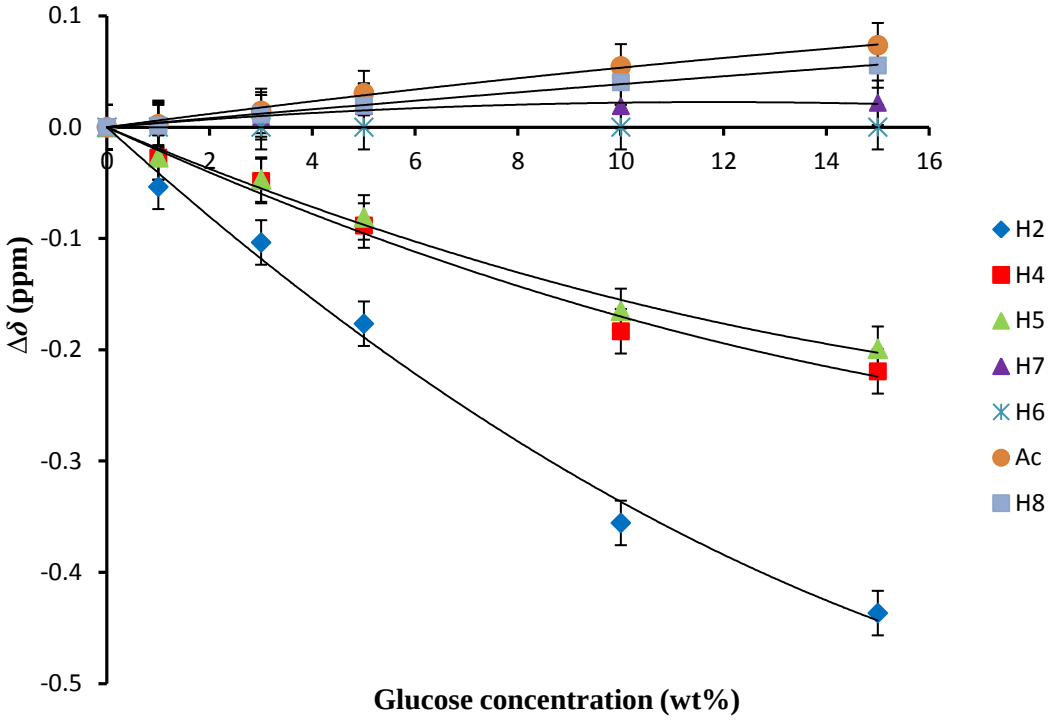

Figure 6.11: Concentration dependence of chemical shift change for all EMIMAc spectral bands in glucose solutions at 40 ^{o}C. The solid lines are presented as an aid to the eye.

Since chemical shift change can be directly observed by NMR spectroscopy, it can be used in a similar way to the self-diffusion coefficient to determine the interaction stoichiometry. For that reason, in an attempt to obtain an insight into the interaction between EMIMAc and carbohydrates, particularly the interaction between hydroxyl groups and EMIMAc, a graph of chemical shift changes for a selected spectral bands as a function of *a* has been plotted.

In Figure 6.12, only chemical shift of H2, H4 and Ac^{-} are displayed. The changes of chemical shift of these spectral bands were observed at 40 ^{o}C. The selection of these spectral bands is follows several previous studies on imidazolium based ILs where these protons have been shown playing an important role in any interaction with

solute or solvents and to be largely affected by their environmental condition [49, 87]. The behaviour of concentration dependence of the chemical shifts observed for all systems are similar even though the changes are different in magnitude.

As shown in Figure 6.12 the changes of chemical shift fall together when plotted in this way. This trend again corroborates the idea that IL interacts with carbohydrates, mainly with the hydroxyl groups. This result is therefore consistent with other previous studies that proposed mechanisms of cellulose dissolution through co-ordination of cation and anion with cellulose hydroxyl groups. Therefore the largest changes in chemical shift in glucose solutions mentioned before results from the highest hydroxyl group per glucose ring possessed by glucose which is then followed by cellobiose and cellulose. The concentration dependence of chemical shift changes in these three solutions reflecting their different abilites to form hydrogen bonding with these carbohydrates, which results in different changes in the microscopic structure.

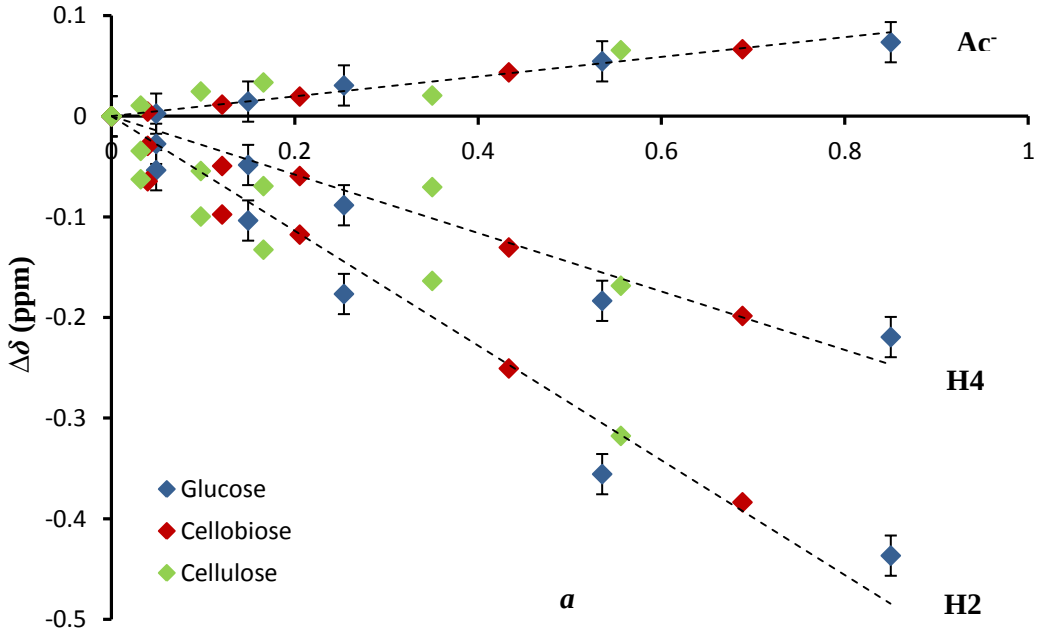

Figure 6.12: *a* dependence of chemical shift change of selected spectral bands in glucose, cellobiose and cellulose solutions at 40 ^{o}C. The dashed lines are presented as an aid to the eye. The size of the uncertainties is shown for glucose data and each series has a similar size uncertainty, which has been left off the figure for clarity.

6.3.4 NMR Relaxometry

The influence of carbohydrates on NMR relaxation times is also studied. In Figure 6.13, carbohydrates concentration dependence of relaxation time, T_1 are plotted for the three solutions. Similar to the self-diffusion coefficient results, it was found that the shortest T_1 is observed in glucose solutions followed by cellobiose and cellulose. A similar trend was also observed for the spin-spin relaxation, T_2. Again this suggests that the presence of glucose molecules provides more restriction to the mobility of EMIMAc molecules than cellobiose or cellulose molecules.

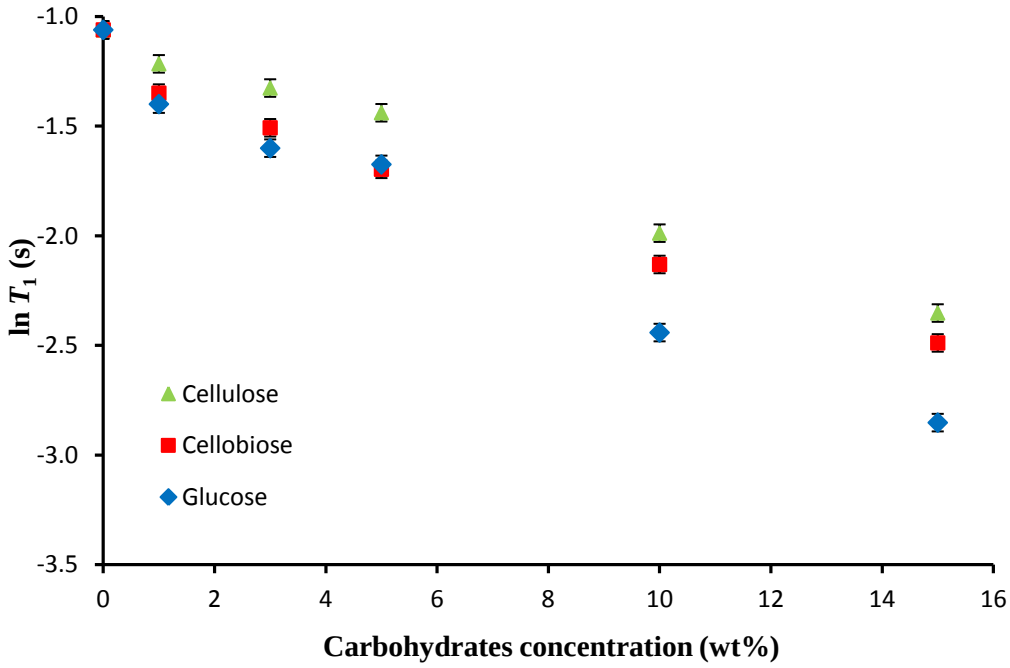

Figure 6.13: Carbohydrates concentration dependence of ln T_1 at 50 ^{o}C. Glucose is more effective at bringing about relaxation of protons whilst cellulose is the least effective.

A similar method has been emplyed to correlate the relaxation times with the number of hydroxyl groups associated with each carbohydrate. In Figure 6.14, a graph of ln T_1 against a is plotted to verify whether the variation of relaxation times with carbohydrates also depends on the stoichiometric interaction proposed in the earlier section. As shown in Figure 6.14, T_1 values collapse onto one straight line when plotting against a. This indicates that the number of hydroxyl group possessed by the carbohydrates not only affect the diffusivity of EMIMAc ions but also the

rotational relaxation time of EMIMAc in a similar manner. The mobility both rotational and translational of EMIMAc molecules is affected by the presence of the number of free hydroxyl groups in carbohydrates. In general, the NMR relaxation results corroborate the intuition that additional microscopic interactions have an effect on the microscopic relaxation times.

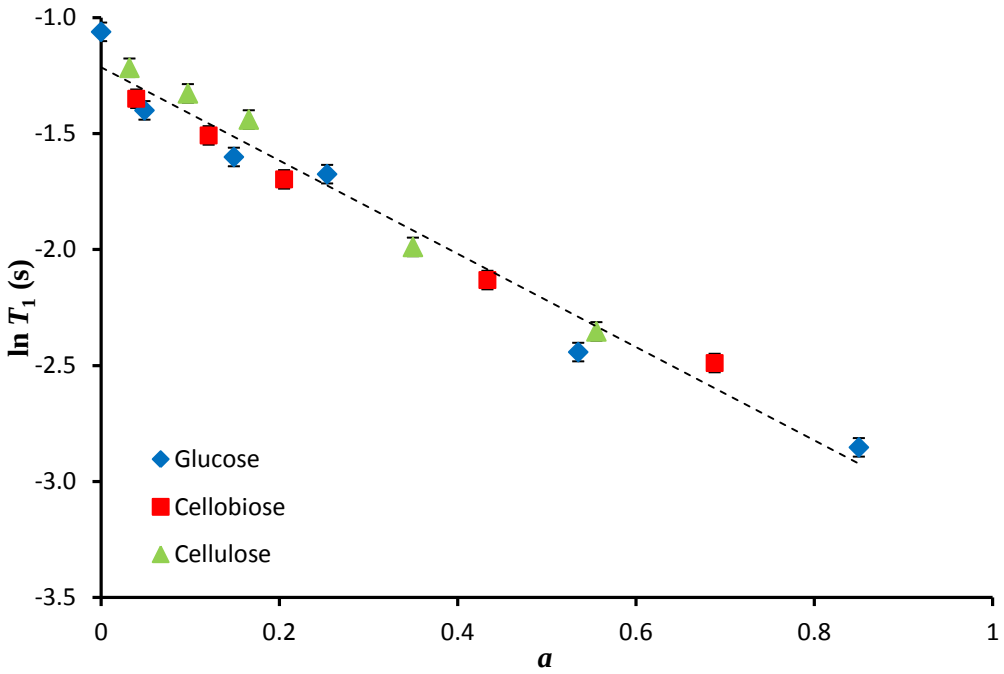

Figure 6.14: A graph of ln T_1 against a at 50 ^{o}C. T_1 values collapse onto one straight line when plotting against a with $R^2 > 0.98$.

Figure 6.15 shows an Arrhenius plot of the relaxation time T_1 for 15 wt% glucose, cellobiose and cellulose solutions. However, at this concentration, the plot of T_1 against temperature does not follow Arrhenius behaviour. EMIMAc in cellulose solution gave the longest T_1 and did not exhibit a T_1 minimum while EMIMAc in glucose solution has the shortest T_1 and starts to exhibit T_1 minimum. T_1 of EMIMAc in glucose solution shows a trasition from an extreme narrowing condition to a diffusion limit in the range of temperatures studied. When the T_1 minimum is observed, it is then possible to calculate a correlation time. The calculation of correlation time from T_1 relaxation will be explained in the next section.

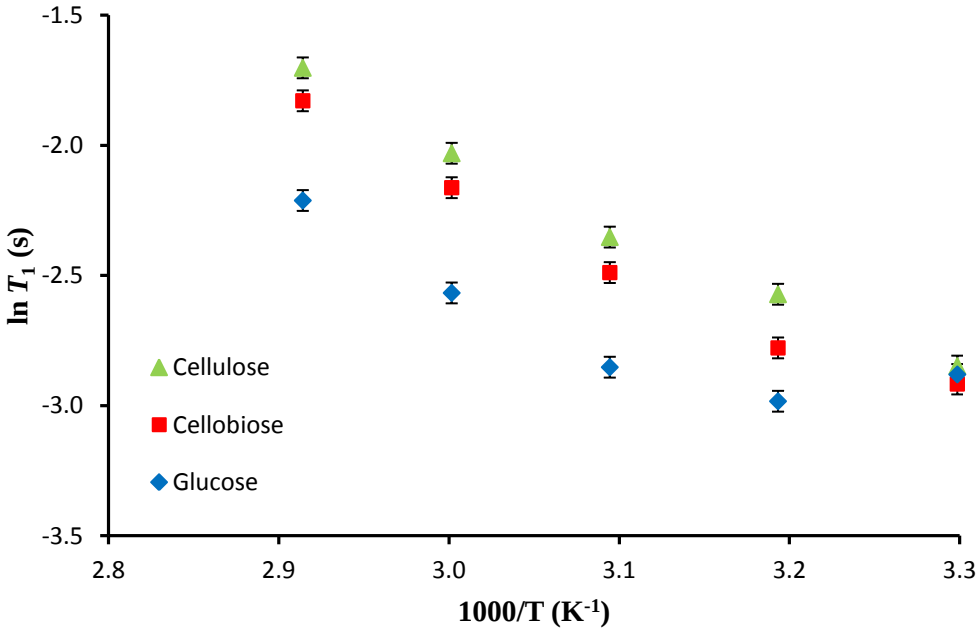

Figure 6.15: Arrhenius plot of spin lattice relaxation, T_1 in 15 wt% carbohydrate concentration. In 15 wt% glucose solution, T_1 shows a transition from an extreme narrowing condition to the diffusion limit.

Since T_1 shows a transition from an extreme narrowing condition to the diffusion limit at ~ 40 ^{o}C (in the case of glucose solution), therefore it is interesting to see how T_1 and T_2 for all carbohydrate concentrations changed with *a* at lower temperature, i.e. 30 ^{o}C. In Figure 6.16, it can readily be seen that all the data for T_1 collapses onto one curve and exhibits a minimum while T_2 simply decreased with *a*. The more hydroxyl groups present in the solution, the more effective the solution is at

relaxating the NMR signal. All this is strong evidence that the parameter *a* is the correct one to describe the effect of the carbohydrate solute on the NMR relaxation of the EMIMAc in these systems.

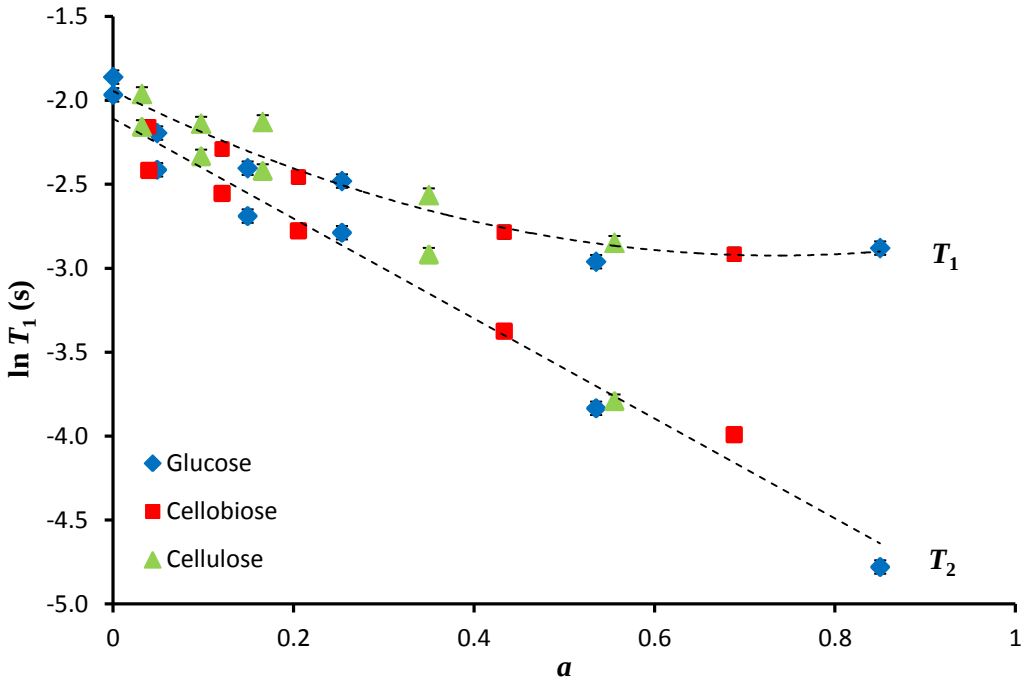

Figure 6.16: A graph of ln T_1 and ln T_2 against *a* at lower temperature, 30 ^{o}C. In both cases, all the data collapses onto one line with T_1 showing a minimum with *a* while T_2 simply decreased with *a*.

6.4 Discussion

6.4.1 Microviscosity correction factor, f_μ analysis

Our earliest findings showed that the diffusion results of all systems are in the reverse order of viscosity results which implies that macroscopic zero shear rate viscosity would be an incorrect term to use in the classical Stokes-Einstein equation. For that reason, instead of using macroviscosity to correlate diffusion to viscosity, it has been suggested that a microviscosity be used to describe the relationship between diffusion and viscosity. Therefore, an adjustment to the classical Stokes-Einstein equation has been made by introducing a microviscosity correction factor, f_μ to quantify the local microviscosity of the EMIMAc molecules (*recall* Section 4.4.2).

$$D = \frac{kT}{6\pi f_\mu R_H \eta} \qquad 6.4$$

Hence for this study, the graphs of D against T/η for both $EMIM^+$ in glucose and cellobiose solutions are plotted in Figure 6.17. The ratio of the size of diffusing molecules is determined from the slope to the theoretical hydrodynamic radius (calculated from empirical relation) which is calculated to determine the value of f_μ. If the value of f_μ is close to unity ($f_\mu \sim 1$), then the molecules are said to be in sticky condition whereas if it is less than unity ($f_\mu < 1$), the molecules are in slip boundary conditions [40].

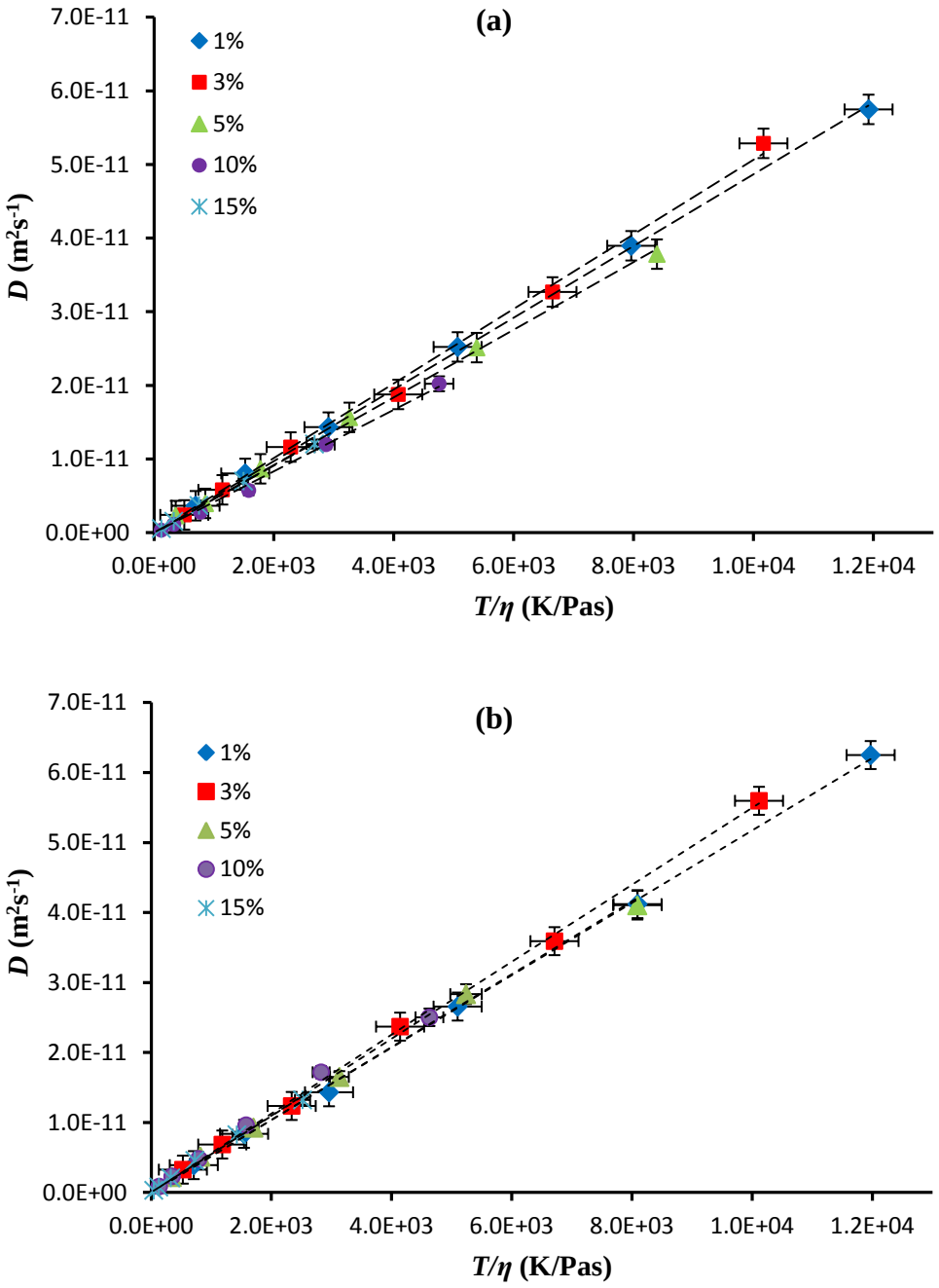

Figure 6.17: D against log T/η for $EMIM^+$ in a) glucose and b) cellobiose solutions. The lines are fit to the classical Stokes-Einstein equation.

The value of f_μ for both $EMIM^+$ and Ac^- in each solution is listed in Table 6.1. It is apparent from this table that the value of f_μ for Ac^- significantly increases with the addition of glucose or cellobiose. In contrast for the $EMIM^+$, increasing of glucose and cellobiose concentration does not significantly alter the value of f_μ.

Indeed the value of f_μ for $EMIM^+$ remains approximately constant at 0.58 ± 0.04 and 0.50 ± 0.02 in glucose and cellobiose respectively. It is interesting to note that the value of f_μ for Ac^- is close to unity. This indicates that Ac^- ions are exposed to stick boundary conditions. Meanwhile the value of f_μ for $EMIM^+$ which is less than 4/6 (*recall* Section 4.4.2) suggests that $EMIM^+$ ions find themselves in the slip condition. The variation of the f_μ value gives insight into the local microviscosity of the ions. As explained before, there are several factors that affect the local microviscosity of molecules in solution. One of the factors can be related to the specific interactions between the diffusing ion and surroundings in the solution that leads to a decrease in the diffusion coefficient.

Table 6.1: Microviscosity factor, f_μ of $EMIM^+$ and Ac^- in EMIMAc/glucose and EMIMAc/cellobiose solutions.

Solute concentration (wt%)	**Microviscosity factor, f_μ**			
	EMIMAc/glucose		**EMIMAc/cellobiose**	
	$EMIM^+$	**Ac^-**	**$EMIM^+$**	**Ac^-**
0	0.55 ± 0.01	0.76 ± 0.01	0.55 ± 0.01	0.76 ± 0.01
1	0.55 ± 0.01	0.77 ± 0.02	0.52 ± 0.02	0.71 ± 0.03
3	0.53 ± 0.04	0.75 ± 0.06	0.49 ± 0.02	0.67 ± 0.03
5	0.58 ± 0.02	0.85 ± 0.02	0.51 ± 0.03	0.75 ± 0.03
10	0.64 ± 0.04	1.08 ± 0.07	0.47 ± 0.05	0.76 ± 0.06
15	0.58 ± 0.03	1.05 ± 0.04	0.49 ± 0.05	0.84 ± 0.04

In this study, the local microviscosity of both $EMIM^+$ and Ac^- were found to be larger in glucose solution than in cellobiose. The data showed that the local microviscosity of Ac^- is always larger than $EMIM^+$ and significantly increase with solute concentration. It can therefore be assumed that Ac^- forms stronger interactions with carbohydrates than its counterpart $EMIM^+$. Significant increase of Ac^- in local microviscosity with solute concentration while its counterpart, $EMIM^+$ does not, explains a further decrease of the $Ac^-/EMIM^+$ ratio with increase of carbohydrate concentration as shown earlier.

This is in agreement with previous studies, which suggested that interaction energy of anion-glucan is higher than the interaction energy of cation-glucan. The higher interaction energies of anion-glucan are from the formation of hydrogen bonds while the interaction energies of cation-glucan is from weaker interactions, i.e. van der Waals interaction [63, 65].

6.4.2 Relaxometry analysis

As shown in Figure 6.18, T_1 and T_2 relaxation values exhibit simple dipolar relaxation behaviour as described by the Bloembergen, Purcell and Pound (BPP) theory. Using the BPP theory, both T_1 and T_2 data were analyzed. Recall Section 3.1.5.4, T_1 and T_2 can be described as [119]:

$$\frac{1}{T_1} = K\left(\frac{\tau_c}{1+\omega_o^2\tau_c^2} + \frac{4\tau_c}{1+4\omega_o^2\tau_c^2}\right) \qquad 6.5$$

$$\frac{1}{T_2} = \frac{K}{2}\left[3\tau_c + \frac{5\tau_c}{1+\ \omega^2\ \tau_c^2} + \frac{2\tau_c}{1+4\omega^2\tau_c^2}\right] \qquad 6.6$$

Due to the terms in parentheses in Equation 6.5, the spin lattice relaxation time is a minimum when $\omega_o\tau_c = 2\pi\upsilon_o\tau_c = 0.616$. From the Arrhenius plot in Figure 6.15, it was shown that EMIMAc in 15 wt% glucose solution exhibits T_1 minimum while the other solutions have no clear minimum at this concentration. The τ_c at this minimum point is simply calculated to be 4.90 x 10^{-9} s. Similar to previous studies (*see* Section 5.4.1) K is then calculated from the T_1 value observed at the minimum point and given a value of 1.74 x 10^9 s^{-2}. Using the same K value and based on the Arrhenius equation, the $E_a[\tau_c]$ for all solutions were determined using a least-squares analysis. It was found that the NMR relaxometry data are best fit with an Arrhenius equation.

$$\tau_c = \tau_o exp\left(\frac{E_a[\tau_c]}{k_B T}\right) \qquad 6.7$$

where τ_o is pre-exponential factor and $E_a[\tau_c]$ is correlation time activation energy. For this purpose, τ_o is treated as a single global fitting parameter across all

carbohydrate concentrations while activation energy, $E_a[\tau_c]$ is a variable parameter and has a single value for each concentration/solute. In this fitting the value of τ_o was found to be 1.00 x 10^{-15} s. Comparison between experimental and theoretical data that have been generated from this fitting method are presented in Figure 6.18.

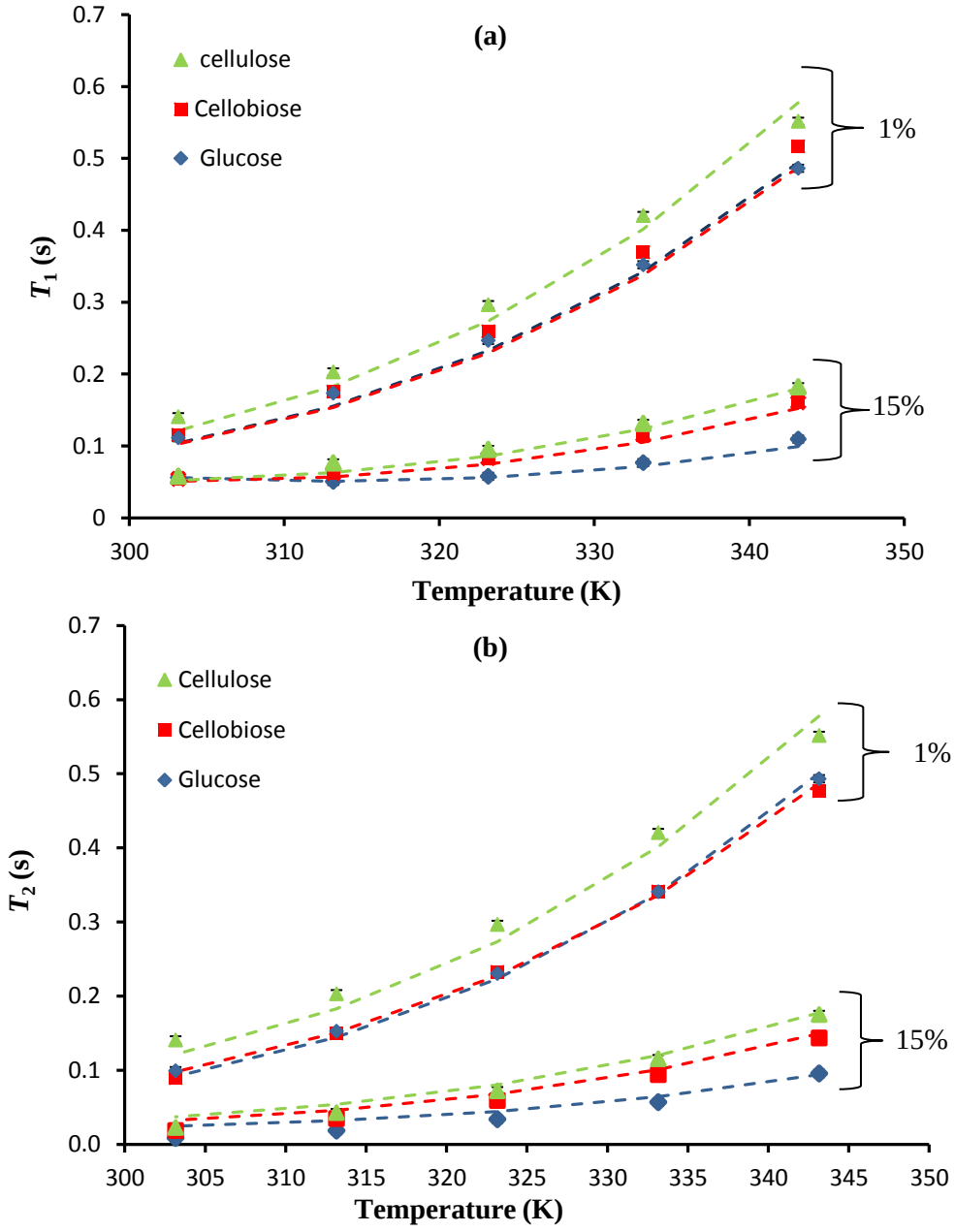

Figure 6.18: a) Spin lattice relaxation, T_1 b) Spin spin relaxation, T_2 value of EMIMAc in 1% and 15% solute. The dotted lines represent theoretical values calculated from BPP theory where the T_1 and T_2 values have been determined using a constrained fitting method.

The value of K calculated from the T_1 value observed at the minimum point allows the determination of the effective inter-proton distance of EMIMAc (*see* Equation 3.20 in Section 3.1.5.4). From the calculation, it was found that the effective inter-proton distance in EMIMAc molecules is 2.15 Å. The value of inter-proton distance here is assumed to be the shortest inter-proton distance in the EMIMAc molecule. This value is comparable to the inter-distance proton for aliphatic protons and aromatic protons which have values of 1.77 Å and 2.48 Å respectively [171].

As can be seen from Figure 6.19, a plot of correlation time against solute concentration exhibits a similar trend to the diffusion coefficient data, with the mobility of EMMAc molecules being found to be slower in glucose solutions.

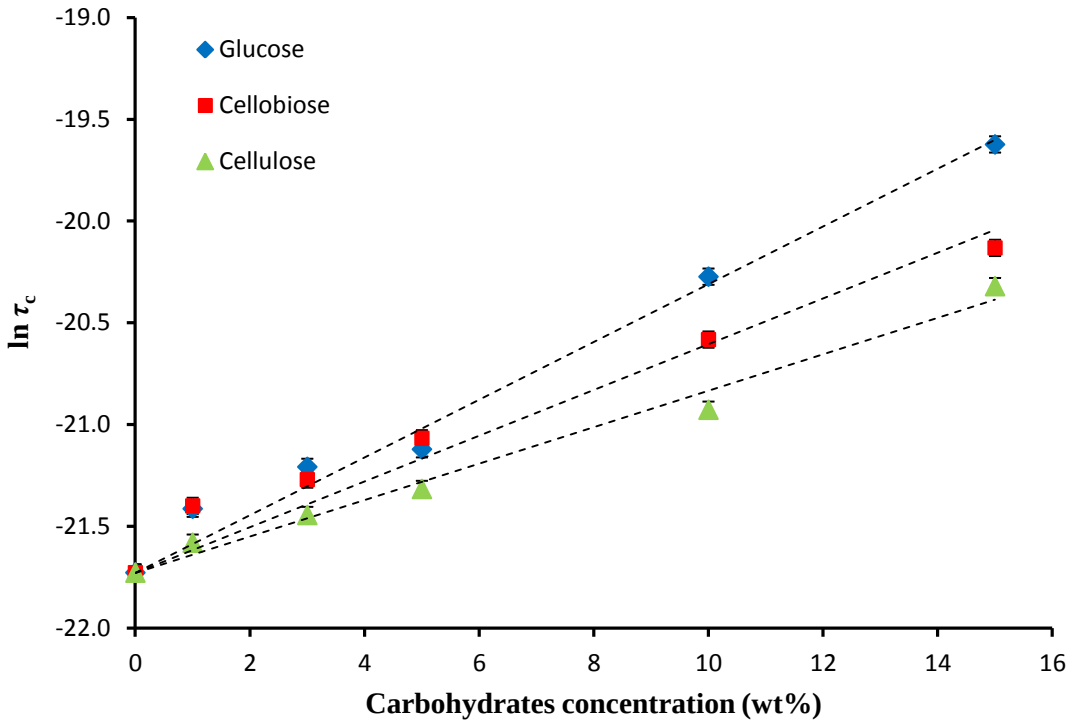

Figure 6.19: Carbohydrates concentration dependence of correlation time at 50 ^{o}C in all solutions.

Again, an attempt has been made to correlate the correlation time with the number of hydroxyl groups associated with the solute. In Figure 6.20 the value of ln τ_c as a function of a at 50 ^oC is plotted. The full line represents the best linear fit through the points, with $R^2 > 0.98$. Plots analogous to Figure 6.20 have been constructed for all temperature ranges studied. In each case, the data nearly falls on a straight line. It is apparent from the result that, to a good approximation, the correlation time is also a function of a at a given temperature. Specific solute/solvent interactions cause the smooth variation of τ_c with a. Note that the solutes used in this study differ considerably in molecular size, structure and chemical nature. Again, there is a clear relationship between the molecular motion of the EMIMAc molecules and the presence of free hydroxyl groups of the carbohydrates.

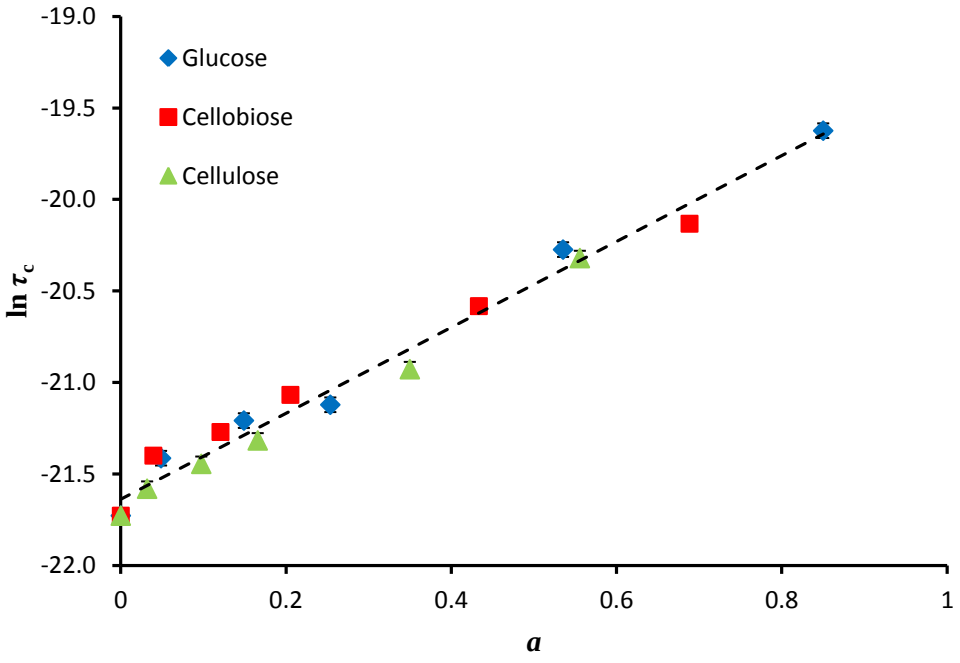

Figure 6.20: τ_c values at 50 ^oC as a function of a. The dotted line is the best fit line through the points and has a $R^2 > 0.98$.

6.4.3 Activation Energy

6.4.3.1 Self-Diffusion Coefficient

Based on an Arrhenius equation, the activation energies of $EMIM^+$ and Ac^- from diffusion measurements have been determined using a least-squares analysis:

$$D = D_o exp\left(\frac{-E_a[D]}{k_B T}\right) \qquad 6.8$$

Using this method, $E_a[D]$ for both $EMIM^+$ and Ac^- for each concentration and carbohydrate system are determined independently. D_o for $EMIM^+$ and Ac- across all the samples is treated as a global fitting parameter which means that for all $EMIM^+$ and Ac- data, there is only one D_o for each ion. With a single value of D_o, this fitting is more rigorous as D_o should be independent of the concentration or the types of carbohydrates present in the solutions. A least squares analysis yields the value of D_o for $EMIM^+$, 1.43 x 10^{-3} m^2/s while for Ac- is 1.60 x 10^{-3} m^2/s. These values are not at first sight in agreement with our experimental finding, where the relatively smaller anion diffused more slowly than the larger cation (*recall* Section 6.3.2). Taking into consideration the hydrodynamic radius of imidazolium cation, $EMIM^+$ (2.74 Å) and anion, Ac^- (2.27 Å) in pure EMIMAc calculated from empirical equation (*see* Equation 3.45), one should expect that the larger $EMIM^+$ to diffuse more slowly than the smaller Ac^-. The value of D_o obtained from a least-squares analysis revealed that at infinite temperature or when the condition/reaction is 'barrier less' (zero activation energy), the diffusion of the ions is in accordance with their relative molecular sizes. With the Ac^- diffusing faster than the $EMIM^+$.

In Figure 6.21 the $E_a[D]$ for both $EMIM^+$ and Ac^- for each carbohydrate system are plotted as a function of bound fraction *a*. The results show a clear trend of linear increase of activation energies with bound fraction *a*. This trend corroborates the earlier hypothesis that it is the number of hydroxyl groups associated with carbohydrates that determines the diffusion of ions in EMIMAc/carbohydrate solutions.

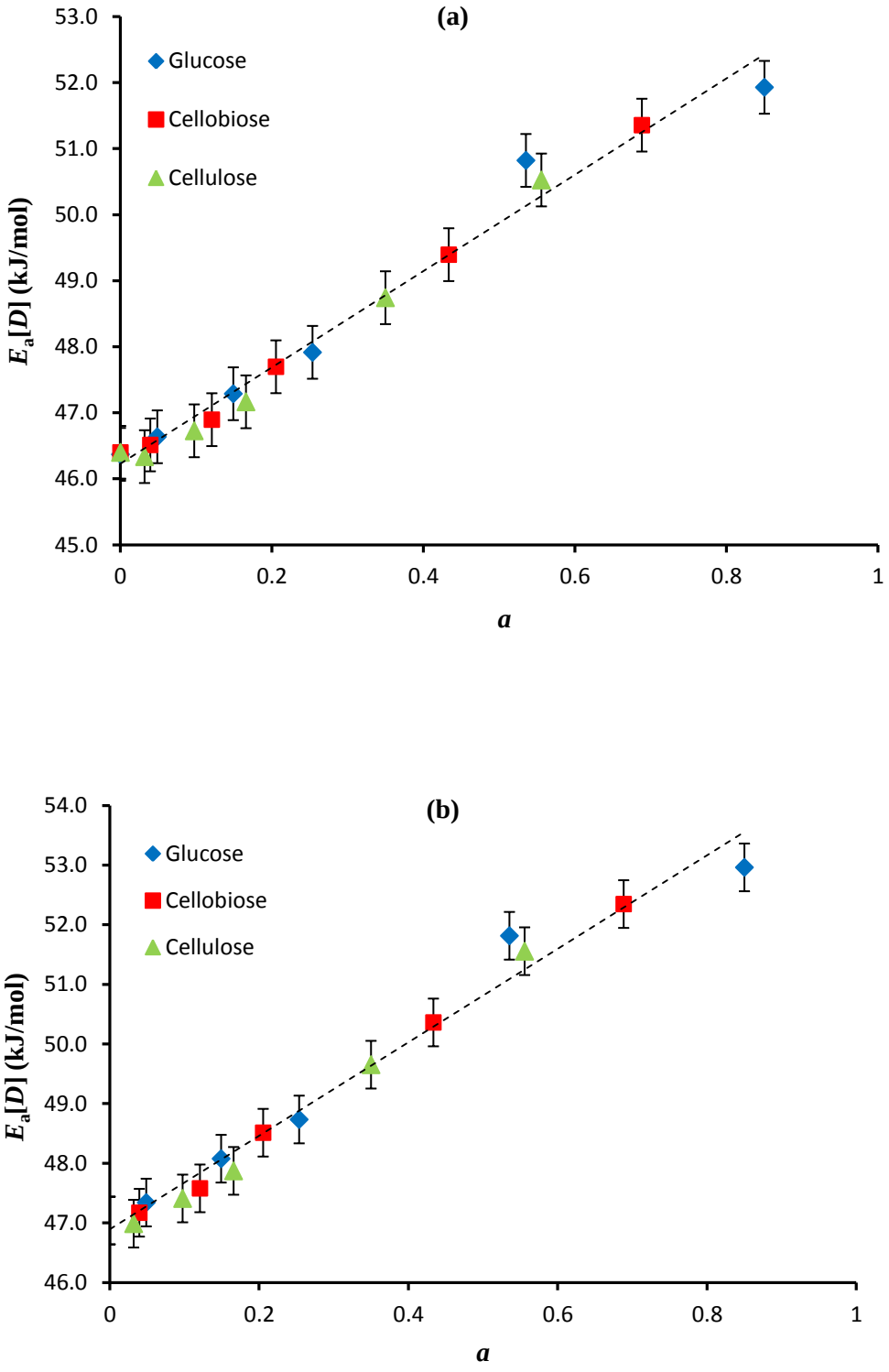

Figure 6.21: *a* dependence of the activation energy for a) $EMIM^+$ and b) Ac^- in the glucose, cellobiose and cellulose solutions. Both $EMIM^+$ and Ac^- show a linear relationship with *a*.

6.4.3.2 NMR Relaxometry

The activation energies of EMIMAc from NMR relaxometry measurement for each concentration and carbohydrate system is presented in Figure 6.22. A plot of activation energy as a function of solute concentration showed that activation energy was highest in glucose solutions followed by cellobiose and cellulose. These results reveal that the mobility of EMIMAc is more hindered and requires more energy to reorient itself in glucose solutions.

The variation of activation energies with carbohydrate types is examined further in Figure 6.23 by showing the *a* dependences of the activation energies. A remarkably similar $E_a[\tau_c]$ as with $E_a[D]$ has been observed, where it was found that the activation energies increase linearly with bound fraction *a* (*see* Figure 6.21). Similar to diffusion measurement, the rotational molecular motion of EMIMAc must be highly correlated with the number of hydroxyl groups associated with the glucose, cellobiose and cellulose molecules. The activation energies determined from the correlation times range from 34 ± 0.2 kJ/mol to 38 ± 0.2 kJ/mol. These values are 12-13 kJ/mol smaller than those determined from diffusion coefficient measurements. However, it is worth noting that the slope of activation energy, $dE_a[\tau_c]/dE_{a[\tau_c]}$ from NMR measurement is similar to the slope of diffusion measurement which lies between (5-6 kJ/mol).

If comparing the activation energy from viscosity, diffusion and NMR relaxometry, if was found that the activation energies obtained from microscopic dynamics were not in parallel with that obtained from viscosity dynamics.

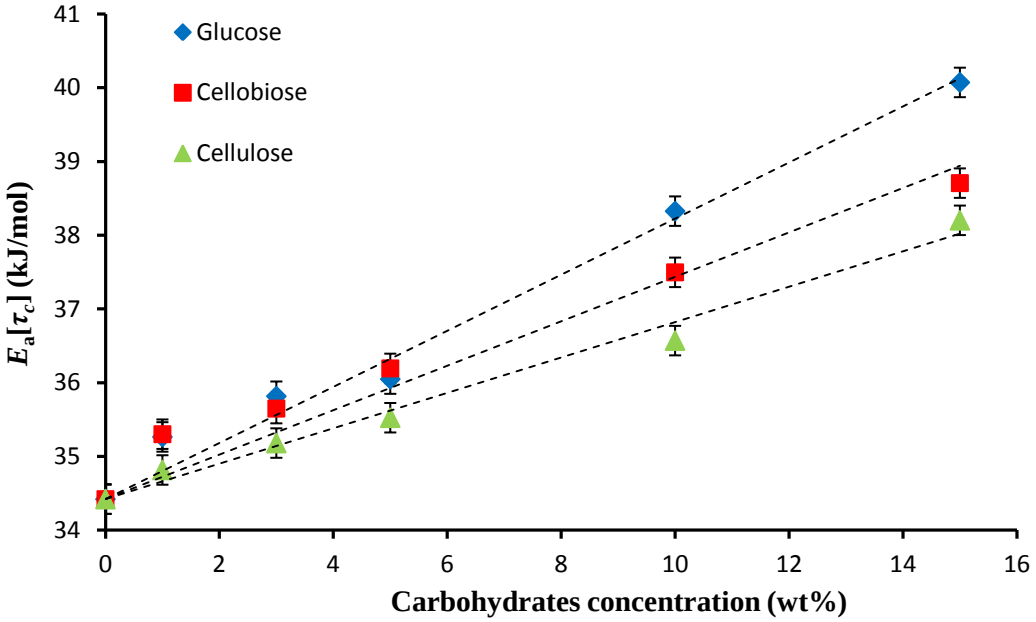

Figure 6.22: Carbohydrates concentration dependence of the activation energy for EMIMAc in glucose, cellobiose and cellulose solutions.

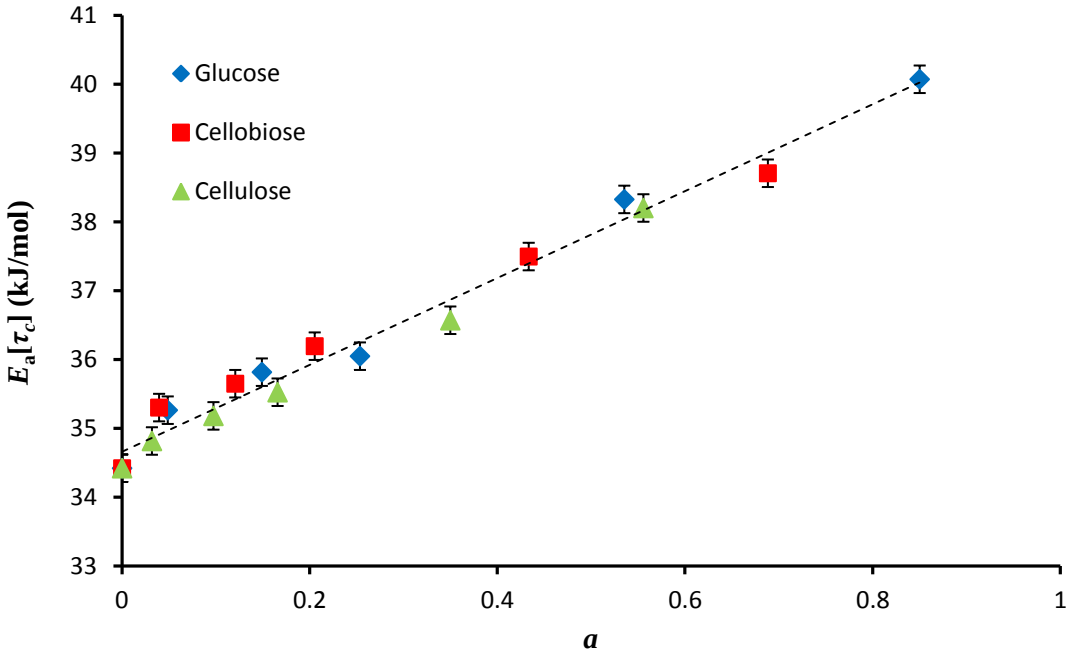

Figure 6.23: *a* dependence of the activation energy for EMIMAc in the EMIMAc/ glucose, EMIMAc/cellobiose and EMIMAc/cellulose solutions.

6.4.4 Self-Diffusion Coefficients and Reorientational Correlation Times

Based on the derivation discussed in Section 6.4.4, correlation time, τ_c can be correlated to translational diffusion by hydrodynamic radius and is given by:

$$\tau_c = \frac{2R_H^2}{9D} \qquad 6.9$$

Figure 6.24 shows the classical plot of reorientational correlation time, τ_c of 10 wt% carbohydrates versus the reciprocal self-diffusion coefficient. The dependence of τ_c upon 1/*D* has zero intercept and is clearly non-linear. The non-linear dependence of τ_c upon 1/*D* suggests that the microscopic translational mobility of the EMIMAc molecules in these systems is not fully responsible for the NMR obtained reorientational correlation times. It is likely that the reorientational correlation time is governed by both translational and rotational motion of the EMIMAc molecules. The most important feature is that all the data comes together on one curve. This suggests that the microscopic motion of EMIMAc molecules is sensitive to a similar environment regardless which types of solute it is in.

In Figure 6.24, the non-linear of τ_c on 1/*D* can be divided into two region in which the variation of τ_c is roughly linear. From Figure 6.24, it can be seen that in a region where the diffusion coefficient is large, τ_c shows a linear dependent with 1/*D*. This indicated that in a dilute region (left side), the correlation time is predominantly determined by translational diffusion while at concentrated region (right side), the rotational motion is more dominant.

In Figure 6.25, a master plot of τ_c against 1/*D* for all systems (EMIMAc/glucose, EMIMAc/cellobiose and EMIMAc/cellulose) and temperature is shown. The trend in which all the data points collapsed onto one curve regardless of which carbohydrate group they are belonged to verified the Equation 6.9, which only depends on the hydrodynamic radius of molecule.

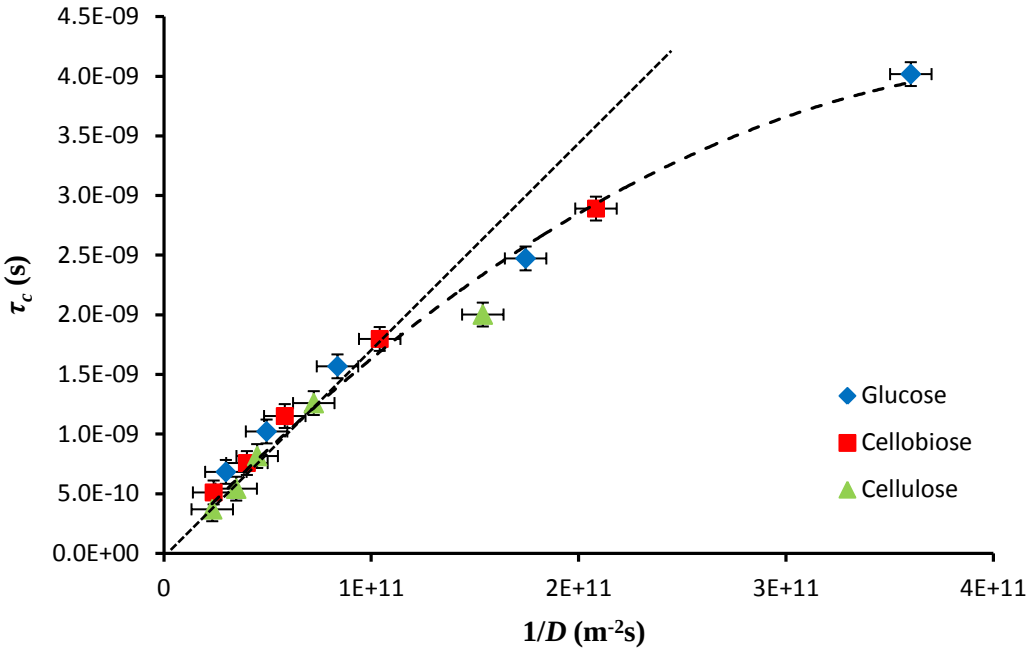

Figure 6.24: τ_c against the reciprocal of the self-diffusion coefficient of $EMIM^+$ for 10% carbohydrates concentration shows that all the data points collapsed onto one curve regardless of which carbohydrate group they are belonged to.

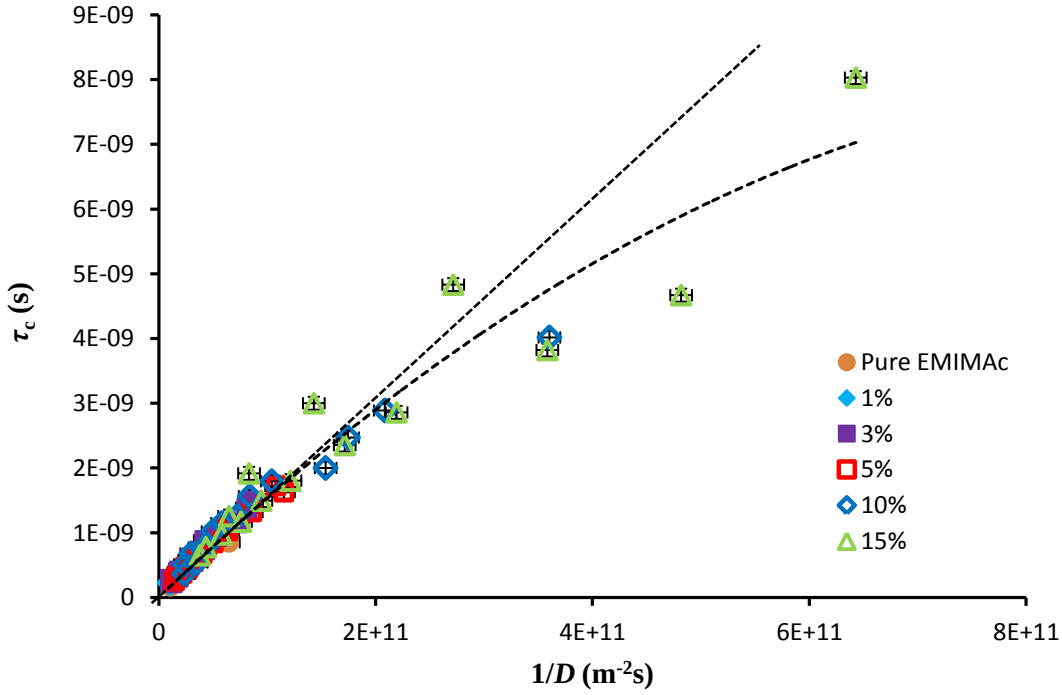

Figure 6.25: Master plot of τ_c against 1/*D* for all data at all temperatures and systems.

The relationship between D_o and τ_o that has been derived in Section 5.4.4 is here verified using the results obtained from diffusion and NMR relaxometry of glucose, cellobiose and cellulose solutions.

$$D_o = \frac{2}{9} R_H^2 \frac{1}{\tau_o} exp^{\Delta E/kT} \qquad 6.10$$

In this study, the value of τ_o and D_o of $EMIM^+$ determined from an Arrhenius fitting is given by 1.00 x 10^{-15} s and 1.43 x 10^{-3} m^2/s respectively. If the temperature takes the average value of 293 K and hydrodynamic radius of $EMIM^+$, R_H, 2.74 Å, it is possible to determine the value of ΔE for $EMIM^+$. Based on the Equation 6.10, the value of ΔE for $EMIM^+$ is found to be 10.8 kJ/mol. These values, which have been independently determined from τ_o and D_o of $EMIM^+$, matches extremely well with the ΔE of $EMIM^+$ (12.6 ± 0.5 kJ/mol) found from the previous analysis.

6.5 Conclusions

This study has shown that the microscopic properties of the EMIMAc molecules are influenced almost exclusively by the presence of free hydroxyl groups associated with the carbohydrates. It was found that EMIMAc molecules in the system having more free hydroxyl groups tended to show the slowest mobility, i.e. glucose is the most effective at slowing down the mobility of EMIMAc while cellulose is the least effective. However, in terms of viscosity this order is reversed in that cellulose becomes the most effective molecule for increasing the zero shear rate viscosity. The results indicate that both the translational and rotational motion of EMIMAc cannot be directly related to solution shear viscosity and therefore cannot be interpreted by means of the classical hydrodynamic theory.

The most obvious finding to emerge from this study is that, both diffusion and correlation times are dependent on the associated fraction, a which is proportional to the number of hydroxyl groups associated with the dissolved carbohydrate.

Low field (20 MHz) proton spin-lattice, T_1 and spin-spin relaxation T_2 times were measured. The trend which all the data for T_1 collapses onto one curve and exhibits a minimum while T_2 simply decreased with a indicated that the more hydroxyl groups present in the solution, the more effective the solution is at relaxating the NMR signal (*recall* Figure 6.16).

In the case of diffusion, both cation and anion show a strong dependence on the number of hydroxyl groups which indicated that the mobility of both anion and cation is affected by the presence of hydroxyl groups. However, a consistent value of the microviscosity factor, f_μ for cation across all the concentration suggested that the cation is less likely to interact with the solute compared to its counterpart anion. Therefore, the dependence of cation diffusivity on hydroxyl groups could be resulted from the indirect effect of interaction between anion and hydroxyl groups.

Additionally, the $E_a[D]$ and $E_a[\tau_c]$ of EMIMAc also obey the diffusion and reorientational process in which the activation energies are strongly dependent on the number of free hydroxyl groups associated with the carbohydrates. A trend which $E_a[D]$ and $E_a[\tau_c]$ merges into single straight line when plotting against bound

fraction, *a* suggested that the presence of more hydroxyl groups in carbohydrates as a binding site for EMIMAc molecules resulted in a higher energy required for EMIMAc to diffuse and reorient itself in the solutions.

This study also provides additional evidence with respect to the peculiarity of the self-diffusion coefficients of the anion and cation where the smaller anion diffuses slower than the larger cation. However the result obtained from a least-squares analysis showed that the value of D_o for the anion is larger than that for the cation, which one would expect from it being a smaller diffusing entity. This explained that the anomalous behaviour of the anion and cation in this IL is due to the interactions of the ions with their surroundings.

A classical plot of reorientational correlation time, τ_c versus the reciprocal self-diffusion coefficient, $1/D$ for all solutions in one graph showed that all the data collapsed onto one master curve (*recall* Figure 6.24 and Figure 6.25). This implied that the microscopic motion of EMIMAc molecules is sensitive to a similar environment regardless which carbohydrate group they are belonged to. A non-linear relationship between τ_c and $1/D$ suggested that the reorientational correlation time is likely governed by both translational and rotational motion of the EMIMAc molecules. Apart from that, this result also contributes additional evidence to the derivation of relationship between correlation time, τ_c and translational diffusion, D which expressed that the τ_c is correlated to D by a hydrodynamic radius (*recall* Equation 6.9)

By combining the molecular reorientational correlation times with self-diffusion coefficient data, the relationship between τ_o and D_o of EMIMAc that depends on the hydrodynamic radius of the molecules and the difference in activation energy between diffusion and NMR correlation times were also developed. It was found that the value of D_o or τ_o estimated from ΔE or vice versa matches extremely well.

Chapter 7
Kinetics of Cellulose Coagulation from EMIMAc/DMSO/Cellulose Systems

7.1 Introduction

The precipitation of cellulose dissolved in ILs could be accomplished by immersing cellulose/IL solution in a bath of anti-solvents [8]. This is not only a physical process (solvent exchange), but also a phase separation process. During coagulation, mass transfer and phase equilibrium between the cellulose solution and the coagulation bath occurs and results in the precipitation of the cellulose structure. In order to ensure the precipitation process is successful, the ILs and co-solvent (if employed together) must be miscible in anti-solvent that has been used. Ideally, polar liquids such as water, ethanol and acetone are the most suitable anti-solvent that can be used to precipitate cellulose as their miscibility in ILs has already been investigated and understood [201, 202].

It is well known that interaction energies between IL and cellulose are very strong as a result of strong interaction between ions with cellulose hydroxyl groups. Nevertheless, the interaction energies of the IL-cellulose system decreased with further addition of water molecules into the system which implies that addition of water into the system has weakened and destroyed the hydrogen bonds between IL and cellulose [203]. During the coagulation process the preference of IL to form stronger interaction with water than cellulose consequently caused the intermolecular interaction between cellulose monomer to reform and precipitate out from the IL-cellulose system.

Several attempts have been made to study the factors affecting the morphological features of precipitated cellulose. These factors vary from the condition of pre-treatment of cellulose such as polymer solution state to the condition during the precipitation/coagulation process, such as type of anti-solvent, temperature and concentration of coagulation bath [10, 106, 204, 205]. Among all those stages, the coagulation condition is the most crucial procedure to the formation

of the morphological features of cellulose. The morphological features of cellulose depend on the mode and kinetics of the coagulation. The diffusion rate of the solvent molecules is important in determining the microstructure of the cellulose membrane/fibre [9].

Composition and phase changes of cellulose solution at different position during coagulation process have been extensively studied by Laity et al. using Magnetic Resonance Imaging (MRI) [206, 207]. Using this technique, the structural changes can be inferred from measurements of diffusion coefficients and relaxation time constants. Their studies demonstrated that the coagulation occurs in several stages. On the onset of coagulation, a rapid exchange of solvent and anti-solvent takes place at the surface of polymer sample in contact with the coagulant and caused the polymer to precipitate. At this stage, the diffusion rate of anti-solvent is higher than the diffusion rate of the solvent, i.e. the anti-solvent penetrating the polymer sample is quicker than the extraction of the solvent out of the sample. However, deeper inside the sample, the exchange takes place more slowly as a result of precipitation of polymer at the surface. The slower phase change deeper within the polymer sample resulted in the formation of larger pores. Later in the coagulation, the situation is reversed in which a greater volume of solvent diffused out than anti-solvent diffused in.

A microscopic insight into the mechanism of cellulose regeneration with a focus on the effects of water concentration and temperature found that the number of cellulose contacts rises upon increasing the temperature of the water bath [106]. W. Xiao et al. studied the effect of anti-solvent on regenerated cellulose and they found that the use of water is most beneficial compared to methanol and ethanol. This is because the yield of the total reducing sugar from regenerated cellulose is found to be higher when water is used as anti-solvent [208]. There were similar findings by Li and co-workers which reported that the use of water as anti-solvent gave higher efficiencies of cellulolytic enzymatic hydrolyses [209].

In this study, the diffusion dynamics of 1-Ethyl-3-Methylimidazolium Acetate (EMIMAc) and dimethyl sulfoxide (DMSO) during the coagulation process of cellulose with water as non-solvent were investigated in detail. Particularly, three cellulose concentrations (5, 10 and 15 wt%) and four different concentrations of

DMSO (20, 30, 40, and 50 wt%) were considered to explore the effect of both cellulose and DMSO concentration on the kinetics of cellulose coagulation from cellulose/ EMIMAc-DMSO solution.

7.2 Experimental Methods

7.2.1 Materials and Sample Preparation

Avicel PH-101 microcrystalline cellulose, (cellulose) with a degree of polymerization of 180 was purchased from Sigma Aldrich. Prior to the sample preparation, cellulose was dried under vacuum at 80 ^{o}C for a period of 12 hours. In this work, cellulose, EMMIMAc and DMSO were mixed and magnetically stirred at a total of 5 g per solution in the sealed reaction vessel at 70 ^{o}C, for about 24 hours, to ensure they had completely dissolved. Three different cellulose concentrations (5, 10 and 15 wt%) were dissolved in 60 wt% EMIMAc/40 wt% DMSO to study the effect of cellulose concentration on the coagulation process while 10 wt% cellulose was dissolved in a series of EMIMAc-DMSO solution with various DMSO concentrations (20, 30 40, and 50 wt%) to study the effect of DMSO concentration on the coagulation process. Concentration of cellulose dissolved in EMIMAc-DMSO was calculated using the equation below:

$$C_{cellulose} = \frac{m_{cellulose}}{m_{cellulose} + m_{EMIMAc} + m_{DMSO}} .100\% \qquad 7.1$$

while concentration of DMSO was calculated using the equation below:

$$C_{DMSO} = \frac{m_{DMSO}}{m_{EMIMAc} + m_{DMSO}} .100\% \qquad 7.2$$

In Equations 7.1 and 7.2, $C_{\text{cellulose}}$ and C_{DMSO} are the concentration of cellulose and DMSO whereas $m_{\text{cellulose}}$, m_{EMIMAc} and mm_{DMSO} are the mass of cellulose, EMIMAc and DMSO respectively.

In this study, distilled water was used as a coagulation bath.

7.2.2 Coagulation rate measurements

In order to study the kinetics of the cellulose regeneration, the Fickian approach was used. The infinite plane source approximation was chosen for the ease of calculations and sample preparation. The approximation assumed the thickness of the disk (*l)* must not be larger than 1/10 of its diameter. A cylindrical pan of 26.74 mm diameter and thickness 2*l* = 3.02 mm was selected. The mould had walls which were constructed from a stainless steel grid with pore sizes of 50 μm x 50 μm. The solution was decanted into the pan, closed with an identical grid (the same as the bottom of the pan) and removed from the glove box. The pan was then immersed into a regenerating bath with 100 ml distilled water at 20 ^{o}C. This set-up allowed diffusion through the grid walls and kept the sample size roughly constant during the regeneration process.

Once in the regenerating bath the stop watch was started immediately and the magnetic stirrer was set at a gentle stirring rate (~100 rpm) to provide a homogenised concentration throughout. The proportion between a sample/bath weight was about 1/50 with a bath mass of 100 g. At each time interval a small amount of sample (~2 g) was removed from the regenerating bath and placed into a small beaker. The same amount of distilled water was then added to compensate for the water removed. The same procedure was carried out with every sample.

Due to the extremely small ratio of EMIMAc and DMSO to water, it was not possible to directly detect the EMIMAc and DMSO spectral peaks. To increase EMIMAc and DMSO concentrations and therefore improve the visibility of the spectral peaks, water was evaporated in a controlled manner (gently heating at 100 ^{o}C). Each sample was then placed into a standard 5 mm NMR tube and stored in a cool dry place.

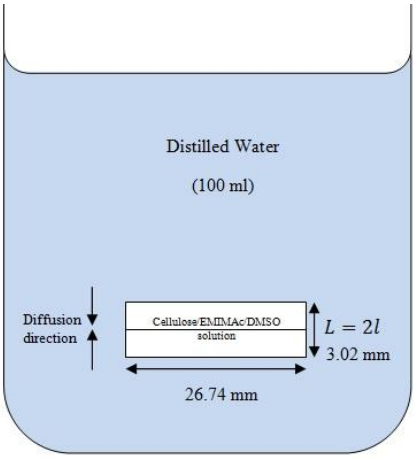

Figure 7.1: Set up of the regeneration process with the cellulose solution inside the pan.

7.2.3 Determination of the EMIMAc and DMSO concentration in the coagulation bath.

The concentration of EMIMAc and DMSO that was released from the cellulose solution to the regeneration bath was determined using high field ^{1}H NMR spectroscopy. The NMR spectrum of EMIMAc and DMSO at set time intervals was obtained by applying a one dimensional (1D) 90^{o} pulse sequence.

Each spectral peak with its corresponding molecule was analysed using Bruker's Biospin 1.5 software. The intensity of each signal was integrated using the integration tool. The integrated intensity of each signal in the spectrum provides a ratio for the number of hydrogen that gives rise to the signal (*see* Figure 7.2). The proportionality of the spectrum intensity with the number of protons makes it possible to calculate the total number of hydrogen present in a sample. The fraction of each component, i.e. EMIMAc, DMSO and water presented in a sample was determined using Equation 7.3 (EMIMAc used as an example throughout):

$$f = \frac{I}{N_H} . M \qquad 7.3$$

where I is the spectrum intensity of the EMIMAc, N_H is the number of protons in the EMIMAc molecule and M is a molar mass of the EMIMAc.

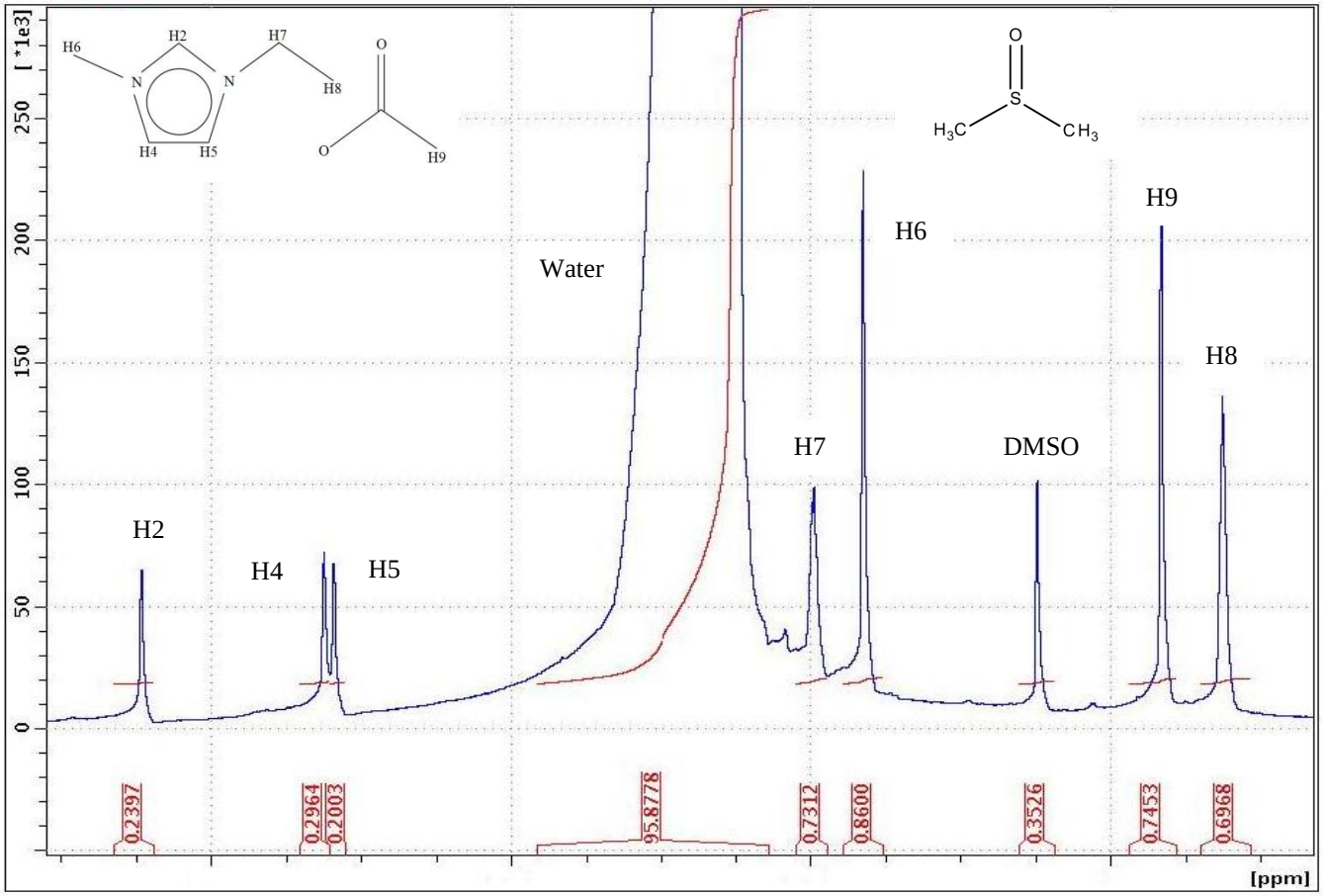

Figure 7.2: Integrations of ^{1}H NMR spectra of a sample from the regenerating bath after evaporation. (Insert: Chemical structure of EMIMAc (left), labelled with H2-H9 and DMSO (right).

Mass fraction, *f'* of each component (e.g. EMIMAc) is then calculated using equation below:

$$f'_{EMIMAc} = \frac{f_{EMIMAc}}{f_{EMIMAc} + f_{DMSO} + f_{water}} \quad 7.4$$

The masses of EMIMAc (m'_{EMIMAc}), DMSO (m'_{DMSO}) and water (m'_{Water}) in the NMR tubes were calculated by multiplying the known mass of sample in the NMR tube (m') by the mass fraction as shown

$$m'_{EMIMAc} = f'_{EMIMAc} * m' \quad 7.5$$

The same process was repeated to find the mass fraction of the EMIMAc (F_{EMIMAc}) and DMSO (F_{DMSO}) in the regenerating bath.

$$F_{EMIMAc} = \frac{m'_{EMIMAc}}{m'_{EMIMAc} + m'_{DMSO} + m'_{Water} + \Delta m} \quad 7.6$$

The total mass also contained the evaporated water (Δm) from the beakers. The mass of EMIMAc (M_{EMIMAc}) and DMSO (M_{DMSO}) were simply calculated again by multiplying the known mass of solution in the bath (m) by the mass fraction as shown

$$m_{EMIMAc} = F_{EMIMAc} * m \quad 7.7$$

Each mass taken from the bath was added to a summation of all the previous masses in the NMR tubes to produce the total mass of EMIMAC ($m_{Total\ EMIMAc}$) and DMSO ($m_{Total\ DMSO}$) as shown

$$m_{Total\ EMIMAc} = m_{EMIMAc} + \sum_{n} m'_{EMIMAc} \quad 7.8$$

where *n* is the number up to and including the NMR tube used. The mass of the EMIMAc and DMSO was mapped to describe the mass evolution of the regeneration. An example of the mass evolution of the EMIMAc and DMSO in the water bath at time, *t* is shown in Figure 7.3.

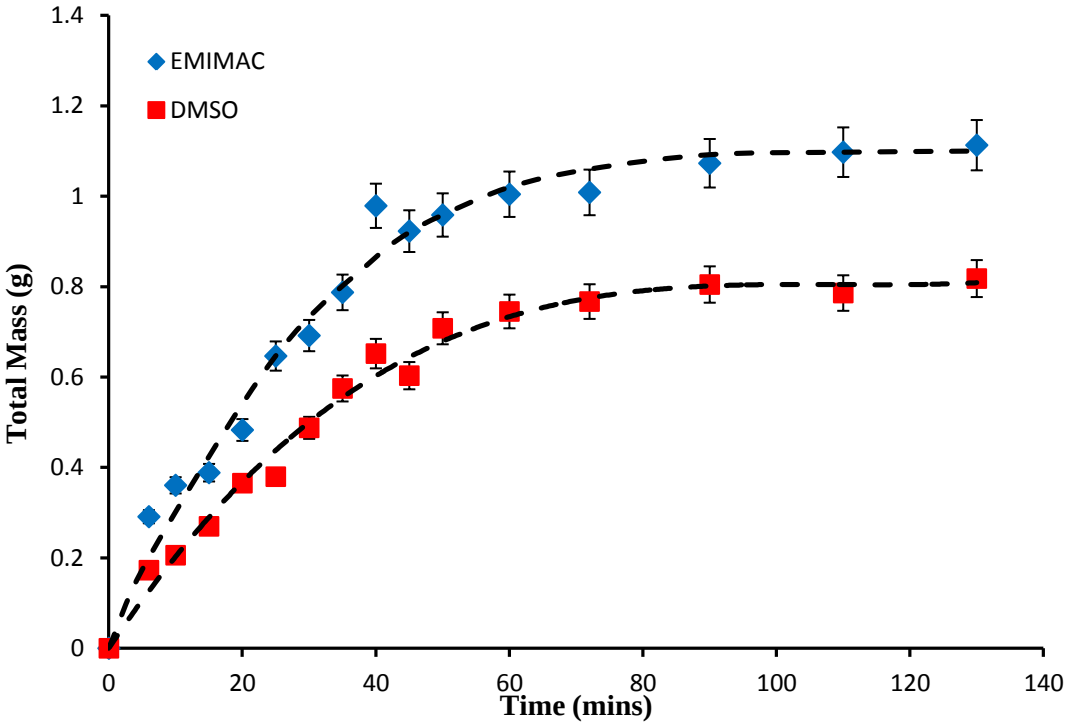

Figure 7.3: The amount of EMIMAc and DMSO released by a sample at time *t*, for 5% cellulose in 60 wt% EMIMAc - 40 wt% DMSO. The dashed lines are presented as an aid to the eye.

7.3 Results

7.3.1 Measurement of diffusion coefficient

The increase of EMIMAc and DMSO in the regenerating bath as a function of time and under different conditions (various cellulose concentration and co-solvent) is analysed using a diffusion controlled model that has been derived from Fick's second law of diffusion. This model is widely used especially in the drug release field [210, 211], and to study the formation of membranes due to phase separation.

In this study the cumulative amount of substance $M(t)/M_\infty$ (here, EMIMAc and DMSO) released in time *t* is proportional to the square root of time. As shown in Figure 7.4 the graphs of $M(t)/M_\infty$ against $\sqrt{t}$ show a straight line within 10% experimental error, up to 70-80 % of the total mass released providing a reliable measure of coagulation rate. The linear dependence of $M(t)/M_\infty$ as a function of $\sqrt{t}$ indicated that the process is a diffusion-controlled process. Therefore, all samples that coagulated from the water bath allowed the application of the diffusion controlled model.

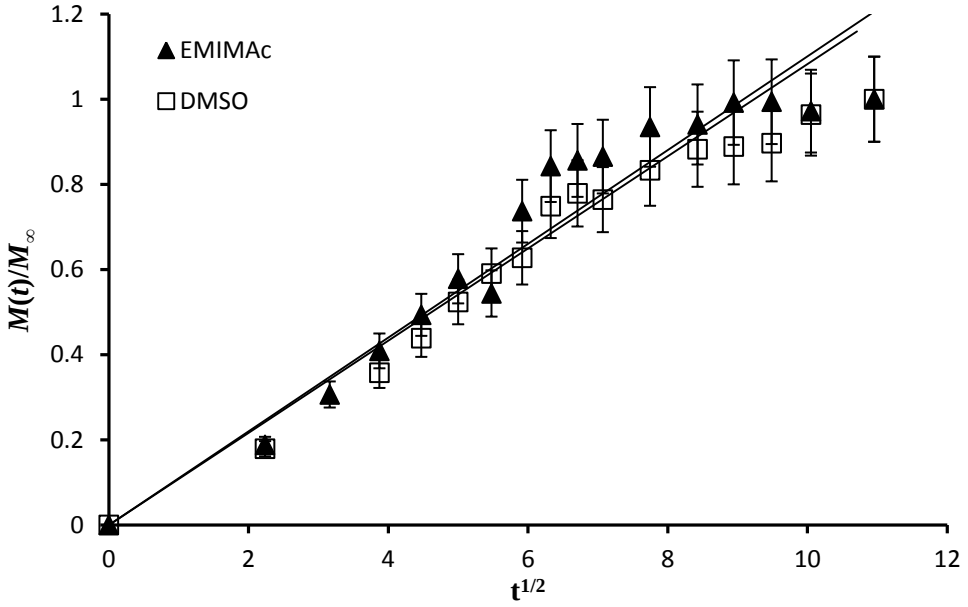

Figure 7.4: The total mass of EMIMAc and DMSO released during the coagulation process as a function of square root time. The data approximated by a straight line up to 70-80 % of *M*(*t*) indicates a diffusion-controlled process.

In the case of a semi infinite plane, the amount of substance released in time can be described as follows [212]:

$$\frac{M(t)}{M_\infty} = 1 - \frac{8}{\pi^2}\sum_{n=0}^{\infty}\frac{1}{(2n+1)^2}e^{-\left(\frac{\pi^2 Dt(2n+1)^2}{l^2}\right)} \qquad 7.9$$

where $M(t)$ is the amount of accumulated substance released at the certain time and M_∞ is the equilibrium mass, i.e. total amount of substance released at $t = \infty$. In this equation, l is equal to half of the sample thickness because the diffusion takes place from both sides of the sample. The solution is valid if the sample does not start with any vapour of a diffusing substance (water) and if the concentration of the solution has reached equilibrium at the sample's surface and is therefore constant [212]. These specific conditions make it possible to deduce an average diffusion coefficient from the slope of three intervals of the curve.

Early time approximation which holds for the release of the first 40% of cumulative release i.e $0 \leq M(t)/M_\infty \leq 0.4$ is described as follows:

$$\frac{M(t)}{M_\infty} = 4\left(\frac{Dt}{\pi l^2}\right)^{1/2} \qquad 7.10$$

Half time approximation $M(t)/M_\infty = 0.5$

$$D = \frac{0.049}{\left(\frac{t}{l^2}\right)_{At\ M(t)/M_\infty = 0.5}} \qquad 7.11$$

Late time approximation which holds for the final portion of the solvent release, i.e. $0.4 \leq M(t)/M_\infty \leq 1$ can be described by the following equation:

$$\frac{M(t)}{M_\infty} = 1 - \frac{8}{\pi^2}e^{-\left(\frac{\pi^2 Dt}{l^2}\right)} \qquad 7.12$$

Table 7.1:Total amount of EMIMAc and DMSO used during sample preparation and their total amount accumulated in water bath after coagulation process was completed.

Solvent (wt %)	Cellulose concentration (wt %)	Total amount of EMIMAc & DMSO used (g)		Total amount of EMIMAc & DMSO accumulated in the water bath (g)		Differences (g)	
		EMIMAc	DMSO	EMIMAc	DMSO	EMIMAc	DMSO
60 % EMIMAc - 40% DMSO	5	1.348 ± 0.020	0.899 ± 0.020	1.25 ± 0.06	0.86 ± 0.04	0.103 ± 0.060	0.039 ± 0.040
60 % EMIMAc - 40% DMSO	10	1.316 ± 0.020	0.877 ± 0.020	1.11 ± 0.06	0.82 ± 0.04	0.208 ± 0.060	0.062 ± 0.040
60 % EMIMAc - 40% DMSO	15	1.146 ± 0.020	0.764 ± 0.020	1.20 ± 0.06	0.57 ± 0.03	-0.068 ± 0.060	0.194 ± 0.040
50 % EMIMAc - 50% DMSO	10	1.100 ± 0.020	1.100 ± 0.020	1.10 ± 0.06	0.92 ± 0.05	0.000 ± 0.020	0.180 ± 0.050
70 % EMIMAc - 30% DMSO	10	1.449 ± 0.020	0.621 ± 0.020	1.26 ± 0.06	0.59 ± 0.03	0.192 ± 0.060	0.031 ± 0.040
80 % EMIMAc - 20% DMSO	10	1.716 ± 0.020	0.429 ± 0.020	1.35 ± 0.07	0.36 ± 0.02	0.368 ± 0.070	0.074 ± 0.030

The determination of the EMIMAc and DMSO diffusion coefficients is illustrated in Figure 7.5. In this case, the cellulose concentration is 10% and the solvent is 50% EMIMAc and 50% DMSO. Figure 7.5 shows the dependence of the ratio $M(t)/M_\infty$ versus t/l^2 for the EMIMAc and DMSO loss from the solution. From Figure 7.5, it can be seen that, $M(t)$, i.e. the mass of EMIMAc and DMSO that left the cellulose solution at time t as well as M_∞, i.e. the mass of EMIMAc and DMSO that left the cellulose solution at the end of the precipitation process, can be estimated as a function of time. The coefficients of diffusion of EMIMAc and DMSO from cellulose/EMIMAc-DMSO solution into the bath were calculated from the slope at the origin of the curve presented in Figure 7.5.

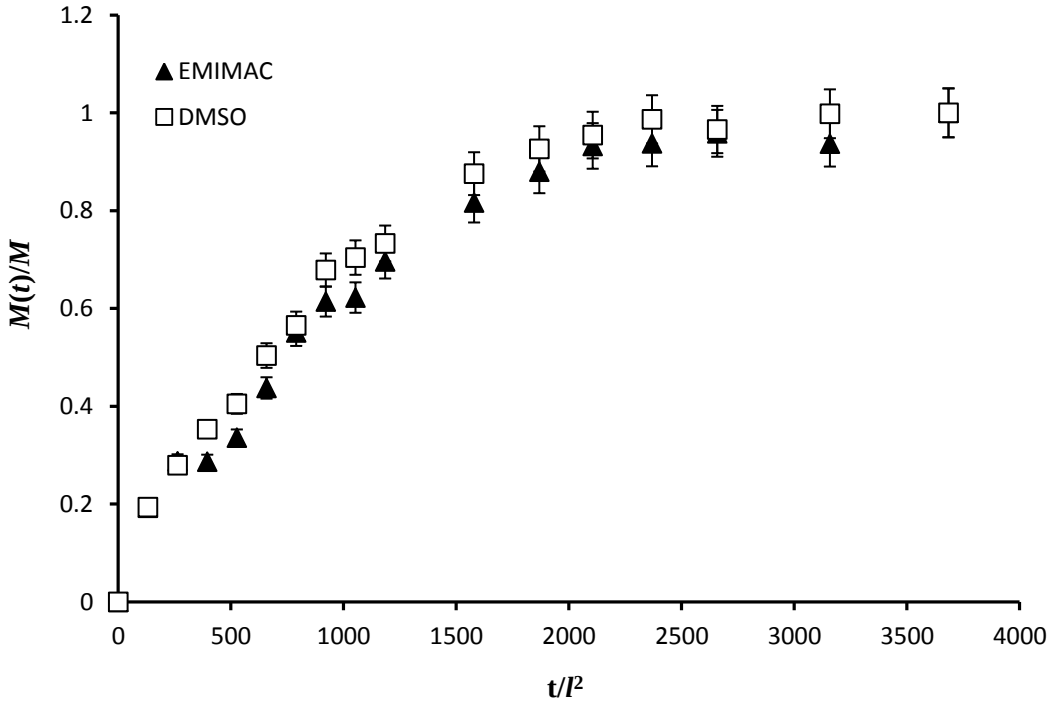

Figure 7.5: The mass of EMIMAc and DMSO released during the regeneration process of 10% cellulose in 50 wt% EMIMAc-50 wt% DMSO solution at 20 ^{o}C.

7.3.2 Effect of cellulose concentration on the coagulation process

The curve in Figure 7.6 shows the development of the content of EMIMAc and DMSO in the coagulation bath during the coagulation process in a distilled water bath. At the beginning of the coagulation process, the amount of EMIMAc and DMSO released to the water bath is very rapid. However, after a sufficiently long coagulation period, the equilibrium was reached where no further addition of EMIMAc and DMSO in the water bath was observed.

The diffusion coefficient of EMIMAc and DMSO at each stage (early, mid and late) is determined using three approximate equations (Equations 7.10, 7.11 and 7.12) described in previous section. As shown in Table 7.2, at the onset of coagulation, the rate of diffusion of both EMIMAc and DMSO is slow. This is in agreement with previous findings by Laity et al. which found that the solvent content in a sample appeared to remain unaffected at early stage [207]. The authors proposed that this phenomenon is due to the extraction of the solvent out of the sample was hindered by their strong interaction (i.e. hydrogen bonding) with cellulose. However, at later stage, cellulose starts to form stronger hydrogen bonds with water molecules subsequently wash away the solvent out of the sample more quickly. From this study, it was found that the average diffusion coefficient of EMIMAc for 5 wt%, 10 wt% and 15 wt% of cellulose are $1.01 \times 10^{-10} \pm 0.6$ m^2/s, $0.83 \times 10^{-10} \pm 0.6$ m^2/s and $0.95 \times 10^{-10} \pm 0.5$ m^2/s respectively.

The present finding seems to be consistent with the research by Sescousse et al. which found that the diffusion coefficient of EMIMAc for 5, 10 and 15 wt% cellulose solutions ranged from $3 - 4 \times 10^{-10}$ m^2/s [11]. In addition, our result is also in agreement with that of the cellulose/BMIMCl solution studied by Jiang and co-workers which found that the values of diffusion coefficient of BMIMCl calculated from their model were in the range of $1.0 - 2.5 \times 10^{-11}$ m^2/s. In their work, the diffusion dynamic of BMIMCl with the initial cellulose concentration 5 - 12 wt% and the temperature of the coagulation bath at 20 ^oC was determined using a spinneret device. Compared with their work, the orders of magnitude of diffusion coefficients of EMIMAc is the same even though it is slightly higher than that of BMIMCl. This is owing to the fact that, cellulose/EMIMAc-DMSO solutions have

significantly lower zero shear viscosities than those of the cellulose/BMIMCl systems [172].

In the case of co-solvent (DMSO), it was found that the average diffusion coefficient of DMSO for 5 wt%, 10 wt% and 15 wt% of cellulose are $0.94 \pm 0.5 \times 10^{-10}$ m^2/s, $0.84 \pm 0.2 \times 10^{-10}$ m^2/s and $0.94 \pm 0.6 \times 10^{-10}$ m^2/s respectively. The orders of magnitude of diffusion coefficient for DMSO are similar to the EMIMAc. It shows that DMSO is leaving the cellulose solution as fast as EMIMAc is leaving. Similar to the case of EMIMAc, the diffusion coefficient of DMSO also does not change with cellulose concentration.

There are several factors including the viscosity of the medium that control the diffusion of species in a medium. Using cellulose with different concentration, and thus different viscosity, should influence the diffusion coefficient of EMIMAc and DMSO. It does not. There is no measurable difference between each concentration and their values coincide within an experimental error. The diffusion coefficient of EMIMAc and DMSO was consistent at approximately $9.3 \pm 0.9 \times 10^{-11}$ m^2s^{-1} and $9.1 \pm 0.6 \times 10^{-11}$ m^2s^{-1} respectively. This suggested that, the viscosity of the solution in a small disc does not affect the coagulation rate of the solvent. These findings suggest that cellulose concentration only had a little effect on the diffusion coefficient of the solvent. A narrow range of cellulose concentration used in this study did not significantly alter the total amount of solvent presented in each solution (*see* Table 7.1). This finding is in agreement with Sescousse's findings which showed the diffusion rate of EMIMAc released from EMIMAc/cellulose solutions did not vary with cellulose concentration [11].

Another important finding in this study was that, the average diffusion coefficient of EMIMAc is found to be equivalent with the diffusion coefficient of EMIMAc in EMIMAc-water mixtures at water molar fraction, *ca*. 0.80 [40]. The present findings seem to be consistent with other research which found that phase separation in IL/water mixtures occurred at water molar fraction between 0.7-0.8 [213].

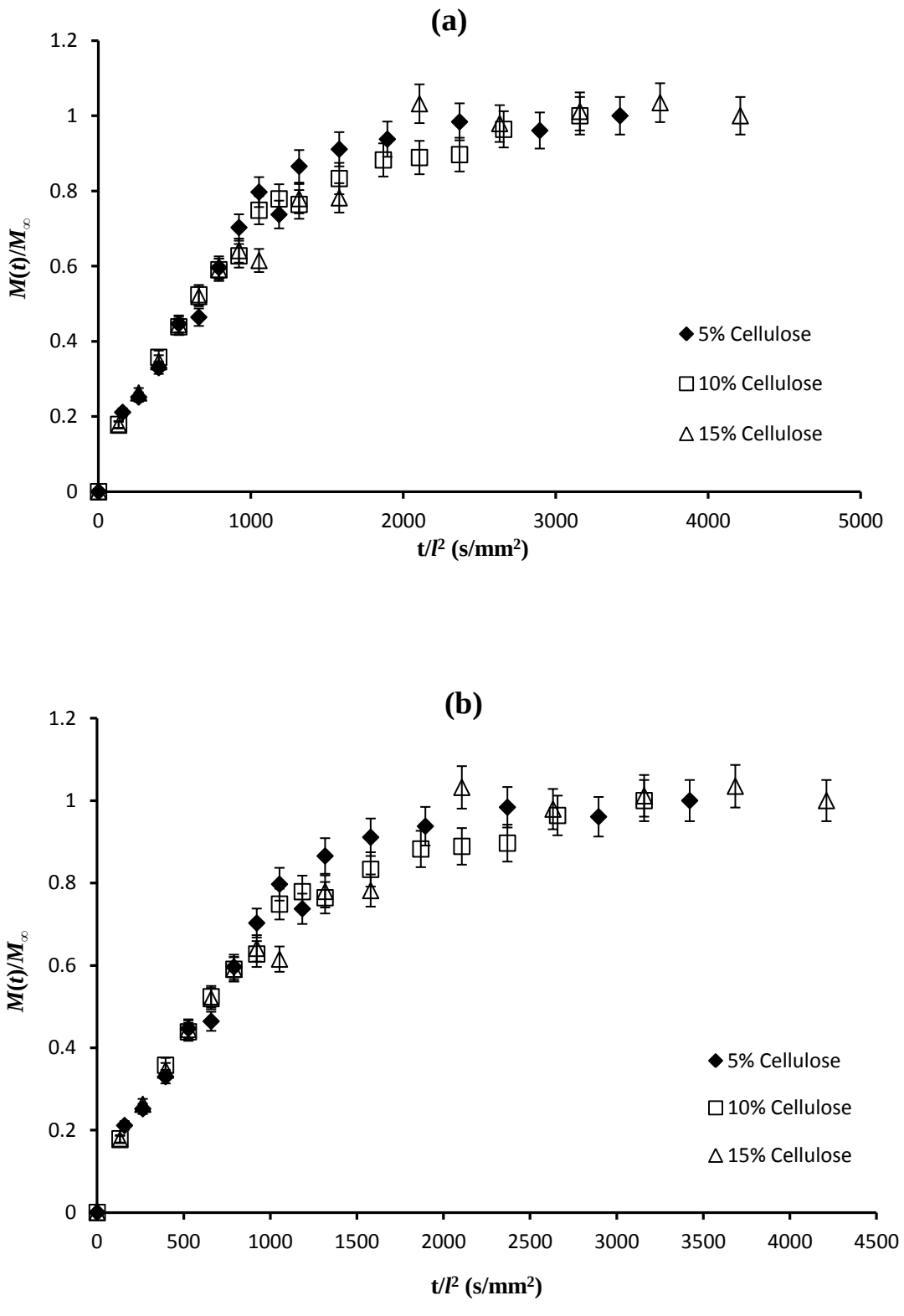

Figure 7.6: The mass of a) EMIMAc and b) DMSO released during the regeneration process of 5, 10 and 15 % cellulose in 60 wt% EMIMAc-40 wt% DMSO solutions at 20 ^{o}C.

Table 7.2: Evolution of the self diffusion coefficient at early, middle and long times for EMIMAc and DMSO for 5, 10 and 15 wt% cellulose concentrations in a 60 wt% EMIMAc-40 wt% DMSO solution.

	Cellulose concentration (wt%)	**Diffusion coefficient, (10^{-10} m^2/s)**	
		EMIMAc	**DMSO**
Early time; $\frac{M(t)}{M_\infty} = 4\left(\frac{Dt}{\pi l^2}\right)^{1/2}$	**5**	0.69	0.59
	10	0.73	0.66
	15	0.48	0.56
Middle time; $D = \frac{0.049}{\left(\frac{t}{l^2}\right)_{At\ M(t)/M_\infty = 0.5}}$	**5**	0.62	0.62
	10	0.93	0.75
	15	0.93	0.75
Late time; $\frac{M(t)}{M_\infty} = 1 - \frac{8}{\pi^2} e^{-\left(\frac{\pi^2 Dt}{l^2}\right)}$	**5**	1.72	1.62
	10	1.82	1.11
	15	1.42	1.52

7.3.3 Effect of co-solvent composition on the coagulation process

The influence of co-solvent concentration on the kinetics of cellulose regeneration was also studied. Since the coagulation of cellulose is mainly accomplished through molecular diffusion of both solvent and anti-solvent, therefore an increase in the amount of co-solvent in cellulose solutions by some means reduced its viscosity. The drop in viscosity of cellulose solution caused easier transport of liquid and increased the mobility of the molecular chain which is beneficial to diffusion of the solvent and anti-solvent molecules. One would expect that solvent molecules will move more quickly and the diffusion coefficient of solvent molecules increase under these conditions. However, there is no measurable difference between each concentration and their values coincide with experimental error. The diffusion coefficients of EMIMAc and DMSO calculated were in the range of 0.8 - 1.0 x 10^{-10} m^2/s and 0.7-0.9 x 10^{-10} m^2/s respectively. Such a weak dependence of solvent diffusion coefficient on co-solvent concentration is rather unusual.

There are a few reasons for this different concentration behaviour. First, the driving force that governs the diffusion of solvent into the coagulation bath is the water itself. As for IL, water also formed a hydrogen bond with DMSO as strong as it is in aqueous IL. Similar to water-IL mixtures, the transport properties of water-DMSO mixtures also showed non-ideal behaviour. The strong hydrogen bond association between water and DMSO molecules at 60-70 % molar fraction of water is said to be the main factor responsible for the strong non-ideal behaviour of this mixture [214] . Evidence of the existence of some structures of the form 1-DMSO:2-water or 1-DMSO:3-water is also supported by molecular simulation studies [215] as well as neutron diffraction experiments [216]. This finding is in parallel with the transport properties of water-IL mixtures which showed a strong deviation from ideal mixing law with the maximum deviation occurred at ~70 % molar fraction of water [40].

In the process of cellulose coagulation, the ratio between sample and bath mass was approximately 1/50 with a bath mass of 100 g. The presence of a large quantity of water molecules enabled them to form an association with both IL and DMSO

molecules simultaneously and eventually remove them from the cellulose solution with more or less the same diffusion rate.

Based on our previous study on EMIMAc-water mixtures, the self-diffusion coefficients of EMIM+, Ac- and water at 303 K with 0.99 mole fraction of water are 1.2×10^{-9}, 1.29×10^{-9} and 2.41×10^{-9}. This indicates that in very dilute regions, the self-diffusion coefficient of IL is approximately comparable to the self-diffusion of water.

Another possible reason for a constant value of diffusion coefficient of EMIMAc and DMSO with variable co-solvent concentrations could possibly be explained by the morphology of the cellulose solutions. Mass transfer through polymeric membranes not only depends on the penetrant molecules, but also the morphology of the membrane. Hedenqvist et al has explained that polymers with high crystallinity are less penetrable because the crystallites have fewer holes through which penetrant molecules may pass [217]. In our study, a further increase of the concentration ratio of DMSO to EMIMAc has weakened the ability of EMIMAc to significantly reduce the crystanallity of cellulose for dissolution. Tian et al has studied the effect of co-solvent on cellulose dissolution in AMIMCl. In their study, the crystallinity of the cellulose treated with AMIMCl/DMSO was analysed using X-ray diffraction (XRD) and found that the crystallinity of cellulose decreased from 0.834 to -0.319 as the ratio of EMIMAc to DMSO is increased from 0 to 1 [94]. During the coagulation process, as soon as the cellulose solution is immersed in the water bath, the cellulose immediately started to precipitate. The morphology of cellulose that regenerated might have a different crystanallity which eventually affected the diffusivity of the solvents.

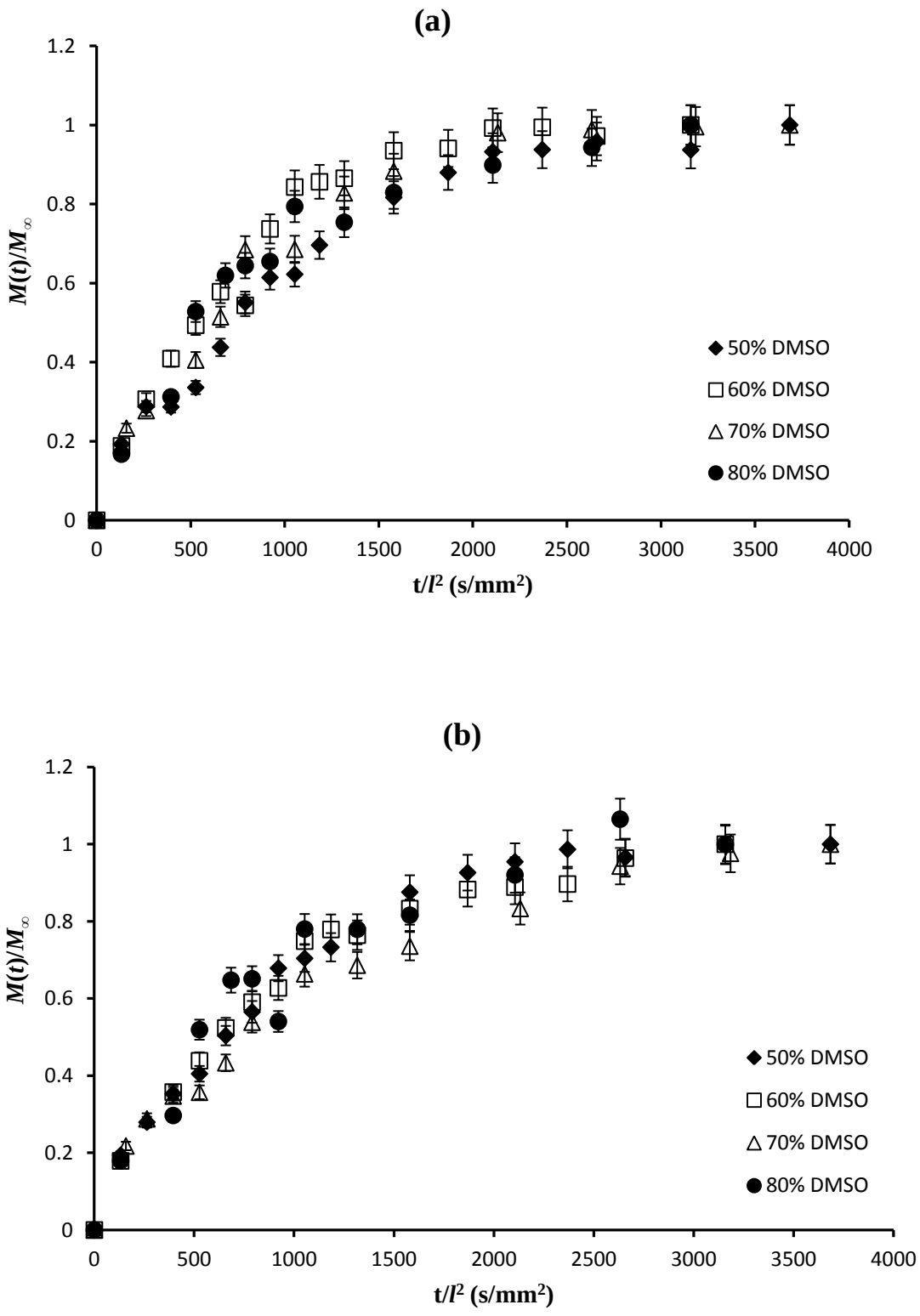

Figure 7.7: The mass of a) EMIMAc and b) DMSO released during the regeneration process of 10 % cellulose in 50, 60, 70 and 80 wt% DMSO-EMIMAc solutions at 20 ^{o}C.

Table 7.3: Evolution of the self diffusion coefficient at early, middle and long times for EMIMAc and DMSO for 10% cellulose in 20, 30, 40 and 50 wt% DMSO-EMIMAc solutions.

	DMSO concentration (wt%)	**Diffusion coefficient, (x 10^{-10} m^2/s)**	
		EMIMAc	**DMSO**
Early time; $\frac{M(t)}{M_\infty} = 4\left(\frac{Dt}{\pi l^2}\right)^{1/2}$	**20**	0.47	0.45
	30	0.62	0.55
	40	0.73	0.66
	50	0.39	0.57
Middle time; $D = \frac{0.049}{\left(\frac{t}{l^2}\right)_{At\ M(t)/M_\infty = 0.5}}$	**20**	0.93	0.93
	30	0.75	0.62
	40	0.93	0.75
	50	0.62	0.75
Late time; $\frac{M(t)}{M_\infty} = 1 - \frac{8}{\pi^2} e^{-\left(\frac{\pi^2 Dt}{l^2}\right)}$	**20**	1.01	1.01
	30	1.52	0.81
	40	1.82	1.11
	50	1.52	1.42

In this study, it is worth noting that, in all cases, the diffusion coefficient of EMIMAc and DMSO coincided within an experimental error. For instance, in a solution of 10% cellulose in 60% EMIMAc - 40%DMSO, the diffusion coefficients of EMIMAc and DMSO are $D_{EMIMAc} = 0.8 \pm 0.6 \times 10^{-11}$ m^2/s and $D_{DMSO} = 0.8 \pm 0.3 \times 10^{-11}$ m^2/s respectively. As we know, the diffusion coefficient of bulk DMSO is approximately two times larger than that of EMIMAc (*see* Section 4.3.5). Therefore the diffusion coefficient of DMSO should be larger which does not match with this result. It appears that the diffusivity of EMIMAc and DMSO in a coagulation bath is based on their affinity to water. Both EMIMAc and DMSO can form a hydrogen bond with water which is a strong proton donor and acceptor.

7.4 Conclusions

The influences of cellulose and DMSO concentration on the diffusion rate of EMIMAC and DMSO during cellulose coagulation were investigated. In this study, the diffusion dynamics of EMIMAc and DMSO provided a basis for the study of mass transport mechanism that is involved during the coagulation process of cellulose.

Based on Fick's second law of diffusion, the calculated diffusion coefficient of both EMIMAc and DMSO were in the range of 0.4 - 1.8 x 10^{-10} m^2/s and 0.4 - 1.5 x 10^{-10} m^2/s respectively. The study of the effect of cellulose concentration on the coagulation process showed that the diffusion coefficients of EMIMAc and DMSO were not significantly changed by the increase of cellulose concentration in the solutions.

Similar behaviour was also observed in the study of the effect of co-solvent (DMSO) on the coagulation process. The changes in DMSO concentration from 20 - 50 wt% were not altering the diffusion coefficient of either EMIMAc or DMSO. Over the range of concentration studied, it was found that the diffusion coefficient of EMIMAc and DMSO was consistent at approximately 0.8 - 1.0 x 10^{-10} m^2/s and 0.7 - 0.9 x 10^{-10} m^2/s respectively.

It is worth noting that in both studies the diffusion coefficient of DMSO always coincides within an experimental error with the diffusion coefficient of EMIMAc. This showed that DMSO was leaving the cellulose solution as fast as EMIMAc was leaving. A constants diffusion dynamic of both EMIMAc and DMSO with variation concentrations of cellulose and co-solvent indicated that the kinetics of cellulose coagulation is similar. This demonstrated that the water molecules were the governing factor determining the kinetics of cellulose coagulation. Therefore, we suggest that any changes in cellulose or DMSO concentration would not significantly affect the morphology of the regenerated cellulose as the diffusion of the solvent occurs at the same rate.

Since the coagulation rate of the solvents is predominantly determined by the anti-solvent hence, if we want to change the coagulation rate and therefore the morphology, we would need to change the anti-solvent.

Chapter 8
Conclusions

8.1 General Conclusion

The works presented here outlines a series of studies that have led to a fundamental understanding of the dissolution and coagulation process of cellulose in ILs. In this study, the experiments carried out using NMR have provided molecular insight into ionic liquid mixtures. A complete relaxation analysis of a given system using rotational correlation functions has provided useful information at the molecular level. The results allow the determination of the structure and relative motion of ILs in both cellulose/IL and IL/co-solvent solutions.

- The influences of dimethyl sulfoxide (DMSO) on 1-Ethyl-3-Methylimidazolium Acetate (EMIMAc) properties and its potential use as a co-solvent in cellulose dissolution process have been investigated. The dynamic properties of IL-DMSO solution at macroscopic and microscopic levels have been analysed using ideal mixing laws and the deviation of these properties from ideal mixing behaviour is reported. In spite of the maximum deviation of all measurements at DMSO molar fraction, $x = 0.65 \pm 0.14$, the deviations are relatively small compared with IL/water mixture. In EMIMAc-DMSO system the percentage of deviation is about one order of magnitude smaller than the deviation in EMIMAc-water system. This suggests that interactions between IL and polar aprotic solvent such as DMSO is weak and might not significantly alter the capability of IL to interact with cellulose. Such a relationship (macro- and micro-scopic properties) will likely aid in the development of new solvent for cellulose/biomass pre-treatment. This study has provided a microscopic insight into the interaction between IL and co-solvent with a focus on the effect of co-solvent concentration and temperature. Experimental data for IL mixtures with DMSO are important and helpful in general, due to the need to

reduce the processing cost and at the same time increase the efficiency of cellulose processing.

- Solutions of 1-Butyl-3-Methylimidazolium Chloride-cellulose were investigated across a range of cellulose concentrations and temperatures using NMR- spectroscopy and relaxometry, diffusion and viscosity measurements. In the course of this investigation it proved useful to correlate the NMR relaxometry results with those obtained from viscosity and diffusion studies. The Stokes-Einstein-Debye (SED) model produces unreasonable values for the Stokes radius of IL which can be corrected by the use of microviscosity correction factor. Derivation of (Stokes-Einstein) SE and SED equation yields the relationship between τ_o and D_o that depends on the hydrodynamic radius of the molecules and the difference of activation energy between translational diffusion and rotational correlation time. Experimental results from this system demonstrated that the value of τ_o or D_o calculated from ΔE or vice versa matches well with the τ_o and D_o found from an Arrhenius analysis indicating that the derivation is correctly relating the translational diffusion to the rotational correlation time and vice versa well within one order of magnitude.

- Three different types of carbohydrates (glucose, cellobiose and cellulose) were dissolved in EMIMAc and the effect of these carbohydrates on the transport properties of EMIMAc was investigated. Our finding illustrates that the origin of the decrease in transport properties at microscopic level is due to the number of hydroxyl groups available. The present results provide direct evidence to confirm that the dissolution of carbohydrate occurred resulting from the interaction of hydroxyl group of the carbohydrates with anion and cation of the IL with the interaction stoichiometry of ionic liquid:hydroxyl group 1:1. Additionally, it was found that at infinite temperature or when the condition/reaction is 'barrier less' (zero activation energy), the D_o for anion is larger than cation, which one would expect for the smaller diffusing ion. This explained that, the anomalous behaviour of anion and cation in IL is due to the interaction of ion with its surrounding.

Analysis of the dynamic properties of the mixtures suggests that in solutions the bulk viscosity, η is best replaced by a microviscosity, $\eta_\mu = f_\mu \eta$, where f_μ is the microviscosity correction factor.

- A new method to study the kinetics of cellulose coagulation in water from cellulose/IL/co-solvent using NMR has been successfully developed. Diffusion coefficients of EMIMAc and DMSO obtained are found not to be significantly affected by cellulose and DMSO concentration which suggests that if we want to change the coagulation rate and therefore the morphology, we would need to change the anti-solvent.

In summary, NMR techniques have been proven to be efficient methods to study the structure and dynamics of ILs. The usefulness of NMR studies is also evidenced for both cellulose dissolution and regeneration studies. However, since the use of ILs as a cellulose solvent is an area of new research, it still requires a better fundamental understanding of the mechanisms of dissolution and a more comprehensive database on the physiochemical properties of the ILs. The higher cost of ILs is still a major obstacle that needs to overcome. This could be accomplished in many ways such as; by combining a co-solvent with ILs; and by recycling ILs after cellulose dissolution and regeneration.

References

1. Skinner, H.J., *Cellulose in Industry*. Industrial & Engineering Chemistry, 1932. **24**(6): p. 694-704.
2. Gloor, W.E., *Properties of cellulose as applied in plastic materials.* Journal of Chemical Education, 1947. **24**(5): p. 214.
3. Horvath, A.L., *Solubility of structurally complicated materials: I. Wood.* Journal of Physical and Chemical Reference Data, 2006. **35**(1): p. 77-92.
4. Johnson, D.L., *Method of preparing polymers from a mixture of cyclic amine oxides and polymers*. 1970, Eastman Kodak Co: United States.
5. Johnson, D.L., *Compounds dissolved in cyclic amine oxides*. 1969, Eastman Kodak Co: United States.
6. Rosenau, T., et al., *The chemistry of side reactions and byproduct formation in the system NMMO/cellulose (Lyocell process).* Progress in Polymer Science, 2001. **26**(9): p. 1763-1837.
7. Fink, H.P., et al., *Structure formation of regenerated cellulose materials from NMMO-solutions.* Progress in Polymer Science, 2001. **26**(9): p. 1473-1524.
8. Swatloski, R.P., et al., *Dissolution of Cellose with Ionic Liquids.* Journal of the American Chemical Society, 2002. **124**(18): p. 4974-4975.
9. Biganska, O. and P. Navard, *Morphology of cellulose objects regenerated from cellulose–N-methylmorpholine N-oxide–water solutions.* Cellulose, 2009. **16**(2): p. 179-188.
10. Jiang, G., et al., *Diffusion dynamics of 1-Butyl-3-methylimidazolium chloride from cellulose filament during coagulation process.* Cellulose, 2011. **18**(4): p. 921-928.
11. Sescousse, R., R. Gavillon, and T. Budtova, *Aerocellulose from cellulose–ionic liquid solutions: Preparation, properties and comparison with cellulose–NaOH and cellulose–NMMO routes.* Carbohydrate Polymers, 2011. **83**(4): p. 1766-1774.
12. Mitchell, R.L., *Viscose Processing of Cellulose.* Industrial & Engineering Chemistry, 1949. **41**(10): p. 2197-2201.
13. Sihtola, H., *Process for manufacturing cellulose xanthate and viscose prepared from said cellulose xanthate* 1973: Findland.
14. Chanzy, H., M. Paillet, and R. Hagège, *Spinning of cellulose from N-methyl morpholine N-oxide in the presence of additives.* Polymer, 1990. **31**(3): p. 400-405.
15. Eckelt, J., et al., *Phase diagram of the ternary system NMMO/water/cellulose.* Cellulose, 2009. **16**(3): p. 373-379.
16. Braverman, L.P., et al., *Rheological properties of concentrated cellulose solutions in N-methylmorpholine-N-oxide.* Fibre Chemistry, 1990. **22**(6): p. 397-400.
17. Wendler, F., et al., *Thermal Stability of Lyocell Solutions: Experimental Results and Modeling Using Cluster Analysis and Partial Least Squares Regression.* Macromolecular Theory and Simulations, 2008. **17**(1): p. 32-38.

18. Gagnaire, D., D. Mancier, and M. Vincendon, *Cellulose organic solutions: A nuclear magnetic resonance investigation.* Journal of Polymer Science: Polymer Chemistry Edition, 1980. **18**(1): p. 13-25.
19. Holbrey, J.D., et al., *Physicochemical Properties.* Ionic Liquids in Synthesis. 2008: Wiley-VCH Verlag GmbH & Co. KGaA. 57-174.
20. Reddy, R., *Ionic liquids: How well do we know them?* Journal of Phase Equilibria and Diffusion, 2006. **27**(3): p. 210-211.
21. Tokuda, H., et al., *Physicochemical Properties and Structures of Room Temperature Ionic Liquids. 1. Variation of Anionic Species.* The Journal of Physical Chemistry B, 2004. **108**(42): p. 16593-16600.
22. Tokuda, H., et al., *Physicochemical Properties and Structures of Room Temperature Ionic Liquids. 2. Variation of Alkyl Chain Length in Imidazolium Cation.* The Journal of Physical Chemistry B, 2005. **109**(13): p. 6103-6110.
23. Welton, T., *Room-Temperature Ionic Liquids. Solvents for Synthesis and Catalysis.* Chemical Reviews, 1999. **99**(8): p. 2071-2084.
24. Fredlake, C.P., et al., *Thermophysical Properties of Imidazolium-Based Ionic Liquids.* Journal of Chemical & Engineering Data, 2004. **49**(4): p. 954-964.
25. Kowsari, M.H., et al., *Molecular dynamics simulation of imidazolium-based ionic liquids. I. Dynamics and diffusion coefficient.* The Journal of Chemical Physics, 2008. **129**(22): p. 224508.
26. López-Martin, I., et al., *Anion and Cation Effects on Imidazolium Salt Melting Points: A Descriptor Modelling Study.* ChemPhysChem, 2007. **8**(5): p. 690-695.
27. Hunt, P.A., B. Kirchner, and T. Welton, *Characterising the Electronic Structure of Ionic Liquids: An Examination of the 1-Butyl-3-Methylimidazolium Chloride Ion Pair.* Chemistry – A European Journal, 2006. **12**(26): p. 6762-6775.
28. Crowhurst, L., et al., *Solvent-solute interactions in ionic liquids.* Physical Chemistry Chemical Physics, 2003. **5**(13): p. 2790-2794.
29. Anderson, J.L., et al., *Characterizing Ionic Liquids On the Basis of Multiple Solvation Interactions.* Journal of the American Chemical Society, 2002. **124**(47): p. 14247-14254.
30. Weingärtner, H., *Understanding Ionic Liquids at the Molecular Level: Facts, Problems, and Controversies.* Angewandte Chemie International Edition, 2008. **47**(4): p. 654-670.
31. Dong, K., et al., *Understanding Structures and Hydrogen Bonds of Ionic Liquids at the Electronic Level.* The Journal of Physical Chemistry B, 2011. **116**(3): p. 1007-1017.
32. Bagno, A., F. D'Amico, and G. Saielli, *Computing the 1H NMR Spectrum of a Bulk Ionic Liquid from Snapshots of Car–Parrinello Molecular Dynamics Simulations.* ChemPhysChem, 2007. **8**(6): p. 873-881.
33. Chang, H.-C., et al., *Hydrogen Bond Stabilization in 1,3-Dimethylimidazolium Methyl Sulfate and 1-Butyl-3-Methylimidazolium Hexafluorophosphate Probed by High Pressure: The Role of Charge-Enhanced C−H···O Interactions in the Room-Temperature Ionic Liquid.* The Journal of Physical Chemistry B, 2006. **110**(7): p. 3302-3307.
34. Dong, K., et al., *Hydrogen Bonds in Imidazolium Ionic Liquids.* The Journal of Physical Chemistry A, 2006. **110**(31): p. 9775-9782.

35. Bowron, D.T., et al., *Structure and Dynamics of 1-Ethyl-3-methylimidazolium Acetate via Molecular Dynamics and Neutron Diffraction.* The Journal of Physical Chemistry B, 2010. **114**(23): p. 7760-7768.
36. Dong, K. and S. Zhang, *Hydrogen Bonds: A Structural Insight into Ionic Liquids.* Chemistry – A European Journal, 2012. **18**(10): p. 2748-2761.
37. Downard, A., et al., *Structural Studies of Crystalline 1-Alkyl-3-Methylimidazolium Chloride Salts.* Chemistry of Materials, 2003. **16**(1): p. 43-48.
38. Olivier-Bourbigou, H., L. Magna, and D. Morvan, *Ionic liquids and catalysis: Recent progress from knowledge to applications.* Applied Catalysis A: General, 2010. **373**(1–2): p. 1-56.
39. Seddon, K.R., A. Stark, and M.J. Torres, *Influence of chloride, water, and organic solvents on the physical properties of ionic liquids.* Pure and Applied Chemistry, 2000. **72**(12): p. 2275-2287.
40. Hall, C.A., et al., *Macroscopic and Microscopic Study of 1-Ethyl-3-methyl-imidazolium Acetate–Water Mixtures.* The Journal of Physical Chemistry B, 2012. **116**(42): p. 12810-12818.
41. Avent, A.G., et al., *Evidence for hydrogen bonding in solutions of 1-ethyl-3-methylimidazolium halides, and its implications for room-temperature halogenoaluminate(III) ionic liquids.* Journal of the Chemical Society, Dalton Transactions, 1994. **0**(23): p. 3405-3413.
42. Huddleston, J.G., et al., *Characterization and comparison of hydrophilic and hydrophobic room temperature ionic liquids incorporating the imidazolium cation.* Green Chemistry, 2001. **3**(4): p. 156-164.
43. Ries, L.A.S., et al., *Evidence of change in the molecular organization of 1-n-butyl-3-methylimidazolium tetrafluoroborate ionic liquid solutions with the addition of water.* Polyhedron, 2008. **27**(15): p. 3287-3293.
44. Fumino, K., et al., *The influence of hydrogen bonding on the physical properties of ionic liquids.* Physical Chemistry Chemical Physics, 2011. **13**(31): p. 14064-14075.
45. Fumino, K., A. Wulf, and R. Ludwig, *Hydrogen Bonding in Protic Ionic Liquids: Reminiscent of Water.* Angewandte Chemie International Edition, 2009. **48**(17): p. 3184-3186.
46. Seki, S., et al., *Effects of cation and anion on physical properties of room-temperature ionic liquids.* Journal of Molecular Liquids. **152**(1-3): p. 9-13.
47. Wang, X., et al., *Cellulose extraction from wood chip in an ionic liquid 1-allyl-3-methylimidazolium chloride (AmimCl).* Bioresource Technology, 2011. **102**(17): p. 7959-7965.
48. Lucas, M., et al., *Ionic Liquid Pretreatment of Poplar Wood at Room Temperature: Swelling and Incorporation of Nanoparticles.* ACS Applied Materials & Interfaces, 2010. **2**(8): p. 2198-2205.
49. Zhang, J., et al., *NMR spectroscopic studies of cellobiose solvation in EmimAc aimed to understand the dissolution mechanism of cellulose in ionic liquids.* Physical Chemistry Chemical Physics, 2010. **12**(8): p. 1941-1947.
50. Doherty, T.V., et al., *Ionic liquid solvent properties as predictors of lignocellulose pretreatment efficacy.* Green Chemistry, 2010. **12**(11): p. 1967-1975.

51. Fukaya, Y., A. Sugimoto, and H. Ohno, *Superior Solubility of Polysaccharides in Low Viscosity, Polar, and Halogen-Free 1,3-Dialkylimidazolium Formates.* Biomacromolecules, 2006. **7**(12): p. 3295-3297.
52. Fukaya, Y., et al., *Cellulose dissolution with polar ionic liquids under mild conditions: required factors for anions.* Green Chemistry, 2008. **10**(1): p. 44-46.
53. Erdmenger, T., et al., *Homogeneous Tritylation of Cellulose in 1-Butyl-3-methylimidazolium Chloride.* Macromolecular Bioscience, 2007. **7**(4): p. 440-445.
54. Xu, A., J. Wang, and H. Wang, *Effects of anionic structure and lithium salts addition on the dissolution of cellulose in 1-butyl-3-methylimidazolium-based ionic liquid solvent systems.* Green Chemistry, 2010. **12**(2): p. 268-275.
55. Vitz, J., et al., *Extended dissolution studies of cellulose in imidazolium based ionic liquids.* Green Chemistry, 2009. **11**(3): p. 417-424.
56. Zhao, H., et al., *Designing enzyme-compatible ionic liquids that can dissolve carbohydrates.* Green Chemistry, 2008. **10**(6): p. 696-705.
57. del Olmo, L., R. López, and J.M. García de la Vega, *Effect of the molecular structure in the prediction of thermodynamic properties for 1-butyl-3-methylimidazolium chloride ionic liquid.* International Journal of Quantum Chemistry, 2013. **113**(6): p. 852-858.
58. Holbrey, J.D., et al., *Crystal polymorphism in 1-butyl-3-methylimidazolium halides: supporting ionic liquid formation by inhibition of crystallization.* Chemical Communications, 2003. **0**(14): p. 1636-1637.
59. Yamamuro, O., et al., *Hierarchical structure and dynamics of an ionic liquid 1-octyl-3-methylimidazolium chloride.* Journal of Chemical Physics, 2011. **135**(5).
60. Quijada-Maldonado, E., et al., *Experimental densities, dynamic viscosities and surface tensions of the ionic liquids series 1-ethyl-3-methylimidazolium acetate and dicyanamide and their binary and ternary mixtures with water and ethanol at T (298.15 to 343.15 K).* The Journal of Chemical Thermodynamics, 2012. **51**(0): p. 51-58.
61. Almeida, H.F.D., et al., *Thermophysical Properties of Five Acetate-Based Ionic Liquids.* Journal of Chemical & Engineering Data, 2012. **57**(11): p. 3005-3013.
62. Wendler, F., L.-N. Todi, and F. Meister, *Thermostability of imidazolium ionic liquids as direct solvents for cellulose.* Thermochimica Acta, 2012. **528**(0): p. 76-84.
63. Liu, H., et al., *Understanding the Interactions of Cellulose with Ionic Liquids: A Molecular Dynamics Study.* The Journal of Physical Chemistry B, 2010. **114**(12): p. 4293-4301.
64. Liu, H., et al., *Simulations Reveal Conformational Changes of Methylhydroxyl Groups during Dissolution of Cellulose Iβ in Ionic Liquid 1-Ethyl-3-methylimidazolium Acetate.* The Journal of Physical Chemistry B, 2012. **116**(28): p. 8131-8138.
65. Youngs, T.G.A., C. Hardacre, and J.D. Holbrey, *Glucose Solvation by the Ionic Liquid 1,3-Dimethylimidazolium Chloride: A Simulation Study.* The Journal of Physical Chemistry B, 2007. **111**(49): p. 13765-13774.

66. Chiappe, C., C.S. Pomelli, and S. Rajamani, *Influence of Structural Variations in Cationic and Anionic Moieties on the Polarity of Ionic Liquids.* The Journal of Physical Chemistry B, 2011. **115**(31): p. 9653-9661.
67. Zhao, Y., et al., *Effects of Cationic Structure on Cellulose Dissolution in Ionic Liquids: A Molecular Dynamics Study.* ChemPhysChem, 2012. **13**(13): p. 3126-3133.
68. Huang, M.-M., et al., *Static Relative Dielectric Permittivities of Ionic Liquids at 25 °C.* Journal of Chemical & Engineering Data, 2011. **56**(4): p. 1494-1499.
69. Brandt, A., et al., *The effect of the ionic liquid anion in the pretreatment of pine wood chips.* Green Chemistry, 2010. **12**(4): p. 672-679.
70. Xu, A., et al., *Cellulose dissolution at ambient temperature: Role of preferential solvation of cations of ionic liquids by a cosolvent.* Carbohydrate Polymers, 2013. **92**(1): p. 540-544.
71. Hauru, L.K.J., et al., *Role of Solvent Parameters in the Regeneration of Cellulose from Ionic Liquid Solutions.* Biomacromolecules, 2012. **13**(9): p. 2896-2905.
72. Ohno, H. and Y. Fukaya, *Task Specific Ionic Liquids for Cellulose Technology.* Chemistry Letters, 2009. **38**(1): p. 2-7.
73. Zhang, J., et al., *Reply to "Comment on 'NMR spectroscopic studies of cellobiose solvation in EmimAc aimed to understand the dissolution mechanism of cellulose in ionic liquids'" by R. C. Remsing, I. D. Petrik, Z. Liu and G. Moyna, Phys. Chem. Chem. Phys., 2010, 12, DOI: 10.1039/c004203j.* Physical Chemistry Chemical Physics, 2010. **12**(44): p. 14829-14830.
74. Ab Rani, M.A., et al., *Understanding the polarity of ionic liquids.* Physical Chemistry Chemical Physics, 2011. **13**(37): p. 16831-16840.
75. Bini, R., et al., *A rationalization of the solvent effect on the Diels-Alder reaction in ionic liquids using multiparameter linear solvation energy relationships.* Organic & Biomolecular Chemistry, 2008. **6**(14): p. 2522-2529.
76. Hon, D.N.S., *Cellulose: a random walk along its historical path.* Cellulose, 1994. **1**(1): p. 1-25.
77. Brown, R.M., I.M. Saxena, and T. Kondo, *Nematic Ordered Cellulose: Its Structure and Properties*, in *Cellulose: Molecular and Structural Biology*. 2007, Springer Netherlands. p. 285-305.
78. Haworth, W.N., *The structure of carbohydrates.* Helvetica Chimica Acta, 1928. **11**(1): p. 534-548.
79. Kulichikhin, V.G., E.B. Kostikova, and D.P. Olenin, *The concentration and degree of polymerization of the cellulose as factors in the viscosity properties of the viscose.* Fibre Chemistry, 1973. **4**(2): p. 155-159.
80. Maréchal, Y. and H. Chanzy, *The hydrogen bond network in I[beta] cellulose as observed by infrared spectrometry.* Journal of Molecular Structure, 2000. **523**(1-3): p. 183-196.
81. Viswanathan, A. and S.G. Shenouda, *On the hydrogen bonds in the helical structure proposed for cellulose I.* Journal of Applied Polymer Science, 1971. **15**(10): p. 2597-2599.

82. Liu, W., et al., *The physical properties of aqueous solution of room-temperature ionic liquids based on imidazolium: Database and evaluation.* Journal of Molecular Liquids, 2008. **140**(1–3): p. 68-72.
83. Seddon, K.R. and A. Stark, *Selective catalytic oxidation of benzyl alcohol and alkylbenzenes in ionic liquids.* Green Chemistry, 2002. **4**(2): p. 119-123.
84. Ding, Z.-D., et al., *Theoretical and experimental investigation of the interactions between [emim]Ac and water molecules.* Journal of Molecular Structure, 2012. **1015**(0): p. 147-155.
85. Hanke, C.G., N.A. Atamas, and R.M. Lynden-Bell, *Solvation of small molecules in imidazolium ionic liquids: a simulation study.* Green Chemistry, 2002. **4**(2): p. 107-111.
86. Wang, Y., H. Li, and S. Han, *A Theoretical Investigation of the Interactions between Water Molecules and Ionic Liquids.* The Journal of Physical Chemistry B, 2006. **110**(48): p. 24646-24651.
87. Zhao, Y., et al., *Aggregation of Ionic Liquids [Cnmim]Br (n = 4, 6, 8, 10, 12) in D2O: A NMR Study.* The Journal of Physical Chemistry B, 2008. **112**(7): p. 2031-2039.
88. Bowers, J., et al., *Aggregation Behavior of Aqueous Solutions of Ionic Liquids.* Langmuir, 2004. **20**(6): p. 2191-2198.
89. Dorbritz, S., W. Ruth, and U. Kragl, *Investigation on Aggregate Formation of Ionic Liquids.* Advanced Synthesis & Catalysis, 2005. **347**(9): p. 1273-1279.
90. Li, N., et al., *Aggregation Behavior of a Fluorinated Surfactant in 1-Butyl-3-methylimidazolium Ionic Liquids.* The Journal of Physical Chemistry B, 2008. **112**(39): p. 12453-12460.
91. Tsuchiya, H., et al., *NMR Study for Self-aggregation of 1-Butyl-3-methylimidazolium Bromide in Aqueous Solution.* Analytical Sciences, 2008. **24**(10): p. 1369-1371.
92. Sui, X., et al., *Preparation of Cellulose Nanofibers/Nanoparticles via Electrospray.* Chemistry Letters, 2008. **37**(1): p. 114-115.
93. Rinaldi, R., *Instantaneous dissolution of cellulose in organic electrolyte solutions.* Chemical Communications, 2011. **47**(1): p. 511-513.
94. Tian, X.-f., et al., *Pretreatment of microcrystalline cellulose in organic electrolyte solutions for enzymatic hydrolysis.* Biotechnology for Biofuels, 2011. **4**(1): p. 53.
95. Hovermale, R.A. and P.G. Sears, *Dipolar Ions in Non-aqueous Solvents. I. Dielectric Increments as Supporting Evidence for the Dipolar Structure of Sulfamic Acid.* The Journal of Physical Chemistry, 1956. **60**(11): p. 1579-1580.
96. Catalán, J., et al., *A Generalized Solvent Basicity Scale: The Solvatochromism of 5-Nitroindoline and Its Homomorph 1-Methyl-5-nitroindoline.* Liebigs Annalen, 1996. **1996**(11): p. 1785-1794.
97. Luzar, A., A.K. Soper, and D. Chandler, *Combined neutron diffraction and computer simulation study of liquid dimethyl sulphoxide.* The Journal of Chemical Physics, 1993. **99**(9): p. 6836-6847.
98. Holz, M., S.R. Heil, and A. Sacco, *Temperature-dependent self-diffusion coefficients of water and six selected molecular liquids for calibration in accurate 1H NMR PFG measurements.* Physical Chemistry Chemical Physics, 2000. **2**(20): p. 4740-4742.

99. Senapati, S., *A molecular dynamics simulation study of the dimethyl sulfoxide liquid--vapor interface.* The Journal of Chemical Physics, 2002. **117**(4): p. 1812-1816.
100. Romanowski, S.J., C.M. Kinart, and W.J. Kinart, *Physicochemical properties of dimethyl sulfoxide-methanol liquid mixtures. Experimental and semiempirical quantum chemical studies.* Journal of the Chemical Society, Faraday Transactions, 1995. **91**(1): p. 65-70.
101. Poole, C.F., *Chromatographic and spectroscopic methods for the determination of solvent properties of room temperature ionic liquids.* Journal of Chromatography A, 2004. **1037**(1–2): p. 49-82.
102. Clever, H.L. and E.F. Westrum, *Dimethyl sulfoxide and dimethyl sulfone. Heat capacities, enthalpies of fusion, and thermodynamic properties.* The Journal of Physical Chemistry, 1970. **74**(6): p. 1309-1317.
103. Srivastava, A.K. and S.L. Shankar, *Ionic Conductivity in Binary Solvent Mixtures. 3. Dimethyl Sulfoxide + Propylene Carbonate at 25 °C.* Journal of Chemical & Engineering Data, 1998. **43**(1): p. 25-28.
104. Vishnyakov, A., A.P. Lyubartsev, and A. Laaksonen, *Molecular Dynamics Simulations of Dimethyl Sulfoxide and Dimethyl Sulfoxide−Water Mixture.* The Journal of Physical Chemistry A, 2001. **105**(10): p. 1702-1710.
105. Stewart, J.P., *MOPAC: A semiempirical molecular orbital program.* Journal of Computer-Aided Molecular Design, 1990. **4**(1): p. 1-103.
106. Gupta, K.M., Z. Hu, and J. Jiang, *Molecular insight into cellulose regeneration from a cellulose/ionic liquid mixture: effects of water concentration and temperature.* RSC Advances, 2013. **3**(13): p. 4425-4433.
107. Dadi, A.P., S. Varanasi, and C.A. Schall, *Enhancement of cellulose saccharification kinetics using an ionic liquid pretreatment step.* Biotechnology and Bioengineering, 2006. **95**(5): p. 904-910.
108. Dadi, A., C. Schall, and S. Varanasi, *Mitigation of cellulose recalcitrance to enzymatic hydrolysis by ionic liquid pretreatment.* Applied Biochemistry and Biotechnology, 2007. **137-140**(1-12): p. 407-421.
109. Haerens, K., et al., *Challenges for recycling ionic liquids by using pressure driven membrane processes.* Green Chemistry, 2010. **12**(12): p. 2182-2188.
110. Scurto, A.M., S.N.V.K. Aki, and J.F. Brennecke, *Carbon dioxide induced separation of ionic liquids and water.* Chemical Communications, 2003. **0**(5): p. 572-573.
111. Gan, Q., M. Xue, and D. Rooney, *A study of fluid properties and microfiltration characteristics of room temperature ionic liquids [C10-min][NTf2] and N8881[NTf2] and their polar solvent mixtures.* Separation and Purification Technology, 2006. **51**(2): p. 185-192.
112. Levitt, M.H., *Spin Dynamics: Basics of Nuclear Magnetic Resonance*. 2008: John Wiley & Sons.
113. Callaghan, P.T., *Principles of nuclear magnetic resonance microscopy*. 1991, Oxford: Clarendon Press. xvii, 492 p., 4 p. of plates.
114. Hore, P.J., *Nuclear magnetic resonance*. Oxford chemistry primers. 1995, Oxford: Oxford University Press. v, 90 p.
115. Keeler, J., *Understanding NMR Spectroscopy*. 2010: John Wiley & Sons.
116. Balci, M., *Basic H-1- and C-13-NMR Spectroscopy Introduction.* Basic 1h- and I3c-Nmr Spectroscopy, 2005: p. 235-239.

117. Imanari, M., et al., *Characterization of the molecular reorientational dynamics of the neat ionic liquid 1-butyl-3-methylimidazolium bromide in the super cooled state using 1H and 13C NMR spectroscopy.* Magnetic Resonance in Chemistry, 2009. **47**(1): p. 67-70.
118. Burrell, G.L., et al., *NMR Relaxation and Self-Diffusion Study at High and Low Magnetic Fields of Ionic Association in Protic Ionic Liquids.* The Journal of Physical Chemistry B, 2010. **114**(35): p. 11436-11443.
119. Bloembergen, N., E.M. Purcell, and R.V. Pound, *Relaxation Effects in Nuclear Magnetic Resonance Absorption.* Physical Review, 1948. **73**(7): p. 679-712.
120. Boeré, R.T. and R.G. Kidd, *Rotational Correlation Times in Nuclear Magnetic Relaxation,* in *Annual Reports on NMR Spectroscopy*, G.A. Webb, Editor. 1983, Academic Press. p. 319-385.
121. Gutowsky, H.S. and D.E. Woessner, *Nuclear Magnetic Spin-Lattice Relaxation in Liquids.* Physical Review, 1956. **104**(3): p. 843-844.
122. Price, W.S., *NMR studies of translational motion: principles and application*. 2009, New York: Cambridge University Press.
123. Cotts, R.M., et al., *Pulsed field gradient stimulated echo methods for improved NMR diffusion measurements in heterogeneous systems.* Journal of Magnetic Resonance (1969), 1989. **83**(2): p. 252-266.
124. Walser, R., A.E. Mark, and W.F. van Gunsteren, *On the validity of Stokes' law at the molecular level.* Chemical Physics Letters, 1999. **303**(5–6): p. 583-586.
125. Cappelezzo, M., et al., *Stokes-Einstein relation for pure simple fluids.* The Journal of Chemical Physics, 2007. **126**(22): p. -.
126. Ribeiro, A.C.F., et al., *Binary Mutual Diffusion Coefficients of Aqueous Solutions of Sucrose, Lactose, Glucose, and Fructose in the Temperature Range from (298.15 to 328.15) K.* Journal of Chemical & Engineering Data, 2006. **51**(5): p. 1836-1840.
127. Berner, B. and D. Kivelson, *Paramagnetically enhanced relaxation of nuclear spins. Measurement of diffusion.* The Journal of Physical Chemistry, 1979. **83**(11): p. 1401-1405.
128. Chen, B., E.E. Sigmund, and W.P. Halperin, *Stokes-Einstein Relation in Supercooled Aqueous Solutions of Glycerol.* Physical Review Letters, 2006. **96**(14): p. 145502.
129. Bordat, P., et al., *The breakdown of the Stokes–Einstein relation in supercooled binary liquids.* Journal of Physics: Condensed Matter, 2003. **15**(32): p. 5397.
130. Chirico, G., M. Placidi, and S. Cannistraro, *Fractional Stokes−Einstein Relationship in Biological Colloids: Role of Mixed Stick−Slip Boundary Conditions.* The Journal of Physical Chemistry B, 1999. **103**(10): p. 1746-1751.
131. Koenderink, G.H. and A.P. Philipse, *Rotational and Translational Self-Diffusion in Colloidal Sphere Suspensions and the Applicability of Generalized Stokes−Einstein Relations.* Langmuir, 2000. **16**(13): p. 5631-5638.
132. Horn, F.M., et al., *Hydrodynamic and Colloidal Interactions in Concentrated Charge-Stabilized Polymer Dispersions.* Journal of Colloid and Interface Science, 2000. **225**(1): p. 166-178.

133. Koenderink, G.H., et al., *On the validity of Stokes-Einstein-Debye relations for rotational diffusion in colloidal suspensions.* Faraday Discussions, 2003. **123**(0): p. 335-354.
134. Li, J.C.M. and P. Chang, *Self-Diffusion Coefficient and Viscosity in Liquids.* The Journal of Chemical Physics, 1955. **23**(3): p. 518-520.
135. Brady, J.E. and F. Senese, *Chemistry: matter and its changes*. 2004: Wiley.
136. Silverstein, T.P., *The Real Reason Why Oil and Water Don't Mix.* Journal of Chemical Education, 1998. **75**(1): p. 116.
137. Heerklotz, H. and R.M. Epand, *The Enthalpy of Acyl Chain Packing and the Apparent Water-Accessible Apolar Surface Area of Phospholipids.* Biophysical journal, 2001. **80**(1): p. 271-279.
138. Petkov, V., Y. Ren, and M. Suchomel, *Molecular arrangement in water: random but not quite.* Journal of Physics: Condensed Matter, 2012. **24**(15): p. 155102.
139. Fitter, J., *A Measure of Conformational Entropy Change during Thermal Protein Unfolding Using Neutron Spectroscopy.* Biophysical journal, 2003. **84**(6): p. 3924-3930.
140. Powell, R.E., W.E. Roseveare, and H. Eyring, *Diffusion, Thermal Conductivity, and Viscous Flow of Liquids.* Industrial & Engineering Chemistry, 1941. **33**(4): p. 430-435.
141. Cullinan, H.T., *Concentration Dependence of the Binary Diffusion Coefficient.* Industrial & Engineering Chemistry Fundamentals, 1966. **5**(2): p. 281-283.
142. Vignes, A., *Diffusion in Binary Solutions. Variation of Diffusion Coefficient with Composition.* Industrial & Engineering Chemistry Fundamentals, 1966. **5**(2): p. 189-199.
143. Zhang, L., et al., *Comparison of the Blue-Shifted C−D Stretching Vibrations for DMSO-d6 in Imidazolium-Based Room Temperature Ionic Liquids and in Water.* The Journal of Physical Chemistry B, 2009. **113**(17): p. 5978-5984.
144. Stoppa, A., J. Hunger, and R. Buchner, *Conductivities of Binary Mixtures of Ionic Liquids with Polar Solvents†.* Journal of Chemical & Engineering Data, 2008. **54**(2): p. 472-479.
145. Wang, N.-N., et al., *Hydrogen Bonding Interactions between a Representative Pyridinium-Based Ionic Liquid [BuPy][BF4] and Water/Dimethyl Sulfoxide.* The Journal of Physical Chemistry B, 2010. **114**(26): p. 8689-8700.
146. Canongia Lopes, J.N., et al., *Polarity, Viscosity, and Ionic Conductivity of Liquid Mixtures Containing [C4C1im][Ntf2] and a Molecular Component.* The Journal of Physical Chemistry B, 2011. **115**(19): p. 6088-6099.
147. Rai, G. and A. Kumar *Probing Thermal Interactions of Ionic Liquids with Dimethyl Sulfoxide.* ChemPhysChem, 2012. **13**(7): p. 1927-1933.
148. Govinda, V., et al., *Thermophysical properties of dimethylsulfoxide with ionic liquids at various temperatures.* Fluid Phase Equilibria, 2011. **304**(1–2): p. 35-43.
149. Geppert-Rybczyńska, M., et al., *Volumetric Properties of Binary Mixtures Containing Ionic Liquids and Some Aprotic Solvents.* Journal of Chemical & Engineering Data, 2010. **55**(9): p. 4114-4120.

150. Liu, X., T.J.H. Vlugt, and A. Bardow, *Maxwell–Stefan Diffusivities in Binary Mixtures of Ionic Liquids with Dimethyl Sulfoxide (DMSO) and H2O.* The Journal of Physical Chemistry B, 2011. **115**(26): p. 8506-8517.
151. Padmanabhan, S., et al., *Solubility and rate of dissolution for Miscanthus in hydrophilic ionic liquids.* Fluid Phase Equilibria, 2011. **309**(1): p. 89-96.
152. MacGregor, W.S., *THE CHEMICAL AND PHYSICAL PROPERTIES OF DMSO.* Annals of the New York Academy of Sciences, 1967. **141**(1): p. 3-12.
153. Liu, H., F. Mueller-Plathe, and W.F. van Gunsteren, *A Force Field for Liquid Dimethyl Sulfoxide and Physical Properties of Liquid Dimethyl Sulfoxide Calculated Using Molecular Dynamics Simulation.* Journal of the American Chemical Society, 1995. **117**(15): p. 4363-4366.
154. Shiflett, M.B. and A. Yokozeki, *Phase Behavior of Carbon Dioxide in Ionic Liquids: [emim][Acetate], [emim][Trifluoroacetate], and [emim][Acetate] + [emim][Trifluoroacetate] Mixtures.* Journal of Chemical & Engineering Data, 2008. **54**(1): p. 108-114.
155. Freire, M.G., et al., *Thermophysical Characterization of Ionic Liquids Able To Dissolve Biomass.* Journal of Chemical & Engineering Data, 2011. **56**(12): p. 4813-4822.
156. Zafarani-Moattar, M.T. and R. Majdan-Cegincara, *Viscosity, Density, Speed of Sound, and Refractive Index of Binary Mixtures of Organic Solvent + Ionic Liquid, 1-Butyl-3-methylimidazolium Hexafluorophosphate at 298.15 K.* Journal of Chemical & Engineering Data, 2007. **52**(6): p. 2359-2364.
157. Syal, V.K., S. Chauhan, and R. Gautam, *Ultrasonic velocity measurements of carbohydrates in binary mixtures of DMSO + H2O at 25°C.* Ultrasonics, 1998. **36**(1–5): p. 619-623.
158. Zhou, Q., et al., *Density and Excess Molar Volume for Binary Mixtures of Naphthenic Acid Ionic Liquids and Ethanol.* Journal of Chemical & Engineering Data, 2009. **55**(3): p. 1105-1108.
159. Lehmann, J., et al., *Densities and Excess Molar Volumes for Binary Mixtures of Ionic Liquid 1-Ethyl-3-methylimidazolium Ethylsulfate with Solvents.* Journal of Chemical & Engineering Data, 2010. **55**(9): p. 4068-4074.
160. Ren, R., et al., *Density, Excess Molar Volume and Conductivity of Binary Mixtures of the Ionic Liquid 1,2-Dimethyl-3-hexylimidazolium Bis(trifluoromethylsulfonyl)imide and Dimethyl Carbonate.* Journal of Chemical & Engineering Data, 2010. **56**(1): p. 27-30.
161. Moreno, M., et al., *Interaction of Water with the Model Ionic Liquid [bmim][BF4]: Molecular Dynamics Simulations and Comparison with NMR Data.* The Journal of Physical Chemistry B, 2008. **112**(26): p. 7826-7836.
162. Mele, A., C.D. Tran, and S.H. De Paoli Lacerda, *The Structure of a Room-Temperature Ionic Liquid with and without Trace Amounts of Water: The Role of C□H···O and C□H···F Interactions in 1-n-Butyl-3-Methylimidazolium Tetrafluoroborate.* Angewandte Chemie International Edition, 2003. **42**(36): p. 4364-4366.
163. Remsing, R.C., et al., *Solvation and Aggregation of N,N'-Dialkylimidazolium Ionic Liquids: A Multinuclear NMR Spectroscopy and Molecular Dynamics Simulation Study.* The Journal of Physical Chemistry B, 2008. **112**(25): p. 7363-7369.

164. Khupse, N. and A. Kumar, *Dramatic Change in Viscosities of Pure Ionic Liquids upon Addition of Molecular Solvents.* Journal of Solution Chemistry, 2009. **38**(5): p. 589-600.
165. Remsing, R.C., et al., *Solvation and Aggregation of N,Nâ€²-Dialkylimidazolium Ionic Liquids: A Multinuclear NMR Spectroscopy and Molecular Dynamics Simulation Study*. The Journal of Physical Chemistry B, 2008. **112**(25): p. 7363-7369.
166. Jiang, J., *Association structures of ionic liquid/DMSO mixtures studied by high-pressure infrared spectroscopy.* J. Chem. Phys., 2011. **134**(4): p. 044506.
167. Fort, R.J. and W.R. Moore, *Viscosities of binary liquid mixtures.* Transactions of the Faraday Society, 1966. **62**(0): p. 1112-1119.
168. Bowron, D.T., et al., *Structure and Dynamics of 1-Ethyl-3-methylimidazolium Acetate via Molecular Dynamics and Neutron Diffraction.* The Journal of Physical Chemistry B. **114**(23): p. 7760-7768.
169. Jiang, J.-C., et al., *Association structures of ionic liquid/DMSO mixtures studied by high-pressure infrared spectroscopy.* The Journal of Chemical Physics, 2011. **134**(4): p. 044506.
170. Salari, H., et al., *Preferential Solvation and Behavior of Solvatochromic Indicators in Mixtures of an Ionic Liquid with Some Molecular Solvents.* The Journal of Physical Chemistry B, 2010. **114**(29): p. 9586-9593.
171. Moniz, W.B., W.A. Steele, and J.A. Dixon, *Nuclear Spin Relaxation in Liquids. Spheroidal Molecules.* The Journal of Chemical Physics, 1963. **38**(10): p. 2418-2426.
172. Sescousse, R., et al., *Viscosity of Cellulose−Imidazolium-Based Ionic Liquid Solutions.* The Journal of Physical Chemistry B, 2010. **114**(21): p. 7222-7228.
173. Remsing, R.C., et al., *Solvation of Carbohydrates in N,N′-Dialkylimidazolium Ionic Liquids: A Multinuclear NMR Spectroscopy Study.* The Journal of Physical Chemistry B, 2008. **112**(35): p. 11071-11078.
174. Gross, A.S., A.T. Bell, and J.-W. Chu, *Thermodynamics of Cellulose Solvation in Water and the Ionic Liquid 1-Butyl-3-Methylimidazolim Chloride.* The Journal of Physical Chemistry B, 2011. **115**(46): p. 13433-13440.
175. Cho, H.M., A.S. Gross, and J.-W. Chu, *Dissecting Force Interactions in Cellulose Deconstruction Reveals the Required Solvent Versatility for Overcoming Biomass Recalcitrance.* Journal of the American Chemical Society, 2011. **133**(35): p. 14033-14041.
176. Simpson, J.H. and H.Y. Carr, *Diffusion and Nuclear Spin Relaxation in Water*. Physical Review, 1958. **111**(5): p. 1201-1202.
177. Bagno, A., F. Rastrelli, and G. Saielli, *Toward the Complete Prediction of the 1H and 13C NMR Spectra of Complex Organic Molecules by DFT Methods: Application to Natural Substances.* Chemistry – A European Journal, 2006. **12**(21): p. 5514-5525.
178. Bagno, A., F. Rastrelli, and G. Saielli, *Prediction of the 1H and 13C NMR Spectra of α-d-Glucose in Water by DFT Methods and MD Simulations.* The Journal of Organic Chemistry, 2007. **72**(19): p. 7373-7381.

179. Bubb, W.A., *NMR spectroscopy in the study of carbohydrates: Characterizing the structural complexity.* Concepts in Magnetic Resonance Part A, 2003. **19A**(1): p. 1-19.
180. Kohagen, M., et al., *How Hydrogen Bonds Influence the Mobility of Imidazolium-Based Ionic Liquids. A Combined Theoretical and Experimental Study of 1-n-Butyl-3-methylimidazolium Bromide.* The Journal of Physical Chemistry B, 2011. **115**(51): p. 15280-15288.
181. Lynden-Bell, R.M. and T.G.A. Youngs, *Simulations of imidazolium ionic liquids: when does the cation charge distribution matter?* Journal of Physics-Condensed Matter, 2009. **21**(42).
182. Heimer, N.E., et al., *13C NMR Relaxation Rates in the Ionic Liquid 1-Ethyl-3-methylimidazolium Butanesulfonate.* The Journal of Physical Chemistry A, 2005. **110**(3): p. 868-874.
183. Carper, W.R., P.G. Wahlbeck, and A. Dölle, *13C NMR Relaxation Rates: Separation of Dipolar and Chemical Shift Anisotropy Effects.* The Journal of Physical Chemistry A, 2004. **108**(29): p. 6096-6099.
184. Antony, J.H., et al., *13C NMR Relaxation Rates in the Ionic Liquid 1-Methyl-3-nonylimidazolium Hexafluorophosphate.* The Journal of Physical Chemistry A, 2005. **109**(30): p. 6676-6682.
185. O'Reilly, D.E., *Self-Diffusion Coefficients and Rotational Correlation Times in Polar Liquids.* The Journal of Chemical Physics, 1968. **49**(12): p. 5416-5420.
186. Mitchell, R.W. and M. Eisner, *Nuclear Spin-Lattice Relaxation in Solutions.* The Journal of Chemical Physics, 1960. **33**(1): p. 86-91.
187. Mitchell, R.W. and M. Eisner, *Concentration Dependence of NMR Spin-Lattice Relaxation Times in Solutions.* The Journal of Chemical Physics, 1961. **34**(2): p. 651-654.
188. Kivelson, D., M.G. Kivelson, and I. Oppenheim, *Rotational Relaxation in Fluids.* The Journal of Chemical Physics, 1970. **52**(4): p. 1810-1821.
189. Meng, Z., A. Dölle, and W. Robert Carper, *Gas phase model of an ionic liquid: semi-empirical and ab initio bonding and molecular structure.* Journal of Molecular Structure: THEOCHEM, 2002. **585**(1–3): p. 119-128.
190. Hu, C.-M. and R. Zwanzig, *Rotational friction coefficients for spheroids with the slipping boundary condition.* The Journal of Chemical Physics, 1974. **60**(11): p. 4354-4357.
191. Dhumal, N.R., H.J. Kim, and J. Kiefer, *Molecular Interactions in 1-Ethyl-3-methylimidazolium Acetate Ion Pair: A Density Functional Study.* The Journal of Physical Chemistry A, 2009. **113**(38): p. 10397-10404.
192. Giraud, G., et al., *The effects of anion and cation substitution on the ultrafast solvent dynamics of ionic liquids: A time-resolved optical Kerr-effect spectroscopic study.* The Journal of Chemical Physics, 2003. **119**(1): p. 464-477.
193. Köddermann, T., R. Ludwig, and D. Paschek, *On the Validity of Stokes–Einstein and Stokes–Einstein–Debye Relations in Ionic Liquids and Ionic-Liquid Mixtures.* ChemPhysChem, 2008. **9**(13): p. 1851-1858.
194. Lovell, C.S., et al., *Influence of Cellulose on Ion Diffusivity in 1-Ethyl-3-Methyl-Imidazolium Acetate Cellulose Solutions.* Biomacromolecules, 2010. **11**(11): p. 2927-2935.

195. Umecky, T., M. Kanakubo, and Y. Ikushima, *Self-diffusion coefficients of 1-butyl-3-methylimidazolium hexafluorophosphate with pulsed-field gradient spin-echo NMR technique.* Fluid Phase Equilibria, 2005. **228–229**(0): p. 329-333.
196. Tokuda, H., et al., *Physicochemical Properties and Structures of Room-Temperature Ionic Liquids. 3. Variation of Cationic Structures.* The Journal of Physical Chemistry B, 2006. **110**(6): p. 2833-2839.
197. Tsuzuki, S., et al., *Molecular Dynamics Simulations of Ionic Liquids: Cation and Anion Dependence of Self-Diffusion Coefficients of Ions.* The Journal of Physical Chemistry B, 2009. **113**(31): p. 10641-10649.
198. Urahata, S.M. and M.C.C. Ribeiro, *Single particle dynamics in ionic liquids of 1-alkyl-3-methylimidazolium cations.* The Journal of Chemical Physics, 2005. **122**(2): p. 024511.
199. Remsing, R.C., et al., *Mechanism of cellulose dissolution in the ionic liquid 1-n-butyl-3-methylimidazolium chloride: a 13C and 35/37Cl NMR relaxation study on model systems.* Chemical Communications, 2006. **0**(12): p. 1271-1273.
200. Liu, H., et al., *Molecular Dynamics Study of Polysaccharides in Binary Solvent Mixtures of an Ionic Liquid and Water.* The Journal of Physical Chemistry B, 2011. **115**(34): p. 10251-10258.
201. Rausch, M.H., et al., *Binary Diffusion Coefficients for Mixtures of Ionic Liquids [EMIM][N(CN)2], [EMIM][NTf2], and [HMIM][NTf2] with Acetone and Ethanol by Dynamic Light Scattering (DLS).* The Journal of Physical Chemistry B, 2013. **117**(8): p. 2429-2437.
202. Feng, S. and G.A. Voth, *Molecular dynamics simulations of imidazolium-based ionic liquid/water mixtures: Alkyl side chain length and anion effects.* Fluid Phase Equilibria, 2010. **294**(1–2): p. 148-156.
203. Ding, Z.-D., et al., *Theoretical and experimental investigation on dissolution and regeneration of cellulose in ionic liquid.* Carbohydrate Polymers, 2012. **89**(1): p. 7-16.
204. Gavillon, R. and T. Budtova, *Kinetics of Cellulose Regeneration from Cellulose−NaOH−Water Gels and Comparison with Cellulose−N-Methylmorpholine-N-Oxide−Water Solutions.* Biomacromolecules, 2007. **8**(2): p. 424-432.
205. Biganska, O. and P. Navard, *Kinetics of Precipitation of Cellulose from Cellulose−NMMO−Water Solutions.* Biomacromolecules, 2005. **6**(4): p. 1948-1953.
206. Laity, P.R., et al., *Studies of non-solvent induced polymer coagulation by magnetic resonance imaging.* Polymer, 2001. **42**(18): p. 7701-7710.
207. Laity, P.R., P.M. Glover, and J.N. Hay, *Composition and phase changes observed by magnetic resonance imaging during non-solvent induced coagulation of cellulose.* Polymer, 2002. **43**(22): p. 5827-5837.
208. Xiao, W., et al., *The study of factors affecting the enzymatic hydrolysis of cellulose after ionic liquid pretreatment.* Carbohydrate Polymers, 2012. **87**(3): p. 2019-2023.
209. Li, B., et al., *Factors Affecting Wood Dissolution and Regeneration of Ionic Liquids.* Industrial & Engineering Chemistry Research, 2010. **49**(5): p. 2477-2484.

210. Wada, R., S.-H. Hyon, and Y. Ikada, *Kinetics of diffusion-mediated drug release enhanced by matrix degradation.* Journal of Controlled Release, 1995. **37**(1–2): p. 151-160.
211. Fu, Y. and W.J. Kao, *Drug release kinetics and transport mechanisms of non-degradable and degradable polymeric delivery systems.* Expert Opinion on Drug Delivery, 2010. **7**(4): p. 429-444.
212. Crank, J., *The mathematics of diffusion*. 1956, Oxford: Clarendon Press. 347 p.
213. Niazi, A.A., B.D. Rabideau, and A.E. Ismail, *Effects of Water Concentration on the Structural and Diffusion Properties of Imidazolium-Based Ionic Liquid–Water Mixtures.* The Journal of Physical Chemistry B, 2013. **117**(5): p. 1378-1388.
214. Nieto-Draghi, C., J.B. Avalos, and B. Rousseau, *Transport properties of dimethyl sulfoxide aqueous solutions.* The Journal of Chemical Physics, 2003. **119**(9): p. 4782-4789.
215. Luzar, A. and D. Chandler, *Structure and hydrogen bond dynamics of water--dimethyl sulfoxide mixtures by computer simulations.* The Journal of Chemical Physics, 1993. **98**(10): p. 8160-8173.
216. Soper, A.K. and A. Luzar, *Orientation of Water Molecules around Small Polar and Nonpolar Groups in Solution: A Neutron Diffraction and Computer Simulation Study.* The Journal of Physical Chemistry, 1996. **100**(4): p. 1357-1367.
217. Hedenqvist, M. and U.W. Gedde, *Diffusion of small-molecule penetrants in semicrystalline polymers.* Progress in Polymer Science, 1996. **21**(2): p. 299-333.